

# Electroweak Working Group Report

D. Bardin<sup>ab</sup>, W. Beenakker<sup>c</sup>, M. Bilenky<sup>ad</sup>, W. Hollik<sup>e</sup>, M. Martinez<sup>f</sup>,  
G. Montagna<sup>gl</sup>, O. Nicrosini<sup>h\*</sup>, V. Novikov<sup>i</sup>, L. Okun<sup>i</sup>, A. Olshevsky<sup>d</sup>,  
G. Passarino<sup>jk</sup>, F. Piccinini<sup>gl</sup>, S. Riemann<sup>a</sup>, T. Riemann<sup>a</sup>, A. Rozanov<sup>im</sup>,  
F. Teubert<sup>f</sup>, M. Vysotsky<sup>i</sup>

<sup>a</sup> Deutsches Elektronen-Synchrotron DESY  
Institut für Hochenergiephysik IfH, Zeuthen, Germany

<sup>b</sup> Bogoliubov Laboratory of Theoretical Physics  
Joint Institute for Nuclear Research, Dubna, Moscow Region, Russia

<sup>c</sup> Deutsches Elektronen-Synchrotron DESY, Hamburg, Germany

<sup>d</sup> Laboratory for Nuclear Problems  
Joint Institute for Nuclear Research, Dubna, Moscow Region, Russia

<sup>e</sup> Institut für Theoretische Physik  
Universität Karlsruhe, Karlsruhe, Germany

<sup>f</sup> Institut de Fisica d'Altes Energies  
Universitat Autònoma de Barcelona, Barcelona, Spain

<sup>g</sup> Dipartimento di Fisica Nucleare e Teorica, Università di Pavia, Pavia, Italy

<sup>h</sup> CERN, TH Division, Geneva, Switzerland

<sup>i</sup> ITEP, Moscow, Russia

<sup>j</sup> Dipartimento di Fisica Teorica, Università di Torino, Torino, Italy

<sup>k</sup> INFN, Sezione di Torino, Torino, Italy

<sup>l</sup> INFN, Sezione di Pavia, Pavia, Italy

<sup>m</sup> CPPM, IN2P3-CNRS, Marseille, France

emails:

bardindy@cernvm.cern.ch, t00bee@dsyibm.desy.de, bilenky@ifh.de, woh@dmumpiwh.mppmu.mpg.de, martinez@ifae.es, montagna@pv.infn.it, nicrosini@pv.infn.it, novikov@vxitep.itep.ru, okun@vxitep.itep.ru, olshevsk@vxcern.cern.ch, giampiero@to.infn.it, piccinini@pv.infn.it, riemanns@cernvm.cern.ch, riemann@cernvm.cern.ch, rozanov@cernvm.cern.ch, teubert@ifae.es, vysotsky@vxitep.itep.ru

\*On leave from INFN, Sezione di Pavia, Italy.

# Contents

<b>1</b>	<b>Theoretical basics</b>	<b>4</b>
1.1	Introduction . . . . .	4
1.2	Input parameters . . . . .	5
1.3	Codes to calculate electroweak observables . . . . .	8
1.4	The language of effective couplings . . . . .	9
1.4.1	The Born Approximation for $e^+e^- \rightarrow f\bar{f}$ . . . . .	9
1.4.2	Electroweak non-photonic corrections . . . . .	10
1.4.3	$Z$ pole approximation . . . . .	11
1.4.4	Effective couplings for $Z$ decay. . . . .	13
1.5	Pseudo-observables . . . . .	15
1.6	Realistic observables . . . . .	16
1.7	Computational schemes . . . . .	17
1.8	Main features of different approaches . . . . .	18
1.8.1	BHM/WHO, ZFITTER . . . . .	19
1.8.2	LEPTOP . . . . .	22
1.8.3	TOPAZ0 . . . . .	24
1.9	Phenomenology of $Z$ boson decays . . . . .	26
1.10	Electroweak corrections: Basic notions . . . . .	28
1.10.1	Comparison of notations of different codes . . . . .	28
1.10.2	Basic notions of different codes . . . . .	29
<b>2</b>	<b>Options, theoretical uncertainties</b>	<b>35</b>
2.1	Factorization of QCD Corrections . . . . .	35
2.2	Genuinely Weak Uncertainties . . . . .	36
2.2.1	Leading-Remainder splitting . . . . .	37
2.2.2	Scale in vertex corrections . . . . .	38
2.2.3	Linearization . . . . .	38
2.2.4	Resummation . . . . .	39
2.2.5	Estimate of the missing terms in higher orders . . . . .	41
2.3	QCD Corrections on Electroweak Loops . . . . .	42
2.4	Parametric Uncertainties . . . . .	44
2.5	Structure of the Comparisons . . . . .	45
2.6	Experimental data and theoretical predictions . . . . .	47
2.7	More on Theoretical Uncertainties . . . . .	53
2.7.1	TOPAZ0 . . . . .	54
2.7.2	ZFITTER . . . . .	55
<b>3</b>	<b>Realistic distributions</b>	<b>57</b>
3.1	De-Convolved Distributions . . . . .	58
3.2	Final-State Radiation . . . . .	58
3.3	Initial-State Pair Production and QED Interference . . . . .	59
3.4	Imaginary Parts of the Formfactors . . . . .	61
3.5	Initial-State QED Uncertainties . . . . .	61

3.6	Comparisons . . . . .	62
<b>4</b>	<b>Basic Formulae for Electroweak Radiative Corrections</b>	<b>68</b>
4.1	BHM/WOH basics . . . . .	68
4.1.1	Self-energies, propagators, and $\Delta r$ . . . . .	68
4.1.2	Vertex corrections . . . . .	71
4.1.3	$e^+e^- \rightarrow f\bar{f}$ amplitudes . . . . .	73
4.1.4	Effective neutral current couplings . . . . .	73
4.2	LEPTOP basics . . . . .	74
4.2.1	Electroweak loops for hadron-free observables: functions $V_i$ . . . . .	74
4.2.2	Corrections $\delta V_i$ . . . . .	76
4.2.3	Hadronic decays of $Z$ boson . . . . .	78
4.2.4	Specific features of the decay $Z \rightarrow b\bar{b}$ . . . . .	79
4.2.5	Appendix: Auxiliary functions $F_t$ and $F_h$ . . . . .	80
4.3	TOPAZ0 basics . . . . .	80
4.3.1	Appendix 1: The self-energies . . . . .	84
4.3.2	Appendix 2: The $Zff$ vertices . . . . .	85
4.4	ZFITTER basics . . . . .	86
4.4.1	Muon life-time . . . . .	86
4.4.2	Partial widths of the $Z$ boson . . . . .	87
4.4.3	Auxiliary functions . . . . .	87
4.4.4	Form factors of the process $e^+e^- \rightarrow f\bar{f}$ . . . . .	90
4.4.5	The $\mathcal{O}(\alpha\alpha_s)$ corrections to electroweak observables . . . . .	90
<b>5</b>	<b>Description of options in different approaches</b>	<b>92</b>
5.1	BHM options . . . . .	92
5.2	LEPTOP options . . . . .	93
5.3	TOPAZ0 options . . . . .	95
5.4	ZFITTER options . . . . .	98
	<b>References</b>	<b>100</b>
	<b>Figures</b>	<b>106</b>
	Pseudo-observables . . . . .	106
	Realistic-observables . . . . .	119
	<b>Tables</b>	<b>133</b>
	Pseudo-observables . . . . .	133
	Realistic-observables . . . . .	144
	Bhabha scattering . . . . .	149
	Effect of working options for different codes . . . . .	156
	<b>Note added in proof</b>	<b>158</b>

# 1 Theoretical basics

## 1.1 Introduction

The radiative corrections (RC) for observables related to the  $Z$  resonance have been described in great detail in the 1989 CERN Yellow Report ‘ $Z$  Physics at LEP 1’ [1]. About  $1.5 \times 10^7$   $Z$  decays have been recorded and analysed during the years of operation of the four LEP experiments — from autumn of 1989 to the end of 1994. In order to match the actual experimental precision, a completely revised analysis of radiative corrections at the  $Z$  resonance is needed. The aim of this contribution to the present Report is threefold. We will:

- (i) introduce a common language for presentation of the results emerging from different approaches;
- (ii) update the predictions of  $Z$  resonance observables within the Minimal Standard Model (MSM);
- (iii) estimate the intrinsic theoretical uncertainties of these predictions, which are mainly caused by the neglect of higher order contributions.

The results, which are presented in this Report, are based on several different approaches and on a comparison of their numerical predictions.

The findings of the Report are based on the following computer codes:

BHM [2], LEPTOP [3], TOPAZO [4], WOH [5], and ZFITTER [6].

The design of some of these codes can be traced back to the 1989 Workshop on ‘ $Z$ -Physics at LEP 1’; others have been developed later. All of them contain a so-called electroweak library, which allows the calculation of virtual higher order electroweak and QCD corrections to selected quantities for example, a weak mixing angle or a partial or total  $Z$  width. Strictly speaking, these are ‘*pseudo-observables*’ and not directly measurable in an experiment. Some packages (codes) contain, in addition, virtual and real photonic corrections (bremsstrahlung) with simple kinematical and geometrical cuts similar to those used in experiments, thus allowing for the calculation of (idealized) measurable cross-sections and asymmetries, which we will call ‘*realistic observables*’.

Apart from a comparison of the numerical results of different codes, we attempted a simulation of the theoretical uncertainties of each code. To do so we had to reach an agreement on the principles on which these simulations are based. We hope that as a result of this project the prospects of the quantitative tests of the MSM at LEP and SLC, and their sensitivity to potential New Physics beyond the MSM, will become clearer.

The Report is organized as follows. In the first section we define the exact framework for the analysis of the electroweak data in the MSM, beginning with ‘Input parameters’ and ending with ‘Basic notions’, which are needed for discussing the numerical results collected in the subsequent sections. These deal with pseudo-observables and realistic observables in the sense introduced above. The first three sections represent a homogenous presentation of the material related to or obtained with the above mentioned codes. In the fourth and fifth sections we have collected items particular to the different codes, such as

explicit analytical formulae and descriptions of the design and of the use of the packages. All the authors of the report agree on the following conclusions from this study:

- The differences between results of different codes are small compared to existing experimental uncertainties. Thus improvement of experimental accuracy at LEP 1 and SLC is welcome even at the present level of theoretical accuracy.
- At present the most promising are measurements of  $g_V/g_A$  in various  $P$ - and  $C$ -violating asymmetries and polarizations.
- The real bottleneck for improved theoretical accuracy in  $g_V/g_A$  is presented by the uncertainty of the input parameter  $\bar{\alpha} \equiv \alpha(M_Z)$ . The improved accuracy of this important parameter calls for new accurate measurements of the cross-section  $e^+e^- \rightarrow \text{hadrons}$  at low energies (Novosibirsk and Beijing accelerators, etc.)
- The estimates of theoretical uncertainties are highly subjective and their values partly reflect the internal philosophy of the actual implementation of radiative corrections in a given code.
- In many cases the one-loop approximation in the electroweak gauge coupling is adequate enough at the present level of experimental accuracy. At the same time, however, it should be stressed that a complete evaluation of the sub-leading corrections,  $\mathcal{O}(G_\mu^2 M_Z^2 m_t^2)$  would greatly reduce the uncertainty that we observe, one way or the other, for all observables.
- In case the next generation of experiments at LEP 1 and SLC improves accuracy considerably (a problem not only of statistics but mainly of systematics) the full program of two-loop electroweak calculations should be carried out.

## 1.2 Input parameters

Within the MSM, any measured quantity can be calculated in terms of a small set of input parameters. Once all possible relations between the parameters of the Lagrangian in the MSM are exploited, we may choose a set of them which, in the electroweak part, consists of *one interaction constant* — say, the fine structure constant  $\alpha$  — of the *masses* of all particles and of the CKM fermionic *mixing angles*. The latter ones are of little importance for  $Z$  resonance observables, which are dominated by flavour-diagonal neutral current interactions.

In practical calculations one prefers to make use of the most precisely measured parameters. Three of them characterize the gauge sector of the MSM:

$$\begin{aligned}\alpha &\equiv \alpha(0) = 1/137.0359895(61), \\ G_\mu &= 1.16639(2) \times 10^{-5} \text{ GeV}^{-2}, \\ M_Z &= 91.1887 \pm 0.0044 \text{ GeV},\end{aligned}\tag{1}$$

where  $G_\mu$ , the four-fermion  $\mu$  decay coupling constant, is defined through the muon lifetime  $\tau_\mu$  by

$$\frac{1}{\tau_\mu} = \frac{G_\mu^2 m_\mu^5}{192\pi^3} \left(1 - \frac{8m_e^2}{m_\mu^2}\right) \left[1 + \frac{\alpha}{2\pi} \left(1 + \frac{2\alpha}{3\pi} \ln \frac{m_\mu}{m_e}\right) \left(\frac{25}{4} - \pi^2\right)\right]. \quad (2)$$

Light fermion masses contribute via the electromagnetic coupling constant  $\alpha$ , running from very small momenta up to  $M_Z$ , the typical scale of the  $Z$  resonance, and yielding

$$\alpha(M_Z) \equiv \bar{\alpha} = \frac{\alpha}{1 - \Delta\alpha}, \quad (3)$$

with  $\Delta\alpha$  consisting of *leptonic* and *hadronic* contributions

$$\Delta\alpha = \Delta\alpha_l + \Delta\alpha_h. \quad (4)$$

The leptonic contribution is known explicitly:

$$\Delta\alpha_l = \frac{\alpha}{3\pi} \sum_l \left[ -\frac{5}{3} - 4 \frac{m_l^2}{M_Z^2} + \beta_l \left(1 + 2 \frac{m_l^2}{M_Z^2}\right) \ln \frac{\beta_l + 1}{\beta_l - 1} \right], \quad (5)$$

where

$$\beta_l = \sqrt{1 - 4 \frac{m_l^2}{M_Z^2}}. \quad (6)$$

With lepton masses taken from the last edition of the Review of Particle properties [7], from (5) we get

$$\Delta\alpha_l = 0.0314129. \quad (7)$$

In the small mass approximation, (5) reduces to the well-known expression

$$\Delta\alpha_l = \frac{\alpha}{3\pi} \sum_l \left( \ln \frac{M_Z^2}{m_l^2} - \frac{5}{3} \right) = 0.0314177. \quad (8)$$

The hadronic contribution is being calculated by a dispersion relation,

$$\Delta\alpha_h = \frac{\alpha M_Z^2}{3\pi} \mathcal{R}e \int_{4m_\pi^2}^{\infty} \frac{ds}{s(M_Z^2 - i\epsilon - s)} R(s), \quad (9)$$

from experimental data on the cross-section ratio  $R(s) = \sigma_{e^+e^-}(s)/\sigma_0(s)$ , where  $\sigma_{e^+e^-}(s) = \sigma(e^+e^- \rightarrow \gamma^* \rightarrow \text{hadrons})$  and  $\sigma_0 = 4/3\pi\alpha^2/s$ . In 1990, the value  $\Delta\alpha_h$  has been updated to

$$\Delta\alpha_h = 0.0282(9), \quad (10)$$

leading to  $\alpha^{-1}(M_Z) = 128.87 \pm 0.12$  [8]<sup>1</sup>.

By using  $\bar{\alpha}$  instead of  $\alpha$ , the electromagnetic coupling constant at the correct scale for  $Z$  physics is chosen and one automatically avoids the problem of the light quark mass

---

<sup>1</sup> Very recently, three new analyses have been published. The first, [9], leads to  $\Delta\alpha_h = 0.02666 \pm 0.00075$  and  $\alpha^{-1}(M_Z) = 129.08 \pm 0.10$ . The second, [10], leads to  $\Delta\alpha_h = 0.02732 \pm 0.00042$  and  $\alpha^{-1}(M_Z) = 128.99 \pm 0.06$ . The third, [11], leads to  $\Delta\alpha_h = 0.0280 \pm 0.0007$  and  $\alpha^{-1}(M_Z) = 128.899 \pm 0.090$ .

singularities. So the relevant input parameter is  $\bar{\alpha}$ , and not  $\alpha$  in — spite of the extremely high accuracy of the latter. It should be stressed that the quantity  $\bar{\alpha}$  used by us is not only numerically, but also in principle, different from the quantity  $\hat{\alpha}(M_Z) = 1/127.9(1)$  (see, for example Ref. [7], page 1304). The latter is defined in the modified minimal subtraction scheme ( $\overline{MS}$ ) in terms of a bare electric charge, while the former is a physical quantity expressed in terms of charged fermion masses.

The treatment of the light fermion masses (all but the top quark mass) in the electroweak corrections is not the same in different codes. First we should mention that the exact expression (5) for the photonic vacuum polarization is not the only place where fermionic power corrections,  $m_f^2/M_Z^2$ , may appear <sup>2</sup>. There are fermionic contributions to the self-energy insertions of the heavy gauge bosons, which also contain power mass corrections. Moreover additional power corrections appear, due to the presence of axial couplings. The latter may be explicitly calculated for leptons; for quarks, they are not taken into account by the dispersion integral (9). In principle, there are also finite mass corrections in three- and four-point functions. In some codes these finite mass terms are neglected completely, some other codes retain them in the two- and three-point functions. In the latter case, for the quarks some *effective* masses are used, which are selected in order to reproduce with a sufficiently high accuracy the hadronic vacuum polarization contribution  $\Delta\alpha_h$  <sup>3</sup>. We emphasize that these finite mass terms have no numerical relevance. They are being retained just in order to investigate the sensitivity of corrections to finite light fermion masses. They also help sometimes to compare results of independent calculations. Such a comparison has been done once for  $\Delta r$ , and an agreement of up to 12 digits (computer precision) was found [14].

The  $\tau$  lepton mass has been retained in all codes in the phase-space corrections and in the Born-level matrix element. The masses of the heavy quarks  $b$  and  $c$  also give rise to phase-space corrections, but are treated together with QCD final state interaction corrections (see the QCD part of this Report). We take the following input values for  $m_\tau$ ,  $m_b$  and  $m_c$  [7]:

$$\begin{aligned} m_\tau &= 1.7771 \pm 0.0005 \text{ GeV}, \\ m_b &= 4.7 \pm 0.3 \text{ GeV}, \\ m_c &= 1.55 \pm 0.35 \text{ GeV}, \end{aligned} \tag{11}$$

where  $m_b, m_c$  are the pole masses converted in the actual calculation of radiative corrections to  $\overline{MS}$  masses using QCD perturbation theory. The meaning of these  $\overline{MS}$  mass definitions and their relation to the *pole* masses are explained in the QCD Part of this Report by Chetyrkin, Kühn and Kwiatkowski. The QCD part of the MSM is characterized by these running quark masses, and by the strong coupling constant  $\alpha_s(M_Z)$ , which will be assumed to be [15] and [16]:

$$\alpha_s(M_Z) \equiv \hat{\alpha}_s = 0.125 \pm 0.007. \tag{12}$$

---

<sup>2</sup>One should emphasize that the dispersion integral (9) automatically includes all these power corrections for the hadronic part of the photonic vacuum polarization.

<sup>3</sup>Details on *effective quark masses* be found in [12] or [13].

Note, that from pure QCD observables at the  $Z$  peak one obtains [17]

$$\alpha_s(M_Z) \equiv \hat{\alpha}_s = 0.123 \pm 0.006 . \quad (13)$$

Finally, there are two yet unknown input parameters left: the top quark mass and the Higgs boson mass,

$$m_t , \quad M_H , \quad (14)$$

although the situation has considerably improved with the recent CDF indication [18] of evidence for the  $t$  quark with  $m_t = 174 \pm 17$  GeV. In the following, by  $m_t$  we will always imply the  $t$ -quark *pole* mass.

### 1.3 Codes to calculate electroweak observables

The radiative corrections for the measured physical observables must be included into the theoretical predictions for them, and the consistency of the theory is verified by comparison with the data. This particular step may assume different aspects related to the actual implementation of the comparisons, but in the end it usually takes the form of some constraint on  $m_t$  and  $\hat{\alpha}_s$  and to a lesser extent on  $M_H$  and  $\bar{\alpha}$ . It is our main goal to present and discuss the most accurate theoretical predictions for the measured quantities and to introduce a reliable estimate of the associated theoretical uncertainties.

The results of this Report have been obtained by a critical comparison and examination of:

- the variations in the results following from the different, although not antithetic, formulations of the various groups;
- the *internal* estimates of the uncertainties induced by the still missing higher order corrections.

The groups participating in this project can be identified by the names of the codes that they have assembled, namely:

BHM [2]

Burgers, Hollik, Martinez, Teubert;

LEPTOP [3] – ITEP Moscow group

Novikov, Okun, Rozanov, Vysotsky;

TOPAZO [4] – Torino-Pavia group

Montagna, Nicrosini, Passarino, Piccinini, Pittau;

WOH [5]

Beenakker, Burgers, Hollik;

ZFITTER [6] – Dubna-Zeuthen group

Bardin, Bilenky, Chizhov, Olchevsky, S.Riemann, T.Riemann, Sachwitz, Sazonov, Sedykh, Sheer.



All these codes may be used to calculate pseudo-observables. Three of them, **BHM**, **TOPAZO**, and **ZFITTER**, may calculate also realistic observables. One code, **TOPAZO**, is additionally able to calculate the full Bhabha cross-section, including complete  $s$  and  $t$  channel exchange contributions. Concerning the electroweak corrections, four codes are based on completely independent theoretical computational schemes, while **BHM/WOH** use basically the same framework. The treatment of QED corrections in the three QED dressers is based on completely independent theoretical methods. As a consequence, it is extremely difficult to describe them in a common language. On the other hand, the treatment of QCD corrections is to a large extent common in all five codes. It is based on papers included in Part II of this volume and on references quoted therein.

In this Report, we will attempt to present the collected material homogeneously as for long as possible. Because of this, all complicated description of what is entering in the various, alternative theoretical formulations, has been shifted to the last two sections of the Report.

## 1.4 The language of effective couplings

A natural and familiar but approximate language for the basic ingredients of the physical observables of the  $Z$  resonance is that of *effective couplings*. How it will translate into the particular realizations and schemes of the various codes can be studied in References [2]-[6] and in the references quoted in these. The more theoretically oriented reader should, however, be aware that basic differences do indeed exist and that the language of effective couplings is not universally realized in all the approaches. The basic notions of effective couplings, which are common to all approaches, can be easily introduced. Nevertheless, this deserves to be seen in several logical steps.

### 1.4.1 The Born Approximation for $e^+e^- \rightarrow f\bar{f}$

The matrix element of the process

$$e^+e^- \rightarrow (\gamma, Z) \rightarrow f\bar{f}, \quad f \neq e, \quad (15)$$

depicted in Fig. 1 may be written as follows:

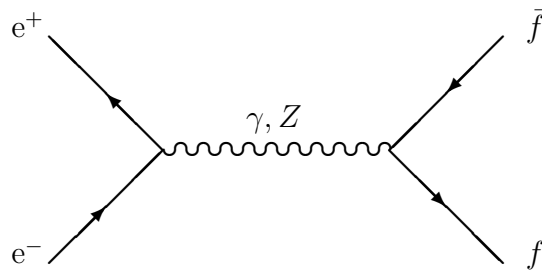


Figure 1: Feynman graph for the reaction (15) in the Born approximation

$$\mathcal{M}^{Born} \sim \frac{1}{s} \left[ Q_e Q_f \gamma_\alpha \otimes \gamma^\alpha + \chi \gamma_\alpha (g_v^e - g_a^e \gamma_5) \otimes \gamma^\alpha (g_v^f - g_a^f \gamma_5) \right] \quad (16)$$

$$= \frac{1}{s} \left[ Q_e Q_f \gamma_\alpha \otimes \gamma^\alpha + \chi \left( g_v^e g_v^f \gamma_\alpha \otimes \gamma^\alpha - g_v^e g_a^f \gamma_\alpha \otimes \gamma^\alpha \gamma_5 - g_a^e g_v^f \gamma_\alpha \gamma_5 \otimes \gamma^\alpha + g_a^e g_a^f \gamma_\alpha \gamma_5 \otimes \gamma^\alpha \gamma_5 \right) \right], \quad (17)$$

with  $\chi$  being the propagator ratio

$$\chi = \frac{s}{s - M_Z^2 + i s \Gamma_Z / M_Z}. \quad (18)$$

And in the Minimal Standard Model (MSM)

$$g_a^f = I_f^{(3)}, \quad g_v^f = I_f^{(3)} - 2Q^f \sin^2 \theta, \quad (19)$$

where  $g_a^f$ ,  $g_v^f$  are vector and axial vector couplings of the  $Z$ -boson,  $Q^f$  are the electric charges of fermions in units of position charge,  $I_f^{(3)}$  the projection of weak isospin, and  $\theta$  the weak mixing angle in the Born approximation. Its value depends on the choice of computational scheme. In (16) and (17) a short notation for bilinear combinations of spinors  $u$  and  $v$  is used:

$$A_\beta \otimes B^\beta = [\bar{v}_e A_\beta u_e] \times [\bar{u}_f B^\beta v_f]. \quad (20)$$

In the matrix element (16) and (17) the contributions from  $\gamma$  and  $Z$  exchange diagrams are unambiguously separated, and the  $Z$  exchange contribution is presented in a *factorized* form (16).

#### 1.4.2 Electroweak non-photonic corrections

The *higher order* electroweak non-photonic corrections are indicated symbolically by the blobs in Fig. 2. They include all possible self-energy and  $Z\bar{f}f$  vertex insertions, together with *non-photonic boxes* insertions (the  $WW$  and  $ZZ$  boxes in the one-loop approximation), and lead to a slightly more complicated structure in the matrix element, which is valid as long as we neglect the external fermion masses:

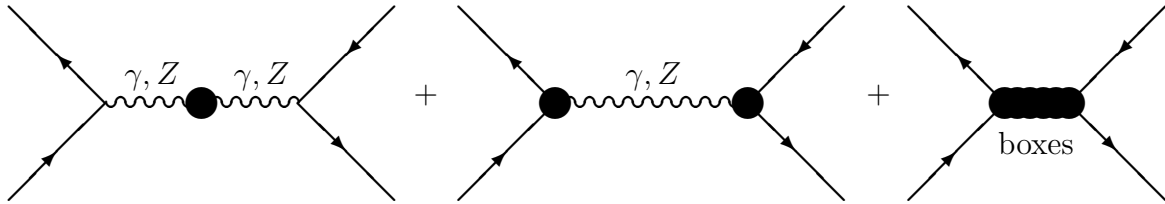


Figure 2: Feynman graphs for higher-order corrections to the reaction (15)

$$\mathcal{M}^{eff} \sim \frac{1}{s} \left\{ \alpha(s) \gamma_\alpha \otimes \gamma^\alpha + \chi \left[ \mathcal{F}_{vv}^{ef}(s, t) \gamma_\alpha \otimes \gamma^\alpha - \mathcal{F}_{va}^{ef}(s, t) \gamma_\alpha \otimes \gamma^\alpha \gamma_5 \right. \right. \\ \left. \left. - \mathcal{F}_{av}^{ef}(s, t) \gamma_\alpha \gamma_5 \otimes \gamma^\alpha + \mathcal{F}_{aa}^{ef}(s, t) \gamma_\alpha \gamma_5 \otimes \gamma^\alpha \gamma_5 \right] \right\}. \quad (21)$$

The products of interaction constants in (17) are replaced by the *running*  $\alpha(s)$  — this time including the imaginary part — and by four *running electroweak form factors*,  $\mathcal{F}_{ij}^{ef}$ . In the MSM, the explicit expressions for the form factors result from an order-by-order calculation and are certain explicit functions of the input parameters (1), (3), (11), (12) and (14).

Several comments should be given on the structure of the matrix element (21) after inclusion of higher order electroweak corrections:

- This structure is unique, but implies the introduction of complex valued form factors which depend on the two Mandelstam variables  $s, t$ ; the dependence on  $t$  is due to the weak box diagrams.
- The separation into insertions for the  $\gamma$  and  $Z$  exchanges is lost. In the proposed realization, the first term in (21) contains the running QED coupling where only fermionic insertions are retained. This ensures a gauge invariant separation.
- The weak boxes are present in (21) as non-resonating ( $\sim s - M_Z^2$ ) insertions to the electroweak form factors  $\mathcal{F}_{ij}^{ef}$ . At the  $Z$  resonance, the one-loop weak  $WW$  and  $ZZ$  box terms are small, with relative contribution  $\leq 10^{-4}$ . If we neglect them, the  $t$  dependence is turned off. The  $t$ -dependence would also spoil factorization of the form factors into products of effective vector and axial vector couplings.
- Full factorization is re-established by neglecting, in addition, the other non-resonating loop contributions, such as the bosonic insertions to the photon propagator, and photon-fermion vertex corrections. All the neglected terms are of the order  $\mathcal{O}(\alpha \frac{\Gamma_Z}{M_Z})$ . The resulting effective vector and axial -vector couplings are complex valued and dependent on  $s$ . The factorization is the result of a variety of approximations, valid at the  $Z$  resonance to the accuracy needed, and indispensable in order to relate the pseudo-observables to actually measured quantities.

In the complete codes — BHM, TOPAZ0, ZFITTER — it is possible to control the numerical influence of all of these approximations.

### 1.4.3 $Z$ pole approximation

After the above-mentioned series of approximations, we arrive at the so called  $Z$  boson pole approximation, which is actually equivalent to the setting  $s = M_Z^2$  in the form factors. In the  $Z$  pole approximation, the one-loop diagrams contributing to the blobs in Fig. 2 can be visualized in the diagrams of Fig. 3.

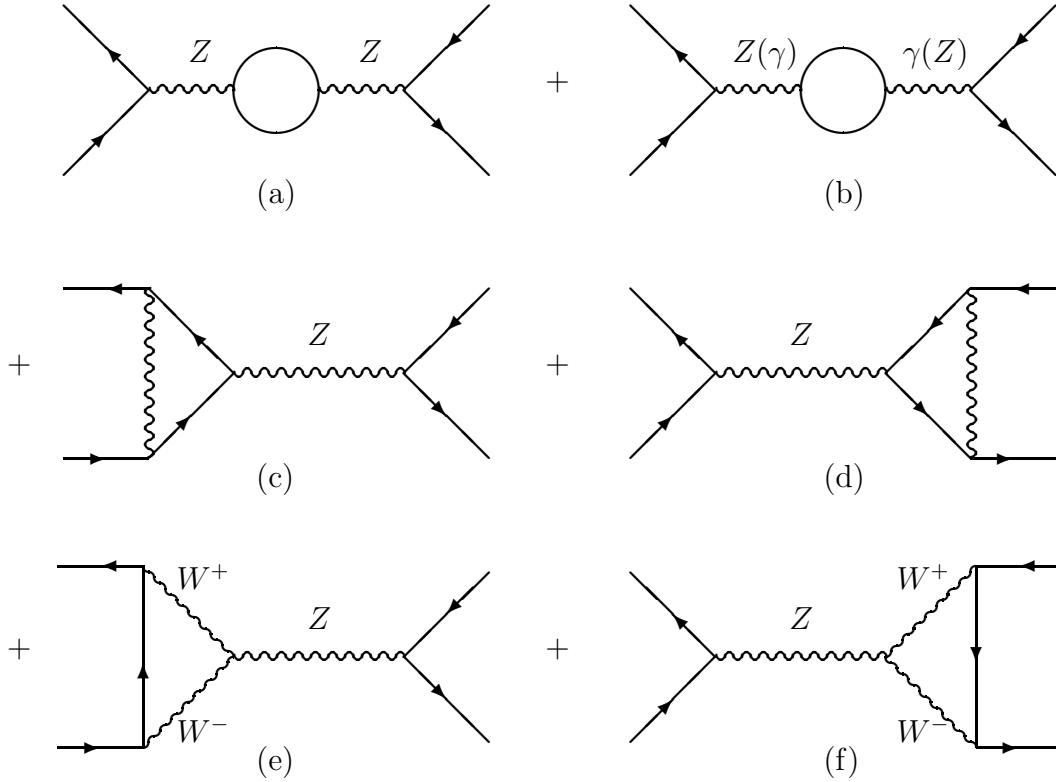


Figure 3: The one-loop Feynman graphs at the  $Z$  boson pole

In Fig. 3 (a) all particles ( $Z$ ,  $H$ ,  $W$ ,  $q$ ,  $l$ ,  $\nu$ ) contribute through their weak neutral currents, while in the  $Z\gamma$  mixing (b) only charged ones contribute. This, of course, is strictly true only in the unitary gauge, while in the renormalizable gauge, Faddeev-Popov and Higgs-Kibble ghosts will also appear. The vertex diagrams (c) and (d) contain  $Z$ ,  $W$ , as vertical lines. The vertex diagrams (e) and (f) contain trilinear gauge boson interactions. The vertex diagrams contain, in principle, also Higgs boson exchanges — as vertical lines in diagrams (c) and (d), and as  $Z$ ,  $H$  virtual states in diagrams (e) and (d). They give, however, a negligible contribution because of small  $Hf\bar{f}$  Yukawa couplings<sup>4</sup>.

The set of the diagrams of Fig. 3 has to be complemented by the contributions from the bare ‘unphysical’ parameters (masses and couplings) in order to get the physical amplitude of Fig. 2. This is depicted in Fig. 4 as an example, the cross representing the contribution from the bare mass  $M_Z^0$ .

The  $W$  boson self-energy enters the analysis only through the  $W$  mass (see Fig. 5). The  $W$  self-energy contains all types of particles entering through their charged weak currents. Explicit expressions for the decay width of the  $W$  are not discussed in this Report, (see the existing literature [19]).

If the mass of the  $W$  boson were known with the same accuracy as that of the  $Z$ , the conceptual picture of the electroweak corrections would be as simple as that of QED.

<sup>4</sup>In some renormalization schemes one should add also the self-energy insertions for external fermion lines. In some other schemes, they vanish, when the field renormalization counterterms contributions are added.

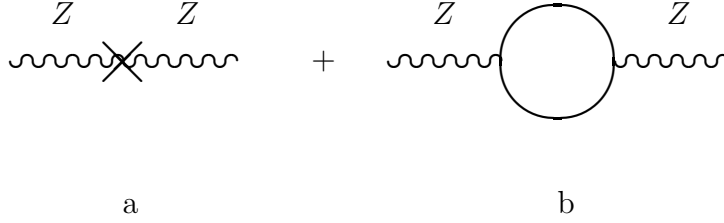


Figure 4: The  $Z$ -boson self-energy

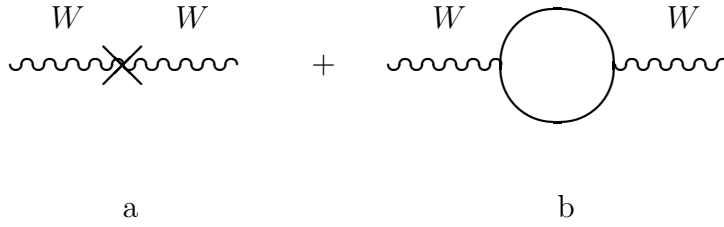


Figure 5: The  $W$  boson self-energy

Every physical observable would be expressed in terms of  $\alpha$ ,  $M_Z$ ,  $M_W$ , the masses of all fermions and the mass of the Higgs boson. Unfortunately,  $M_W$  is not known with an accuracy comparable to that of  $M_Z$ . Therefore, instead of  $M_W$  we have to choose  $G_\mu$  as the most accurately measured dimensional observable.

#### 1.4.4 Effective couplings for $Z$ decay.

Formulae (17) and (21) are very similar in their structure, a property which makes the language of effective couplings so convenient. These formulae refer to a general  $f\bar{f} \rightarrow f'\bar{f}'$  annihilation process. After the simplifications described in 1.4.2–1.4.3, the factorization allows us to write for the form factors

$$\mathcal{F}_{ij}^{ef}(s = M_Z^2, t = 0) = \mathcal{G}_i^e(M_Z^2)\mathcal{G}_j^f(M_Z^2). \quad (22)$$

This implies that the  $Z$  part of the amplitude (21) is obtained from that of (16) by substituting

$$g_{v,a}^{e,f} \rightarrow \mathcal{G}_{v,a}^{e,f}(M_Z^2). \quad (23)$$

Simultaneously, we obtain for the matrix element of the decay process  $Z \rightarrow f\bar{f}$ , Fig. 6, as follows:

$$\mathcal{M}_{Z\bar{f}f}^{eff} = \bar{u}_f \gamma_\alpha [\mathcal{G}_v^f(M_Z^2) - \mathcal{G}_a^f(M_Z^2)\gamma_5] v_f \epsilon_Z^\alpha, \quad (24)$$

where  $\bar{u}_f$ ,  $v_f$ ,  $\epsilon_Z^\alpha$  are wave-functions of the fermion  $f$ , antifermion  $\bar{f}$  and  $Z$  boson.

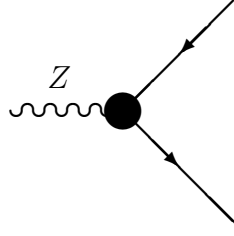


Figure 6: Feynman graph for higher-order corections to the  $Z \rightarrow f \bar{f}$  decay

In the one-loop approximation, the blob in Fig. 6 can be visualized as the diagrams of Fig. 7. Note that Fig. 3 (a) contributes both to initial and final state virtual corrections. The effective decay couplings  $\mathcal{G}_{v,a}^f$ , are nothing else but the reduced electroweak form factors, which are now constant because of the kinematical constraint  $s = M_Z^2$ , which is equivalent to the  $Z$  pole approximation. They will be the basic objects in the following presentation. We will use for them the simplified notations,

$$g_{V,A}^f = \text{Re} \mathcal{G}_{v,a}^f(M_Z^2), \quad (25)$$

where the capital letters  $V, A$  are introduced in order to distinguish effective couplings  $g_{V,A}$ , dressed by higher order interactions, from their Born-like analogs  $g_{v,a}$ .

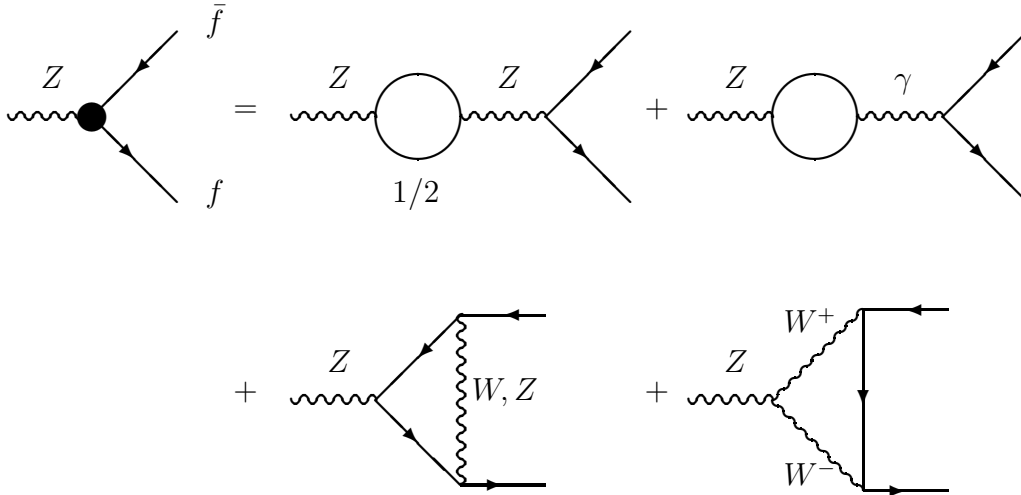


Figure 7: Feynman graphs of the  $Z$  decay in the one-loop approximation

In the next two subsections we will define the quantities to be computed and compared: the pseudo-observables, and the realistic observables.

## 1.5 Pseudo-observables

The *pseudo-variables* are related to measured cross-sections and asymmetries by some de-convolution or *unfolding* procedure. The concept itself of pseudo-observability is rather difficult to define. One way to introduce it is to say that the experiments *measure* some primordial (basically cross-sections and thereby asymmetries also) quantities which are then reduced to secondary quantities under some set of specific assumptions. Within these assumptions, the secondary quantities, the pseudo-observables, also deserve the label of *observability*. Just to give an example, we quote the de-convoluted forward–backward asymmetry, where, typically, only the  $Z$  exchange is included and initial and final state QED corrections, plus eventual final state QCD corrections, are assumed to be subtracted from the experimental data. We have analyzed 25 of such pseudo-observables in details, namely:

mass of the W	$M_W$
hadronic peak cross-section	$\sigma_h$
partial leptonic and hadronic widths	$\Gamma_\nu, \Gamma_e, \Gamma_\mu, \Gamma_\tau, \Gamma_u, \Gamma_d, \Gamma_c, \Gamma_s, \Gamma_b$
the total width	$\Gamma_Z$
the total hadronic width	$\Gamma_h$
the total invisible width	$\Gamma_{\text{inv}}$
ratios	$R_l, R_b, R_c$
asymmetries and polarization	$A_{\text{FB}}^\mu, A_{\text{LR}}^e, A_{\text{FB}}^b, A_{\text{FB}}^c, P^\tau, P^b$
effective sine	$\sin^2 \theta_{\text{eff}}^{\text{lept}}, \sin^2 \theta_{\text{eff}}^b$

The *effective sine* are defined by <sup>5</sup>

$$4 |Q_f| \sin^2 \theta_{\text{eff}}^f = 1 - \frac{g_V^f}{g_A^f}, \quad (26)$$

with  $Q_f$  being the electric charge of the fermion  $f$  in units of the positron charge. By definition, the total and partial widths of the  $Z$  boson include final state QED and QCD radiation. The explicit formulae for partial widths will be presented in subsection 1.9. Moreover, we have defined

$$\Gamma_h = \Gamma_u + \Gamma_d + \Gamma_c + \Gamma_s + \Gamma_b, \quad (27)$$

$$\Gamma_{\text{inv}} = \Gamma_Z - \Gamma_e - \Gamma_\mu - \Gamma_\tau - \Gamma_h, \quad (28)$$

$$R_l = \frac{\Gamma_h}{\Gamma_e}, \quad (29)$$

$$R_{b,c} = \frac{\Gamma_{b,c}}{\Gamma_h}, \quad (30)$$

---

<sup>5</sup>With lepton universality there exists only one *leptonic effective sine*,  $\sin^2 \theta_{\text{eff}}^{\text{lept}} = \sin^2 \theta_{\text{eff}}^l$ .

$$\sigma_h = 12\pi \frac{\Gamma_e \Gamma_h}{M_Z^2 \Gamma_Z^2} . \quad (31)$$

The quantity  $\sigma_h$  is the de-convoluted hadronic peak cross-section, which by definition includes only the  $Z$  exchange. To this end we would like to emphasize that in our calculations we indeed assumed that

$$\Gamma_{\text{inv}} = 3\Gamma_\nu , \quad (32)$$

then the total  $Z$  width becomes

$$\Gamma_Z = 3\Gamma_\nu + \Gamma_e + \Gamma_\mu + \Gamma_\tau + \Gamma_h . \quad (33)$$

Unlike the widths, asymmetries and polarizations do not contain, by definition, QED and QCD corrections; furthermore, they will only refer to pure  $Z$  exchange: they are nothing but simple combinations of the effective  $Z$  couplings, introduced above,

$$\begin{aligned} A_{\text{FB}}^f &= \frac{3}{4} \mathcal{A}^e \mathcal{A}^f , \\ A_{\text{LR}}^e &= \mathcal{A}^e , \\ P^f &= -\mathcal{A}^f , \\ P_{\text{FB}}(\tau) &= -\frac{3}{4} \mathcal{A}^e , \end{aligned} \quad (34)$$

where we define

$$\mathcal{A}^f = \frac{2g_V^f g_A^f}{(g_V^f)^2 + (g_A^f)^2} , \quad (35)$$

and  $g_V^f, g_A^f$  defined by Eq. (25) are the effective neutral current vector and axial-vector couplings of the  $Z$  to a fermion pair  $f\bar{f}$ .  $P_{\text{FB}}(\tau)$  is the  $\tau$  polarization forward-backward asymmetry. One should realize that as a consequence of the adopted definition of pseudo-observables, there exist even more relations among them than are indicated above; it is, for example,  $A_{\text{LR}}^e = -P^\tau$ , if in addition lepton universality is assumed, which is granted automatically in the MSM. For this reason we will present numerical and graphical results only for a selected subset of them.

## 1.6 Realistic observables

Realistic observables are the cross-sections  $\sigma^f(s)$  and asymmetries  $A_{\text{FB}}^f(s)$  of the reactions

$$e^+e^- \rightarrow (\gamma, Z) \rightarrow f\bar{f}(n\gamma) , \quad (36)$$

for a given interval of  $s = 4E^2$  around the  $Z$  resonance, including real and virtual photonic corrections ('dressed by QED'). We will present results for  $f = \mu$  and  $f = \text{had}$ , both in a fully extrapolated set-up or with simple kinematical cuts. For  $f = e$  both the  $s$  channel exchange cross-section and the complete Bhabha reaction will be treated. In total, we



considered 14 cross-sections and asymmetries for different combinations of flavour  $f$  and *cuts*; they will be defined in section 3. The kinematical cuts that will be imposed are of two types:

- $\theta_{\min} < \theta_- < \pi - \theta_{\min}$
- $s' > s'_{\min}$

and:

- $\theta_{\min} < \theta_- < \pi - \theta_{\min}$
- $\theta_{\text{acoll}} < \xi$
- $E_{\pm} > E_{\text{th}}$ .

Where  $s'$  is the invariant mass of two final-state fermions,  $\theta_-$  refers to the outgoing scattering angle of the outgoing fermion,  $\theta_{\text{acoll}}$  is the acollinearity angle between the outgoing fermions and  $E_{\pm}$  the outgoing fermion (anti-fermion) energies. By  $s$  channel Bhabha scattering we mean that the  $s-t$  and  $t-t$  exchange interferences have been subtracted from the observable under consideration.

We would like to mention in passing that the QED dressers have options which allow a model independent interpretation of realistic observables. Since this is beyond our present scope, we refer the reader for details to the existing literature [20]-[21].

## 1.7 Calculational schemes

Before entering into a detailed study of the numerical results it is important to underline how an estimate of the theoretical uncertainty emerges from the many sets of numbers obtained with the five codes. First of all, one may distinguish between *intrinsic* and *parametric* uncertainties. The latter are normally associated with a variation of the input parameters according to the precision with which they are known. Typically, we have  $|\Delta\alpha^{-1}(M_Z^2)| = 0.12$ ,  $|\Delta m_b| = 0.3 \text{ GeV}$ ,  $|\Delta m_c| = 0.35 \text{ GeV}$  etc. These uncertainties will eventually shrink when more accurate measurements become available. In this Report we are mainly devoted to a discussion of the intrinsic uncertainties associated with missing non-leading higher-order corrections, although some results on parametric uncertainties will be also given. An essential ingredient of all calculations for radiative corrections to pseudo-observable is the choice of the renormalization scheme. There are many renormalization schemes in the literature:

- the on-shell schemes in various realizations [22]-[28], [3]
- the  $G_{\mu}$  scheme [29]-[31]
- the  $*$  scheme [32]
- the  $\overline{MS}$  scheme [33]-[34].

One cannot simulate the shift of a given quantity due to a change in the renormalization scheme with one code alone. Thus the corresponding theoretical band in that quantity will be obtained from the differences in the prediction of the codes, which use different renormalization schemes. On top of that we should also take into account the possibility of having different implementations of the full radiative corrections within one code, — within one well specified renormalization scheme. Typically we are dealing here with the practical implementation of resummation procedures, of the exact definition of leading versus non-leading higher order corrections and so on. Many of these implementations are equally plausible and differ by non-leading higher order contributions, which, however, may become relevant in view of the achieved or projected experimental precision. This sort of intrinsic theoretical uncertainty can very well be estimated by staying within each single code. However, since there are no reasons to expect that these will be the same in different codes, only the full collection of different sources will, in the end, give a reliable information on how accurate an observable may be considered from a theoretical point of view.

Of course, only a complete two-loop electroweak calculation, combined with some re-summations of the leading corrections (renormalization group improvements), would ultimately solve the problem of the theoretical accuracy.

## 1.8 Main features of different approaches

In this subsection we will discuss common features of and main differences between the electroweak libraries of the five codes.

Common features:

- All five codes use as input parameters the most accurately known electroweak parameters  $G_\mu$ ,  $M_Z$  and  $\bar{\alpha}$ , (the codes, with the exception of LEPTOP, also use  $\alpha$ ), in order to calculate the less precisely measured pseudo-observables.
- They use the same expressions for final state QED and QCD corrections (radiation factors).
- All codes include essentially the same internal gluon corrections of the order of  $\alpha\alpha_s$  in the  $W$  and  $Z$  self-energy quark loops.
- All codes include leading *two-loop* corrections of the order of  $G_\mu^2 m_t^4$ ; all gluonic corrections of the order of  $\alpha_s G_\mu m_t^2$ ; leading gluonic corrections  $\alpha\alpha_s^2$  in the vector boson self-energies.

Main differences:

- Each code uses a different renormalization framework.
- Some codes define an electroweak Born approximation, others give no physical emphasis to a Born approximation and employ only the notion of an *Improved Born Approximation* (*IBA*) which includes the leading electroweak loop corrections.

- Certain codes include higher-order electroweak corrections, which are documented in the literature but are numerically irrelevant, such as the irreducible two-loop photon vacuum polarization and the Higgs corrections proportional to  $\alpha^2 m_H^2$ . Some codes use, on top of these higher order corrections, resummation of one-loop terms.
- They differ by the choice of the definition of the weak mixing angle.

### 1.8.1 BHM/WOH, ZFITTER

The three codes **BHM** [2], **WOH** [5] and **ZFITTER** [6] rely on different realizations of the on-mass-shell renormalization scheme. They perform the renormalization procedure with systematic use of the counterterm method for the basic parameters  $\alpha$ ,  $M_W$ ,  $M_Z$ . The **BHM** and **WOH** codes lead back to one approach and are thus not completely independent of each other.

The description of the renormalization schemes may be found in [28] for **BHM/WOH** and in [24] for **ZFITTER**. The weak mixing angle formally appears as

$$\begin{aligned} c_w^2 &= \cos^2 \theta_w = (M_W/M_Z)^2, \\ s_w^2 &= \sin^2 \theta_w = 1 - c_w^2. \end{aligned} \quad (37)$$

This corresponds to the definition proposed by Sirlin [35]. The masses in (37) are the physical  $W$  and  $Z$  boson masses. Thus,  $s_w^2$  is not an independent quantity and is used mainly for internal bookkeeping. For fixed values of  $m_t$  and  $M_H$  each observable, including the Fermi constant  $G_\mu$ , is expressed in terms of  $\alpha$ ,  $M_Z$  and  $M_W$  with the corresponding quantum corrections being taken into account. Because of lack of precision in the  $W$  mass,  $M_W$ , it is not taken as an experimentally measured input quantity. It is instead replaced by the more accurate value of  $G_\mu$ .

The quantum corrections for  $\mu$  decay (2) after removing the Fermi-model like QED corrections are contained in the parameter  $\rho_c$  related to  $G_\mu$  by the equation<sup>6</sup>

$$G_\mu = \frac{\pi}{\sqrt{2}} \frac{\alpha}{s_w^2 c_w^2 M_Z^2} \rho_c. \quad (38)$$

Since this equation contains  $\alpha$  instead of  $\alpha(M_Z)$  a large fraction of  $\rho_c$  is of purely electromagnetic origin via  $\Delta\alpha$ . The parameter  $\rho_c$  in (38) takes into account the  $W$  propagator, vertex and box corrections due to one-loop diagrams and presently available higher order terms. The one-loop corrections were first calculated in Refs. [35]-[36]. The correction due to the photon self-energy is QED renormalization group improved: a geometrical progression brings  $\Delta\alpha$  into the denominator of  $\rho_c$ . Hence,  $\rho_c$  is usually written in the form

$$\rho_c = \frac{1}{1 - \Delta r}, \quad (39)$$

---

<sup>6</sup>The naive Born approximation for muon decay of Eq. (38),  $\rho_c = 1$ , was used in the 70's for predictions of the masses of the  $W$  and  $Z$  bosons with a crude accuracy by using the value of  $s_w$  from the ratio of neutral and charged currents in neutrino interactions.

where  $\Delta r$  contains all the one-loop corrections to the muon-decay with the inclusion and the proper arrangement of the higher order terms. (For more details see the explanations presented in subsection 1.10.2.)

For given values of  $m_t$  and  $M_H$ , Eq. (38) fixes  $\theta_w$  and, hence,  $M_w$  by the experimental value of  $G_\mu$ . In practice, Eq. (38) is solved with respect to  $M_w$  iteratively, since  $\Delta r$  is a complicated function of  $M_w$ . This equation for iteration of  $M_w$  reads

$$M_w = M_Z \sqrt{1 - \sqrt{1 - \frac{4\pi\alpha}{\sqrt{2}G_\mu M_Z^2 [1 - \Delta r(M_w)]}}} . \quad (40)$$

Therefore,  $M_w$  appears as an  $m_t$ ,  $M_H$ ,  $\hat{\alpha}_s$  dependent prediction, which can be compared with the experimental values from UA2 and CDF [37].

After fixing  $M_w$  in this way all the other observables are expressed in terms of  $G_\mu$ ,  $\alpha$ ,  $M_Z$ ,  $m_t$ ,  $M_H$  and  $\hat{\alpha}_s$ <sup>7</sup>. As a consequence of this procedure, purely leptonic Feynman graphs (e.g. a vertex correction in the  $Z \rightarrow \bar{\mu}\mu$  decay) also turn out to be implicitly  $m_t$  dependent through the  $M_w$ .

In conclusion, Eq. (38) uses the amplitude of  $\mu$  decay with the inclusion of weak corrections in order to establish the interdependence between  $M_w$ ,  $m_t$  and  $M_H$  and the best measured parameters  $\alpha$ ,  $G_\mu$ ,  $M_Z$ . Thus,  $M_w$  appears as a prediction as well as an intermediate parameter for the calculation of  $Z$ -boson observables.

The flowchart of the BHM/WOH, ZFITTER approach is shown in Fig. 8. One should have in mind that in spite of a common presentation of the basics of these codes there are certain differences in the realization of the on-mass-shell renormalization schemes between BHM/WOH on one side and ZFITTER on the other — for example, in the use of different gauges and in the different treatment of field renormalization.

---

<sup>7</sup> In leptonic processes the dependence on  $\hat{\alpha}_s$  is of higher order; it comes from gluonic exchanges between virtual quarks in  $W$ ,  $Z$ ,  $Z\gamma$  and  $\gamma$  self-energy diagrams with quark loops.

## FLOWCHART OF ZFITTER/BHM/WOH

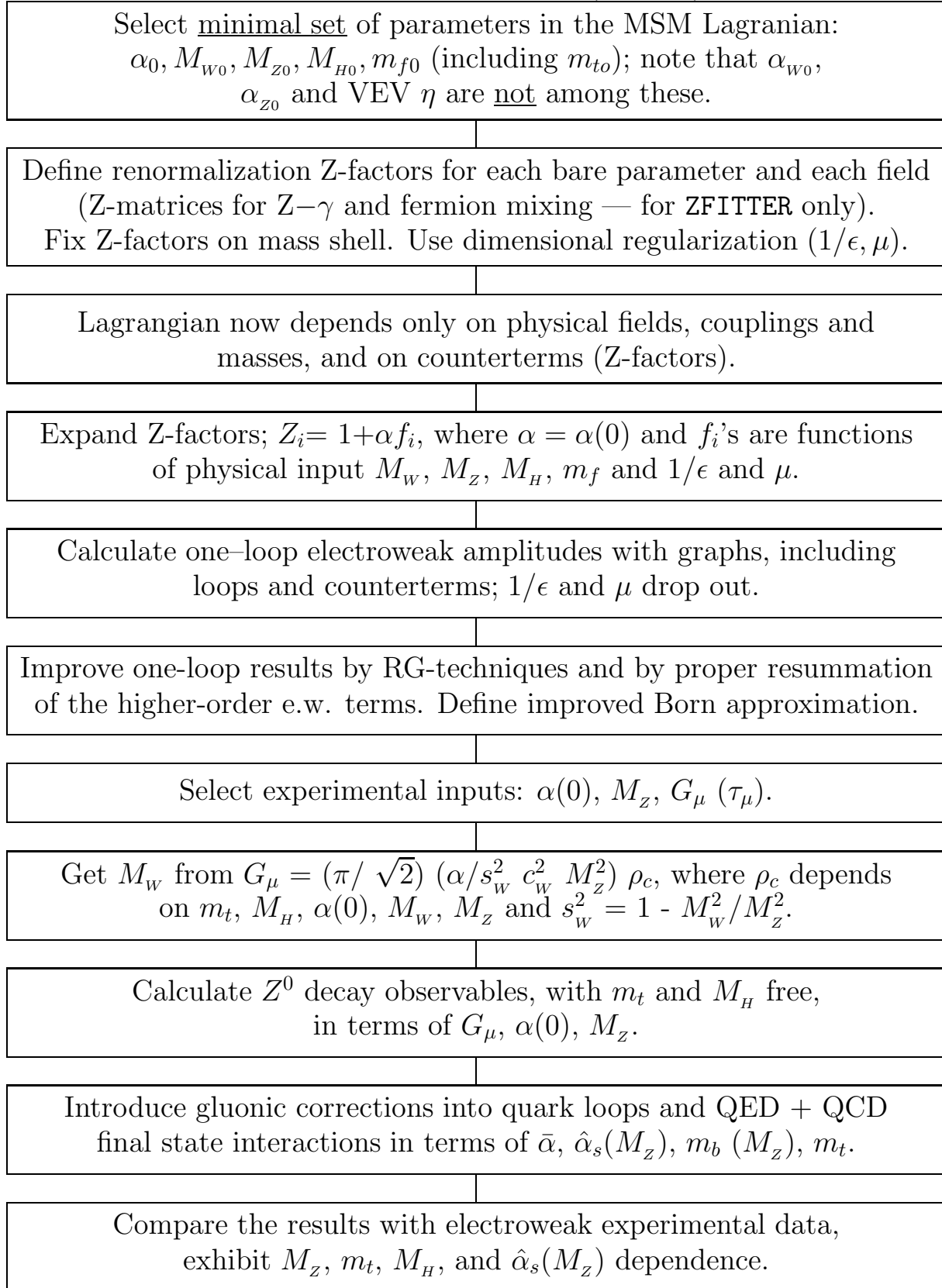


Figure 8: BHM/WOH ZFITTER flowchart

### 1.8.2 LEPTOP

The authors of LEPTOP avoid the use of counterterms in the formulation of the theoretical framework. They do not use resummation of one-loop electroweak corrections, thus limiting themselves to a simple one-loop approximation, completed by selected leading electroweak two-loop corrections. In contrast to all the other codes, LEPTOP uses a Born approximation. According to LEPTOP, the weak mixing angle  $\theta$  is defined by ( $s \equiv \sin \theta$ ,  $c \equiv \cos \theta$ ):

$$G_\mu = \frac{\pi \bar{\alpha}}{\sqrt{2} s^2 c^2 M_Z^2}, \quad (41)$$

$$\sin^2 2\theta = \frac{4\pi \bar{\alpha}}{\sqrt{2} G_\mu M_Z^2}. \quad (42)$$

This gives  $s^2=0.23117(33)$ ,  $c=0.87683(19)$ . Such a  $\theta$ , which by definition does not depend on  $m_t$  and  $M_H$ , is used to determine the so-called  $\bar{\alpha}$ -Born approximations for electroweak observables.

The bare gauge couplings  $\alpha^0$ ,  $\alpha_w^0$  and the bare mass  $M_Z^0$  are expressed in terms of  $\bar{\alpha}$ ,  $G_\mu$  and  $M_Z$ ,  $1/\epsilon$  and  $\mu$ , where  $\mu$  is the 't Hooft's scale parameter and  $2\epsilon = 4 - D$  in dimensional regularization scheme. The  $W$  mass,  $M_W$ , is treated on an equal footing with the other observables.

The  $\bar{\alpha}$ -Born approximation automatically includes purely electromagnetic corrections. In terms of  $s$  and  $c$ , the expressions for the hadron-free pseudo-observables are very simple in that approximation

$$(M_W/M_Z)^B = c, \quad (43)$$

$$(g_A^f)^B = I_f^{(3)}, \quad (44)$$

$$(g_V^f/g_A^f)^B = 1 - 4|Q_f|s^2. \quad (45)$$

The  $\bar{\alpha}$ -Born approximation with the due account of the final state QED and QCD radiation factors gives simple expressions for the observables in the *hadronic* decays of  $Z$  boson as well.

The electroweak corrections for all observables are calculated in the framework of LEPTOP in terms of  $\alpha^0$ ,  $\alpha_w^0$ ,  $M_Z^0$ ,  $m_t^0$ ,  $m_H^0$ , and  $(1/\epsilon, \mu)$  in one-loop approximation. In this approximation  $m_t^0$  and  $M_H^0$  can be replaced by the physical masses  $m_t$  and  $M_H$ .

By expressing  $\alpha^0$ ,  $\alpha_w^0$ ,  $M_Z^0$  in terms of  $\bar{\alpha}$ ,  $G_\mu$ ,  $M_Z$  and  $(1/\epsilon, \mu)$  one derives formulae in which terms  $(1/\epsilon, \mu)$  cancel out. Thus introduction of counterterms is avoided.

The explicit analytical expressions for the LEPTOP electroweak corrections in terms of  $G_\mu$ ,  $\bar{\alpha}$ ,  $c$ ,  $s$ ,  $t = (m_t/M_Z)^2$  and  $h = (M_H/M_Z)^2$  are given in section 4.1.

The flowchart for the LEPTOP approach is shown in Fig. 9.

## FLOWCHART OF LEPTOP

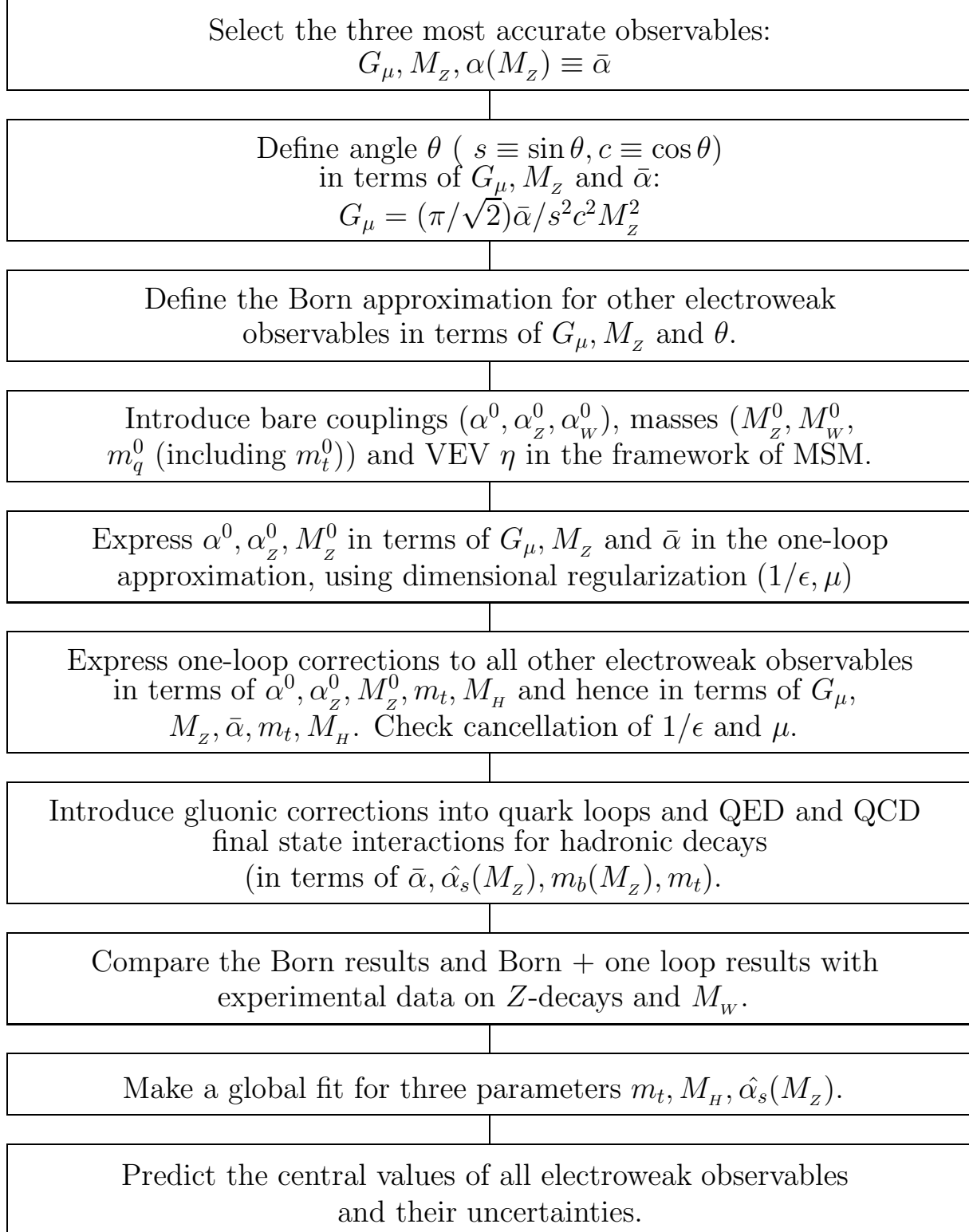


Figure 9: LEPTOP flowchart

### 1.8.3 TOPAZO

The TOPAZO code [4] uses the  $\overline{MS}$  (modified minimal subtraction) scheme for all types of interactions, including the electroweak ones, as introduced in [34]. Its approach is quite different both from those of BHM/WOH, ZFITTER, and LEPTOP. Its main steps are presented in the following items:

- The MSM Lagrangian is assumed. Excluding fermion masses and mixing angles the MSM is a three-parameter theory: i.e.  $g^0$ ,  $M_W^0$  and  $\sin \theta_0$ . At the level of defining a renormalization scheme, two essentially different approaches may be distinguished: to prescribe precisely what a parameter of the Lagrangian is or to prescribe precisely what a counterterm is. It is a matter of convention, since only their combined effect appears in the confrontation with the data, and once the latter is chosen it would then seem natural to follow the consensus with respect to QCD. The bare parameters are fixed by considering three data points —  $\alpha(0)$ ,  $G_\mu$ , and  $M_Z$ . These quantities are computed up to one-loop diagrams and *fitting equations* are written:

$$p_i^0 = f_i(\alpha, G_\mu, M_Z, \Delta), \quad i = 1, 2, 3, \quad (46)$$

where  $p_i^0$  are the bare parameters and  $\Delta = -2/(n-4) + \gamma_E - \ln \pi$ . Everything is worked out explicitly in the 't Hooft–Feynman gauge.

- The *fitting equations* are solved perturbatively (order-by-order renormalization), but gauge invariant (fermionic) higher order leading terms are always re-summed.

Strictly speaking, one usually solves an implicit equation  $f(a, \lambda) = 0$ , where  $a$  is some parameter and  $\lambda$  is a coupling constant, by expanding  $a$  around  $a_0$ , the solution of  $f(a_0, 0) = 0$ . However, one could just as well expand  $a$  around  $\bar{a}$ , the solution of some other equation  $h(\bar{a}, \lambda) = 0$ , as long as  $\bar{a}$  is gauge invariant. Thus in our implementation  $\alpha(0)$  will evolve into  $\alpha(M_Z)$  and the lowest-order approximation for  $s_\theta^2 = \sin^2 \theta_0$  is

$$\hat{s}^2 = \frac{1}{2} \left[ 1 - \sqrt{1 - \frac{4\pi\alpha(M_Z)}{\sqrt{2}G_\mu M_Z^2 \rho_Z^R}} \right], \quad (47)$$

$$(\rho_Z^R)^{-1} = 1 + \frac{G_\mu M_Z^2}{2\sqrt{2}\pi^2} \times \{\text{UV finite combination of two-point functions}\}, \quad (48)$$

where  $(\rho_Z^R)^{-1} - 1$  is determined by an ultraviolet finite combination of two-point functions. The detailed definition of  $\rho_Z^R$  is left for the section 4.2 — Eqs. (227) and (232 – 233).

Eq.(47) is an algebraic solution of the following relation<sup>8</sup>

$$G_\mu = \frac{\pi \bar{\alpha}}{\sqrt{2} M_Z^2 \hat{s}^2 \hat{c}^2 \rho_Z^R}. \quad (49)$$

---

<sup>8</sup>For analogous relations for BHM/WOH, ZFITTER see Eq. (38) and for LEPTOP - Eq.(41).



If no resummation at all is performed in TOPAZ0 then  $\rho_z^R = 1$  and, in this limit, one recovers the weak mixing angle as defined by LEPTOP. The  $\rho_z^R$  parameter is strictly connected to the  $Z$  wave function renormalization and usually all bosonic contributions are expanded up to first order, in this case the  $\rho$  parameter being instead denoted by  $\rho_z$ , Eq.(227), but the possibility of a resummation for a certain gauge invariant subset in the  $\overline{MS}$  framework is built in. It should be noticed that  $\rho_z$  or its variant  $\rho_z^R$  represent the natural extension of the Veltman's  $\rho$ -parameter, as defined at low energy [34], to the scale  $M_z$ . Its asymptotic behavior, for large  $m_t$ , is exactly the same as dictated by  $\Delta\rho$  — see Eq. (80). That is why all the higher-order leading ( $m_t$ ) corrections will simply be added to  $\rho_z^R(\rho_z)$ .

- By a proper redefinition of the bare coupling  $g^0$  [31], corresponding to a gauge field re-diagonalization in the quadratic part of the Lagrangian, in the  $\xi = 1$  (t'Hooft–Feynman) gauge the following properties are fulfilled: the sum of all  $Z\bar{f}f$  vertices,  $\sum_v \{\text{vertex}\}$ , is ultraviolet finite and the  $Z - \gamma$  transition satisfies  $\Sigma_{Z\gamma}(0) = 0$ . In the renormalization procedure of TOPAZ0 it is observed that, unlike QED, no one-to-one correspondence exists between the bare parameters and experimental data points. Therefore no attempt is made to give an all-orders relation as for  $s_w^2$ , but rather it is observed that the mixing angle defines the distribution of the vector current between  $Z$  and  $\gamma$ . It is an accident of the minimal Higgs system (or more generally of representations where the Higgs scalars only occur in doublets) that the vector boson masses are not both free and beyond lowest order different definitions of the weak mixing angle receive different radiative corrections. Also, the  $W$  mass has no special role in TOPAZ0, being computed like any other quantity, once the bare parameters are substituted through their explicit expressions. Typically,

$$\begin{aligned} \sin^2 \theta_0 &= \hat{s}^2 + \{\mathcal{O}(\alpha)\text{UV finite bosonic corrections}\} \\ &\quad + \{\mathcal{O}(\alpha) \Delta\text{-dependent terms}\} , \end{aligned} \tag{50}$$

and in computing for instance  $Z \rightarrow f\bar{f}$  the latter cancel their  $\Delta$  dependence against the  $Z - \gamma$  transition, leading to an ultraviolet finite result. According to the chosen strategy, all bosonic terms are expanded or, alternatively, a gauge invariant sub-set of the bosonic corrections is re-summed in  $\hat{s}^2$  (in the  $\overline{MS}$  environment). In the second case a (usually small) remainder is left, which compensates against vertex corrections. The corrected  $Z$  propagator, leading to mass renormalization and to a  $Z$  wave-function renormalization factor, is ultraviolet finite by inspection.

- The processes  $Z \rightarrow f\bar{f}$ ,  $e^+e^- \rightarrow f\bar{f}$  are computed up to one-loop diagrams with lowest-order (partially re-summed) parameters plus tree diagrams with one-loop corrected parameters. Ultraviolet finiteness is checked both analytically and numerically (independence of  $\Delta$ ). Roughly speaking, the central objects in TOPAZ0 are the  $S$ -matrix elements for a given process, so particular care is devoted to the proper treatment of the wave-function renormalization factors (see Ref. [38]).

## 1.9 Phenomenology of $Z$ boson decays

The decay width of  $Z \rightarrow f\bar{f}$  is described by the following equation used by all five codes:

$$\Gamma_f \equiv \Gamma(Z \rightarrow f\bar{f}) = 4N_c^f \Gamma_0 [(g_V^f)^2 R_V^f + (g_A^f)^2 R_A^f] , \quad (51)$$

where  $g_V^f$  and  $g_A^f$  are effective electroweak couplings defined in section 1.4.4,  $N_c^f = 1$  or 3 for leptons or quarks ( $f = l, q$ ). The factors  $R_V^f$  and  $R_A^f$  describe the final state QED and QCD interactions and take into account the mass  $m_f$ . The radiation factors are universal, to a large extent, and will be described below in this subsection.

The standard width  $\Gamma_0$  in Eq.(51) is known with very high accuracy:

$$\Gamma_0 = \frac{G_\mu M_Z^3}{24\sqrt{2}\pi} = 82.945(12) \text{ MeV} . \quad (52)$$

For the decay into leptons  $l\bar{l}$  the radiation factors  $R_{V,A}^l$  are especially simple. For charged leptons:

$$\Gamma_l = 4\Gamma_0 \left[ (g_V^l)^2 \left( 1 + \frac{3}{4\pi} \bar{\alpha} \right) + (g_A^l)^2 \left( 1 - 6 \frac{m_l^2}{M_Z^2} + \frac{3}{4\pi} \bar{\alpha} \right) \right] . \quad (53)$$

The mass term in Eq. (53) is negligible for  $l = e, \mu$  and is barely visible only for  $l = \tau$  ( $m_\tau^2/M_Z^2 = 3.8 \times 10^{-4}$ ).

For the neutrino decay:

$$\begin{aligned} \Gamma_\nu &= 8(g^\nu)^2 \Gamma_0 , \\ g^\nu &= g_V^\nu = g_A^\nu . \end{aligned} \quad (54)$$

For the decays into quarks  $q\bar{q}$  the radiation factors are given by [39]-[45]

$$R_V^q(s) = 1 + \delta_e^q + \delta_v a_s^2 - 12.76706 a_s^3 + 12 \frac{\bar{m}_q^2(s)}{s} a_s \delta_{vm} , \quad (55)$$

$$\begin{aligned} R_A^q(s) &= 1 + \delta_e^q + \left[ \delta_v - 2I_q^{(3)} \mathcal{I}^{(2)} \left( \frac{s}{m_t^2} \right) \right] a_s^2 \\ &\quad + \left[ -12.76706 - 2I_q^{(3)} \mathcal{I}^{(3)} \left( \frac{s}{m_t^2} \right) \right] a_s^3 \\ &\quad - 6 \frac{\bar{m}_q^2(s)}{s} \delta_{am}^1 - 10 \frac{\bar{m}_q^2(s)}{m_t^2} a_s^2 \delta_{am}^2 , \end{aligned} \quad (56)$$

where

$$\begin{aligned} \delta_e^q &= \frac{3}{4} Q_q^2 a + a_s - \frac{1}{4} Q_q^2 a a_s , \\ \delta_v &= 1.40923 + \left( \frac{44}{675} - \frac{2}{135} \ln \frac{s}{m_t^2} \right) \frac{s}{m_t^2} , \end{aligned}$$

$$\begin{aligned}
\delta_{vm} &= 1 + 8.7 a_s + 45.15 a_s^2, \\
\delta_{am}^1 &= 1 + \frac{11}{3} a_s + \left( 11.286 + \ln \frac{s}{m_t^2} \right) a_s^2, \\
\delta_{am}^2 &= \frac{8}{81} - \frac{1}{54} \ln \frac{s}{m_t^2},
\end{aligned} \tag{57}$$

and

$$\begin{aligned}
a_s &= \frac{\alpha_s(s)}{\pi}, \quad a = \frac{\alpha(s)}{\pi}, \\
\mathcal{I}^{(2)}(x) &= -\frac{37}{12} + l + \frac{7}{81}x + 0.0132 x^2, \\
\mathcal{I}^{(3)}(x) &= -\frac{5651}{216} + \frac{8}{3} + \frac{23}{36} \pi^2 + \zeta(3) + \frac{67}{18}l + \frac{23}{12}l^2,
\end{aligned} \tag{58}$$

where  $l = \ln x$ ,  $m_t = m_{t(pole)}$  (and  $s = M_Z^2$  for  $Z$  decay).

Note that we have automatically absorbed the finite mass terms into the QCD correction factors and that in  $R_A$  the large logarithms  $\ln(m_f^2/s)$  have been absorbed through the use of running parameters

$$\begin{aligned}
\bar{m}(s) &= \bar{m}(m^2) \exp \left\{ - \int_{a_s(m^2)}^{a_s(s)} dx \frac{\gamma_m(x)}{\beta(x)} \right\}, \\
m &= \bar{m}(m^2) \left[ 1 + \frac{4}{3} a_s(m) + K a_s^2(m) \right],
\end{aligned} \tag{59}$$

where  $m = m_{pole}$  and  $K_b \approx 12.4$ ,  $K_c \approx 13.3$ . The various codes may differ in the construction of  $g_V^f$  and  $g_A^f$  but, a general consensus has been reached for final state radiation. In this way we obtain the hadronic and total  $Z$  width as

$$\begin{aligned}
\Gamma_h &= \sum_{f=udcsb} \Gamma(Z \rightarrow f\bar{f}) + 4\Gamma_0 N_c^f R_V^h, \\
R_V^h &= -0.41318 \left( \sum_q v_q \right)^2 a_s^3, \\
\Gamma_Z &= \Gamma_h + \sum_{f=e\mu\tau} \Gamma_f + \Gamma_{inv}.
\end{aligned} \tag{60}$$

Actually, the hadronic width and the partial  $q\bar{q}$  widths deserve some partial comment, while the complete theoretical framework is described in [45]. The singlet QCD contribution which is simple and unambiguous for the hadronic width becomes ambiguous, starting at  $\mathcal{O}(\alpha_s^2)$ , for individual  $q\bar{q}$  channels. In fact, some sort of agreement has recently been reached on these matters but we want to summarize the roots of the problem. From a pragmatic point of view there is a hierarchical description where

$$\Gamma_q = \Gamma [Z \rightarrow q\bar{q}(g) + q'\bar{q}'] \quad (61)$$

for all  $q'$ , such that  $m_{q'} < m_q$ . However, we could have a democratic description where the final states  $q\bar{q} + q'\bar{q}'$  are assigned for  $\frac{1}{2}$  to  $\Gamma_q$  and for the other  $\frac{1}{2}$  to  $\Gamma_{q'}$ . The two descriptions agree — fortunately for the leading terms. In general, one could also decide that such final states should not be assigned to any specific channels in such a way that

$$\sum_q \Gamma_q \neq \Gamma_h = \sum_q \Gamma(Z \rightarrow q\bar{q}) + \sum_{q,q'} \Gamma(Z \rightarrow q\bar{q}q'\bar{q}') + \dots \quad (62)$$

In particular the  $\mathcal{O}(\alpha_s^3)$  contribution to  $\Gamma_V^S$  cannot be assigned to any specific flavour. In our approach the  $\mathcal{I}^{(2,3)}$  corrections terms are included according to isospin, i.e. proportional to  $I_q^{(3)}$ , and therefore cancel in the hadronic width while summing over the first four flavours  $u, d, c, s$ . However, it must be pointed out that no general consensus has been reached on this particular point, so that the prediction for  $\Gamma_u, \Gamma_d, \Gamma_c$  may differ from one code to the other, although the total hadronic width will remain the same.

## 1.10 Electroweak corrections: Basic notions

Above, we introduced a universal language describing the general features of radiative corrections, the language of *effective* couplings. At a secondary level, each computational scheme, being a particular *representation* of the same general concept, may use different building blocks, which, however, are so deeply related that one could even attempt the construction of some sort of ‘Rosetta stone’. Since one of our main motivations was to build up a theoretical framework that includes some estimate of its own uncertainty, we must necessarily spend some time in discussing some of the specific building blocks.

Indeed, even though there is a high degree of universality in the realization of the theoretical uncertainty, in practice the way in which this realization becomes effective is strictly related to the actual implementation of higher-order radiative corrections into the various codes. In order to discuss the numerous effects involved in the calculations we have to introduce additional notions.

### 1.10.1 Comparison of notations of different codes

As explained earlier, all electroweak loop effects in  $Z$  boson decays are concealed in the effective couplings  $g_V^f$  and  $g_A^f$ . The treatment of these couplings, unlike that of the radiation factors  $R_{V,A}^f$ , differs from one code to another (having several different realizations). In order to concentrate on these realizations let us for a moment forget about radiative factors  $R_{V,A}^f$ . Then

$$\Gamma_f = 4N_c^f \Gamma_0 [(g_V^f)^2 + (g_A^f)^2] . \quad (63)$$

The five codes deal with three main realizations.

In BHM/WOH, ZFITTER the following notations are introduced:

$$\rho_f = \frac{1}{1 - \delta\rho_f} = 4(g_A^f)^2 , \quad (64)$$

$$\frac{g_V^f}{g_A^f} = 1 - 4|Q_f|s_w^2\kappa_f, \quad (65)$$

where

$$\kappa_f = 1 + \delta\kappa_f, \quad (66)$$

so that Eq. (63) may be rewritten in the form

$$\Gamma_f = \Gamma_0 N_c^f \rho_f [4(I_f^3 - 2Q_f s_w^2 \kappa_f)^2 + 1]. \quad (67)$$

Here the electroweak corrections affect  $\delta\rho_f$ ,  $\delta\kappa_f$  and  $s_w$ . They will be discussed in the next subsection.

In TOPAZO,

$$\Gamma_f = 4\Gamma_0 N_c^f \rho_Z \left[ \left( I_f^{(3)} - 2Q_f \hat{s}^2 + \delta g_V^f \right)^2 + \left( I_f^{(3)} + \delta g_A^f \right)^2 \right], \quad (68)$$

where  $\hat{s}^2$  is defined in (47),  $\rho_Z$  in (227) and  $\delta g_V^f, \delta g_A^f$  — see (91) — contain (part of) the bosonic corrections as well as the vertex corrections.

In LEPTOP,

$$g_A^f = I_f^{(3)} \left[ 1 + \frac{3}{32\pi s^2 c^2} \bar{\alpha} V_A^f \right], \quad (69)$$

$$\frac{g_V^f}{g_A^f} = 1 - 4|Q_f|s^2 + \frac{3|Q_f|}{4\pi(c^2 - s^2)} \bar{\alpha} V_R^f, \quad (70)$$

and  $V_{A,R}$  are simple functions of  $(m_t/M_Z)^2$  and  $(M_H/M_Z)^2$ , as described in section 4.1.

### 1.10.2 Basic notions of different codes

Here we will concentrate on a specific *realization* of the language of effective couplings in different codes. In particular it is important to clarify the notion of *leading*, *non-leading* and eventually of *remainder* terms in BHM/WOH, TOPAZO and ZFITTER.

We start our presentation by considering two well known objects,  $\Delta r$  (which is used by BHM, TOPAZO, ZFITTER) and the partial  $Z$  width. There are many notions which are common to both these objects.

The quantity  $\Delta r$  is nothing but the effective coupling of the  $\mu$ -decay, when it is being implemented with higher order corrections, see the couple of Eqs. (38) and (39). In this case there is only one effective coupling, as the  $\mu$  decay is a purely weak process mediated by a charged current. For the partial  $Z$  width, the situation is more involved, since we have a decay which is mediated by the neutral current. That is why it is described by two effective electroweak couplings. The introduction of  $\Delta r$  will be very useful in clarifying the notion of leading and of remainder contributions to radiative corrections. However, from a general point of view this is only one of the many specific realizations of the effective coupling in the  $\mu$  decay.

As an example of the leading-remainder splitting we consider  $\rho_c$  and  $\Delta r$  (39, 40),  $\rho_f$  and  $\delta\rho_f$  (64), and  $\kappa_f$  and  $\delta\kappa_f$  (65, 66) — the electroweak corrections to  $\Delta r$  and to  $\Gamma_f$ . Next we subdivide  $\rho_c$  as introduced in Eq. (39) and  $\rho_f$  and  $\kappa_f$  of (64, 65) into a *leading* term,  $\Delta_L$ , and *remainder*,  $\Delta_{\text{rem}}$ , terms as follows:

$$\rho_c = \frac{1}{1 - \Delta r} = \frac{1}{1 - \Delta r_L - \Delta r_{\text{rem}}} = \frac{1}{(1 - \Delta\alpha) \left(1 + \frac{c_W^2}{s_W^2} \Delta\rho_x\right) - \Delta r_{\text{rem}}}, \quad (71)$$

$$\rho_f = \frac{1}{1 - \delta\rho_f} = \frac{1}{1 - \Delta\rho - \Delta\rho_{f,\text{rem}}}, \quad (72)$$

$$\kappa_f = 1 + \delta\kappa_f = (1 + \Delta\kappa_{f,\text{rem}}) \left(1 + \frac{c_W^2}{s_W^2} \Delta\rho_x\right). \quad (73)$$

From Eqs. (71–73) one may notice that each coupling contains some *universal*, flavour-independent piece ( $\Delta\alpha$ ,  $\Delta r_L$ ,  $\Delta\rho$ ,  $\Delta\rho_x$ ), and some flavour-dependent remainder. The former comprise the *leading* terms ( $\Delta\alpha$ ,  $\Delta\rho$ ) they are *re-summed* to all orders in accordance with the renormalization group equation for  $\Delta\alpha$  and with the proper inclusion of leading irreducible terms for  $\Delta\rho$  [46]. The latter are normally small, since all potentially large contributions have already been subtracted and shifted to the leading terms. For this reason, they are placed freely either into the denominators, (71, (72)), or as a factor of the leading contribution, (73); in doing so we follow Ref. [47]. In one case however, namely Eq. (71), there exist arguments in favour of keeping the remainder in the denominator. In Ref. [48] it was proved that the right-hand side of Eq. (71) actually means that, on the two-loop level at least, all fermionic mass singularities are located exclusively in  $\Delta\alpha$ . This may be argued by a partial expansion of a simplified case ( $\Delta\rho = 0$ ) up to the two-loop order terms,

$$\rho_c \approx \frac{1}{1 - \Delta\alpha - \Delta r_{\text{rem}}} \approx \frac{1}{(1 - \Delta\alpha)} \left(1 + \frac{\Delta r_{\text{rem}}}{1 - \Delta\alpha}\right), \quad (74)$$

from which one can see that the scale of  $\Delta r_{\text{rem}}$  is actually  $\alpha(M_Z)$ .

One should emphasize that since there is no  $\Delta\alpha$  in Eqs. (72), (73) and since the non-leading terms of the order  $\Delta_L \Delta_{\text{rem}}$  are unknown, no arguments in favour of putting  $\Delta_{\text{rem}}$  as it is done in (72, 73) can be presented. The size of these uncontrolled terms should be treated as an intrinsic theoretical error.

All the remainder terms have a similar structure:

$$\Delta r_{\text{rem}} = \Delta r^{\text{1loop},\alpha} + \Delta r^{\text{2loop},\alpha\alpha_s} + \frac{c_W^2}{s_W^2} \Delta\bar{\rho}_x - \Delta\alpha, \quad (75)$$

$$\Delta\rho_{f,\text{rem}} = \Delta\rho_f^{\text{1loop},\alpha} + \Delta\rho^{\text{2loop},\alpha\alpha_s} - \Delta\bar{\rho}, \quad (76)$$

$$\Delta\kappa_{f,\text{rem}} = \Delta\kappa_f^{\text{1loop},\alpha} + \Delta\kappa^{\text{2loop},\alpha\alpha_s} - \frac{c_W^2}{s_W^2} \Delta\bar{\rho}_x. \quad (77)$$

They contain all the terms known at present: the complete one-loop  $\mathcal{O}(\alpha)$  corrections (two-, three-, four-point functions) and complete two-loop  $\mathcal{O}(\alpha\alpha_s)$  insertions to two-point functions, from which the leading  $\mathcal{O}(\alpha)$  and  $\mathcal{O}(\alpha\alpha_s)$  terms are subtracted:

$$\begin{aligned}\Delta\bar{\rho}_{(X)} &= \Delta\bar{\rho}^\alpha + \Delta\bar{\rho}^{\alpha\alpha_s} + (\bar{X}) \\ &= \frac{3\alpha}{16\pi s_w^2 c_w^2} \frac{m_t^2}{M_Z^2} \left[ 1 - \frac{2}{3} \left( 1 + \frac{\pi^2}{3} \right) \frac{\alpha_s(m_t^2)}{\pi} \right] + (\bar{X}) ,\end{aligned}\quad (78)$$

where braces in (78) and below mean that this expression describes simultaneously both quantities  $\Delta\bar{\rho}$  and  $\Delta\bar{\rho}_X$ , which appeared in Eqs. (75)-(77).

The term  $\bar{X}$  in (78) is a next-to-leading order term, whose proper treatment is rather important:

$$\bar{X} = \mathcal{R}e \left[ \frac{\Pi_Z(M_Z^2)}{M_Z^2} - \frac{\Pi_W(M_W^2)}{M_W^2} \right]_{\overline{\text{MS}}}^{\text{1loop}} - \Delta\rho^\alpha. \quad (79)$$

In Ref. [49] it was argued that in the on-mass-shell renormalization scheme this term should be re-summed together with  $\Delta\bar{\rho}^\alpha$ , since in the  $\overline{\text{MS}}$  scheme it appears to be automatically incorporated. Similar arguments in favour of such a resummation were presented in Ref. [50]. In  $\bar{X}$  the UV divergences are removed according to the  $\overline{\text{MS}}$  renormalization scheme with  $\mu = M_Z$ . The separation of  $\bar{X}$  is not unique; it makes the resummation dependent on the renormalization procedure.

The leading contribution  $\Delta\rho$  is built out of the same terms as (78). But they are normalized by  $G_\mu$  rather than by  $\alpha/s_w^2 M_W^2$ , as is required by the resummation proposed in Ref. [46]:

$$\begin{aligned}\Delta\rho_{(X)} &= \Delta\rho^\alpha + \Delta\rho^{\alpha^2} + \Delta\rho^{\alpha\alpha_s} + \Delta\rho^{\alpha\alpha_s^2} + (X) \\ &= N_c x_t \left[ 1 + x_t \Delta\rho^{(2)} \left( \frac{m_t^2}{M_H^2} \right) + c_1 \frac{\alpha_s(m_t^2)}{\pi} + c_2 \left( \frac{\alpha_s(m_t^2)}{\pi} \right)^2 \right] + (X) ,\end{aligned}\quad (80)$$

where

$$x_t = \frac{G_\mu}{\sqrt{2}} \frac{m_t^2}{8\pi^2} , \quad (81)$$

$$X = 2s_w^2 c_w^2 \frac{G_\mu M_Z^2}{\sqrt{2}\pi\alpha} \bar{X} , \quad (82)$$

and  $x_t$  is the Veltman heavy top factor [51]. The coefficients  $c_1$  and  $c_2$  describe the first- and second-order QCD corrections for the leading  $x_t$  contribution to  $\Delta\rho$ , calculated in Refs. [52] and [53]. Correspondingly:

$$c_1 = -\frac{2}{3} \left( 1 + \frac{\pi^2}{3} \right) , \quad (83)$$

$$c_2 = -\pi^2 (2.155165 - 0.180981 n_f) . \quad (84)$$

The function  $\Delta\rho^{(2)}(m_t^2/M_H^2)$  describes the leading second order  $x_t$  (two-loop electroweak) correction to  $\Delta\rho$ , calculated first in the  $M_H = 0$  approximation in Ref. [54] and later in Ref. [55] for an arbitrary relation between  $M_H$  and  $m_t$ .

The partial decay width  $Z \rightarrow b\bar{b}$  contains an additional  $m_t$  dependence due to vertex diagrams (see Fig. 10).

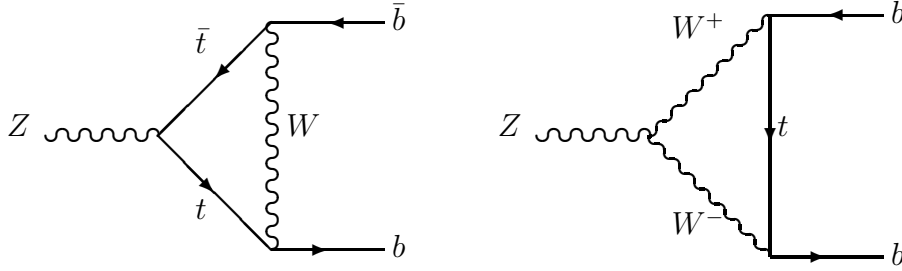


Figure 10: Top quark exchange diagrams which contribute to  $\Gamma_b$  (unitary gauge)

As a consequence, the effective couplings  $\rho_b$  and  $\kappa_b$  contain additional leading terms of the order  $\mathcal{O}(G_\mu m_t^2)$ . The complete one-loop approximation for the  $Z \rightarrow b\bar{b}$  partial width was calculated in Ref. [56]. We first redefine remainder terms by an additional subtraction of the leading one-loop term originating from these diagrams:

$$\begin{aligned}\Delta\rho_{b,\text{rem}} &\rightarrow \Delta\rho_{b,\text{rem}} - 2\Delta\bar{\rho}_b, \\ \Delta\kappa_{b,\text{rem}} &\rightarrow \Delta\kappa_{b,\text{rem}} + \Delta\bar{\rho}_b,\end{aligned}\tag{85}$$

where

$$\Delta\bar{\rho}_b = \frac{\alpha}{8\pi s_w^2} \frac{m_t^2}{M_W^2}.\tag{86}$$

Following papers [55] and [57], the two-loop order QCD and electroweak leading terms in the  $Zb\bar{b}$  vertex are implemented by an additional re-definition of effective couplings  $\rho_b$  and  $\kappa_b$ :

$$\rho_b \rightarrow \rho_b(1 + \tau_b)^2,\tag{87}$$

$$\kappa_b \rightarrow \frac{\kappa_b}{1 + \tau_b},\tag{88}$$

where  $\tau_b$  is given by

$$\tau_b = -2x_t \left[ 1 - \frac{\pi}{3}\alpha_s(m_t) + x_t\tau^{(2)} \left( \frac{m_t^2}{M_H^2} \right) \right].\tag{89}$$

A compact analytic representation for the two-loop functions  $\rho^{(2)}$  and  $\tau^{(2)}$  was also given in Ref [58].

We have just discussed what is known in the literature about the treatment of the corrections of the order  $\mathcal{O}(G_\mu m_t^2)$ . The  $Zb\bar{b}$  vertex also contains a logarithmically enhanced



term,  $\mathcal{O}[\alpha \ln(m_t^2/M_w^2)]$ , whose contribution is comparable to the leading one. Recently, QCD corrections were also calculated for this term, (see contribution by Kwiatkowski and Steinhauser in the QCD Part of this Report). This correction, however, can be nearly completely absorbed into the final-state QCD corrections. What remains is approximately one hundred times less than the QCD correction for the leading term as given in (89).

What has been presented so far in this subsection, is to an extent inherent in all five codes. However, in order to reach a better understanding of our set of theoretical predictions and of the strategy adopted to extract their related *intrinsic* errors we have to devote more time to discussing other realizations of the effective coupling language. In TOPAZO — see, Eq.(68) — the partial  $Z$ -widths reads:

$$\Gamma_f = 4 \Gamma_0 N_c^f \rho_Z \left[ \left( I_f^{(3)} - 2 Q_f \hat{s}^2 + \delta g_V^f \right)^2 + \left( I_f^{(3)} + \delta g_A^f \right)^2 \right], \quad (90)$$

where  $\hat{s}^2$ , defined by (47) and (229) (see also Ref. [31]), and is to be put in partial correspondence with the  $s_w^2 \kappa_f$  of Eq. (65). Moreover,  $\delta g_V^f, \delta g_A^f$  contain bosonic corrections as well as vertex corrections. Again, the basic point under examination is the leading-remainder splitting. The main idea beyond this realization is to write a system of equations that connect the  $\overline{MS}$  parameters of the theory in terms of  $\alpha, G_\mu$  and  $M_Z$ . These equations contain the effects of radiative corrections up to a certain order in perturbation theory and must be solved consistently and respecting gauge invariance. As a result of this procedure we end up in Eq. (90) with a  $\rho_Z$  defined according to Eq. (227). This parameter, which properly re-sums the gauge invariant fermionic corrections, contains all isospin breaking terms and includes, beyond  $\mathcal{O}(\alpha)$ , all the presently known higher-order terms — the  $\mathcal{O}(\alpha^2)$  [55], [58],  $\mathcal{O}(\alpha\alpha_s)$  [52] and  $\mathcal{O}(\alpha\alpha_s^2)$  [53] corrections.

The bare weak mixing angle, according to the previous strategy, will always be expanded around  $\hat{s}$ , Eq.( 229), where  $\rho_Z^R$  from Eq. (232) and (233) is used. These two quantities ( $\rho_Z^R$  and  $\rho_Z$ ) may differ whenever a resummation of bosonic corrections is performed for the weak mixing angle. Once the divergent terms are treated in the  $\overline{MS}$  framework,  $\hat{s}^2$  (the leading term) will receive a correction (the remainder)  $\Delta s^2$ . At this point, when the  $Z$  wave function renormalization factor  $\Pi_Z$  is included, we usually expand all the remaining corrections up to first order — we decompose  $\Pi_Z$  into its leading, fermionic part and a remainder  $\Delta\Pi_Z$  (see Eq. (231)). This  $\Delta\Pi_Z$  is always expanded. After inclusion of vertices and fermion wave-function renormalization factors we end up with

$$\begin{aligned} \delta g_V^f &= \frac{\alpha}{4\pi} \left[ \frac{2F_V^f - \frac{1}{2}v_f \Delta\Pi_Z}{c^2 s^2} - 2Q_f \Delta s^2 \right], \\ \delta g_A^f &= \frac{\alpha}{4\pi} \left[ \frac{2F_A^f - \frac{1}{2}I_f^{(3)} \Delta\Pi_Z}{c^2 s^2} \right], \end{aligned} \quad (91)$$

where  $s^2$  is again defined as (41) and  $F_{V,A}^f$  are the flavour-dependent vertex corrections. Additional versions of this realization will be discussed in the framework of the theoretical options. Here we need only mention some of the problems connected to the resummation of bosonic contributions in this realization (as well as in others). It is strictly related to

the question of gauge invariance. As it is well known, the vertices and the bosonic parts of the vector boson self-energies are not separately gauge invariant. On the one hand there is no rigorous procedure for re-summing the vertices, and on the other hand any attempt to isolate the gauge variant parts and to throw them away is not unambiguously defined. Even when we identify the universal contributions from vertices and boxes (for instance by working in the  $R_\xi$  gauge), to be combined with the vector boson self-energies in order to get the one-loop gauge invariant dressed propagators, we still have the freedom to shift from one part (to be re-summed) to the other some process-independent,  $\xi$ -independent, UV finite function of  $q^2$  with the proper asymptotic behavior. Strict enforcement of gauge invariance is one of the roots of Eq. (91), in that  $\Delta\Pi_z$  is not absorbed into the  $\rho_z$  parameter and that particular care must be devoted to the proper definition of the remainder,  $\Delta s^2$ , when resummation of irreducible terms is performed. This fact accounts for one of the many structural differences with other realizations.

In LEPTOP, due to the proper choice of the  $\bar{\alpha}$ -Born approximation, the electroweak radiative corrections turned out to be small — for  $m_t$  around 175 GeV. The smallness of corrections is a result of the mutual cancellation of different equally important terms. Therefore, functions  $V_{A,R}^f$  representing loop corrections are not subdivided into leading and remainder terms and no resummation is performed.

## 2 Options, theoretical uncertainties

During the completion of this work it has become increasingly evident that there is a need to quantify the effect of our partial lack of knowledge of the missing higher-order terms in radiative corrections. Thus we have introduced the notion of *option*, which refers to a set of possible and plausible alternative implementations of the full machinery of radiative corrections within a given renormalization scheme. In order to explain the treatment of higher-order terms and the interplay between pure electroweak and QCD corrections we must once more remember that the effective coupling description of the  $Z$  width has several different realizations.

Quite independent of specific details, all the realizations single out two main components in each observable:

$$O = O_B + \Delta O . \quad (92)$$

The term  $O_B$ , giving the bulk of the answer, is often called the Born approximation (the  $\bar{\alpha}$ -Born approximation in LEPTOP, or improved Born approximation in BHM/WOH, TOPAZ0 and ZFITTER), or the leading contribution to  $O$ . The term  $\Delta O$  represents a small perturbative correction, often called remainder or non-leading contribution. Different realizations usually have different ways of performing this splitting so that, while they agree at the  $\mathcal{O}(\alpha)$ , there are differences which start at  $\mathcal{O}(\alpha^2)$ .

Independent of the particular realization of  $g_V, g_A$ , these effective couplings are complex valued functions, due to the imaginary parts of the diagrams. This, however, will have some relevance only for realistic distributions while for pseudo-observables they are taken to be strictly real. Given that the universal language has in practice many alternative realizations and that the actual implementation of the options is very much code-dependent, we have not created a common set-up for the electroweak options. From this simple fact follows the need to discuss at length the physical motivations behind our options. Although we have tried, as much as possible, to illustrate them from a general perspective, it is also evident that some space has been left to analyze certain specific issues. A description of the implementation of the options in the various codes, with the relative flags, will be given in section 5.

### 2.1 Factorization of QCD Corrections

No matter which realization we are using, one problem naturally emerges when final-state QCD corrections are switched on. This problem is connected with the folding of the non-corrected widths using the QCD factors  $R_{V,A}^f$ . One can take the point of view that non-universal and flavour-dependent couplings should also be folded or, to the contrary, that only the universal effective couplings should multiply the QCD radiation terms. This option merely reflects our ignorance of the mixed  $\mathcal{O}(\alpha\alpha_s)$  corrections, with the noticeable exception of the  $b\bar{b}$  partial width where the leading  $m_t$  part of these corrections is actually known [57]. If we consider the  $b\bar{b}$  partial width we can write

$$\Gamma_0^b = \frac{G_\mu M_Z^3}{2\sqrt{2}\pi} \left[ (g_v^b)^2 + (g_a^b)^2 \right] ,$$

$$\Gamma_{EW}^b = \Gamma_{EW}(Z \rightarrow \bar{b}b) \approx \Gamma_0^b \left[ 1 - 4x_t \frac{(g_v^b + g_a^b)g_a^b}{(g_v^b)^2 + (g_a^b)^2} \right]. \quad (93)$$

At this point naive factorization would imply

$$\Gamma_b = \Gamma_{EW}^b \left( 1 + \frac{\alpha_s}{\pi} \right), \quad (94)$$

while the computed FTJR term [57] gives

$$\Gamma_b = \Gamma_0^b \left[ 1 + \frac{\alpha_s}{\pi} - 4x_t \frac{(g_v^b + g_a^b)g_a^b}{(g_v^b)^2 + (g_a^b)^2} \left( 1 + \frac{3 - \pi^2}{3} \frac{\alpha_s}{\pi} \right) \right], \quad (95)$$

so that the correct QCD coefficient in front of the heavy top factor turns out to be  $-2.290 \alpha_s/\pi$  instead of  $\alpha_s/\pi$ . Of course, an approximate but factorized expression is still possible and can be written as

$$\Gamma_b = \Gamma_0^b \left[ 1 - 4x_t \frac{(g_v^b + g_a^b)g_a^b}{(g_v^b)^2 + (g_a^b)^2} \left( 1 - \frac{\pi^2}{3} \frac{\alpha_s}{\pi} \right) \right] \left( 1 + \frac{\alpha_s}{\pi} \right), \quad (96)$$

where the uncertainty has now moved to order  $\alpha_s^2 G_\mu m_t^2$ . Actually, we have not yet specified the scale of  $\alpha_s$  in the previous equations but these corrections have been implemented such that the universal QCD factor is computed as  $1 + \alpha_s(M_Z)/\pi$ , while the specific FTJR term is computed with  $\alpha_s(m_t)$ . As a consequence the  $1 + \alpha_s(M_Z)/\pi$  factor is not included for the  $b$ -quark asymmetries and for the effective  $b$ -quark mixing angle. In general, however, the  $\mathcal{O}(\alpha\alpha_s)$  corrections for the  $Zf\bar{f}$  vertex is presently not known and we must accept an intrinsic uncertainty associated with the two procedures, i.e. factorization or non-factorization of electroweak and QCD corrections. Once again, if  $\Gamma_0^q$  is the (improved) Born  $q\bar{q}$  partial width and

$$\Gamma_{EW}^q = \Gamma_0^q \left( 1 + \delta_{EW}^{\text{univ}} \right) + \Delta_{EW}^q \quad (97)$$

then

$$\frac{\Delta_{EW}^q}{\Gamma_0^q} \frac{\alpha_s(M_Z)}{\pi} \quad (98)$$

is roughly assumed as the corresponding uncertainty. This type of uncertainty can be illustrated very well by asking how correct it is to shrink an electroweak blob to a point before allowing for QCD radiation.

## 2.2 Genuinely Weak Uncertainties

In this section we briefly discuss the main ingredients which enter the pure weak corrections to the pseudo-observables — the resummation of the one-particle irreducible vector boson self-energies, the scale in vertex corrections and the linearization of the corresponding S-matrix elements. We have avoided in this chapter any intensive usage of the lengthy formulae introduced in the first part of this Report and summarized in some

detail in section 5. Indeed, there is a simple set of problems in the implementation of radiative corrections which is inherent to perturbation theory and does not depend on any specific approach. Only formulae belonging to different realizations represent the technical transcription of these implementations. Real progress is usually achieved whenever a new term becomes available, otherwise we are left with heuristic arguments or with ingenious attempts to improve upon perturbation theory. Different paths along this road represent our present degree of inaccuracy and to understand these differences already gives a hint on how to proceed. The structural and logical essence of these differences can be explained without a massive use of equations.

### 2.2.1 Leading–Remainder splitting

Before we move to discuss the next source of uncertainty we must recall again that, generally speaking, the effective couplings  $g_V^f, g_A^f$  contain a leading and usually re-summed part and a non-leading (remainder) one, quite independent of the specific realization. For instance, in one of the realizations the building blocks are  $\rho_f$  and  $\kappa_f$ , while in another they are  $\rho_z, \hat{s}^2$  and  $\delta g_V^f, \delta g_A^f$ , and in a third they are  $s^2, V_A$  and  $V_R$ . The way in which the non-leading terms can be treated and the exact form of the *leading–remainder* splitting give rise to several possible options in the actual implementation of radiative corrections that in turn become another source of theoretical uncertainty. For instance, for all the objects  $\Delta r, \Delta \rho_f$  and  $\Delta \kappa_f$ , we can introduce the decomposition into leading and remainder. Since we know how to proceed with all objects in the leading approximation the only ambiguity is due to the treatment of the remainders. Clearly, after the splitting  $\Delta r = \Delta r_L + \Delta r_{\text{rem}}$  there are in principle several possible ways of handling the remainder<sup>9</sup>:

$$\frac{1}{1 - \Delta r} = \frac{1}{1 - \Delta r_L - \Delta r_{\text{rem}}} = \left\{ \begin{array}{l} \frac{1}{1 - \Delta r_L - \Delta r_{\text{rem}}} \\ \frac{1}{1 - \Delta r_L} \left( 1 + \frac{\Delta r_{\text{rem}}}{1 - \Delta r_L} \right) \\ \frac{1 + \Delta r_{\text{rem}}}{1 - \Delta r_L} \\ \frac{1}{1 - \Delta r_L} + \Delta r_{\text{rem}} \cdot \end{array} \right. \quad (99)$$

Actually, these options differ among themselves but the difference can be related to the choice of the scale in the remainder term. A complete evaluation of the sub-leading  $\mathcal{O}(G_\mu^2 M_z^2 m_t^2)$  would greatly reduce the associated uncertainty. At the moment these sub-leading terms are simulated just by varying the scale in the remainder. Typical choices are described in section 5 and may vary from realization to realization. A different approach to the problem [3] will be illustrated in section 2.2.5.

---

<sup>9</sup>In case of  $\Delta r$ , the last two expansions are not valid indeed, see a discussion around Eq. (74). We present them here nevertheless for the sake of illustration.

### 2.2.2 Scale in vertex corrections

Another possible option, which is realized by some of the codes (but not all), has to do with the scale of  $\alpha$  in the non-leading corrections, in particular the vertex corrections. To make this point clear we use one of the *realizations* of the effective couplings and analyse the  $Z \rightarrow \bar{b}b$  decay in some details. The essential ingredient will be  $\Delta\rho_b$  which we write as

$$\begin{aligned}\Delta\rho_b &= \Delta\rho_d + \delta\rho_b(m_t) \\ \delta\rho_b(m_t) &= -\frac{G_\mu m_t^2}{2\sqrt{2}\pi^2} \left[ 1 + \mathcal{O}(G_\mu m_t^2) + \mathcal{O}(\alpha_s) \right] + \mathcal{O}(\alpha \ln m_t^2) + \delta\rho_b^{NL},\end{aligned}\quad (100)$$

where  $\delta\rho_b$  is a correction specific to the  $b\bar{b}$  channel. The question naturally arises as to what to use for the scale in  $\delta^{NL}$  and in the sub-leading logarithmic term —  $G_\mu$ ,  $\alpha(M_Z)$  or  $\alpha(0)$ . Obviously the same kind of option will be present in the vertex corrections for light fermions where the expansion parameter is formally  $\alpha/(4\pi \sin^2 \theta \cos^2 \theta)$ . Different ways to interpret  $\alpha$  in these expressions give rise to different results, from  $\alpha(0)/(4\pi \sin^2 \theta \cos^2 \theta)$  to  $G_\mu M_Z^2/(2\sqrt{2}\pi^2)$ . The difference between possible identifications of coupling constants in the  $\mathcal{O}(\alpha)$  corrections represents, of course, effects of  $\mathcal{O}(\alpha^2)$ . The fact that the neutral current amplitude is automatically expressed in terms of  $G_\mu M_Z^2$  is a possible heuristic argument to adopt the same strategy in the evaluation of the presently known  $\mathcal{O}(\alpha)$  corrections, but in order to be on the safe side, the differences should be considered as a theoretical uncertainty, at least according to many authors. For instance, we know from a specific calculation [41] that for inclusive quantities the final state QED radiation is controlled by  $\alpha(M_Z)$  and not by  $\alpha(0)$ . The option of variation of the scale of non-leading corrections has been implemented by the majority of the codes.

### 2.2.3 Linearization

Another example to be discussed is the following. In almost any realization we have the possibility of using an *expanded* versus a *non-expanded* option — to linearize our expressions. To give a partial illustration of this possibility we use the realization of Ref. [4] where we have

$$\sin^2 \theta_{\text{eff}}^l = \frac{1}{4} \left( 1 - \frac{g_V^l}{g_A^l} \right) = \begin{cases} \hat{s}^2 + \frac{1}{2} \delta g_V^l + \frac{1}{2} (4\hat{s}^2 - 1) \delta g_A^l & \text{expanded} \\ \frac{\hat{s}^2 + \frac{1}{2} (\delta g_V^l - \delta g_A^l)}{1 - 2\delta g_A^l} & \text{non-expanded .} \end{cases}$$

On the same footing, the  $\delta g_V^f, \delta g_A^f$  terms in each partial width will be expanded up to first order in the *expanded* option. More generally, the difference between the two options in the evaluation of  $O^2$ , where  $O$  is given by Eq. (92), is equal to  $(\Delta O)^2$ , a two-loop reducible but non-leading contribution, and from this point of view we clearly do not need a specific exemplification. By comparing the two options we obtain a rough estimate of the importance of the missing non-leading two-loop effects. It goes almost without saying that when this option is implemented on top of the leading-remainder splitting and of the

choice  $G_\mu$  versus  $\alpha(0)$  we can have rather different behaviours in the global theoretical error according to the size of the remainder. Thus whenever we need to quantify the effect then the remainder must be considered in detail and the effect becomes realization-dependent. This has some relevance for the de-convoluted leptonic forward-backward asymmetry, where the leading term is small by itself due to accidental cancellations. To summarize we can say that the theoretical error on  $A_{\text{FB}}^l$  is very sensitive to the sum of various factors:

- *expansion* versus *non-expansion*
- definition of the *leading* part of  $\sin^2 \theta_{\text{eff}}^l$
- scale of  $\alpha$  for the non-leading terms.

A further exemplification of what we call option for radiative corrections, in part connected to a selection of the scale in the coupling but generalizable to all parameters appearing in the remainder, can be illustrated as follows. Suppose that a given quantity  $A$ , function of the parameter  $a$ , is given in perturbation theory by the following expansion:

$$\begin{aligned} A &= a + g [a^2 + f_1(a)] + g^2 [a^3 + f_2(a)] + \mathcal{O}(g^3) \\ &= \bar{a} + g f_1(a) + \mathcal{O}(g^2) \\ \bar{a} &= a / (1 - ga) , \end{aligned} \tag{101}$$

and that only the  $f_1$  term is actually known. It could be decided that  $\bar{a}$  is the effective expansion parameter (or that in the full expression we change variable  $a \rightarrow \bar{a}$ ), which of course in the truncated expansion introduces the option,

$$\begin{aligned} A &= \bar{a} + g f_1(a) \\ &= \bar{a} + g f_1(\bar{a}) , \end{aligned} \tag{102}$$

so that  $\Delta A = g^2 a^2 f_1'(a)$  would be our estimate of the associated theoretical uncertainty. Sometimes it is only a rough estimate, since there is no guarantee that the irreducible terms  $g^2 f_2$  are essentially small in size.

#### 2.2.4 Resummation

Another source of theoretical uncertainty is connected with the treatment of the physical Higgs contribution. As we know for large Higgs masses ( $M_H \gg M_Z$ ) there is a correction term in  $\Delta\rho$  which is only logarithmic, in contrast to the heavy fermion case, the so-called Veltman's screening effect [59]. With respect to this correction  $\Delta\rho_H$  we can:

- expand it to first order in  $\alpha$  as is sometimes done for all bosonic corrections;
- re-sum the leading part of it,  $\Delta\rho_H^L$ , for relatively large values of  $M_H$ , e.g.  $M_H > M_W \exp 5/12$ ;

- re-sum in  $\rho$  the whole physical Higgs contribution. This requires a further comment, since this term is not UV finite by itself and therefore the resummation procedure must be understood strictly in the  $\overline{MS}$  scheme with a scale  $\mu = M_Z$ .

As an additional and rather general comment, which somehow collects many of the previous considerations, we stress once more that there are different ways of implementing the resummation of the vector boson self-energies. These choices, which in turn are deeply related to the proper definition of remainder, differ from code to code — at least in their default settings. We have already illustrated the splitting  $\Delta r_L - \Delta r_{\text{rem}}$  and simply add a few additional considerations. Resummation is very often the main recipe for separating a small remainder from the bulk of the effect.

- One choice consists in a resummation which includes the square of the  $Z - \gamma$  mixing-term [2, 5] with the option of strictly keeping in the resummation only the one-loop irreducible terms. The default thus corresponds to an additional mass counter-term which enters the field and coupling renormalization constants and modifies the quantity  $\Delta r$ . The resummation of the modified  $\Delta r$  leads automatically to the factorization property which takes into account the proper summation of all the leading higher-order reducible terms.
- Even more generally we can distinguish among complete expansion of the one-loop self-energies, partial resummation of fermionic self-energies or partial inclusion of bosonic self-energies in the resummation. There are two considerations to be made at this point. Sometimes accidental cancellations occur among the fermionic and the bosonic sectors, which would suggest a similar treatment for both; however, the bosonic sector is not gauge invariant by itself. Thus any resummation of bosonic parts must properly identify some numerically relevant but gauge invariant sub-set.

For completeness we recall that one of these identifications gives in the  $\xi = 1$  gauge [60]

$$\begin{aligned}
\mathcal{S}_{\gamma\gamma}(p^2) &= S_{\gamma\gamma}(p^2)|_{\xi=1} - 4e^2 p^2 I(p^2) , \\
\mathcal{S}_{Z\gamma}(p^2) &= S_{Z\gamma}(p^2)|_{\xi=1} - 2e^2 \frac{\cos\theta}{\sin\theta} (2p^2 - M_Z^2) I(p^2) , \\
\mathcal{S}_{ZZ}(p^2) &= S_{ZZ}(p^2)|_{\xi=1} - 4e^2 \frac{\cos^2\theta}{\sin^2\theta} (p^2 - M_Z^2) I(p^2) , 
\end{aligned} \tag{103}$$

where  $I(p^2) = -B_0(p^2, M_W^2, M_W^2)/(16\pi^2)$ ,  $B_0$  is a scalar formfactor [22] and  $\mathcal{S}$  denotes a possible identification of the gauge invariant part of  $S$ .

To spend an additional word on electroweak uncertainties and to understand the implications of some of the procedures used as a possible estimator of the theoretical error we consider a fictitious quantity  $X$  defined as  $X = 1 - 4 \sin^2 \theta_{\text{eff}}^l$ . Each code will define some effective Born approximation to  $\sin^2 \theta_{\text{eff}}^l$  and here we distinguish between three basic possibilities: complete expansion of the corrections (E), a resummation which only includes the fermionic self-energies (FR), or a global resummation (R). We refer here to the complete set of formulae given in section 4 and simply quote the adopted strategies:



- BHM/WOH adopted as the default of the resummation of the entire set of self-energies, including the  $Z - \gamma$  mixing term;
- LEPTOP, which expands all those contributions not re-absorbed in the running of  $\alpha$  into  $\bar{\alpha}$ ;
- TOPAZO's default, which re-sums in the  $\overline{MS}$  framework the  $\Sigma_R$  term of Eq. (233), while an option is left in which only its fermionic content is re-summed;
- ZFITTER's default, which also re-sums in the  $\overline{MS}$  framework the  $X$  term of Eq. (82), allowing asr options the resummations of the leading terms only.

Let us define  $X_0$  as the effective Born approximation of  $X$  and define a non-leading (remainder) part,  $X = X_0 + [\alpha(M_Z)/\pi]X_1 + \mathcal{O}(\alpha^2)$ . The three different procedures, E or FR or R, will find  $X_0 = 0.07528, 0.08672, 0.07184$  (for  $m_t = 175$  GeV,  $M_H = 300$  GeV and  $\alpha_s = 0.125$ ). In fact, there is no unique way for global resummation (R), so that the last number can vary a little (say, from 0.07184 to 0.07416). Using the corresponding value for  $\sin^2 \theta_{\text{eff}}^l$  we get  $X_1 = -1.344, -5.976, -0.016$ . Whenever we compute  $X^2$  and use the square of the remainder to estimate part of the uncertainty (there are other options around) we are bound to see rather different behaviors, depending on the adopted leading-remainder splitting. It should be clear that the remainder itself is subject to several possible options, from the scale of the coupling to the choice of those terms which are to be considered small and perturbative. These options themselves contribute, sometimes sizably, to the final uncertainty, quite independently from linearization (expansion) and in the end every adopted procedure is somehow equivalent to a proper choice of the scale. Thus a preferred set of options is equivalent, in some sense, to an ideal optimization of the perturbative expansion.

### 2.2.5 Estimate of the missing terms in higher orders

While some of the realizations of the effective coupling description make use of a (partial) resummation of higher-order terms, thus trying to improve upon ordinary perturbation theory, we have other realizations where the mixing angle is defined only in terms of  $G_\mu, M_Z$  and of the running constant  $\alpha(M_Z)$  while everything else is strictly expanded. Thus, a Born approximation is defined in terms of an  $s^2$ , the definition of which was given in Eq. (42) and the realization is constructed in terms of the one-loop approximation with respect to the genuinely electroweak interactions. As has become clear from the previous discussion, there is no common set of implemented procedures for describing the theoretical uncertainties but only some rather general guidelines. Certainly, when we move to a concrete implementation, it happens that every code has its own internal ways of estimating the missing higher-order effects. Codes which do not foresee, for theoretical reasons, the possibility of expanding the remainders with respect to the leading terms or of playing with the choice of the scale in the remainders, introduce another set of options based on a different estimate of the not-yet-calculated diagrams or terms in a given diagram. The basic and alternative idea is that each of the Born relations (43–45) will receive a genuinely electroweak correction proportional to  $\bar{\alpha}V_i$ , as given by Eq. (180).

The main point is related to the recent observation [61] that the sub-leading two-loop corrections to the vector boson self-energies, of order  $\mathcal{O}(G_\mu^2 m_t^2 M_Z^2)$ , could be numerically close to the leading ones, of  $\mathcal{O}(G_\mu^2 m_t^4)$ . Thus the latter can be considered as an estimate of the uncertainties in the  $V_i$ . At the same level the  $\mathcal{O}(\alpha_s^2 m_t^2)$  corrections, to be discussed in the next section, can also be used as an estimate of the uncertainty. In order to have the correct asymptotic behavior of the uncertainties for  $m_t \gg M_Z$ , it is assumed that these universal corrections are multiplied by a factor  $2/t = 2 M_Z^2/m_t^2$ . Indeed, the  $\mathcal{O}(t^2)$  is completely under control, although the sub-leading  $\mathcal{O}(t)$  is not and thereby  $1/t$  follows with the usual safety factor of 2. Thus if the leading higher-loop corrections calculated in Refs. [55] and [53] are denoted respectively by

$$\delta V_i^{t^2}, \quad \delta V_i^{\alpha_s^2}, \quad (104)$$

then the corresponding estimates of the missing terms are assumed to be

$$\Delta V = (2/t) \delta V, \quad \text{with} \quad t = \frac{m_t^2}{M_Z^2}. \quad (105)$$

There is also a specific correction to the  $Z \rightarrow b\bar{b}$  vertex dependent on  $M_H^2/m_t^2$ , which is presently computed up to  $\mathcal{O}(G_\mu^2 m_t^4)$  term [55], while the sub-leading terms are still unknown. If we denote it by  $\delta\phi^{t^2}$  — see the second term in Eq. (220) — then an upper bound on the ‘Higgs theoretical uncertainty’ can be estimated as

$$\Delta\Gamma_b = -\frac{\alpha(M_Z)}{\pi} \Gamma_0 \delta\phi^{t^2}. \quad (106)$$

For  $m_t = 175 \text{ GeV}$  and  $M_H = 300 \text{ GeV}$  this amounts to  $0.02 \text{ MeV}$ , which is much smaller than other uncertainties and could therefore be neglected.

## 2.3 QCD Corrections on Electroweak Loops

The effect of QCD corrections is not confined to the final-state radiation or the  $\mathcal{O}(\alpha\alpha_s)$  vertex corrections to  $Z \rightarrow b\bar{b}$  but it will influence all vector boson self-energies through virtual gluon exchanges within quark-loop insertions. All codes include these two-loop diagrams [52] by first decomposing the  $WW, ZZ, Z\gamma$ , and  $\gamma\gamma$  self-energies into two basic building blocks,  $\Pi_V(m_i, m_j)$  and  $\Pi_A(m_i, m_j)$ , which are given by the expansion

$$\Pi_{V,A} = N_c \left( \Pi_{V,A}^{(1)} + \frac{\alpha_s}{\pi} \frac{C_F}{4} \Pi_{V,A}^{(2)} + \dots \right), \quad (107)$$

with  $C_F = (N_c^2 - 1)/(2 N_c)$ . For instance for each isodoublet,

$$\begin{aligned} \gamma - \gamma &\rightarrow e^2 \sum_{i=1}^2 Q_i^2 \Pi_V(p^2, m_i, m_i), \\ Z - Z &\rightarrow e^2 \sum_{i=1}^2 \left[ v_i^2 \Pi_V(p^2, m_i, m_i) + a_i^2 \Pi_A(p^2, m_i, m_i) \right]. \end{aligned} \quad (108)$$

In the limit where we neglect light quark masses, four different cases have to be considered:

$$\Pi_V(m_t, m_t), \quad \Pi_A(m_t, m_t), \quad \Pi_{V,A}(m_t, 0), \quad \Pi_{V,A}(0, 0). \quad (109)$$

An important issue is related to the renormalization scale to choose for  $\alpha_s$ . The default that we have adopted is to select  $\mu = m_t$  for contributions from the  $t - b$  doublet while  $\mu = M_Z$  is assumed for light quark contributions. A practical difference emerges in the various implementations of  $\Pi^{(2)}$ , where sometimes the full expression is used, while in other cases a Taylor expanded (in  $q^2/m_t^2$ ) version has been used. A step forward has been made with the evaluation of the  $\mathcal{O}(\alpha_s^2)$  corrections to  $\Delta\rho$ , the AFMT term [53]. Given the usual definition of  $\Delta\rho$  as

$$\begin{aligned} \rho &= \frac{1}{1 - \Delta\rho}, \\ \Delta\rho &= N_c x_t \left(1 + \delta^{\text{EW}} + \delta^{\text{QCD}}\right), \end{aligned} \quad (110)$$

we have the QCD contribution to  $\Delta\rho$ , up to three loops and in the heavy top limit, as

$$\begin{aligned} \Delta\rho^{\text{QCD}} &= N_c x_t \delta^{\text{QCD}} \\ &= N_c x_t a_s \left(\delta_2^{\text{QCD}} + a_s \delta_3^{\text{QCD}}\right), \end{aligned} \quad (111)$$

with  $a_s = \alpha_s/\pi$ . As stated, this correction has been computed in the heavy top limit and therefore only the leading part of  $\delta_3^{\text{QCD}}$  is available. Actually, this new calculation makes the QCD corrections to  $\Delta\rho$  much more stable with respect to the renormalization scale, since we now have

$$\delta^{\text{QCD}}(\mu) \approx -0.910 \alpha_s(m_t) - 1.069 \alpha_s^2(m_t) + 2.609 \alpha_s^3(m_t) \ln\left(\frac{\mu^2}{m_t^2}\right) + \mathcal{O}(\alpha_s^4), \quad (112)$$

where  $\alpha_s(m_t)$  is evaluated with five flavours and the  $n_f$  that appears in the final AFMT result is interpreted as the total number of flavours contributing in the Feynman diagrams —  $n_f = 6$ . Recently the same result has been cast [62] into a slightly different form by use of the notion that the corrections to  $\Delta\rho$  in terms of  $m_t$  are almost entirely contained in  $\hat{m}^2(m_t)/m_t^2$ ;  $\hat{m}(m_t)$  being the running mass evaluated at the pole mass. The corresponding differences in  $\delta^{\text{QCD}}$  amount to  $\approx 5\%$  of the total QCD correction. Concerning the treatment of the AFMT term it should be noted that there is, at present, some disagreement on the value for  $n_f$  — for instance, LEPTOP uses  $n_f = 5$  on the basis of decoupling of heavy fermions in vector theories, leading to a 2% change in  $\delta^{\text{QCD}}$  <sup>10</sup>.

A strictly related topic concerns the inclusion and the magnitude of the  $t\bar{t}$  threshold effects on  $\Delta\rho$  and therefore on all the electroweak parameters. These effects have recently

---

<sup>10</sup>A recent and independent evaluation of the QCD corrections to the  $\rho$ -parameter has been presented by K.G. Chetyrkin, J.H. Kühn and M. Steinhauser [63], showing disagreement with the original AFMT result. Meanwhile, a revised version of the AFMT calculation has appeared in hep-ph 16.02.1995 showing agreement with the CKS result. For understanding the effect we have added a **Note in proof**.

been estimated by both dispersion relation and perturbative methods [64] however an uncertainty remains as to their magnitude (see Ref. [65] for a detailed discussion). Most of the QCD corrections to  $\Delta\rho$  beyond the leading-order QCD terms can be discussed and evaluated by absorbing them into the  $\mathcal{O}(\alpha_s)$  term computed with an adjusted scale  $\mu = \xi m_t$ :

$$\Delta\rho^{\text{QCD}} = N_c x_t \left[ 1 - \frac{2}{3} \left( 1 + \frac{\pi^2}{3} \right) \frac{\alpha_s(\xi m_t)}{\pi} \right] + \Delta\rho_{\text{NL}}^{\text{QCD}}, \quad (113)$$

where  $\Delta\rho_{\text{NL}}^{\text{QCD}}$  takes into account the non-leading top effect with the scale set to  $\mu = m_t$ , as well as the light quark effects with  $\mu = M_Z$ . For instance the result of Ref. [62] can be summarized by saying that it corresponds to a very high accuracy, to a scale,

$$\xi = 0.321^{+0.110}_{-0.073}. \quad (114)$$

Incidentally, the original AFMT formulation corresponds in this language to a scale  $\xi = 0.444$ . We note that the absorption of the non-leading QCD terms into a rescaling of  $\alpha_s$  has only been performed, so far, at the level of the leading  $\delta_2^{\text{QCD}}$  term, even if we have at our disposal the full  $\mathcal{O}(\alpha\alpha_s)$  correction factor.

A comment is in order here. Our original idea was to incorporate the  $\bar{t}t$  threshold effects through an opportune rescaling factor  $\xi$ . However, the intrinsic theoretical error on  $\xi$  deriving from the threshold analysis is very difficult to assess, since non-relativistic approximations also play a certain role. In view of the present situation, the majority of the codes has agreed with a specific strategy:

- The default is represented by computing the pseudo-observables to include the complete three-loop AFMT term at a scale of  $\xi = 1$ , Eq. (112), which is equivalent to the use of Eq. (113) with  $\xi = 0.444$ .
- In order to estimate the size of the non-leading QCD effects, the  $\delta^{\text{QCD}}$  correction factor has been implemented according to the formulation of Ref. [62], with a scale which gives the maximum variation with respect to the AFMT term —  $\xi = 0.248$  — and the difference between this and the AFMT calculation is used as an estimate of the corresponding uncertainty. It is certainly not the ideal solution, but we cannot rely on other analyses, not incorporating the  $\mathcal{O}(\alpha\alpha_s^2)$  term. In this context a further subtlety arises, since the effective scale for the AFMT term ( $\xi = 0.444$ ) gives a correction outside the range required by the present Green function analysis [65]. In fact, the result of Ref. [62] and the corresponding error estimate, Eq. (114), also leave the AFMT expansion at the edge or even a bit outside the error range.

## 2.4 Parametric Uncertainties

The parametric uncertainties are those related to the input parameters,  $\alpha(M_Z)$ ,  $G_\mu$  and the masses,  $M_Z, m_b$  etc. Among them the largest uncertainty comes from  $\alpha(M_Z)$ :  $\alpha^{-1}(M_Z) = 128.87 \pm 0.12$  (see, however, the new results [9]-[11]), while the relative uncertainty in  $M_Z$  is an order of magnitude smaller and that in  $G_\mu$  is 50 times smaller. For the  $b$  quark mass we used  $4.7 \pm 0.3 \text{ GeV}$  as a sort of conservative average. We have tried

to compare the effects of variations in the input parameters in a way which, hopefully, will also give useful informations in the future, providing some sort of evolution of the uncertainties as a function of the errors in the input parameters. Assuming independence from the actual central values of  $\alpha(M_Z)$  and of  $m_b$  we computed the derivatives of the pseudo-observables with respect to  $\alpha(M_Z), m_b$ . Assuming, also, that the errors are small enough and that the dependence is therefore approximately linear, this result will allow us to give the uncertainties, even when the input parameters or the errors on them change with time. Actually, a linear approximation is good enough for the derivative with respect to  $\bar{\alpha}^{-1}$  but not with respect to  $m_b$ . In order not to have problems with the latter near a local extremum we have defined a maximum derivative given by

$$\begin{aligned}\mathcal{D}f &= \text{sign}(f') \frac{\max(\delta_h, \delta_l)}{\Delta x}, \\ \delta_h &= |\max(f) - \bar{f}|, \\ \delta_l &= |\bar{f} - \min(f)|,\end{aligned}\tag{115}$$

where  $\bar{f}$  is the corresponding central value. In order to avoid lengthy tables we have computed this set of derivatives for our pseudo-observables at the standard reference point, where  $m_t = 175 \text{ GeV}$ ,  $M_H = 300 \text{ GeV}$  and  $\alpha_s(M_Z) = 0.125$ . The results are shown in Tables 1 and 2 for BHM, LEPTOP, TOPAZO and ZFITTER.

## 2.5 Structure of the Comparisons

Having introduced the main ingredients of the calculations we are now ready to explain in more detail the structure of the comparison. As already pointed out, we focus on 25 pseudo-observables and vary  $m_t, M_H$  and  $\alpha_s(M_Z)$  in a given range of values. It is worth mentioning that we could introduce at this point the notion of an *adapted* set-up, in the sense that prior to the introduction of options we have made an effort to show that different codes running under as similar as possible conditions give very close answers.

In fact, each code will produce a set of results according to some well specified *preferred* set-up relative to the various options briefly discussed. As far as the external building blocks are concerned — QCD and QED correction factors — some effort has been made in order to reach a common default.

- The QED final state radiation for the partial widths is computed at the scale  $M_Z$  [41].
- The FTJR correction [57] has been split into a universal QCD factor computed at a scale  $\mu = M_Z$  and an internal correction factor computed at the scale  $\mu = m_t$ . The former is not included for the  $b$ -quark asymmetries (effective mixing angle  $\sin^2 \theta_{\text{eff}}^b$ ).
- The AFMT three-loop effect [53] with  $n_f = 6$  is included in the default with a scale  $\mu = m_t$ .
- The  $\mathcal{O}(\alpha\alpha_s)$  vector boson self-energies ( $\Pi^{(2)}$ ) are included (almost always the full expression) with two scales:  $\mu = m_t$  for the  $t - b$  doublet and  $\mu = M_Z$  for the light quarks.

- The introduction of an effective scale  $\xi m_t$  is not part of the *preferred* set-up but rather is included in the uncertainty.

This procedure for estimating the size of the non-leading QCD effects has been implemented in all codes but **LEPTOP**, which uses the  $(2/t) \times \text{AFMT}$  term as an estimator of the uncertainty.

In this way the *preferred* set-up of a code refers to a specific choice of the electroweak options, everything of course embedded in a given choice of the renormalization scheme. The result of this procedure is given by five sets of predictions for the 25 pseudo-observables as functions of  $m_t$ ,  $M_H$  and  $\alpha_s(M_Z)$ . On top of our predictions, each group has adapted the various codes to run under all its options (typically up to  $2^5 \div 2^6$ ). It must be clearly realized that no common set of options has been created and that the options of one code have been designed independent of the options of all other codes. In the end, the  $2^n$  electroweak options are folded with 2 QCD options, the inclusion of AFMT being the default versus a rescaling  $m_t \rightarrow 0.248 m_t$  in the  $\mathcal{O}(\alpha\alpha_s)$  term representing the uncertainty. **LEPTOP**, however, is using a different procedure (see above). Note, that electroweak-QCD factorization simulates  $\mathcal{O}(\alpha\alpha_s)$  non-controlled terms, therefore it can also be considered a QCD option. For each pseudo-observable  $O$  we have collected  $O_{\text{adapt}}$  and  $O_+$ ,  $O_-$ , i.e.

$$\begin{aligned} O_+ &= \max_i O_i \\ O_- &= \min_i O_i \end{aligned} \tag{116}$$

where the index  $i$  is running over the options. The differences  $O_+ - O_{\text{adapt}}$  and  $O_{\text{adapt}} - O_-$  calculated by a given code are our *internal* estimates of the theoretical uncertainty associated with  $O$ , while the different results for  $O_{\text{adapt}}$  as obtained by the various codes may be considered as giving our estimation of the scheme dependence. Here *internal* must be understood as the estimate that one particular code can produce by varying internally its options on the implementation of radiative corrections. The corresponding error bars on the theoretical predictions are in some cases very asymmetric, merely reflecting the specific ideas or, even better, personal taste, beyond the choice of preferred set-up. Clearly the way in which the different realizations have been built into the codes is very indicative of the original strategy. To give an example, we may note that the reason why some code does not include the one-loop corrected axial-vector coupling of the  $Z$  to fermions in the definition of the  $\rho$  parameter is because its preferred set-up is the expanded solution. In some cases, the theoretical uncertainty internally estimated by one code could turn out to be large with respect to those of other codes. Basically, we do not attribute any particular relevance to this fact, as the global indication should include some sort of average among the codes. In the general discussion of the results we have tried as much as possible to trace the roots of the phenomenon, whenever it appears, and any further consideration should be left to the potential users of our analysis. Each point in the error bars has the same content of probability and the width of the theoretical bands associated with each pseudo-observable should be taken as an indication of the relevance of that quantity for the analysis of the LEP data. Sometimes the theoretical error, which cannot be reduced

unless we come up with a full two-loop calculation, becomes of the same order as the present or projected experimental error. Even before entering into a full discussion of the results we may anticipate the predictions for  $\sin^2 \theta_{\text{eff}}^l$  by choosing some reference point, such as  $m_t = 175 \text{ GeV}$ ,  $M_H = 300 \text{ GeV}$  and  $\alpha_s(M_Z) = 0.125$ . The prediction is

$$\sin^2 \theta_{\text{eff}}^l = \begin{cases} 0.23197^{+0.00004}_{-0.00007} & \text{BHM} \\ 0.23200^{+0.00008}_{-0.00008} & \text{LEPTOP} \\ 0.23200^{+0.00004}_{-0.00004} & \text{TOPAZO} \\ 0.23194^{+0.00003}_{-0.00007} & \text{WOH} \\ 0.23205^{+0.00004}_{-0.00014} & \text{ZFITTER} . \end{cases}$$

The corresponding width for the theoretical band is therefore 0.00011, 0.00016, 0.00008, 0.00010 or 0.00018 for BHM, LEPTOP, TOPAZO, WOH and ZFITTER. This can be compared with what we obtain by combining the LEP results on all the asymmetries:  $\sin^2 \theta_{\text{eff}}^l = 0.2321 \pm 0.0004$  [15]-[16].

In order to present our results we have focused on the  $W$  mass, on the primary set of pseudo-observables chosen by the LEP collaborations for fitting —  $\Gamma_Z, R_l, A_{\text{FB}}^l$ , and on the  $b$ - and  $c$ -quark related charge asymmetries and ratios of partial widths.

## 2.6 Experimental data and theoretical predictions

To set the scene for our discussion we must first introduce, in Table 3, the relevant experimental data. Clearly a detailed discussion of our results should take into account the whole range of values for the input parameters but many of the relevant conclusions can already be drawn by considering Tables 4–7, where we have reported  $M_W$  [37] and a sample of 11 quantities as measured by the LEP collaborations. For comparison we have fixed a reference point,  $m_t = 175 \text{ GeV}$ ,  $M_H = 300 \text{ GeV}$  and  $\alpha_s = 0.125$ , and reported the predictions from BHM/LEPTOP/TOPAZO/WOH/ZFITTER, including the estimated theoretical errors and the average. The content of the tables should not be confused with a fit but should only be taken as a first introduction to the theoretical results. Our reference point is a mere consequence of the range indicated by CDF for the top quark mass and of the most recent prediction for  $\alpha_s(M_Z)$  from LEP. As far as  $M_H$  is concerned, we must admit a high degree of arbitrariness. As we have detailed, the differences among the (theoretical) central values for each quantity are basically (even though not totally) a measure of the effect induced by a variation in the renormalization scheme. As can be seen from Tables 4–7 the ratios of the maximal half-differences among the five codes over the experimental errors are:

$$\Delta_c(M_W) = 2.5 \times 10^{-2}$$

$$\begin{aligned}
\Delta_c(\Gamma_e) &= 6.7 \times 10^{-2} \\
\Delta_c(\Gamma_Z) &= 3.9 \times 10^{-2} \\
\Delta_c(R_l) &= 1.0 \times 10^{-1} \\
\Delta_c(R_b) &= 3.3 \times 10^{-2} \\
\Delta_c(R_c) &= 2.0 \times 10^{-3} \\
\Delta_c(\sin^2 \theta_{\text{eff}}^l) &= 1.4 \times 10^{-1} \\
\Delta_c(A_{\text{FB}}^l) &= 5.6 \times 10^{-2} \\
\Delta_c(A_{\text{FB}}^b) &= 7.8 \times 10^{-2} \\
\Delta_c(A_{\text{FB}}^c) &= 2.5 \times 10^{-2} .
\end{aligned} \tag{117}$$

Another piece of information is obtained by looking at the theoretical uncertainties as estimated internally by each code. A very conservative attitude would be to report the half-difference between the global maxima and minima among the five codes. By considering again the ratio with the experimental errors we obtain

$$\begin{aligned}
\Delta_g(M_W) &= 7.2 \times 10^{-2} \\
\Delta_g(\Gamma_e) &= 1.6 \times 10^{-1} \\
\Delta_g(\Gamma_Z) &= 3.7 \times 10^{-1} \\
\Delta_g(R_l) &= 2.3 \times 10^{-1} \\
\Delta_g(R_b) &= 8.0 \times 10^{-2} \\
\Delta_g(R_c) &= 4.1 \times 10^{-3} \\
\Delta_g(\sin^2 \theta_{\text{eff}}^l) &= 2.8 \times 10^{-1} \\
\Delta_g(A_{\text{FB}}^l) &= 1.2 \times 10^{-1} \\
\Delta_g(A_{\text{FB}}^b) &= 1.6 \times 10^{-1} \\
\Delta_g(A_{\text{FB}}^c) &= 5.2 \times 10^{-2} .
\end{aligned} \tag{118}$$

By comparing the various  $\Delta_c$  and  $\Delta_g$  we can obtain a rough evaluation of the global theoretical error associated with the most relevant quantities in the analysis of the LEP data. As far as the differences among codes in their preferred(adapted) set-up is concerned, we can safely conclude that the ratios of their predictions to the experimental errors are usually less than 0.15. However, the most important message to be derived from this simple exercise is that very often the theoretical uncertainty can be larger than what is to be expected on the basis of a simple comparison of the results from different calculations.

A wider sample of results is shown in Figures 11–23, where, again, we have fixed some reference point —  $M_H = 300$  GeV and  $\alpha_s(M_Z) = 0.125$  and where  $100 \text{ GeV} < m_t < 250 \text{ GeV}$ . In every figure the corresponding experimental points(data), as they are given in ref. ([15]), are shown at  $m_t = 178$  GeV. The full collection of our results refers instead to  $M_H = 60, 300, 1000$  GeV and to  $\alpha_s(M_Z) = 0.118, 0.125, 0.132$ <sup>11</sup>.

Here we discuss the main features of the comparison and for each quantity we indulge in presenting an estimate of the *global uncertainty* by roughly considering the half-difference

---

<sup>11</sup>A preliminary version of the comparison among our results has been presented in [66]



between the maximum and minimum among all predictions. Admittedly this is not a very rigorous procedure and therefore it should be treated with due caution. It should be stressed again that the  $\Delta_c, \Delta_g$  factors presented above show the half-difference of the predictions over the experimental errors. In the following discussion we will mainly analyze two quantities:

$d_c, d_g$  — the half-differences, either among central predictions or between the maximum and the minimum among all predictions.

It should be noted that we will not address in this section the question of how the transformation from primordial distributions to the secondary quantities will affect their precision. In the following we have examined some of the pseudo-observables at the standard reference point and tried to present the state of the art for their theoretical predictions without including all sorts of parametric uncertainties, but rather we have limited our discussion to the genuinely theoretical ones. Below we discuss 13 pseudo-observables.

- $M_W$   
There is a certain spread in the predictions for increasing values of  $m_t$  substantially independent of  $\alpha_s$  and increasing for large  $M_H$ , with the formation of two clusters, represented by **BHM/WOH** and **ZFITTER** on one side and **LEPTOP/TOPAZO** on the other. The maximum difference in central values is seen for  $m_t = 250$  GeV where  $d_c$  reaches a 10.5(12) MeV for  $M_H = 300(1000)$  GeV, made even more significant by the additional fact that the bands essentially do not overlap. The situation improves for central values of  $m_t$ , where we see at most a half-difference of  $\approx 4.5$  MeV even if the clustering is already evident.
- $\Gamma_e$   
No pattern of any particular relevance is observed. Almost independent of  $\alpha_s$  we notice that for intermediate  $m_t$  there is a substantial agreement for all  $M_H$ , while for high  $m_t$  the agreement is better at large values of  $M_H$ , and for small  $m_t$  it improves for low values of  $M_H$ . All the error bars tend to become wider for increasing  $m_t$  and  $M_H$ , with the possible exception of **TOPAZO/ZFITTER**. The largest half-difference among central values is for low  $M_H$  and high  $m_t$  where  $d_c$  can reach  $\approx 0.03$  MeV. A safe estimate of the overall theoretical error at  $m_t = 175$  GeV is of about 0.03 MeV ( $0.030 < d_g < 0.031$  for the full range of  $\alpha_s$  and  $M_H$ ).
- $\Gamma_Z$   
Due to the final state QCD corrections  $\Gamma_Z$  is much more sensible to variations in  $\alpha_s$ . However, we have verified that there is no substantial variation among the codes as a function of  $\alpha_s$ , a sign that final state QCD corrections are well under control. For instance we find  $1.4 \text{ MeV} < d_g < 1.5 \text{ MeV}$  for  $0.118 < \alpha_s < 0.132$  at  $m_t = 175$  GeV and  $M_H = 300$  GeV<sup>12</sup>. For low  $m_t$  the result of the comparison does not show any particular pattern, while for high  $m_t$  the agreement improves with high  $M_H$ , showing again some sort of correlation between the two variables. For intermediate

---

<sup>12</sup>This is not a trivial consequence of the fact that all five codes use the same radiation functions, since their implementation is usually different.

$m_t$ , instead we find smaller differences around central values of  $M_H$ . In general for  $m_t > 150 \div 175$  GeV the various error bands, while growing, have a tendency to overlap. The maximum deviation among codes is for high  $m_t$  and low  $M_H$ , where  $d_c$  can reach approximately 0.6 MeV. For  $m_t = 175$  GeV  $\alpha_s = 0.125$  instead we get, as the global estimate of the uncertainty, 1.3, 1.4 and 1.4 MeV for  $M_H = 60, 300$  and 1000 GeV (with tiny variations in respect of  $\alpha_s$ ).

- $R_l$

This quantity has a role of its own since quite often it is used for extracting a precise determination of  $\alpha_s(M_Z)$ . Indeed, up to some degree of accuracy, the two variables are related by  $\Delta\alpha_s \approx \pi\Delta R/R$  so that a difference of 0.01 in  $R_l$  is equivalent to an error of 0.002 in  $\alpha_s$ . There is some common trend in all our results for  $R_l$ , namely the BHM predictions always stay a little higher, while the other codes tend to cluster, apart from the TOPAZ0 results, which, for very low  $m_t$  and high  $M_H$  tend to converge towards those of BHM. For  $m_t > 175$  GeV the error bands tend to overlap so that each code has a central prediction within the other error bands, again apart from the BHM point, which sometimes is fully contained only within the WOH predictions and lies at the upper boundary of the LEPTOP/ZFITTER ones. Error bars are often very asymmetric, especially for WOH/ZFITTER. The maximal deviation is for high  $m_t, M_H$ , where  $d_c$  may reach 0.006, whereas the global estimate of the uncertainty for  $m_t = 175$  GeV gives 0.0085, 0.0090 and 0.0095 for  $\alpha_s(M_Z) = 0.118, 0.125$  and 0.132, independent of  $M_H$ . These values correspond to an error of  $0.002 \div 0.003$  in the determination of  $\alpha_s(M_Z)$ . We have also analyzed in more detail the  $\alpha_s$  dependence of the ratio  $R_l$  for  $m_t = 175$  GeV and  $M_H = 300$  GeV, including the case when QCD is switched off. Indeed, a determination of  $\alpha_s$  from  $R_l$  is usually achieved by writing  $R_l = R_l(\alpha_s = 0)(1 + \delta^{\text{QCD}})$  and by using the most updated formulation of QCD corrections (see for instance Ref. [67]). In this way, some relevance should also be attributed to a comparison of various predictions for the ratio  $R_l$ , unfolded of QCD correction terms. For  $\alpha_s = 0$  the WOH prediction is lower than the others, which cluster around 19.946 (WOH is  $-0.78 \times 10^{-2}$  below the average). When QCD corrections become active, BHM remains higher ( $0.5 \div 0.6 \times 10^{-2}$  above average) while the other codes form a cluster.

- $R_b, R_c$

The ratios of the  $b\bar{b}$  and  $c\bar{c}$  partial widths to the total hadronic width share some common features. The experimental errors are 0.0020 and 0.0098 and the two quantities are  $-38\%$  correlated. Our central predictions for  $R_b$  are all within  $2 \times 10^{-4}$  and even the inclusion of the theoretical uncertainty only gives  $d_g \approx 6 \times 10^{-4}$ . The overall theoretical error at  $m_t = 175$  GeV is  $1.7 \times 10^{-4}$ . For  $R_c$  the global uncertainty is well contained within  $6.0 \times 10^{-5}$ .  $R_b$  shows some clustering which becomes more and more evident for large  $m_t$ , with BHM giving the higher prediction and LEPTOP/TOPAZ0/WOH/ZFITTER forming a lower cluster. The behavior of  $d_g$  as a function of  $\alpha_s$  is practically flat.

- $\sin^2 \theta_{\text{eff}}^{\text{lept}}$

The reported value of the leptonic effective weak mixing angle is the average of all

forward–backward and polarization asymmetries from LEP. Therefore the analysis relies on the hypothesis that the peak forward–backward asymmetry can simply be connected with the remaining asymmetries through the use of the same  $\sin^2 \theta_{\text{eff}}^l$ . For all values of  $M_H$  and  $\alpha_s$  the agreement is less satisfactory for low  $m_t$  where ZFITTER remains on the higher side, BHM/WOH form a lower cluster and LEPTOP/TOPAZO are somewhere in between. The general trend is to have a convergence of all codes for high  $m_t$ . The maximal half-difference among central values is as for low  $m_t$ , where for all  $M_H, \alpha_s$  we find  $d_c \approx 9.0 \times 10^{-5}$ . For  $m_t = 175 \text{ GeV}$  the overall uncertainty is estimated to be  $d_g \approx 1.1 \div 1.4 \times 10^{-4}$  over the whole range  $M_H - \alpha_s$ . For  $M_H = 300 \text{ GeV}$  and  $\alpha_s = 0.125$  we find  $d_g = 1.3, 1.1, 2.1 \times 10^{-4}$  for  $m_t = 100, 175, 250 \text{ GeV}$ . In view of the supposed relevance of this parameter and of its projected experimental error we have to admit that the status of the theoretical predictions is far from satisfactory but totally related to the unknown higher order effects. To give an example, we could say that the knowledge of the sub-leading  $\mathcal{O}(G_\mu^2 M_Z^2 m_t^2)$  corrections to  $\Delta r$  would greatly improve the situation — for instance for ZFITTER, which dominates the error.

- $\sin^2 \theta_{\text{eff}}^b$

From many points of view the situation is very similar to that described for  $\sin^2 \theta_{\text{eff}}^l$ . Let us remember that  $\sin^2 \theta_{\text{eff}}^b$  differs from  $\sin^2 \theta_{\text{eff}}^l$  because of flavour-dependent corrections, which are  $m_t$ -dependent and not negligible. There is some kind of crossed behavior in our predictions, with an agreement substantially better for intermediate values of  $m_t$  and deteriorating at the boundaries. For low  $m_t$  the comparison is similar to that for  $\sin^2 \theta_{\text{eff}}^l$ : a higher prediction from ZFITTER, a central cluster LEPTOP/TOPAZO and a lower one BHM/WOH. For high  $m_t$  the highest prediction is from BHM, with a lower cluster of the other codes. The global estimate of the uncertainty for  $m_t = 175 \text{ GeV}$  and  $\alpha_s = 0.125$  is of  $1.15(1.05, 1.45) \times 10^{-4}$  for  $M_H = 60(300, 1000) \text{ GeV}$ , with an uncertainty  $\pm 0.1 \times 10^{-4}$  due to a variation in  $\alpha_s$ .

- $A_{\text{FB}}^l$

In presenting results for the leptonic forward–backward (peak) asymmetry, as well as for any other leptonic asymmetries, we follow the indication of the experimentalists who keep  $A_{\text{FB}}^l$  until the end in their standard model fits, without necessarily identifying it directly with  $\sin^2 \theta_{\text{eff}}^l$ . We first start by analyzing the comparison among the central values. Here the result of the comparison is rather good and essentially we always start at low  $m_t$  with two clusters — a higher one containing BHM/WOH and a lower one containing TOPAZO/ZFITTER and with LEPTOP somewhere in between. There is a fast convergence of all results for increasing  $m_t$ , especially for high  $M_H$ . Typically for  $m_t = 175 \text{ GeV}$  and  $M_H = 300 \text{ GeV}$  we find a half-difference of about  $8.4(8.9, 9.5) \times 10^{-5}$  for  $\alpha_s = 0.118(0.125, 0.132)$ . When we come to the inclusion of the theoretical uncertainty it is immediately evident that the previous comment still applies and the global error for the standard reference point becomes  $1.9 \div 2.0 \times 10^{-4}$  at  $\alpha_s = 0.118$ ,  $2.0 \div 2.2 \times 10^{-4}$  for  $\alpha_s = 0.125$  and  $2.0 \div 2.3 \times 10^{-4}$  for  $\alpha_s = 0.132$ , where the variation with  $M_H$  is illustrated. We will come back to  $A_{\text{FB}}^l$  and to the related uncertainty while discussing additional theoretical options which have not been included in the working set.

- $A_{\text{LR}}$

Also for the left–right (peak) asymmetry there is some general behavior in our predictions. At low  $m_t$  we start with maximal disagreement, two clusters with **BHM/WOH** in the higher one and **LEPTOP/TOPAZO** in the central one, to reach convergence of results for high  $m_t$ . For low  $m_t$  there is also a considerable spreading of the error bands. Given the fact that the SLD measurement seems to require a much higher value of  $m_t$ , we have considered the overall uncertainty for  $m_t = 250$  GeV with the result of  $1.82(1.59, 1.74) \times 10^{-3}$  for  $M_H = 60(300, 1000)$  GeV for  $\alpha_s = 0.118$ . These values become  $1.84(1.61, 1.74) \times 10^{-3}$  and  $1.86(1.63, 1.77) \times 10^{-3}$  for  $\alpha_s = 0.125$  and  $0.132$ .

- $A_{\text{FB}}^b, A_{\text{FB}}^c$

Practically everything we state for the general behavior of  $A_{\text{LR}}$  can be repeated for the  $b$ - and  $c$ - quark charge asymmetries. As for  $A_{\text{LR}}$ , the agreement is worst at low  $m_t$  and there is a general convergence at high  $M_H$  when  $m_t$  is growing. For low  $M_H$  and large  $m_t$  **TOPAZO** has the tendency to give a higher prediction. The global uncertainty for  $A_{\text{FB}}^b$  at  $m_t = 175$  GeV is  $6.2 \div 7.4 \times 10^{-4}$ . There is no general agreement among codes on the definition of  $A_{\text{FB}}^b$ . In particular **LEPTOP** and **TOPAZO** include mass effects into the definition of this pseudo-observable. For the  $b$  quark, the effect of its non-vanishing mass leads to:

$$\mathcal{A}^b = \frac{2g_v^b g_A^b}{[\frac{1}{2}(3 - v^2)(g_v^b)^2 + v^2(g_A^b)^2]} v, \quad (119)$$

where  $v$  is the  $b$  quark velocity:

$$v = \sqrt{1 - \frac{4\bar{m}_b^2(M_Z^2)}{M_Z^2}}, \quad (120)$$

where  $\bar{m}_b(M_Z^2)$  is the running  $b$ -mass in  $\overline{MS}$ -scheme defined by Eq.(59) below. However this is a very tiny effect. An estimate of it, based on **TOPAZO** results, gives an absolute deviation between the massless and massive definitions of  $1.6, 1.0, 2.0 \times 10^{-5}$  at  $m_t = 100, 175, 250$  GeV for  $M_H = 300$  GeV and  $\alpha_s = 0.125$ . Similar conclusion can be drawn for  $A_{\text{FB}}^c$ . The global uncertainty at  $m_t = 175$  GeV is  $d_g = 4.5 \div 6.0 \times 10^{-4}$ .

- $\sigma_h$

For the hadronic cross-section the theoretical error  $d_g$  is always contained in a range of  $0.0075 \div 0.0095$  nb, with very little dependence on  $\alpha_s$ . Indeed, for our standard reference point ( $m_t = 175$  GeV and  $M_H = 300$  GeV) the largest half-difference among central values is  $0.0065$  nb,  $0.0065$  nb and  $0.0070$  nb for  $\alpha_s = 0.118, 0.125$  and  $0.132$ . Our estimate of the overall theoretical error at  $m_t = 175$  GeV is of about  $0.009$  nb and the largest half-difference is seen at large  $m_t$  and  $M_H$  where it reaches  $0.0095$  nb. Over the whole range of the parameters the prediction of **WOH** remains higher with a tendency for **ZFITTER**, though only at very low values of  $m_t$ , to slightly converge towards **WOH**. In any case, the **WOH** error bands are sufficiently large to include the other predictions or to overlap with the other bands.

To summarize our results we have also presented in Table 8 the largest half-differences between central values or between maximal and minimal predictions among codes in the range  $150 \text{ GeV} < m_t < 200 \text{ GeV}$ ,  $60 \text{ GeV} < M_H < 1 \text{ TeV}$  and  $0.118 < \alpha_s < 0.125$ . In Tables 9 and 10 we have fixed  $m_t = 175 \text{ GeV}$  and illustrated the largest half-differences among central values or those between the maximum of the maxima and the minimum of the minima among the five codes in two situations:  $\alpha_s = 0.125$  fixed and  $60 \text{ GeV} < M_H < 1 \text{ TeV}$ , or  $M_H = 300 \text{ GeV}$  and  $0.118 < \alpha_s < 0.125$ . In this way the separate contributions from  $M_H$  or  $\alpha_s$  to the theoretical errors are indicatively given. A final but partial indication of our results can be provided by computing some of the quantities which usually enter the SM fits (at  $m_t = 175 \text{ GeV}$ ) and by collecting all available sources of error

$$\begin{aligned}
\text{BHM} \quad \Gamma_Z &= 2497.4^{+0.9}_{-1.0}(th.)^{+7.9}_{-8.8}(M_H, \alpha_s) \pm 6.7 \Delta\bar{\alpha}^{-1} \pm 0.8 \Delta m_b \text{ MeV} \\
\text{LEPTOP} \quad \Gamma_Z &= 2497.2 \pm 1.1(th.)^{+8.0}_{-8.5}(M_H, \alpha_s) \pm 6.8 \Delta\bar{\alpha}^{-1} \pm 0.8 \Delta m_b \text{ MeV} \\
\text{TOPAZO} \quad \Gamma_Z &= 2497.4^{+0.2}_{-0.9}(th.)^{+8.2}_{-9.1}(M_H, \alpha_s) \pm 6.8 \Delta\bar{\alpha}^{-1} \pm 0.8 \Delta m_b \text{ MeV} \\
\text{WOH} \quad \Gamma_Z &= 2497.4^{+1.5}_{-0.6}(th.)^{+8.0}_{-8.8}(M_H, \alpha_s) \text{ MeV} \\
\text{ZFITTER} \quad \Gamma_Z &= 2497.5^{+0.6}_{-0.5}(th.)^{+7.9}_{-8.7}(M_H, \alpha_s) \pm 6.8 \Delta\bar{\alpha}^{-1} \pm 0.8 \Delta m_b \text{ MeV} \quad (121)
\end{aligned}$$

$$\begin{aligned}
\text{BHM} \quad \sigma_0^h &= 41.436^{+0.006}_{-0.003}(th.) \pm 0.042(M_H, \alpha_s) \pm 0.013 \Delta\bar{\alpha}^{-1} \pm 0.007 \Delta m_b \text{ nb} \\
\text{LEPTOP} \quad \sigma_0^h &= 41.439^{+0.003}_{-0.004}(th.) \pm 0.040(M_H, \alpha_s) \pm 0.012 \Delta\bar{\alpha}^{-1} \pm 0.008 \Delta m_b \text{ nb} \\
\text{TOPAZO} \quad \sigma_0^h &= 41.437^{+0.007}_{-0.002}(th.)^{+0.041}_{-0.040}(M_H, \alpha_s) \pm 0.012 \Delta\bar{\alpha}^{-1} \pm 0.007 \Delta m_b \text{ nb} \\
\text{WOH} \quad \sigma_0^h &= 41.449^{+0.000}_{-0.012}(th.)^{+0.041}_{-0.040}(M_H, \alpha_s) \text{ nb} \\
\text{ZFITTER} \quad \sigma_0^h &= 41.441^{+0.000}_{-0.005}(th.)^{+0.041}_{-0.040}(M_H, \alpha_s) \pm 0.013 \Delta\bar{\alpha}^{-1} \pm 0.007 \Delta m_b \text{ nb} \quad (122)
\end{aligned}$$

$$\begin{aligned}
\text{BHM} \quad R_l &= 20.788^{+0.004}_{-0.008}(th.)^{+0.061}_{-0.060}(M_H, \alpha_s) \pm 0.047 \Delta\bar{\alpha}^{-1} \pm 0.009 \Delta m_b \\
\text{LEPTOP} \quad R_l &= 20.780^{+0.006}_{-0.005}(th.)^{+0.061}_{-0.059}(M_H, \alpha_s) \pm 0.046 \Delta\bar{\alpha}^{-1} \pm 0.010 \Delta m_b \\
\text{TOPAZO} \quad R_l &= 20.782^{+0.002}_{-0.005}(th.)^{+0.052}_{-0.059}(M_H, \alpha_s) \pm 0.046 \Delta\bar{\alpha}^{-1} \pm 0.010 \Delta m_b \\
\text{WOH} \quad R_l &= 20.780^{+0.013}_{-0.000}(th.)^{+0.062}_{-0.059}(M_H, \alpha_s) \\
\text{ZFITTER} \quad R_l &= 20.781^{+0.006}_{-0.001}(th.)^{+0.061}_{-0.060}(M_H, \alpha_s) \pm 0.047 \Delta\bar{\alpha}^{-1} \pm 0.009 \Delta m_b, \quad (123)
\end{aligned}$$

where we have allowed, as usual,  $60 \text{ GeV} < M_H < 1 \text{ TeV}$  and  $0.118 < \alpha_s < 0.132$ . Whenever available, the parametric uncertainties have been inserted. It is assumed that  $\Delta m_b$  is given in GeV.

## 2.7 More on Theoretical Uncertainties

There are some options on electroweak radiative corrections which, although implemented in the codes, have not been used as working options for producing our comparisons with the experimental data. The main argument for this exclusion is related to their tendency

to produce results deviating sensibly from the average. As a matter of fact, this is the visible consequence of their inclusion, but quite often we have theoretical reasons against them. This short section is devoted to a summary of those effects and of their eventual influence on the comparisons. At the end one should not forget that the design and the implementation of options is indeed something very peculiar to a given realization. The following short considerations give another illustration of a very important fact: theoretical uncertainties should be treated with due caution, realizing that they contain, in any case, a large degree of arbitrariness.

### 2.7.1 TOPAZO

With TOPAZO, the most striking effect is related to an expansion of the non-leading terms to  $\mathcal{O}(\alpha)$ , once bosonic self-energies were not re-summed. Roughly speaking, we can assume that a certain quantity  $X$  is given by (see also 2.2.4)

$$X = X_0 + \frac{\alpha}{\pi} X_1 + \mathcal{O}(\alpha^2) , \quad (124)$$

where  $X_0$ , by construction, will include all the re-summed contributions. As soon as we allow the two options,

$$X^2 = \begin{cases} \left(X_0 + \frac{\alpha}{\pi} X_1\right)^2 \\ X_0^2 + 2 \frac{\alpha}{\pi} X_0 X_1 , \end{cases}$$

and interpret the resulting difference as a theoretical uncertainty, then, under some circumstances, we end up with errors considerably larger than those presented above. The main problem is represented here by a clash between accidental cancellations and gauge invariance (even the notion of cancellation between fermionic and bosonic sector is gauge-dependent). As it is well known, the bosonic self-energies are gauge-dependent and, moreover, the fermionic ones tend to dominate away from the intermediate  $m_t$  region. That is how TOPAZO allows, among other options, for a strict resummation of the fermionic self-energies alone. Of course, one could just avoid resummation altogether, but the option of expanding versus non-expanding the remainders, with respect to the leading terms, still applies and the theoretical uncertainties would become, in this case, sensibly  $m_t$  dependent. Finally, we stress once more that the identification of a gauge invariant part of the bosonic self-energies is not at all a unique procedure and therefore some degree of arbitrariness is always hidden in a global resummation. We admit that, this option allows for a nice construction of a small remainder, in a situation, however, where we are working with one-loop contributions and higher order reducible ones. What is left out of our analysis is, in any case, related to the two-loop irreducible terms, about which nothing is presently known. To summarize we could say that in one case it is approximately the ‘square’ of the one-loop bosonic corrections that we use to estimate the theoretical error, while in the other we can decide to re-sum part of it into the leading term and make the remainder small, even though we are still missing information about not-yet-computed higher orders and their effects, which could make the smallness of the remainder inadequate.

The final reason why TOPAZO has excluded this option in presenting the pseudo-observable Tables is therefore totally related to the abnormal (as compared to the other codes) size of the errors for some of the quantities, noticeably  $A_{\text{FB}}^l$ . Here we say again that the expansion option is bounded to produce larger errors whenever the remainders are not (one way or another) kept small and in some codes this effect is not seen, simply because nothing equivalent to the expansion has been implemented. To give a quick idea of the effect we present in Table 11 the shift in the central values and in the error bands for some of the pseudo-observables. Clearly the largest effect is seen for the leptonic forward–backward asymmetry where the theoretical error becomes comparable in size to the experimental counterpart. Needless to say, when this option is activated, a large fraction of the uncertainties become TOPAZO dominated. Additional consequences will be introduced and discussed in the next chapter.

### 2.7.2 ZFITTER

About ZFITTER, one can also mention several peculiar moments, related to the specific design of its options. We begin with by making clear that nothing resembling what is described in the previous section was observed. To a large extent this is due to the fact that the coefficient  $X_1$  (see discussion in 2.2.4) happened to be small in the framework of the ZFITTER renormalization scheme. Having accepted this statement, however, one should not conclude that it has particular advantages over the other schemes. The size of the coefficient is simply a numerical accident, without any deep physical meaning.

However, ZFITTER does contain additional options, which eventually were not left among its *working options*. An example is given by the array of expansions (99). All four expansions have been implemented, and it was noted that the third and fourth expansions enlarge the theoretical uncertainty for some observables ( $M_W$  and  $\sin^2 \theta_{\text{eff}}^l$ ), roughly by factors of two and four correspondingly. As it was pointed out in section 1.10.2, the third and the fourth expansions contradict to the conclusion of paper [48] about fermionic mass singularities. It not surprising that this was the argument in favour of excluding these options from the working set.

Another interesting example is related to the leading–remainder splitting problem. Three variants of the resummation of the leading terms in  $\Delta\rho$ , see Eq. (80), were implemented as different sub-options:

- 1) only the first term, i.e.  $\Delta\rho^\alpha$ , is re-summed;
- 2) all but X terms of (80) — the content of square brackets is re-summed;
- 3) the whole expression (80) is re-summed (ZFITTER default).

There is a noticeable increase in the uncertainty when we include the second option with respect to a situation where only the first and the third are retained among the working options. One should emphasize, however, that this increase in the error is not dramatic: for example for  $\sin^2 \theta_{\text{eff}}^l$  it amounts to a nearly  $m_t$  independent uncertainty, of the order  $5 \times 10^{-5}$ . Examining the reasons for this enhancement, it was revealed that for the second option the remainder terms are about 5–10 times bigger compared to those for the first and

the third options. Moreover, they are only several times smaller than the leading terms. On the basis of this observation, the second option was termed *a pathological* option and initially excluded from the working set, since its effect contradicted to an accepted strategy. In playing more with **ZFITTER** options a striking property was observed. Some of the **ZFITTER** options do not possess the additivity property. As an example, we mention that the ‘scale of remainder option’ alone produces nearly the same uncertainty as when it is applied ‘in conjunction’ with the following two other options:

- the one dealing with expansion (99), first two rows;
- the one dealing with the three above-mentioned variants of resummation for  $\Delta\rho$ : 1)  $\div$  3).

As a consequence, the combined effect of all three options leads practically to the same uncertainty, and the latter is independent from the actual number of options included — two or three  $\Delta\rho$  resummation sub-options are left in the working set. This eventually lead to a decision to retain all 1)  $\div$  3) among working options.



### 3 Realistic distributions

To give predictions for pseudo-observables has not been our only task and we have also devoted a noticeable effort in order to present the most updated analysis for realistic observables. This process requires as fundamental ingredients a QED *dresser* and therefore the comparisons have been restricted to BHM, TOPAZO and ZFITTER, since they allow for the treatment of QED diagrams involving the emission of real photons with results which are dependent on energies and experimental cuts. Roughly speaking we can distinguish between  $s$ -channel processes and Bhabha scattering,  $e^+e^- \rightarrow e^+e^-$ . For Bhabha scattering the commonly accepted procedure is the so-called  $t$ -channel subtraction, where the  $s - t$  and  $t - t$  contributions are subtracted from the data by using the code ALIBABA [68]. In the procedure the ‘most reasonable’ values of  $m_t$  and of  $M_H$  are used leading to additional sources of errors in the analysis. Given the present situation we have also performed a comparison between ALIBABA and TOPAZO inspite of the fact that the electroweak library of ALIBABA has not been constantly updated. Thus in the comparison will emerge an intrinsic difference due to the improved electroweak and QCD formulation of TOPAZO. Our comparisons can be divided according to the following scheme:

- Fully extrapolated set-up for muonic and hadronic channel with the possible inclusion of a cut on the invariant mass of the final fermion pair, the so-called  $s'$  cut (BHM, TOPAZO, ZFITTER);
- $e^+e^- \rightarrow \mu^+\mu^-$  ( $e^+e^-$ ,  $s$ -channel for  $40^\circ < \theta_- < 140^\circ$ ,  $\theta_{\text{acoll}}^{\text{max}} = 10^\circ, 25^\circ$ , and  $E_{\text{th}}(\mu^\pm) = 20 \text{ GeV}$  ( $E_{\text{th}}(e^\pm) = 1 \text{ GeV}$ ), (TOPAZO, ZFITTER);
- $e^+e^- \rightarrow e^+e^-$  for  $40^\circ < \theta_- < 140^\circ$ ,  $\theta_{\text{acoll}}^{\text{max}} = 10^\circ, 25^\circ$ , and  $E_{\text{th}}(e^\pm) = 1 \text{ GeV}$ , (ALIBABA, TOPAZO).

Moreover, we have fixed the following set of values for the c.m.energy: 88.45, 89.45, 90.20, 91.1887, 91.30, 91.95, 93.00, 93.70 GeV. All the results refer to a given reference point,  $m_t = 175 \text{ GeV}$ ,  $M_H = 300 \text{ GeV}$  and  $\alpha_s(M_Z) = 0.125$ . A first comment concerns the  $s'$  cut, which should not be confused with a cut on the invariant mass of the event after initial state radiation (sometimes also used in the experiments). For realistic observables we have avoided all references to any specific set of *effective* formulas and to their realizations, the interested reader having available the existing literature [68]-[69]. Weak radiative corrections, depending on the assumptions of the electroweak theory, have already been discussed from the point of view of the options that arise in their practical implementation. Here we only mention that we have fully propagated those theoretical uncertainties from the pseudo-observables to the realistic ones with the result that — for the fully convoluted cross-sections and forward–backward asymmetries — the final results include a theoretical error bar. In the following we present a short discussion of the main ingredients entering the calculation of realistic observables and critically compare some of the results obtained with BHM, TOPAZO and ZFITTER.

### 3.1 De-Convoluted Distributions

To illustrate in more detail the construction of realistic observables (RO) we start from the concept of de-convoluted quantities. For a given process we construct  $\sigma_F(\sigma_B)$ , the forward(backward) kernel cross-section, including electroweak corrections, and eventually the comprehensive of a cut on the angular acceptance. QCD corrections are included while all QED corrections are left out. After a first comparison at this level we proceeded by introducing QED final-state radiation (FSR), initial-state leptonic and hadronic pair production (PP), initial-final-state QED interference (INT) and, finally, the kernel distributions folded with initial-state QED radiation (ISR). One should emphasize, however, that the INT contribution was simply added — at  $\mathcal{O}(\alpha)$  — and was not folded with the ISR. As far as the ISR is concerned we did not find it opportune to fully review the various treatments and implementations but have tried as much as possible to illustrate the origin of possible discrepancies whenever they arise. For instance, the differences that we find in the results of the various codes are dominated by pure weak (and QCD) corrections around the region of the peak and by QED radiation along the tails, where, however, the experimental error is considerably larger. Among the de-convoluted quantities, the most relevant are those computed at  $s = M_Z^2$ , which have an obvious counterpart in the pseudo-observables, that we have already computed,  $A_{\text{FB}}^l$  and  $\sigma^h$ , which hereafter will be characterized by an index 0, as  $A_{\text{FB}}^{l,0}$  and  $\sigma_0^h$ . There is, however, a noticeable difference between the two sets, represented by the interference of the  $Z - \gamma$   $s$ -channel diagrams and by the presence of imaginary parts in the formfactors, the latter being particularly relevant for the leptonic forward-backward asymmetry.

As far as the propagation of electroweak uncertainties from pseudo-observables to realistic ones is concerned we notice that all three codes see an enhancement of the theoretical errors. For instance for the standard reference point we denote with  $\sigma_0^h$  the PO hadronic (peak) cross-section and with  $\sigma^h(M_Z^2)$  the realistic one and get:

$$\begin{array}{lll}
\text{BHM} & \sigma_0^h & = 41.436_{-0.003}^{+0.006} \text{ nb} & \sigma^h(M_Z^2) = 30.366_{-0.002}^{+0.015} \text{ nb} \\
\text{TOPAZO} & \sigma_0^h & = 41.437_{-0.002}^{+0.007} \text{ nb} & \sigma^h(M_Z^2) = 30.375_{-0.005}^{+0.016} \text{ nb} \\
\text{ZFITTER} & \sigma_0^h & = 41.441_{-0.005}^{+0.000} \text{ nb} & \sigma^h(M_Z^2) = 30.373_{-0.002}^{+0.005} \text{ nb} ,
\end{array} \tag{125}$$

the enhancement factor being 1.9, 2.3 and 1.4 for the three codes respectively. The reason behind this increase of the induced theoretical error is that for  $\sigma_0^h$ , as defined in Eq. (31), we first compute  $\Gamma_e, \Gamma_h$  and  $\Gamma_Z$  and then construct the combination  $\Gamma_e \Gamma_h / \Gamma_Z^2$  without any further expansion in  $\alpha$ , while for  $\sigma^h(M_Z^2)$  we include the expansion in the option set (linearization of the cross-section), thus enlarging the error.

### 3.2 Final-State Radiation

A substantial difference exists between fully extrapolated RO and RO in the presence of cuts. This is illustrated by the fact that without cuts we can simply use the well known correction factor  $1 + \frac{3}{4} Q_f^2 \frac{\alpha}{\pi}$  for each partial channel and there is therefore no ambiguity in FSR. A possible source of discrepancy can instead be introduced when cuts are present, due to a different treatment of final-state higher-order QED effects. This can lead to

differences which in general depend on the experimental cuts required and may grow for particularly severe cuts. It has already been shown [4] that two possible prescriptions, — completely factorized final-state QED correction versus factorized leading-terms and non-leading contributions summed up — lead to differences in the cross-section for Bhabha scattering of the order of 0.5% far from the peak, whereas the asymmetry is substantially left unchanged. To be more specific, the final-state QED corrections amount to a leading correction term:

$$F_{\text{cut}}^l(s) = 2\frac{\alpha}{\pi}Q_f^2 \ln\left(1 - \frac{s_0}{s}\right) \left[ \ln\left(\frac{s}{m_f^2}\right) - 1 \right] , \quad (126)$$

where  $s_0$  represents a cut in the reduced invariant mass. Renormalization group arguments suggest that such a leading term should be exponentiated, which is of no practical importance at low thresholds but could give sizeable effects at high thresholds. By defining

$$F_{\text{cut},r}^\pm(s) = F_{\text{cut},\alpha}^\pm(s) - F_{\text{cut}}^l(s) , \quad (127)$$

the leading term resummation can be implemented as follows:

$$F_{\text{cut}}^\pm(s) = \exp\left[F_{\text{cut}}^l(s)\right] \left[1 + F_{\text{cut},r}^\pm(s) - F_{\text{cut},r}^\pm(s)F_{\text{cut}}^l(s)\right] , \quad (128)$$

where spurious terms  $F_{\text{cut}}^l(s) \times F_{\text{cut},r}^\pm(s)$  are confined at least at  $\mathcal{O}(\alpha^3)$ . Indeed, several prescriptions for treating final-state correction are possible, all equivalent at  $\mathcal{O}(\alpha)$ . One reasonable recipe could be to define the leading term in a different way. For instance, in the presence of an acollinearity cut, the infrared logarithm could be defined as

$$l = \ln(1 - x) , \quad (129)$$

where  $x$  is given by

$$x = \max(s_0/s, y_T) , \quad (130)$$

$y_T$  being

$$y_T = \frac{1 - \sin(\zeta/2)}{1 + \sin(\zeta/2)} , \quad (131)$$

and  $\zeta$  the maximum acollinearity allowed. Another possibility would be to exponentiate the full  $\mathcal{O}(\alpha)$  contribution  $F_{\text{cut},\alpha}^\pm$ , even though there is no guarantee that the experimental cut-dependent terms do exponentiate; in this case spurious terms appear already at  $\mathcal{O}(\alpha^2)$ . Alternatively, one could choose to factorize only a leading  $\mathcal{O}(\alpha)$  term and simply add the  $\mathcal{O}(\alpha)$  correction due to the acollinearity cut (this simulates the choice in Ref. [68]).

### 3.3 Initial-State Pair Production and QED Interference

Next we come to the inclusion of initial-state pair production in the realistic distributions. A fermionic pair of four-momentum  $q^2$  radiated from the  $e^+$  or  $e^-$  line gives a correction [70]:

$$\begin{aligned}
\sigma_{rm\text{pair}} &= \sigma_{\text{pair}}^{S+V} + \sigma_{\text{pair}}^H, \\
\sigma^S &= \int_{4m^2}^{\Delta^2} dq^2 \int_{(\sqrt{s}-\Delta)^2}^{(\sqrt{s}-\sqrt{q^2})} ds' \frac{d^2\sigma}{dq^2 ds'}, \\
\frac{d\sigma^H}{dz} &= s \int_{4m^2}^{(1-\sqrt{z})^2 s} dq^2 \frac{d^2\sigma}{dq^2 ds'}.
\end{aligned} \tag{132}$$

Also for this term there are different treatments — we can exponentiate the pair production according to the YFS formalism [71] or the same pairs can be included at  $\mathcal{O}(\alpha^2)$ . In the end, however, we found a reasonable agreement among the results of the three codes relative to the specific inclusion of pair production. The main features of this correction term are as follows.

- **TOPAZ0/ZFITTER** employ the KKKS formulation [70] without exponentiating the soft+virtual part, which is added linearly to the cross-section. **BHM**, instead employs the YFS formalism [71]. The independence of the results from the soft–hard separator has also been successfully investigated.
- $\tau$ -pairs are not included.
- The lower limit of integration  $z_{\min}$ , adopted for leptonic pair production, is 0.25 and the soft–hard separator  $\Delta$  has been fixed in the region where we see a plateau of stability.

Initial–final QED interference has been introduced in the calculations, including the effects of hard photons. For a fully extrapolated set-up this means that all photons, up to the maximum available energy, are taken into account, while  $s'$  cuts or energy thresholds and acollinearity cuts will restrict the available phase space. In order to proceed step-by-step we have introduced the procedure of comparing our results in the sequence  $\sigma_{F(B)}(NN, NY, YN, YY)$ , where the first argument in parenthesis denotes inclusion or exclusion of PP, and the second refers to the interference. In this way the relative influence of QED corrections has been checked and kept under control. To illustrate the trend, we present in Tables 12 and 13 a comparison for the hadronic cross-section and the muonic forward–backward asymmetry. In particular, to continuously keep under control our comparisons, we have introduced and analyzed the ratios

$$r(\text{C-TOPAZ0, conf}, O) = \frac{dO(\text{C-TOPAZ0, conf})}{dO(\text{C-TOPAZ0, NN})}, \tag{133}$$

where  $O = \sigma^h, \sigma^\mu, A_{\text{FB}}^\mu$ , conf = YN/NY/YY and C = **BHM**, **ZFITTER**. Moreover,  $dO$  denotes the relative variation for cross-sections and the absolute deviation for the asymmetry. Whenever pair production or QED interference have similar effects, the corresponding ratio assumes values of around 1. When the ratio goes to zero it is a signal that the apparent agreement does not reflect a similar agreement in the NN quantities and is therefore due to accidental compensations. Finally, if this ratio grows in modulus it gives

an indication that the agreement at the NN level is not respected when PP or INT are introduced.

To illustrate this fact, consider Table 12, which refers to  $\sigma^h$ . We find, for instance, that the YY cross-sections for ZFITTER-TOPAZO agree in five digits at  $\sqrt{s} = 89.45$  GeV, 90.20 GeV and 91.30 GeV, giving 10.042 nb, 17.992 nb and 30.514 nb respectively. Moreover, a closer look reveals that

$$\begin{aligned}
\sqrt{s} &= 89.45 \text{ GeV} & 10.067 - 10.068 \text{ nb} \\
\sqrt{s} &= 90.20 \text{ GeV} & 18.039 - 18.040 \text{ nb} \\
\sqrt{s} &= 91.30 \text{ GeV} & 30.590 - 30.590 \text{ nb}
\end{aligned} \tag{134}$$

for ZFITTER/TOPAZO in the NN configuration.

### 3.4 Imaginary Parts of the Formfactors

The presence of imaginary parts in the weak formfactors introduces additional possibilities for the implementation of radiative corrections with respect to pseudo-observables. At the level of the kernel cross-sections and remembering the quite general subdivision into leading parts and remainders introduced in section 2.2.1, we can basically select two possible options:

- Imaginary parts confined in the remainders,
- Imaginary parts inserted into the leading terms.

To illustrate the effect of imaginary parts we select  $f = \mu$  and consider the asymmetric part of the angular distribution for  $e^+e^- \rightarrow \mu^+\mu^-$ . If we denote with  $\chi_\gamma$  and  $\chi_Z$  the corrected  $\gamma - \gamma$  and  $Z - Z$  propagators, this asymmetric part is proportional to

$$\begin{aligned}
\sigma_F - \sigma_B &\propto \text{Re} \left[ \left( g_A^* \right)^2 \chi_\gamma \chi_Z^* \right] + \left[ \text{Re} \left( g_V g_A^* \right) \right]^2 |\chi_Z|^2 + \text{boxes} \\
&= \text{Reg}_A^2 \text{Im} \chi_\gamma \text{Im} \chi_Z + 2 \text{Reg}_A \text{Im} g_A \text{Re} \chi_\gamma \text{Im} \chi_Z \\
&\quad + (\text{Reg}_A)^2 (\text{Reg}_V)^2 + \mathcal{O}(\text{Re} \chi_Z) + \mathcal{O}(\text{Reg}_V \times \text{Im}^2) + \mathcal{O}(\text{Im}^4), \tag{135}
\end{aligned}$$

where  $\text{Re} \chi_Z$  is suppressed around the  $Z$  peak and  $\text{Reg}_V$  is usually small.

### 3.5 Initial-State QED Uncertainties

An estimate of the theoretical uncertainty due to QED radiation can also be derived, so that our results may contain two sources of theoretical error,  $\pm \Delta(EW) \pm \Delta(QED)$ . For instance such an estimate can be performed by using the following algorithm. Since the main source of QED theoretical uncertainty is the treatment of final-state radiation, namely the use of a completely factorized formula versus a leading-log factorized plus a

non-log additive one, whenever the theoretical error is required, we can run over the two possible options and return the corresponding uncertainty. Moreover, when the large-angle Bhabha scattering is considered, we must realize that the main approximation adopted by TOPAZ0 is to treat the  $t$  and  $s + t$  contributions to the cross-section at the leading logarithmic level. Thus the size of the convoluted  $t$  and  $s + t$  terms is computed as the difference between the full Bhabha prediction and the pure  $s$ -channel one and the theoretical error is estimated by assuming 1% of the difference. In particular, this means that the QED theoretical error depends on the detailed experimental set-up, growing when tightening the experimental cuts and, for the Bhabha case, when enlarging the angular acceptance to smaller angles, since this increases the contribution of the non- $s$  terms to the Bhabha cross-section. In the case of Bhabha scattering, the calorimetric measurement problem arises if a cross-section not inclusive of the energy of the outgoing fermion is considered. For thresholds of the order of  $\approx 1$  GeV the effect is of order  $0.01 \div 0.02\%$ , but for higher energy thresholds ( $E_{\text{th}}$ ) the contribution can grow considerably.

### 3.6 Comparisons

Let us now consider the question of de-convoluting the peak quantities in order to extract pseudo-observables like  $\sigma_0^h$  and  $A_{\text{FB}}^{l,0}$ . By definition the de-convoluted asymmetry does not include final-state QED radiation, while the de-convoluted cross-sections include both QED and QCD final-state corrections. For  $\sqrt{s} = M_Z$  GeV the three codes predict a hadronic cross-section of 30.366 nb, 30.375 nb and 30.373 nb respectively. The corresponding de-convoluted quantities — no QED corrections — are 41.400 nb, 41.409 nb and 41.402 nb which, in turn, means that for BHM the effect of extracting QED corrections amounts to 11.034 nb, for ZFITTER 11.029 nb, and for TOPAZ0, also 11.034 nb with a 0.045% difference. If we introduce

$$\sigma^h = \mathcal{D}[\sigma^h] (1 + \delta_{\text{conv}}) , \quad (136)$$

where  $\mathcal{D}$  denotes de-convolution, we get

$$\delta_{\text{conv}}(\text{B,T,Z}) = -0.2665 , \quad -0.2665 , \quad -0.2664 . \quad (137)$$

From our previous tables we also find that for the same choice of input parameters

$$\sigma_0^h(\text{B,T,Z}) = 41.436 , \quad 41.437 , \quad 41.441 \text{ nb} . \quad (138)$$

The corresponding differences as compared to the de-convoluted observables, which are 0.036 nb, 0.028 nb and 0.039 nb, give an estimate of about 0.011 nb for the uncertainty in the effect of the imaginary parts from the weak formfactors. Coming now to the asymmetry we find:

$$A_{\text{FB}}(\text{B,T,Z}) = -0.00082 , \quad -0.00125 , \quad -0.00109 \quad (139)$$

at  $\sqrt{s} = M_Z$ , becoming after de-convolution,

$$\mathcal{D}A_{\text{FB}}(\text{B,T,Z}) = 0.0169 , \quad 0.0166 , \quad 0.0166 . \quad (140)$$

Thus the effect of de-convolution is 0.0177, 0.0179 and 0.0177 in BHM , TOPAZO and ZFITTER, with a BHM/ZFITTER-TOPAZO difference of  $2.0 \times 10^{-4}$ . It must be noted that the quantity usually reported in the literature is the de-convoluted peak asymmetry with a pure  $Z$  exchange. In this case our predictions become

$$\mathcal{D}A_{\text{FB}}(\text{B,T,Z}) = 0.01544(0.01544) , \quad 0.01536(0.01536) , \quad 0.01528(0.01531) , \quad (141)$$

where in parenthesis we have included the corresponding prediction for  $A_{\text{FB}}^{l,0}$ . Therefore this additional and conventional filtering of the asymmetry brings the BHM-TOPAZO difference to  $8.5 \times 10^{-5}$  and the ZFITTER-TOPAZO difference to  $-8.0 \times 10^{-5}$ . The various combinations of de-convoluted asymmetries are presented in Table 14. The complete set of de-convoluted quantities is presented in Table 15, where, around the peak, we see the largest difference among codes of 0.04% and of 0.02% for  $\sigma^\mu, \sigma^h$ . For the muonic cross-section we find at  $\sqrt{s} = M_Z$  1.4785 nb, 1.4790 nb and 1.4794 nb, while the corresponding de-convoluted quantities are 2.0015 nb, 2.0019 nb and 2.0022 nb respectively. Thus the effect of de-convolution in  $\sigma^\mu$  is  $-0.2613, -0.2611$  and  $-0.2611$  for BHM, TOPAZO and ZFITTER. An interesting question, which arises in this contest, is related to the possibility of performing a real and significant test of the QED corrections by comparing the predictions of different codes. We could define

$$\delta_{\text{QED}}^i(O^i) = \frac{O^i}{O_0^i} - 1 \quad (142)$$

for a given observable  $O$ , with  $O_0^i$  being the de-convoluted observable as predicted by the  $i$ -th code. For a given code this  $\delta_{\text{QED}}$  represents the effect of the convolution over an electroweak-corrected observable. It must however be noted that the comparison of  $\delta_{\text{QED}}$  of different codes does not give an unambiguous information on QED corrections since we start already from slightly different kernels. Let us quantify this statement. Let  $\Delta_{\text{QED}}^i$  be the absolute QED correction for some observable  $O$  as computed by the  $i$ -th code:

$$O^i = O_0^i + \Delta_{\text{QED}}^i . \quad (143)$$

Then

$$\delta_{\text{QED}}(O^i) = \frac{\Delta_{\text{QED}}^i}{O_0^i} , \quad (144)$$

so that the difference between  $\delta_{\text{QED}}$  of different codes can be written as

$$\delta_{\text{QED}}(O^i) - \delta_{\text{QED}}(O^j) = \frac{\Delta_{\text{QED}}^i}{O_0^i} - \frac{\Delta_{\text{QED}}^j}{O_0^j} . \quad (145)$$

By adding and subtracting  $\Delta_{\text{QED}}^i/O_0^j$  one obtains

$$\delta_{\text{QED}}(O^i) - \delta_{\text{QED}}(O^j) = \Delta_{\text{QED}}^i \frac{O_0^j - O_0^i}{O_0^i O_0^j} + \frac{1}{O_0^j} (\Delta_{\text{QED}}^i - \Delta_{\text{QED}}^j) . \quad (146)$$

Now it is clear that the difference between  $\delta_{\text{QED}}$  of different codes depends also on the differences in the pure weak and QCD libraries of the codes. In particular, for the leptonic asymmetries in the  $Z$  peak region, which are small, the first term in the r.h.s. of the last equation becomes very large, so that  $\delta_{\text{QED}}(O^i) - \delta_{\text{QED}}(O^j)$  is weak- and QCD- dominated, whereas it becomes QED-dominated far from the peak only.

Coming back to our original strategy we have made a constant effort to understand the systematics inherent in the extraction of pseudo-observables from the realistic distributions that the experiments should consider as a theoretical uncertainty. The main ingredient contributing to the systematics is of course the QED radiation, inclusive of initial-final interference and of initial-state pair-production. But in the extraction, some relevance must also be attributed to the imaginary parts of the formfactors and to the  $Z - \gamma$  interference. The latter may have some influence, since not all the codes have the same splitting of the  $\gamma f \bar{f}$  vertices among the formfactors. We have already devoted some detailed discussion to the differences among the convolutions around the peak. In Table 16, we give all the remaining results, corresponding to the full set of the energy points. With due caution as to the correct interpretation of our comparison we observe a somehow larger difference in the convolution around the tails with respect to the peak region, notably 0.23% at  $\sqrt{s} = 88.45$  GeV and 0.59% at  $\sqrt{s} = 93.70$  GeV. Since these are differences in  $\delta_{\text{conv}}$  and not in the total prediction, even 0.6% away from the peak is quite reasonable.

Our results are presented in Figures 24 – 37 where we have reported  $\sigma^\mu$  and  $A_{\text{FB}}^\mu$  for four different set-ups: fully extrapolated,  $s' > 0.5 s$  and  $40^\circ < \theta_- < 140^\circ$ ,  $E_{\text{th}} > 20$  GeV,  $\theta_{\text{acoll}} < 10^\circ, 25^\circ$ . Also reported are  $\sigma^h$  for two set-ups, fully extrapolated and  $s' > 0.01 s$  and the  $s$  channel  $\sigma^e, A_{\text{FB}}^e$  where, however,  $E_{\text{th}} > 1$  GeV.

In all these figures we have also shown the deviations (relative for cross-sections and absolute for the asymmetry) BHM-TOPAZO (when available) and ZFITTER-TOPAZO with the corresponding theoretical error bars. The choice of TOPAZO as a reference point is purely technical and avoids the necessity of introducing an average among the codes. It emerges from these comparisons that for a fully extrapolated set-up, the agreement for the muonic cross-section for energies below the peak and around it is quite reasonable, always taking the intrinsic error as a reference. Given the reasonable agreement at the level of de-convoluted cross-sections and once we have observed that the de-convolution is satisfactory for hadrons, we come to the conclusion that for muons the low- $q^2$  region, where mass effects may become relevant, gives the dominant difference in  $\sigma^\mu$ . Indeed, a comparison for  $s' > 0.5 s$  shows a much better agreement, giving 1.4391 nb, 1.4396 nb and 1.4397 nb for the three codes (instead of 1.4785, 1.4790, 1.4794). Since the corresponding de-convoluted quantities are 1.9599 nb for BHM and 1.9605 nb for TOPAZO we conclude that de-convolutions amount to  $-0.2657$  for both codes, while for fully extrapolated they are  $-0.2613$  versus  $-0.2611$  with a 0.08% of relative difference. Around the peak, the energy-dependence of the observables as predicted by BHM looks different — a difference which should probably be related to the way in which BHM implements the effective coupling language. For the hadronic cross-section we observe a consistent agreement among the three codes. Finally, for the muonic asymmetry the agreement at the peak is again quite reasonable, but the energy dependence again looks different, with BHM/TOPAZO agreeing below the peak and TOPAZO/ZFITTER agreeing above it. To summarize the status of



the comparison for extrapolated set-up or for  $s'$ -cut we have from Figures 24 — 29 the following.

- $\sigma^\mu$

Around the peak the maximum deviation is  $9 \times 10^{-4}$  nb corresponding to 0.06%, the BHM predictions are always lower, those of ZFITTER higher, and TOPAZ0 is in-between. On the high energy side the BHM behavior with energy tends to differ. For an  $s'$ -cut of 0.5 s the maximum deviation around the peak corresponds to 0.04% and on the low-energy side of the resonance we observe a rather remarkable agreement among all codes.

- $\sigma^h$

For the hadronic cross-section we have found an impressive agreement around the peak, with 0.03% of maximum relative deviation, which is only slightly worse around the tails — 0.08% and 0.06%. The comparison remains substantially unchanged for a low  $s'$  cut.

- $A_{\text{FB}}^\mu$

Here the agreement is quite reasonable at the peak, with an absolute deviation of  $4.3 \times 10^{-4}$  between BHM and TOPAZ0. Not completely satisfactory is the energy dependence, which registers a substantial disagreement with ZFITTER giving higher predictions below the peak and BHM after it. At least on the low-energy side the situation improves if an  $s' = 0.5$  s cut is imposed.

The agreement between TOPAZ0 and ZFITTER remains rather remarkable even when the geometrical acceptance is constrained, and as well, final-state energies and the acollinearity angle are bounded with or without QED initial-final interference. For instance, for the  $s$ -channel leptonic cross-sections at  $\sqrt{s} = M_Z$  and  $40^\circ < \theta_- < 140^\circ$ ,  $E_{\text{th}}(\mu) > 20$  GeV,  $E_{\text{th}}(e) > 1$  GeV, we find

$\sigma^\mu$ ,	$\theta_{\text{acoll}} < 10^\circ$	0.9802 – 0.9801 nb	
$\sigma^\mu$ ,	$\theta_{\text{acoll}} < 25^\circ$	0.9905 – 0.9900 nb	
$\sigma^e$ ,	$\theta_{\text{acoll}} < 10^\circ$	0.9886 – 0.9884 nb	
$\sigma^e$ ,	$\theta_{\text{acoll}} < 25^\circ$	1.0012 – 1.0011 nb ,	(147)

where the first entry is ZFITTER and the second TOPAZ0. More generally, and remembering that we use  $E_{\text{th}} > 20$  GeV for muons and a lower cut of 1 GeV for electrons, we find from Figures 30 – 37:

- $\sigma^{\mu,e}$

for the muonic cross-section there is very good agreement for all energies and  $\theta_{\text{acoll}} < 10^\circ$  — agreement which slightly deteriorates for  $\theta_{\text{acoll}} < 25^\circ$ . At the peak we have a relative difference of 0.02%, 0.05% respectively for two above mentioned  $\theta_{\text{acoll}}$ . (0.03% for a fully extrapolated set-up). For  $s$ -channel electrons the agreement is everywhere of the same quality: in particular at the peak we find a 0.02%, 0.01% of relative TOPAZ0/ZFITTER deviation — for  $\theta_{\text{acoll}} < 10, 25^\circ$ . Thus for  $\sigma^l$  our agreement is not altered by introducing cuts.

- $A_{\text{FB}}^{\mu,e}$

The two leptonic forward–backward asymmetries agree at the peak at the level of  $0.3, 4.3 \times 10^{-4}$  for muons ( $\theta_{\text{acoll}} < 10, 25^\circ$ ) and  $2.9, 0.1 \times 10^{-4}$  for electrons. For  $\theta_{\text{acoll}} < 10^\circ$  the agreement tends to deteriorate at larger energies, reaching  $9.6 \times 10^{-4}$  for muons and  $8.7 \times 10^{-4}$  for electrons at  $\sqrt{s} = 93.70$  GeV, while remaining always very good for  $\theta_{\text{acoll}} < 25^\circ$ . Globally for  $A_{\text{FB}}^\mu$  the TOPAZ0-ZFITTER comparison shows for the fully extrapolated set-up a larger difference on the low-energy side of the resonance ( $1.0 \times 10^{-3}$  at  $\sqrt{s} = 88.45$  GeV), a maximal agreement over the whole range of energies for  $\theta_{\text{acoll}} < 25^\circ$ , and a larger difference on the high-energy side for  $\theta_{\text{acoll}} < 10^\circ$  ( $9.6 \times 10^{-4}$  at  $\sqrt{s} = 93.70$  GeV).

We illustrate the electroweak theoretical error by considering  $\sigma^\mu$  at  $\sqrt{s} = M_Z$ . In the four different set-ups considered — fully extrapolated,  $s'$ -cut of  $0.5$  or  $40^\circ < \theta_- < 140^\circ$ ,  $E_{\text{th}} > 20$  GeV, and  $\theta_{\text{acoll}} < 10^\circ$  or  $< 25^\circ$  — we find  $0.095\%$ ,  $0.097\%$ ,  $0.066\%$  and  $0.068\%$ , respectively, in the relative deviation between the maximum and minimum predictions among the codes.

Finally, we illustrate the effect of different treatments of final state QED radiation in the presence of severe kinematical cuts. By adopting different strategies TOPAZ0 predicts for  $\sigma^\mu$  at  $\sqrt{s} = M_Z$  and  $40^\circ < \theta_- < 140^\circ$ ,  $E_{\text{th}} > 20$  GeV,  $\theta_{\text{acoll}} < 10^\circ$ :

$$\sigma^\mu = 0.9801 - 0.9817 \text{ nb} , \quad (148)$$

while for a loose cut of  $E_{\text{th}} > 1$  GeV we obtain

$$\sigma^\mu = 0.9892 - 0.9893 \text{ nb} . \quad (149)$$

As already discussed, the  $0.16\%$  difference at large  $E_{\text{th}}$  reduces to a mere  $0.01\%$  at low  $E_{\text{th}}$ .

Coming now to the full Bhabha cross-section and forward–backward asymmetry, we have considered in the following a comparison between the results of TOPAZ0 and of ALIBABA. As already explained, the comparison is not fully consistent as it stands now, because the electroweak and QCD libraries of ALIBABA are not up-to-date. Nevertheless, we show it because it gives an impression of the state-of-the-art. For this particular comparison the input parameters are slightly different from our default — namely  $m_t = 174$  GeV and  $\alpha_s = 0.124$  have been used. The ALIBABA-TOPAZ0 comparison for  $\sigma^e$  is shown in Tables 17 for  $40^\circ < \theta_- < 140^\circ$ ,  $E_{\text{th}} > 1$  GeV and  $\theta_{\text{acoll}} < 10^\circ$ . For TOPAZ0 we have shown three sets of numbers, all including QED interference, with the first two showing the effect of a different treatment of QED final-state radiation — I is the TOPAZ0 default, while II is the ZFITTER-like default, and III shows the effect of initial state pair production, which is, however, not included in ALIBABA. It should be mentioned at this point that the insertion of pair production is strictly valid in TOPAZ0 only for s-channel processes [4] and that it is approximate for full Bhabha. The cross-section is shown for ALIBABA with its numerical error, while for TOPAZ0 we give first the electroweak theoretical error and than the numerical one. Expressing due caution in comparing the two codes we observe a relative difference, of  $0.05\%$  at the low-energy side of the resonance, which becomes  $0.003 \div 0.004\%$  around it, with a visible deterioration at high energies where we reach

0.86%. As already discussed [4], this is mainly due to a different treatment of higher-order QED final-state corrections.

A more detailed comparison between **ALIBABA** and **TOPAZ0** is shown in Tables 18-25. We have shown the predictions for the full Bhabha cross-section and the forward-backward asymmetry for two different values of  $\theta_{\text{acoll}}$  in Tables 17-20. In Tables 21-22 we give the relative deviation between the central values of **ALIBABA-TOPAZ0** for full Bhabha or for the  $s$ -channel alone. Next in Table 23 we give the difference between full Bhabha and  $s$ -channel results both in **ALIBABA** and in **TOPAZ0** with the relative contribution, i.e.  $\delta = \sigma/\sigma(s) - 1$  and  $\delta(A)/\delta(T)$ . In Table 24 we show the  $s + t$ ,  $s$  and  $t$  forward-backward asymmetries. Finally in Table 25 we give a rough estimate of the theoretical uncertainty by considering the difference between maximal and minimal predictions from the two codes. For **ALIBABA** this takes into account the numerical error alone while for **TOPAZ0** we have added linearly the electroweak and the numerical uncertainty. With due caution in the interpretation we extract a  $0.1 \div 0.2\%$  before and around the  $Z$  resonance which becomes as large as  $0.9 \div 1.0\%$  at higher energies.

## 4 Basic Formulae for Electroweak Radiative Corrections

In this section we give a more detailed description of the *realizations* of the effective couplings  $g_V$  and  $g_A$ .

### 4.1 BHM/WOH basics

#### 4.1.1 Self-energies, propagators, and $\Delta r$

The radiative corrections to the photon- $Z$  propagator system (considering only the transverse parts  $\sim g_{\mu\nu}$ ) can be obtained by inversion of the matrix

$$(\mathbf{D}_{\mu\nu})^{-1} = i g_{\mu\nu} \begin{pmatrix} k^2 + \hat{\Sigma}^{\gamma\gamma}(k^2) & \hat{\Sigma}^{\gamma Z}(k^2) \\ \hat{\Sigma}^{\gamma Z}(k^2) & k^2 - M_Z^2 + \hat{\Sigma}^{ZZ}(k^2) \end{pmatrix}, \quad (150)$$

with the renormalized self energies specified below, yielding

$$\mathbf{D}_{\mu\nu} = -i g_{\mu\nu} \begin{pmatrix} D_\gamma & D_{\gamma Z} \\ D_{\gamma Z} & D_Z \end{pmatrix}, \quad (151)$$

where ( $s = k^2$ )

$$\begin{aligned} D_\gamma(s) &= \frac{1}{s + \hat{\Sigma}^{\gamma\gamma}(s) - \frac{[\hat{\Sigma}^{\gamma Z}(s)]^2}{s - M_Z^2 + \hat{\Sigma}^{ZZ}(s)}}, \\ D_Z(s) &= \frac{1}{s - M_Z^2 + \hat{\Sigma}^{ZZ}(s) - \frac{[\hat{\Sigma}^{\gamma Z}(s)]^2}{s + \hat{\Sigma}^{\gamma\gamma}(s)}}, \\ D_{\gamma Z}(s) &= -\frac{\hat{\Sigma}^{\gamma Z}(s)}{[s + \hat{\Sigma}^{\gamma\gamma}(s)][s - M_Z^2 + \hat{\Sigma}^{ZZ}(s)] - [\hat{\Sigma}^{\gamma Z}(s)]^2}. \end{aligned} \quad (152)$$

The building blocks of Eq. (150) are the renormalized self-energies  $\hat{\Sigma}$ , which are decomposed into unrenormalized ones  $\Sigma$  and counter terms, as follows:

$$\begin{aligned} \hat{\Sigma}^{\gamma\gamma}(k^2) &= \Sigma^{\gamma\gamma}(k^2) + \delta Z_2^\gamma k^2, \\ \hat{\Sigma}^{ZZ}(k^2) &= \Sigma^{ZZ}(k^2) - \delta M_Z^2 + \delta Z_2^Z (k^2 - M_Z^2), \\ \hat{\Sigma}^{WW}(k^2) &= \Sigma^{WW}(k^2) - \delta M_W^2 + \delta Z_2^W (k^2 - M_W^2), \\ \hat{\Sigma}^{\gamma Z}(k^2) &= \Sigma^{\gamma Z}(k^2) - \delta Z_2^{\gamma Z} k^2 + (\delta Z_1^{\gamma Z} - \delta Z_2^{\gamma Z}) M_Z^2. \end{aligned} \quad (153)$$

In the last line the abbreviations ( $i = 1, 2$ )

$$\delta Z_i^{\gamma Z} = \frac{c_W s_W}{c_W^2 - s_W^2} (\delta Z_i^Z - \delta Z_i^\gamma)$$

and

$$s_w^2 = 1 - M_w^2/M_Z^2, \quad c_w^2 = 1 - s_w^2$$

were used.

The self-energies  $\Sigma^{ij}$  in (153) are the sum of the electroweak one-loop diagrams [2], completed in the quark loops by the  $\mathcal{O}(\alpha\alpha_s)$  two-loop QCD-electroweak contributions.

The mass counter terms for  $W$  and  $Z$  follow from the on-shell conditions for the  $W$  and  $Z$  propagators:

$$\begin{aligned} \delta M_w^2 &= \mathcal{R}e \Sigma^{ww}(M_w^2), \\ \delta M_Z^2 &= \mathcal{R}e \left\{ \Sigma^{ZZ}(M_Z^2) - \frac{[\hat{\Sigma}^{\gamma Z}(M_Z^2)]^2}{M_Z^2 + \hat{\Sigma}^{\gamma\gamma}(M_Z^2)} \right\}. \end{aligned} \quad (154)$$

The other renormalization constants in (153) are given by the following set of equations:

$$\begin{aligned} \delta Z_2^\gamma &= -\Pi^\gamma(0) \equiv -\frac{\partial \Sigma^{\gamma\gamma}}{\partial k^2}(0), \\ \delta Z_1^\gamma &= -\Pi^\gamma(0) - \frac{s_w}{c_w} \frac{\Sigma^{\gamma Z}(0)}{M_Z^2}, \\ \delta Z_2^Z &= -\Pi^\gamma(0) - 2 \frac{c_w^2 - s_w^2}{s_w c_w} \frac{\Sigma^{\gamma Z}(0)}{M_Z^2} + \frac{c_w^2 - s_w^2}{s_w^2} \left( \frac{\delta M_Z^2}{M_Z^2} - \frac{\delta M_w^2}{M_w^2} \right), \\ \delta Z_1^Z &= -\Pi^\gamma(0) - \frac{3c_w^2 - 2s_w^2}{s_w c_w} \frac{\Sigma^{\gamma Z}(0)}{M_Z^2} + \frac{c_w^2 - s_w^2}{s_w^2} \left( \frac{\delta M_Z^2}{M_Z^2} - \frac{\delta M_w^2}{M_w^2} \right), \\ \delta Z_2^W &= -\Pi^\gamma(0) - 2 \frac{c_w}{s_w} \frac{\Sigma^{\gamma Z}(0)}{M_Z^2} + \frac{c_w^2}{s_w^2} \left( \frac{\delta M_Z^2}{M_Z^2} - \frac{\delta M_w^2}{M_w^2} \right), \\ \delta Z_1^W &= -\Pi^\gamma(0) - \frac{3 - 2s_w^2}{s_w c_w} \frac{\Sigma^{\gamma Z}(0)}{M_Z^2} + \frac{c_w^2}{s_w^2} \left( \frac{\delta M_Z^2}{M_Z^2} - \frac{\delta M_w^2}{M_w^2} \right). \end{aligned} \quad (155)$$

The photon vacuum polarization  $\Pi^\gamma(0)$  contains as its light fermion part the quantity  $\Delta\alpha$  discussed in section 1.2. The last two constants  $\delta Z_i^W$  are not independent but are linear combinations of  $\delta Z_i^\gamma$  and  $\delta Z_i^Z$ . They are given here for completeness.

By the presence of the  $(\hat{\Sigma}^{\gamma Z})^2$  term on the r.h.s. the equations (155) are non-linear equations. It is, however, straightforward to solve them for the renormalization constants in terms of the unrenormalized quantities.

The higher-order irreducible contributions to the  $\rho$ -parameter, as far as available, are built in by means of substituting

$$\frac{\delta M_Z^2}{M_Z^2} - \frac{\delta M_w^2}{M_w^2} \rightarrow \frac{\delta M_Z^2}{M_Z^2} - \frac{\delta M_w^2}{M_w^2} + \Delta\rho^{(\text{HO})} \quad (156)$$

for the r.h.s of (155), with

$$\Delta\rho^{(\text{HO})} = 3\bar{x}_t \left[ 1 + x_t \Delta\rho^{(2)}(\xi) + \delta_{(3)}^{\text{QCD}} \right], \quad (157)$$

$$\bar{x}_t = \frac{\alpha}{16\pi s_w^2 c_w^2} \frac{m_t^2}{M_Z^2}, \quad x_t = \frac{G_\mu m_t^2}{8\pi^2 \sqrt{2}}, \quad \xi = \frac{m_t^2}{M_H^2}, \quad (158)$$

comprising the two-loop electroweak and three-loop QCD contributions. For the functions  $\Delta\rho^{(2)}$  and  $\delta_{(3)}^{\text{QCD}}$  see section 1.10.2 and 2.3.

Around the  $Z$  peak, the  $Z$  propagator has the form

$$D_Z(s) \simeq \frac{1}{1 + \hat{\Pi}^Z(M_Z^2)} \frac{1}{s - M_Z^2 + i \frac{s}{M_Z} \Gamma_Z}, \quad (159)$$

with

$$\begin{aligned} \hat{\Pi}^Z(M_Z^2) &= \mathcal{R}e \frac{d\hat{\Sigma}^Z}{ds}(M_Z^2), \\ \hat{\Sigma}^Z(s) &= \hat{\Sigma}^{ZZ}(s) - \frac{[\hat{\Sigma}^{\gamma Z}(s)]^2}{s + \hat{\Sigma}^{\gamma\gamma}(s)}. \end{aligned} \quad (160)$$

The  $Z$  width  $\Gamma_Z$  is calculated from the effective coupling constants given below in Eq. (175) together with the general formulae of section 1.10.1.

The vector boson masses  $M_w, M_Z$  are correlated by the Fermi constant

$$G_\mu = \frac{\pi\alpha}{\sqrt{2}M_w^2 s_w^2} \frac{1}{1 - \Delta r} = \frac{\pi\alpha}{\sqrt{2}M_Z^2 c_w^2 s_w^2} \frac{1}{1 - \Delta r}. \quad (161)$$

The quantity  $\Delta r(\alpha, M_Z, M_w, m_t, M_H)$  has the following representation:

$$\begin{aligned} \Delta r &= \Pi^\gamma(0) - \frac{c_w^2}{s_w^2} \left( \frac{\delta M_Z^2}{M_Z^2} - \frac{\delta M_w^2}{M_w^2} \right) + \frac{\Sigma^{ww}(0) - \delta M_w^2}{M_w^2} \\ &+ 2 \frac{c_w}{s_w} \frac{\Sigma^{\gamma Z}(0)}{M_Z^2} + \frac{\alpha}{4\pi s_w^2} \left( 6 + \frac{7 - 4s_w^2}{2s_w^2} \log c_w^2 \right). \end{aligned} \quad (162)$$

The last term is the sum of the box contributions and renormalized vertex corrections to the muon decay amplitude after removing the Fermi-model-like virtual photonic corrections. Due to the inclusion of the higher-order reducible and irreducible terms the way of writing  $\Delta r$  in the denominator of (161) automatically takes account of the proper resummation of the leading  $\Delta\alpha$  and  $\Delta\rho$  terms and some of the sub-leading terms as discussed in sub-section 1.10.2.

### 4.1.2 Vertex corrections

The vertex corrections can be summarized in terms of  $s$ -dependent vector and axial vector form factors if the masses  $m_f$  of the external fermions are small compared to  $M_w$ , both for the electromagnetic and the weak NC vertex. In our terminology, ‘vertex corrections’ denote the renormalized  $\gamma(Z)ff$  three-point functions in one-loop order, together with the finite wave function renormalizations for external fermions.

In contrast to the propagator corrections, the vertex corrections are not universal and depend on the fermion species. For this reason we have to list them separately for  $\nu$ ,  $e$ ,  $u$ , and  $d$  type fermions. In addition, the  $b$  quark is exceptional due to the virtual top contributions in the vertex.

Our terminology is as follows.

$F_{V,A}^{Zf}$  and  $F_{V,A}^{\gamma f}$  denote the IR finite weak (without the virtual photon diagrams) form factors for the  $Zff$  and  $\gamma ff$  vertex which, together with the lowest order terms, yield the dressed vertices:

$$\begin{aligned}\hat{\Gamma}_\mu^{Zff} &= i \frac{e}{2s_w c_w} \gamma_\mu \left\{ v_f + F_V^{Zf}(s) - \gamma_5 \left[ a_f + F_A^{Zf}(s) \right] \right\} , \\ \hat{\Gamma}_\mu^{\gamma ff} &= -i e Q_f \gamma_\mu - i e \gamma_\mu \left[ F_V^{\gamma f}(s) - F_A^{\gamma f}(s) \gamma_5 \right] .\end{aligned}\tag{163}$$

The lowest order coupling reads:

$$v_f = I_f^{(3)} - 2Q_f s_w^2 , \quad a_f = I_f^{(3)} ,\tag{164}$$

and the weak form factors in (163) are explicitly given by the following set of formulae.

#### Neutral current vertex:

neutrinos:

$$\begin{aligned}F_V^{Z\nu} &= F_A^{Z\nu} \\ &= \frac{\alpha}{4\pi} \left[ \frac{1}{8c_w^2 s_w^2} \Lambda_2(s, M_z) + \frac{2s_w^2 - 1}{4s_w^2} \Lambda_2(s, M_w) + \frac{3c_w^2}{2s_w^2} \Lambda_3(s, M_w) \right] ,\end{aligned}\tag{165}$$

charged fermions:

$$\begin{aligned}F_V^{Zf} &= \frac{\alpha}{4\pi} \left[ \frac{v_f(v_f^2 + 3a_f^2)}{4s_w^2 c_w^2} \Lambda_2(s, M_z) + F_L^f \right] , \\ F_A^{Zf} &= \frac{\alpha}{4\pi} \left[ \frac{a_f(3v_f^2 + a_f^2)}{4s_w^2 c_w^2} \Lambda_2(s, M_z) + F_L^f \right] ,\end{aligned}\tag{166}$$

with

$$\begin{aligned}
F_L^\ell &= \frac{1}{4s_w^2} \Lambda_2(s, M_w) - \frac{3c_w^2}{2s_w^2} \Lambda_3(s, M_w) , \\
F_L^u &= -\frac{1 - \frac{2}{3}s_w^2}{4s_w^2} \Lambda_2(s, M_w) + \frac{3c_w^2}{2s_w^2} \Lambda_3(s, M_w) , \\
F_L^d &= \frac{1 - \frac{4}{3}s_w^2}{4s_w^2} \Lambda_2(s, M_w) - \frac{3c_w^2}{2s_w^2} \Lambda_3(s, M_w) .
\end{aligned} \tag{167}$$

**Electromagnetic vertex:**

$$\begin{aligned}
F_V^{\gamma f} &= \frac{\alpha}{4\pi} \left[ \frac{Q_f(v_f^2 + a_f^2)}{4s_w^2 c_w^2} \Lambda_2(s, M_z) + G_L^f \right] , \\
F_A^{\gamma f} &= \frac{\alpha}{4\pi} \left[ \frac{Q_f 2v_f a_f}{4s_w^2 c_w^2} \Lambda_2(s, M_z) + G_L^f \right] ,
\end{aligned} \tag{168}$$

with

$$\begin{aligned}
G_L^\ell &= -\frac{3}{4s_w^2} \Lambda_3(s, M_w) , \\
G_L^u &= -\frac{1}{12s_w^2} \Lambda_2(s, M_w) + \frac{3}{4s_w^2} \Lambda_3(s, M_w) , \\
G_L^d &= \frac{1}{6s_w^2} \Lambda_2(s, M_w) - \frac{3}{4s_w^2} \Lambda_3(s, M_w) .
\end{aligned} \tag{169}$$

The functions  $\Lambda_2, \Lambda_3$  have the form,

$$\begin{aligned}
\Lambda_2(s, M) &= -\frac{7}{2} - 2w - (2w + 3) \log(-w) \\
&\quad + 2(1 + w)^2 \left[ \text{Li}_2 \left( 1 + \frac{1}{w} \right) - \frac{\pi^2}{6} \right] , \\
\Lambda_3(s, M) &= \frac{5}{6} - \frac{2w}{3} + \frac{(2w + 1)}{3} \sqrt{1 - 4w} \log(x) + \frac{2}{3} w(w + 2) \log^2(x) ,
\end{aligned} \tag{170}$$

with

$$w = \frac{M^2}{s + i\varepsilon}, \quad x = \frac{\sqrt{1 - 4w} - 1}{\sqrt{1 - 4w} + 1} .$$

The functions  $F_L^d$  and  $G_L^d$  cannot be used for  $b$  quarks. The full expressions for  $F_L^b, G_L^b$  can be found, for example, in the second of Ref. [2]<sup>13</sup>.

---

<sup>13</sup> Note that the normalization is different:

$$F_L^b(\text{this report}) = 2s_w c_w F_L^b(\text{Ref. [2]}).$$



#### 4.1.3 $e^+e^- \rightarrow f\bar{f}$ amplitudes

Around the  $Z$  resonance, the amplitude for  $e^+e^- \rightarrow f\bar{f}$  can be cast into a form close to the lowest order amplitude:

$$A(e^+e^- \rightarrow f\bar{f}) = A_\gamma + A_Z + (box) , \quad (171)$$

where  $A_\gamma$  denotes the dressed photon,  $A_Z$  the dressed  $Z$  exchange amplitude, and  $(box)$  summarizes the terms from the massive box diagrams, which, however, can be neglected around the  $Z$ .

The dressed **photon exchange** amplitude can be written in the following way:

$$A_\gamma = \frac{e^2}{1 + \hat{\Pi}^\gamma(s)} \frac{Q_e Q_f}{s} [(1 + F_V^{\gamma e})\gamma_\mu - F_A^{\gamma e}\gamma_\mu\gamma_5] \otimes [(1 + F_V^{\gamma f})\gamma^\mu - F_A^{\gamma f}\gamma^\mu\gamma_5] . \quad (172)$$

$\hat{\Pi}^\gamma$  is the subtracted vacuum polarization  $\hat{\Pi}^\gamma(s) = \Pi^\gamma(s) - \Pi^\gamma(0)$  with

$$\Pi^\gamma(s) = \frac{\Sigma^{\gamma\gamma}(s)}{s} .$$

The vertex form factors  $F_{V,A}^{\gamma f}$  from Eq. (168) are evaluated for  $s = M_Z^2$ .

The  $Z$  **exchange** amplitude without the box diagrams factorizes as follows:

$$A_Z = \sqrt{2}G_\mu M_Z^2 (\rho_e \rho_f)^{1/2} \times \frac{[\gamma_\mu (I_e^{(3)} - 2Q_e s_W^2 \kappa_e) - I_e^{(3)}\gamma_\mu\gamma_5] \otimes [\gamma^\mu (I_f^{(3)} - 2Q_f s_W^2 \kappa_f) - I_f^{(3)}\gamma^\mu\gamma_5]}{s - M_Z^2 + i \frac{s}{M_Z^2} M_Z \Gamma_Z} \quad (173)$$

The weak corrections appear in terms of fermion-dependent form factors  $\rho_f$  and  $\kappa_f$  in the coupling constants and in the width in the denominator.

#### 4.1.4 Effective neutral current couplings

The factorized amplitude (173) allows us to define NC vertices at the  $Z$  resonance with effective coupling constants  $g_{V,A}^f$ , synonymously with the use of  $\rho_f, \kappa_f$ :

$$\begin{aligned} J_\mu^{NC} &= (\sqrt{2}G_\mu M_Z^2 \rho_f)^{1/2} [(I_f^{(3)} - 2Q_f s_W^2 \kappa_f) \gamma_\mu - I_f^{(3)}\gamma_\mu\gamma_5] \\ &= (\sqrt{2}G_\mu M_Z^2)^{1/2} [g_V^f \gamma_\mu - g_A^f \gamma_\mu\gamma_5] . \end{aligned} \quad (174)$$

The effective couplings read as follows:

$$\begin{aligned} g_V^f &= [v_f + 2s_W c_W Q_f \hat{\Pi}^{\gamma Z}(M_Z^2) + F_V^{Zf}] \left[ \frac{1 - \Delta r}{1 + \hat{\Pi}^Z(M_Z^2)} \right]^{1/2} , \\ g_A^f &= [a_f + F_A^{Zf}] \left[ \frac{1 - \Delta r}{1 + \hat{\Pi}^Z(M_Z^2)} \right]^{1/2} . \end{aligned} \quad (175)$$

The building blocks are:

- $\Delta r$  from Eq. (162)
- $\hat{\Pi}^Z(M_Z^2)$  from Eq. (160)
- $\hat{\Pi}^{\gamma Z}(M_Z^2) = \hat{\Sigma}^{\gamma Z}(M_Z^2)/M_Z^2$  from Eq. (153)
- $F_{V,A}^{Zf}$  from Eq. (166) for  $s = M_Z^2$ .

For given  $m_t, M_H$  the values of  $s_W^2$  respectively  $M_W$  are chosen such that Eq. (161) is fulfilled.

For the  $b$  quark couplings the next-order leading corrections  $\sim G_\mu^2 m_t^4$ ,  $\sim \alpha_s G_\mu m_t^2$  are taken into account by performing in the one-loop expression  $F_L^b$  the following substitution:

$$F_L^b \rightarrow F_L^b - \frac{\alpha}{16\pi s_W^2 c_W^2} \frac{m_t^2}{M_Z^2} + \Delta\tau_b, \quad (176)$$

with

$$\Delta\tau_b = x_t \left[ 1 + x_t \tau^{(2)}(\xi) - \alpha_s(m_t) \frac{\pi}{3} \right]. \quad (177)$$

The function  $\tau^{(2)}$  is taken from Refs. [55, 58], and the QCD correction term from Ref. [57].

The alternative form factors  $\rho$  and  $\kappa$  can then be obtained via

$$\frac{g_V^f}{g_A^f} = 1 - 4 |Q_f| \kappa_f s_W^2, \quad \left( \frac{g_A^f}{a_f} \right)^2 = \rho_f. \quad (178)$$

Due to the imaginary parts of the self energies and vertices, the form factors and the effective couplings, respectively, are complex quantities. The effective mixing angles are calculated from the real parts according to

$$\sin^2 \theta_{\text{eff}}^f = \frac{1}{4 |Q_f|} \left( 1 - \frac{\text{Re } g_V^f}{\text{Re } g_A^f} \right). \quad (179)$$

## 4.2 LEPTON basics

### 4.2.1 Electroweak loops for hadron-free observables: functions $V_i$

For hadron-free observables we write the result of one-loop electroweak calculations in the form suggested in ref. [72]:

$$\begin{aligned} M_W/M_Z &= c + \frac{3c}{32\pi s^2(c^2 - s^2)} \bar{\alpha} V_m(t, h), \\ g_A^l &= -\frac{1}{2} - \frac{3}{64\pi s^2 c^2} \bar{\alpha} V_A(t, h), \\ R &= g_V^l/g_A^l = 1 - 4s^2 + \frac{3}{4\pi(c^2 - s^2)} \bar{\alpha} V_R(t, h), \\ g^\nu &= \frac{1}{2} + \frac{3}{64\pi s^2 c^2} \bar{\alpha} V_\nu(t, h), \end{aligned} \quad (180)$$

where  $t = m_t^2/M_Z^2$ ,  $h = M_H^2/M_Z^2$  and functions  $V_i(t, h)$  are normalized by the condition,

$$V_i(t, h) \simeq t, \quad (181)$$

at  $t \gg 1$ .

Each function  $V_i$  is a sum of five terms [72], [73]

$$V_i(t, h) = t + T_i(t) + H_i(h) + C_i + \delta V_i(t, h). \quad (182)$$

The functions  $t + T_i(t)$  are due to  $(t, b)$  doublet contribution to self-energies of the vector bosons,  $H_i(h)$  is due to  $W^\pm$ ,  $Z$  and  $H$  loops, the constants  $C_i$  include light fermion contribution both to self-energies, vertex and box diagrams.

To give explicit expressions for  $T_i(t)$  and  $H_i(h)$  it is convenient to introduce three auxiliary functions  $F_t(t)$ ,  $F_h(h)$  and  $F'_h(h)$  (see subsection 4.2.5 for their expressions).

The equations for  $T_i(t)$  and  $H_i(h)$  have the form [72]:

$$\underline{i = m}$$

$$\begin{aligned} T_m(t) &= \left( \frac{2}{3} - \frac{8}{9}s^2 \right) \ln t - \frac{4}{3} + \frac{32}{9}s^2 + \frac{2}{3} (c^2 - s^2) \left( \frac{t^3}{c^6} - \frac{3t}{c^2} + 2 \right) \ln \left| 1 - \frac{c^2}{t} \right| \\ &\quad + \frac{2}{3} \frac{c^2 - s^2}{c^4} t^2 + \frac{1}{3} \frac{c^2 - s^2}{c^2} t + \left( \frac{2}{3} - \frac{16}{9}s^2 - \frac{2}{3}t - \frac{32}{9}s^2 t \right) F_t(t), \\ H_m(h) &= -\frac{h}{h-1} \ln h + \frac{c^2 h}{h-c^2} \ln \frac{h}{c^2} - \frac{s^2}{18c^2} h - \frac{8}{3}s^2 + \left( \frac{h^2}{9} - \frac{4h}{9} + \frac{4}{3} \right) F_h(h) \\ &\quad - (c^2 - s^2) \left( \frac{h^2}{9c^4} - \frac{4}{9} \frac{h}{c^2} + \frac{4}{3} \right) F_h \left( \frac{h}{c^2} \right) + (1.1205 - 2.59\delta s^2), \end{aligned} \quad (183)$$

where  $\delta s^2 = 0.23117 - s^2$ .

$$\underline{i = A}$$

$$\begin{aligned} T_A(t) &= \frac{2}{3} - \frac{8}{9}s^2 + \frac{16}{27}s^4 - \frac{1 - 2tF_t(t)}{4t - 1} \\ &\quad + \left( \frac{32}{9}s^4 - \frac{8}{3}s^2 - \frac{1}{2} \right) \left[ \frac{4}{3}tF_t(t) - \frac{2}{3}(1 + 2t) \frac{1 - 2tF_t(t)}{4t - 1} \right], \\ H_A(h) &= \frac{c^2}{1 - c^2/h} \ln \frac{h}{c^2} - \frac{8h}{9(h-1)} \ln h + \left( \frac{4}{3} - \frac{2}{3}h + \frac{2}{9}h^2 \right) F_h(h) \\ &\quad - \left( \frac{4}{3} - \frac{4}{9}h + \frac{1}{9}h^2 \right) F'_h(h) - \frac{1}{18}h + (0.7751 + 1.07\delta s^2). \end{aligned} \quad (184)$$

$$\underline{i = R}$$

$$\begin{aligned} T_R(t) &= \frac{2}{9} \ln t + \frac{4}{9} - \frac{2}{9}(1 + 11t)F_t(t), \\ H_R(h) &= -\frac{4}{3} - \frac{h}{18} + \frac{c^2}{1 - c^2/h} \ln \frac{h}{c^2} + \left( \frac{4}{3} - \frac{4}{9}h + \frac{1}{9}h^2 \right) F_h(h) \\ &\quad + \frac{h}{1 - h} \ln h + (1.3590 + 0.51\delta s^2). \end{aligned} \quad (185)$$

$$\underline{i} = \underline{\nu}$$

$$\begin{aligned} T_\nu(t) &= T_A(t) , \\ H_\nu(h) &= H_A(h) . \end{aligned} \quad (186)$$

The constants  $C_i$  are rather complicated functions of  $\sin^2 \theta$  and we present their numerical values near  $s^2 = 0.23117$ :

$$C_m = -1.3500 + 4.13 \, \delta s^2 , \quad (187)$$

$$C_A = -2.2619 - 2.63 \, \delta s^2 , \quad (188)$$

$$C_R = -3.5041 - 5.72 \, \delta s^2 , \quad (189)$$

$$C_\nu = -1.1638 - 4.88 \, \delta s^2 . \quad (190)$$

#### 4.2.2 Corrections $\delta V_i$

Functions  $\delta V_i(t, h)$  in Eq. (182) are small corrections to  $V_i$ . They can be presented as a sum of five terms  $\delta_k V_i (k = 1 \div 5)$ :

1. Corrections to polarization of electromagnetic vacuum due to W boson loop,  $\delta_w \alpha$ , and t-quark loop,  $\delta_t \alpha$ , are traditionally not included in the running of  $\alpha(q^2)$ . We also prefer to consider them together with electroweak corrections. This is especially reasonable because  $W$  contribution  $\delta_w \alpha$  is gauge-dependent, while  $\delta \alpha_t$  is negligibly small. Here and for all other electroweak corrections we use the 't Hooft–Feynman gauge. The corrections  $\delta_w \alpha$  and  $\delta_t \alpha$  were neglected in Ref. [72] and were introduced in Ref. [74]:

$$\delta_1 V_m(t, h) = -\frac{16}{3} \pi s^4 \frac{1}{\alpha} (\delta_w \alpha + \delta_t \alpha) = -0.055 , \quad (191)$$

$$\delta_1 V_R(t, h) = -\frac{16}{3} \pi s^2 c^2 \frac{1}{\alpha} (\delta_w \alpha + \delta_t \alpha) = -0.181 , \quad (192)$$

$$\delta_1 V_A(t, h) = \delta_1 V_\nu(t, h) = 0 , \quad (193)$$

where

$$\frac{\delta_w \alpha}{\alpha} = \frac{1}{2\pi} \left[ (3 + 4c^2) \left( 1 - \sqrt{4c^2 - 1} \arcsin \frac{1}{2c} \right) - \frac{1}{3} \right] = 0.0686 , \quad (194)$$

$$\frac{\delta_t \alpha}{\alpha} = -\frac{4}{9\pi} \left[ (1 + 2t) F_t(t) - \frac{1}{3} \right] \simeq -\frac{4}{45\pi} \frac{1}{t} + \dots \simeq -0.00768 . \quad (195)$$

(Here and in Eqs. (196 – 209) we use  $m_t = 175$  GeV for numerical estimates.)

2. Corrections of the order of  $\bar{\alpha}\hat{\alpha}_s$ , due to the gluon exchange in the quark electroweak loops [56] (see also Ref. [73]),  $\delta_2 V_i = \delta_2^q V_i + \delta_2^t V_i$ . For the two generations of light quarks ( $q = u, d, s, c$ ) this gives:

$$\delta_2^q V_m(t, h) = 2 \left\{ \frac{4}{3} \left[ \frac{\hat{\alpha}_s(M_Z)}{\pi} \right] (c^2 - s^2) \ln c^2 \right\} = \left[ \frac{\hat{\alpha}_s(M_Z)}{\pi} \right] (-0.377) , \quad (196)$$

$$\delta_2^q V_A(t, h) = 2 \left\{ \frac{4}{3} \left[ \frac{\hat{\alpha}_s(M_Z)}{\pi} \right] \left( c^2 - s^2 + \frac{20}{9} s^4 \right) \right\} = \left[ \frac{\hat{\alpha}_s(M_Z)}{\pi} \right] (1.750), \quad (197)$$

$$\delta_2^q V_R(t, h) = 0 , \quad (198)$$

$$\delta_2^q V_\nu(t, h) = \delta_2^q V_A(t, h) . \quad (199)$$

The results of calculations for the third generation are given by rather complicated functions of the top mass and  $s^2$ . Here we present an expansion for large values of  $t$  and for fixed value of  $s^2 = 0.23117$ :

$$\begin{aligned} \delta_2^t V_m(t, h) &= \left[ \frac{\hat{\alpha}_s(m_t)}{\pi} \right] \left[ -2.86 t + 0.46 \ln t - 1.540 - \frac{0.68}{t} - \frac{0.21}{t^2} \right] \\ &= \frac{\hat{\alpha}_s(m_t)}{\pi} (-11.67) , \end{aligned} \quad (200)$$

$$\begin{aligned} \delta_2^t V_A(t, h) &= \left[ \frac{\hat{\alpha}_s(m_t)}{\pi} \right] \left[ -2.86 t + 0.493 - \frac{0.19}{t} - \frac{0.05}{t^2} \right] \\ &= \frac{\hat{\alpha}_s(m_t)}{\pi} (-10.10) , \end{aligned} \quad (201)$$

$$\delta_2^t V_R(t, h) = \left[ \frac{\hat{\alpha}_s(m_t)}{\pi} \right] \left[ -2.86 t + 0.22 \ln t - 1.513 - \frac{0.42}{t} - \frac{0.08}{t^2} \right] \quad (202)$$

$$= \frac{\hat{\alpha}_s(m_t)}{\pi} (-11.88) , \quad (203)$$

$$\delta_2^t V_\nu(t, h) = \delta_2^t V_A(t, h) . \quad (204)$$

As these formulas are valid for  $m_t > M_Z$ , in order to go to the region  $m_t < M_Z$  we either put  $\delta_2^t V_i = 0$  or use a massless limit in which  $\delta_2^t V_i = \frac{1}{2} \delta_2^q V_i$ . In any case, this region gives a tiny contribution to the global fit.

3. Corrections of the order of  $\bar{\alpha}\hat{\alpha}_s^2$  were calculated for the leading term  $\bar{\alpha}\hat{\alpha}_s^2 t$  only [53]

$$\delta_3 V_i(t, h) \simeq -(2.1552 - 0.18094 N_f) \hat{\alpha}_s^2(m_t) t \simeq -1.250 \hat{\alpha}_s^2(m_t) t = -0.06 \quad (205)$$

for  $N_f = 5$  light flavours. [For the numerical estimate we use  $\hat{\alpha}_s(M_Z) = 0.125$ .]

4. The leading correction of the order  $\bar{\alpha}^2 t^2$ , which originates from the second-order Yukawa interaction, was calculated in Refs. [55]-[58]:

$$\delta_4 V_i(t, h) = -\frac{\bar{\alpha}}{16\pi s^2 c^2} A\left(\frac{h}{t}\right) t^2, \quad (206)$$

where function  $A(M_H/m_t)$  can be found in Refs. [55],[58]. For  $m_t = 175$  GeV and  $M_H = 300$  GeV one has  $A = 8.9$  and  $\delta_4 V_i(t, h) = -0.11$ .

5. In the second order in electroweak interactions quadratic dependence appears on the Higgs mass [75]

$$\delta_5 V_m = \frac{\bar{\alpha}}{24\pi} \left(\frac{h}{c^2}\right) 0.747 = 0.0011, \quad (207)$$

$$\delta_5 V_A = \frac{\bar{\alpha}}{24\pi} \left(\frac{h}{s^2}\right) 1.199 = 0.0057, \quad (208)$$

$$\delta_5 V_R = -\frac{\bar{\alpha}}{24\pi} \left(\frac{h}{c^2}\right) \frac{c^2 - s^2}{s^2} 0.973 = -0.0032. \quad (209)$$

(Here for numerical estimates we use  $m_H = 300$  GeV.)

### 4.2.3 Hadronic decays of $Z$ boson

For the partial width of the  $Z$  decay into a pair of quarks  $q\bar{q}$  ( $q = u, d, s, c, b$ ), we use the equation

$$\Gamma_q = 12 \left[ (g_V^q)^2 R_V^q + (g_A^q)^2 R_A^q \right] \Gamma_0,$$

where the final state QED and QCD radiative functions  $R_V^q$  and  $R_A^q$  are given by Eqs. (55) and (56) respectively, and  $\Gamma_0$  is defined by Eq. (52). The electroweak radiative corrections are included in  $g_V^q$  and  $g_A^q$ :

$$g_A^q = I_q^{(3)} \left[ 1 + \frac{3\bar{\alpha}}{32\pi s^2 c^2} V_{Aq}(t, h) \right], \quad (210)$$

$$g_V^q / g_A^q = 1 - 4|Q_q|s^2 + \frac{3|Q_q|}{4\pi(c^2 - s^2)} \bar{\alpha} V_{Rq}(t, h). \quad (211)$$

The functions  $V_{Aq}(t, h)$  and  $V_{Rq}(t, h)$  in the one-loop electroweak approximation are related to the functions  $V_A(t, h)$  and  $V_R(t, h)$  from leptonic decays [76]:

$$V_{Au}(t, h) = V_{Ac}(t, h) = V_A(t, h) + \frac{128\pi s^3 c^3}{3\bar{\alpha}} (F_{Al} + F_{Au}), \quad (212)$$

$$V_{Ad}(t, h) = V_{As}(t, h) = V_A(t, h) + \frac{128\pi s^3 c^3}{3\bar{\alpha}} (F_{Al} - F_{Ad}), \quad (213)$$

$$\begin{aligned} V_{Ru}(t, h) = V_{Rc}(t, h) = V_R(t, h) + \frac{16\pi s c(c^2 - s^2)}{3\bar{\alpha}} \\ \times [F_{Vl} - (1 - 4s^2)F_{Al} + \frac{3}{2}(-1 - \frac{8}{3}s^2)F_{Au} + F_{Vu}], \end{aligned} \quad (214)$$

$$V_{Rd}(t, h) = V_{Rs}(t, h) = V_R(t, h) + \frac{16\pi s c(c^2 - s^2)}{3\bar{\alpha}} \quad (215)$$

$$\times [F_{Vl} - (1 - 4s^2)F_{Al} + 3((1 - \frac{4}{3}s^2)F_{Ad} - F_{Vd})] , \quad (216)$$

where  $F_{Vl} = 0.00197$ ,  $F_{Al} = 0.00186$ ,  $F_{Vu} = -0.00169$ ,  $F_{Au} = -0.00165$ ,  $F_{Vd} = 0.00138$ ,  $F_{Ad} = 0.00137$  [76]. The difference  $V_{i,q} - V_i$  is due to different electroweak corrections to the vertices  $Zq\bar{q}$  and  $Zl\bar{l}$  ( $s^2 = 0.23117$  is assumed: formulas used in the code have explicit  $s^2$  dependence).

The oblique corrections of the order of  $\hat{\alpha}_s$ ,  $\hat{\alpha}_s^2 t$  and  $\bar{\alpha} t^2$  to the  $V_{Aq}(V_{Rq})$  are the same as in the case of  $V_A$  and  $V_R$ . But for  $Z$  boson decay into pair  $q\bar{q}$  there are additional  $\hat{\alpha}_s$  corrections to the vertices that have not yet been calculated. This brings additional uncertainty into the theoretical accuracy.

#### 4.2.4 Specific features of the decay $Z \rightarrow b\bar{b}$

For  $Z \rightarrow b\bar{b}$  decays we have to take into account corrections to the  $Z \rightarrow b\bar{b}$  vertex which depend on  $t$  [52], [57].

$$V_{Ab}(t, h) = V_{Ad}(t, h) - \frac{8s^2 c^2}{3(3 - 2s^2)} [\phi(t) + \delta\phi(t)] , \quad (217)$$

$$V_{Rb}(t, h) = V_{Rd}(t, h) - \frac{4s^2(c^2 - s^2)}{3(3 - 2s^2)} [\phi(t) + \delta\phi(t)] . \quad (218)$$

For  $\phi(t)$  we use the following expansion [52]

$$\begin{aligned} \phi(t) = & \frac{3 - 2s^2}{2s^2 c^2} \left\{ t + c^2 \left[ 2.88 \ln \left( \frac{t}{c^2} \right) - 6.716 + \frac{1}{t} \left( 8.368 c^2 \ln \left( \frac{t}{c^2} \right) - 3.408 c^2 \right) \right. \right. \\ & + \frac{1}{t^2} \left( 9.126 c^4 \ln \left( \frac{t}{c^2} \right) + 2.26 c^4 \right) + \frac{1}{t^3} \left( 4.043 c^6 \ln \left( \frac{t}{c^2} \right) + 7.41 c^6 \right) \\ & \left. \left. + \dots \right] \right\} , \end{aligned} \quad (219)$$

and for  $\delta\phi(t)$  we use the leading approximation calculated in Refs. [57] and [55], [58]

$$\delta\phi(t) = \frac{3 - 2s^2}{2s^2 c^2} \left\{ -\frac{\pi^2}{3} \left[ \frac{\hat{\alpha}_s(m_t)}{\pi} \right] t + \frac{1}{16s^2 c^2} \left( \frac{\bar{\alpha}}{\pi} \right) t^2 \tau_b^{(2)} \left( \frac{h}{t} \right) \right\} , \quad (220)$$

where function  $\tau_b^{(2)}$  has been calculated in Ref. [58].

For  $m_t = 175$  GeV and  $M_H = 300$  GeV

$$\tau_b^{(2)} = 1.245 .$$

Asymmetries are calculated with the loop corrected values of  $g_V$  and  $g_A$ .

#### 4.2.5 Appendix: Auxiliary functions $F_t$ and $F_h$

$$F_t(t) = \begin{cases} 2(1 - \sqrt{4t-1} \arcsin \frac{1}{\sqrt{4t}}) & , \quad 4t > 1 \\ 2(1 - \sqrt{1-4t} \ln \frac{1+\sqrt{1-4t}}{\sqrt{4t}}) & , \quad 4t < 1 \end{cases} \quad (221)$$

$$F_h(h) = \begin{cases} 1 + (\frac{h}{h-1} - \frac{h}{2}) \ln h + h\sqrt{1-\frac{4}{h}} \ln \left( \sqrt{\frac{h}{4}-1} + \sqrt{\frac{h}{4}} \right) & , \quad h > 4 \\ 1 + (\frac{h}{h-1} - \frac{h}{2}) \ln h - h\sqrt{\frac{4}{h}-1} \arctan \sqrt{\frac{4}{h}-1} & , \quad h < 4 \end{cases} \quad (222)$$

$$F'_h(h) = \begin{cases} -1 + \frac{h-1}{2} \ln h + (3-h)\sqrt{\frac{h}{h-4}} \ln \left( \sqrt{\frac{h}{4}-1} + \sqrt{\frac{h}{4}} \right) & , \quad h > 4 \\ -1 + \frac{h-1}{2} \ln h + (3-h)\sqrt{\frac{h}{4-h}} \arctan \sqrt{\frac{4}{h}-1} & , \quad h < 4 \end{cases} \quad (223)$$

### 4.3 TOPAZ0 basics

The *realization* given in Ref. [77] describes the coupling of the  $Z$  as:

$$\sqrt{2}(G_\mu \rho_Z)^{1/2} M_Z \gamma^\mu \left[ I_f^{(3)} - 2Q_f \hat{s}^2 + \delta g_V^f + \left( I_f^{(3)} + \delta g_A^f \right) \gamma_5 \right] . \quad (224)$$

Before giving the specific expression of the various quantities entering the previous equation, we stress that our metric is such that a time-like momentum squared is negative. Next we decompose the unrenormalized vector boson self-energies as:

$$\begin{aligned} S_{\gamma\gamma}(p^2) &= \frac{g^2 s_\theta^2}{16\pi^2} \Pi_{\gamma\gamma}(p^2) p^2 , \\ S_{ZZ}(p^2) &= \frac{g^2}{16\pi^2 c_\theta^2} \Sigma_{ZZ}(p^2) , \\ S_{Z\gamma}(p^2) &= \frac{g^2 s_\theta}{16\pi^2 c_\theta} \Sigma_{Z\gamma}(p^2) , \\ S_{WW}(p^2) &= \frac{g^2}{16\pi^2} \Sigma_{WW}(p^2) , \\ \Sigma_{ZZ}(p^2) &= \Sigma_{33}(p^2) - 2s_\theta^2 \Sigma_{3Q}(p^2) + s_\theta^4 \Pi_{\gamma\gamma}(p^2) p^2 , \\ \Sigma_{Z\gamma}(p^2) &= \Sigma_{3Q}(p^2) - s_\theta^2 \Pi_{\gamma\gamma}(p^2) p^2 , \end{aligned} \quad (225)$$

where  $\theta$  denotes the bare mixing angle. After a re-diagonalization in the neutral sector, which makes  $S_{Z\gamma}(0) = 0$  in the  $\xi = 1$  gauge and replaces  $\Sigma_{WW}, \Sigma_{33}$  and  $\Sigma_{3Q}$  with  $\Sigma_{WW} + 4\Gamma, \Sigma_{33} + 4\Gamma$  and  $\Sigma_{3Q} + 2\Gamma$  with  $\Gamma = M^2 B_0(0, M^2, M^2) - M$  being the bare  $W$  mass — we consider the ultraviolet and infrared finite corrections to the  $\mu$ -decay  $\delta_G$  and introduce

$$\Sigma_{WW}^G = \Sigma_{WW}(0) + \frac{\sqrt{2}\pi\alpha}{G_\mu} \delta_G , \quad (226)$$



which has the virtue of being gauge invariant, a property not satisfied by  $\Sigma_{ww}(0)$  alone. The extra term induced by the diagonalization is gauge invariant by construction. From now on we will denote the fermionic (bosonic) contributions to a given quantity  $A$  with the notation  $A^{\text{ferm}}(A^{\text{bos}})$ . With these quantities we define

$$\begin{aligned}\rho_z &= \frac{1}{1 + \frac{G_\mu M_Z^2}{2\sqrt{2}\pi^2} \Sigma^{\text{ferm}} + \text{h.o.}} , \\ M_Z^2 \Sigma &= \Sigma_{ww}^G - \mathcal{R}e \Sigma_{33}(M_Z^2) + \mathcal{R}e \Sigma_{3Q}(M_Z^2) + s^2 c^2 M_Z^2 \Pi_F^{\text{bos}}(M_Z^2) ,\end{aligned}\quad (227)$$

where

$$s^2 c^2 = \frac{\pi \alpha(M_Z)}{\sqrt{2} G_\mu M_Z^2} , \quad (228)$$

and  $\Pi_F(M_Z^2) = \mathcal{R}e \Pi_{\gamma\gamma}(M_Z^2) - \Pi_{\gamma\gamma}(0)$ . Note that  $\Sigma$  is ultraviolet finite. Next we can introduce  $\hat{s}^2$  as:

$$\hat{s}^2 = \frac{1}{2} \left[ 1 - \sqrt{1 - \frac{4\pi\alpha(M_Z)}{\sqrt{2} G_\mu M_Z^2 \rho_z^R}} \right] , \quad (229)$$

and give the definition of  $\delta g_V^f, \delta g_A^f$ ,

$$\begin{aligned}\delta g_V^f &= \frac{\alpha}{4\pi} \left[ \frac{2F_V^f - \frac{1}{2} v_f \Delta \Pi_Z}{c^2 s^2} - 2Q_f \Delta s^2 \right] , \\ \delta g_A^f &= \frac{\alpha}{4\pi} \left[ \frac{2F_A^f - \frac{1}{2} I_f^{(3)} \Delta \Pi_Z}{c^2 s^2} \right] ,\end{aligned}\quad (230)$$

where  $v_f = I_f^{(3)} - 2Q_f s^2$ , and

$$\begin{aligned}M_Z^2 \Delta \Pi_Z &= \mathcal{R}e \left\{ \left( \Sigma_{ww}^G \right)^{\text{bos}} - \Sigma_{33}^{\text{bos}}(M_Z^2) - \Sigma_{3Q}^{\text{ferm}}(M_Z^2) - M_Z^2 \Sigma'_{33}(M_Z^2) \right. \\ &\quad \left. + 2s^2 \left[ \Sigma_{3Q}(M_Z^2) + M_Z^2 \Sigma'_{3Q}(M_Z^2) \right] + s^4 M_Z^4 \Pi'_{\gamma\gamma}(M_Z^2) \right\} .\end{aligned}\quad (231)$$

Here  $f'$  stands for  $-df/dp^2$ . The  $F$  refers to flavour-dependent vertex corrections.

- If no resummation of bosonic self-energies is performed we have

$$\rho_z^R = \rho_z, \quad \text{and} \quad \Delta s^2 = \frac{\Sigma^{\text{bos}}}{c^2 - s^2} ; \quad (232)$$

- otherwise  $\rho_z^R$  has the same structure of  $\rho_z$  with  $\Sigma^{\text{ferm}}$  replaced by  $\Sigma_R$ :

$$\begin{aligned}
\rho_Z^R &= \frac{1}{1 + \frac{G_\mu M_Z^2}{2\sqrt{2}\pi^2} \Sigma_R + \text{h.o.}} , \\
\Sigma_R &= \left[ \Sigma^{\text{tot}} - (c^2 - s^2) \frac{\text{Re} \Sigma_{Z\gamma}(M_Z^2)}{M_Z^2} \right]_{\overline{MS}} , 
\end{aligned} \tag{233}$$

and

$$M_Z^2 \Delta s^2 = \left[ \text{Re} \Sigma_{Z\gamma}(M_Z^2) \right]_{\overline{MS}} . \tag{234}$$

$\Delta \Pi_Z$  is the residual  $Z$  wave function factor which obtains by writing the  $Z$  propagator  $\chi_Z$  as

$$\begin{aligned}
\text{Re} \chi_Z^{-1} &= \left( 1 + \frac{G_\mu M_Z^2}{2\sqrt{2}\pi^2} \Pi_Z \right) (p^2 + M_Z^2) , \\
M_Z^2 \Pi_Z &= \Sigma_{WW}^G - \frac{1}{p^2 + M_Z^2} \text{Re} \left[ \frac{p^2}{M_Z^2} \Sigma_{ZZ}(M_Z^2) + \Sigma_{ZZ}(p^2) \right] , \\
\Pi_Z &= \Sigma^{\text{ferm}} + \Delta \Pi_Z . 
\end{aligned} \tag{235}$$

The resummation operates on a gauge invariant quantity since it can be proved that

$$\left[ M_Z^2 \frac{\Sigma}{c^2 - s^2} - \text{Re} \Sigma_{Z\gamma}(M_Z^2) \right]^{\text{bos}} = \frac{1}{c^2 - s^2} \left[ \Sigma_{WW}^G - s^2 c^2 M_Z^2 \Pi_{\gamma\gamma}(0) - \text{Re} \Sigma_{ZZ}(M_Z^2) \right]^{\text{bos}} , \tag{236}$$

and the sum of the terms in the last parenthesis is automatically gauge invariant. The same quantity, however, is not ultraviolet-finite and therefore has to be strictly understood in the  $\overline{MS}$  sense at the scale  $\mu = M_Z$ . The higher-order terms in Eq. (227) are given by:

$$\begin{aligned}
\text{h.o.} &= \frac{G_\mu M_Z^2}{2\pi^2} \Delta \Sigma_2 + \frac{1}{2} \frac{\alpha_s(m_t)}{\pi} \left( 1 + \frac{\pi}{3} \right) m_t^2 \left[ 1 + \mathcal{O} \left( \frac{M_Z^2}{m_t^2} \right) \right] \\
&\quad + \frac{\alpha_s(M_Z)}{\pi} \Delta \Sigma_{lq} + 10.55 \left( \frac{\alpha_s(m_t)}{\pi} \right)^2 , 
\end{aligned} \tag{237}$$

where  $\Delta \Sigma_2$  is the two-loop factor proportional to  $m_t^4/M_Z^4$ ,  $\Delta \Sigma_{lq}$  denotes the  $\mathcal{O}(\alpha\alpha_s)$  light quark contribution and the last factor is the three-loop correction computed for six active flavours. In the special case of the  $Z \rightarrow b\bar{b}$  width we include the well known correction factor [55], which modifies the vector and axial-vector couplings into  $1 - 4/3\hat{s}^2 + \tau$  and  $1 + \tau$ .

To illustrate the internal structure of the renormalization procedure we use a well defined and generalizable example. The three bare parameters of the MSM Lagrangian

are related to experimental data by one-loop relations. One example of a solution concerns the bare mixing-angle

$$\begin{aligned}\sin^2 \theta &= s^2 + \frac{\alpha}{4\pi} s_1 + \left(\frac{\alpha}{4\pi}\right)^2 s_2, \\ s_1 &= \frac{1}{c^2 - s^2} \Sigma - \frac{1}{M_Z^2} \mathcal{R}e \Sigma_{Z\gamma}(M_Z^2), \\ s_2 &= \frac{1}{(c^2 - s^2)^3} \Sigma^2 - \Pi_{\gamma\gamma}(0) s_1.\end{aligned}\tag{238}$$

For the  $Z \rightarrow \bar{f}f$  amplitude the self-energy corrections give rise to

$$\gamma^\mu \left[ I_f^{(3)} - 2Q_f V_f + I_f^{(3)} \gamma^5 \right]. \tag{239}$$

Thus:

$$\begin{aligned}V_f &= \sin^2 \theta + \frac{\alpha}{4\pi} \frac{1}{M_Z^2} \frac{\mathcal{R}e \Sigma_{Z\gamma}(M_Z^2)}{1 - \frac{\alpha}{4\pi} \Pi_F} + \mathcal{O}(\alpha^2) \\ &= s^2 + \frac{\alpha}{4\pi} \frac{\Sigma}{c^2 - s^2} + \left(\frac{\alpha}{4\pi}\right)^2 \left[ \frac{\Sigma^2}{(c^2 - s^2)^3} + \frac{\Sigma \Pi_F}{c^2 - s^2} \right] + \mathcal{O}(\alpha^3) \\ &= s^2 + \frac{\alpha(M_Z)}{4\pi} \frac{\Sigma}{c^2 - s^2} + \left[ \frac{\alpha(M_Z)}{4\pi} \right]^2 \frac{\Sigma^2}{(c^2 - s^2)^3} + \mathcal{O}(\alpha^3).\end{aligned}\tag{240}$$

After this result we may perform a partial resummation —

$$V_f = \hat{s}^2 + \frac{\alpha(M_Z)}{4\pi} \frac{1}{c^2 - s^2} \Sigma^{\text{bos}} + \dots \tag{241}$$

As a final comment let us consider the term proportional to the square of the  $Z - \gamma$  transition in the propagators. It would contribute to  $\Pi_Z$  with

$$\begin{aligned}\Delta \Pi_Z &\rightarrow \Delta \Pi_Z - \frac{G_\mu}{2\pi^2} s^2 c^2 \frac{p^2}{M_Z^2(p^2 + M_Z^2)} \left[ \mathcal{R}e \Sigma_{Z\gamma}(M_Z^2) + \frac{M_Z^2}{p^2} \mathcal{R}e \Sigma_{Z\gamma}(p^2) \right]^2 \\ &= -\frac{G_\mu}{2\pi^2} s^2 c^2 \frac{p^2}{M_Z^2} (p^2 + M_Z^2) \left[ -\mathcal{R}e \Sigma'_{Z\gamma}(M_Z^2) + \frac{\mathcal{R}e \Sigma_{Z\gamma}(M_Z^2)}{M_Z^2} + \dots \right]^2,\end{aligned}\tag{242}$$

where  $\dots$  indicates terms of  $\mathcal{O}(p^2 + M_Z^2)$ . Thus the additional term, being  $\mathcal{O}(p^2 + M_Z^2)$ , does not contribute to the  $Z$  wave function renormalization factor. It should be noted that there is an easy dictionary of translation with other realizations, for instance:

$$\begin{aligned}\rho_f &= 4\rho_Z \left( I_f^{(3)} + \delta g_A^f \right)^2, \\ 2Q_f s_W^2 \kappa_f &= I_f^{(3)} \frac{2Q_f \hat{s}^2 + \delta g_A^f - \delta g_V^f}{I_f^{(3)} + \delta g_A^f}.\end{aligned}\tag{243}$$

Once electroweak corrections are included in the formulation, TOPAZ0 implements initial state QED corrections by a convolution on the weakly corrected kernel distributions with a radiator function, or with structure functions — depending on the experimental set-up. Resummation of soft photon effects and hard photon emission up to  $\mathcal{O}(\alpha^2)$  is taken into account, and final state QED radiation with realistic cuts, QED initial–final interference, and initial state leptonic and hadronic pair production are also included. In the next two appendices further details are given for pure electroweak corrections.

#### 4.3.1 Appendix 1: The self-energies

Starting from the decomposition of Eq. (225) for the vector boson self-energies we give their general expression in terms of two-point scalar form factors [22]. In the following, the first argument,  $p^2$ , is always left understood:

$$\begin{aligned}
\Pi_{\gamma\gamma} &= \frac{2}{3} - 12 B_{21}(M_W, M_W) + 7 B_0(M_W, M_W) \\
&\quad + 4 \sum_g \left[ B(m_l, m_l) + \frac{4}{3} B(m_u, m_u) + \frac{1}{3} B(m_d, m_d) \right] , \\
\Sigma_{3Q} &= p^2 \text{Biggl} \left\{ \frac{2}{3} - 10 B_{21}(M_W, M_W) + \frac{13}{2} B_0(M_W, M_W) \right. \\
&\quad \left. + \sum_g [B(m_l, m_l) + 2 B(m_u, m_u) + B(m_d, m_d)] \text{Biggr} \right\} - 2 M_W^2 B_0(M_W, M_W) , \\
\Sigma_{33} &= p^2 \Pi_{33} + \sigma_{33} , \\
\Sigma_{WW} &= p^2 \left[ \Pi_{WW}^0 + s^2 \Pi_{WW}^1 \right] + \left[ \sigma_{WW}^0 + s^2 \sigma_{WW}^1 \right] , \\
\Pi_{33} &= \frac{2}{3} - 9 B_{21}(M_W, M_W) + \frac{25}{4} B_0(M_W, M_W) - B_{21}(M_Z, M_H) \\
&\quad - B_1(M_Z, M_H) - \frac{1}{4} B_0(M_Z, M_H) \\
&\quad + \frac{1}{2} \sum_g [B(m_l, m_l) + B(m_\nu, m_\nu) + 3 B(m_u, m_u) + 3 B(m_d, m_d)] , \\
\sigma_{33} &= -2 M_W^2 B_0(M_W, M_W) + \frac{1}{2} M_Z^2 B_1(M_Z, M_H) + \frac{5}{4} M_Z^2 B_0(M_Z, M_H) \\
&\quad - \frac{1}{2} M_H^2 B_1(M_Z, M_H) - \frac{1}{4} M_H^2 B_0(M_Z, M_H) \\
&\quad - \frac{1}{2} \sum_g \left[ m_\nu^2 B_0(m_\nu, m_\nu) + m_l^2 B_0(m_l, m_l) \right. \\
&\quad \left. + 3 m_u^2 B_0(m_u, m_u) + 3 m_d^2 B_0(m_d, m_d) \right] , \\
\sigma_{WW}^0 &= \frac{9}{2} (M_Z^2 - M_W^2) B_1(M_Z, M_W) + \frac{1}{4} (13 M_Z^2 - 21 M_W^2) B_0(M_Z, M_W) \\
&\quad + \frac{1}{2} (M_W^2 - M_H^2) B_1(M_W, M_H) + \frac{1}{4} (5 M_W^2 - M_H^2) B_0(M_W, M_H) \\
&\quad + \sum_g \left[ (m_l^2 - m_\nu^2) B_1(m_\nu, m_l) - m_\nu^2 B_0(m_\nu, m_l) + 3 (m_d^2 - m_u^2) B_1(m_u, m_d) \right.
\end{aligned}$$

$$\begin{aligned}
& -3 m_u^2 B_0(m_u, m_d) \Big] , \\
\sigma_{ww}^1 &= 2 (M_w^2 - M_z^2) [2B_1(M_z, M_w) + B_0(M_z, M_w)] - 2 M_w^2 [2 B_1(0, M_w) + B_0(0, M_w)] , \\
\Pi_{ww}^0 &= \frac{2}{3} - 9B_{21}(M_z, M_w) - 9B_1(M_z, M_w) + \frac{7}{4} B_0(M_z, M_w) \\
& - B_{21}(M_w, M_H) - B_1(M_w, M_H) - \frac{1}{4} B_0(M_w, M_H) \\
& + 2 \sum_g [B_{21}(m_\nu, m_l) + B_1(m_\nu, m_l) + 3 B_{21}(m_u, m_d) + 3 B_1(m_u, m_d)] , \\
\Pi_{ww}^1 &= 8 [B_{21}(M_z, M_w) + B_1(M_z, M_w) - B_{21}(0, M_w) - B_1(0, M_w)] \\
& + 2 [B_0(0, M_w) - B_0(M_z, M_w)] , \tag{244}
\end{aligned}$$

where  $B = 2 B_{21} - B_0$  and the sum is over the fermionic generations. The factor  $\Delta$  is given by  $\Delta = -2/(n-4) + \gamma_E - \ln 4\pi$ . The functions  $\chi(x)$ ,  $G_n(y)$  are defined by [78]

$$\begin{aligned}
\chi(x) &= -p^2 x^2 + (p^2 + m_2^2 - m_1^2)x + m_1^2 , \\
G_n(y) &= \int_0^1 dx x^{n-1} \ln(x-y) . \tag{245}
\end{aligned}$$

In terms of  $\chi$  (where  $m^2 \rightarrow m^2 - i\epsilon$ ) we have

$$\begin{aligned}
B_0 &= \Delta - \int_0^1 dx \ln \chi , \\
B_1 &= -\frac{1}{2}\Delta + \int_0^1 dx x \ln \chi , \\
B_{21} &= \frac{1}{3}\Delta - \int_0^1 dx x^2 \ln \chi , \tag{246}
\end{aligned}$$

and the corresponding integrals can be written in terms of the  $G_n$ -functions, for which we write recursion formulae to be worked upwards or downwards, according to the magnitude of  $y$ .

The  $\mathcal{O}(\alpha_s)$  contributions to  $\Pi_{\gamma\gamma} \dots \Sigma_{ww}$  are computed according to the formulation of Kniehl (see Ref. [52]). For instance,

$$\begin{aligned}
\Pi_{\gamma\gamma} &= \Pi_{\gamma\gamma} + \Pi_{\gamma\gamma}^{\alpha_s} , \\
\Pi_{\gamma\gamma}^{\alpha_s} &= \frac{64}{9} \frac{\alpha_s(m_t)}{\pi} \frac{m_t^2}{p^2} [rX + V_1(r)] , \tag{247}
\end{aligned}$$

where  $r = -1/4 p^2/m_t^2$  and the functions  $X$  and  $V_1$  are explicitly given in Ref. [52].

#### 4.3.2 Appendix 2: The $Zf\bar{f}$ vertices

In order to introduce the vertex contributions  $F_{v,A}^f$  we first present the fermion wave function renormalization factors ( $f \neq b$ ):

$$\begin{aligned}
W_V^f &= -\frac{1}{32} \left[ \left( I_f^{(3)} - 2Q_f s^2 \right)^2 + 1 \right] F_Z - \frac{1}{8} c^2 F_W, \\
W_A^f &= -\frac{1}{16} \left( 1 - 8I_f^{(3)} Q_f s^2 \right) F_Z - \frac{1}{8} c^2 F_W,
\end{aligned} \tag{248}$$

where  $F_x = \Delta - \ln(M_x^2) - \frac{1}{2}$ . With them we can write ( $f \neq b$ ):

$$\begin{aligned}
F_V^f &= W_V^f v_f + W_A^f I_f^{(3)} - 2v_f \left( v_f^2 + \frac{3}{4} \right) F_1^f + 4I_f^{(3)} c^2 F_2^f - c^4 I_f^{(3)} F_3^f, \\
F_A^f &= W_V^f I_f^{(3)} + W_A^f v_f - 2I_f^{(3)} \left( 3v_f^2 + \frac{1}{4} \right) F_1^f + 4I_f^{(3)} c^2 F_2^f - c^4 I_f^{(3)} F_3^f,
\end{aligned} \tag{249}$$

where again  $v_f = I_f^{(3)} - 2Q_f s^2$ . The functions  $F_i^f$  are given in terms of three-point scalar formfactors [22]. For instance,

$$\begin{aligned}
F_1^e &= -\frac{1}{4} C_{24}(m_e^2, M_Z^2, m_e^2) - \frac{1}{8} p^2 \left[ C_{11}(m_e^2, M_Z^2, m_e^2) + C_{23}(m_e^2, M_Z^2, m_e^2) \right] + \frac{1}{8}, \\
F_2^e &= -\frac{1}{4} C_{24}(m_\nu^2, M_W^2, m_\nu^2) - \frac{1}{8} p^2 \left[ C_{11}(m_\nu^2, M_W^2, m_\nu^2) + C_{23}(m_\nu^2, M_W^2, m_\nu^2) \right] + \frac{1}{8}, \\
F_3^e &= -6 C_{24}(M_W^2, m_\nu^2, M_W^2) - p^2 \left[ C_0(M_W^2, m_\nu^2, M_W^2) + C_{11}(M_W^2, m_\nu^2, M_W^2) \right. \\
&\quad \left. + C_{23}(M_W^2, m_\nu^2, M_W^2) \right] + 1 + \Delta - \ln(M_W^2).
\end{aligned} \tag{250}$$

In TOPAZ0 the most general (arbitrary internal and external masses) two-, three- and four-point scalar functions are available [79]. For  $b\bar{b}$  final states the expression for vertices contains additional  $m_t$ -dependent terms which can be found in Ref. [77].

## 4.4 ZFITTER basics

Here, we introduce explicit expressions for  $\Delta r$  and the weak form factors of  $Z$  decay and of fermion pair production process  $e^+e^- \rightarrow f\bar{f}$   $\rho$ ,  $\kappa$  to order (1loop, $\alpha$ ) and order (2loop, $\alpha\alpha_s$ ) as used in Eqs.(71)-(73) and (75)-(77) of the main text.

### 4.4.1 Muon life-time

The virtual, non-photonic one-loop corrections to the muon life-time are:

$$\begin{aligned}
\Delta r^{\text{1loop},\alpha} &= \frac{\alpha}{4\pi} \left\{ -\frac{2}{3} \left( 1 + 2 \sum_f Q_f^2 \ln \frac{m_f^2}{M_W^2} \right) + \frac{R}{(1-R)^2} \left[ W(M_W^2) - Z(M_Z^2) \right] \right. \\
&\quad \left. + \frac{1}{1-R} \left[ W(0) - W(M_W^2) - \frac{5}{8} R(1+R) + \frac{11}{2} + \frac{9}{4} \frac{R}{1-R} \ln R \right] \right\}.
\end{aligned} \tag{251}$$

Here and in the following sections, we use the abbreviations,

$$R = \frac{M_W^2}{M_Z^2}, \quad r_W = \frac{M_H^2}{M_W^2}, \quad r_Z = \frac{M_H^2}{M_Z^2}. \tag{252}$$

The  $\Delta r$  was introduced in (E.8) and (F.3) of [80]. The  $t$  mass dependent terms may be found in the appendix of [81].

#### 4.4.2 Partial widths of the $Z$ boson

The two form factors for each fermionic partial width of the  $Z$  boson are in one loop order and in the approximation of vanishing external fermion masses [81]:

$$\begin{aligned} \rho_f^{\text{1loop},\alpha} = & 1 + \frac{\alpha}{4\pi(1-R)} \left\{ Z(M_Z^2) + Z^F(M_Z^2) - W(0) \right. \\ & \left. + \frac{5}{8}R(1+R) - \frac{11}{2} - \frac{9R}{4(1-R)} \ln R + u_f + \delta\rho_{ct,f}^t \right\}, \end{aligned} \quad (253)$$

$$\begin{aligned} \kappa_f^{\text{1loop},\alpha} = & 1 + \frac{\alpha}{4\pi(1-R)} \left\{ \frac{R}{1-R} [Z(M_Z^2) - W(M_W^2)] + M(M_Z^2) \right. \\ & \left. + \frac{(1-R)^2}{R} Q_f^2 \left[ V_{1z}(M_Z^2) + \frac{3}{2} \right] - \frac{1}{2} [u_f + \delta\rho_{ct,f}^t] \right\}, \end{aligned} \quad (254)$$

$$\begin{aligned} u_f = & \frac{1}{2R} \left[ 1 - 6|Q_f|(1-R) + 12Q_f^2(1-R)^2 \right] \left[ V_{1z}(M_Z^2) + \frac{3}{2} \right] + \left[ 1 - 2R \right. \\ & \left. - 2|Q_f|(1-R) \right] \left[ V_{1w}(M_Z^2) + \frac{3}{2} \right] + 2R \left[ V_{2w}(M_Z^2) + \frac{3}{2} \right]. \end{aligned} \quad (255)$$

#### 4.4.3 Auxiliary functions

All  $W$  and  $Z$  boson self-energy functions are sums of bosonic and fermionic parts, e.g.

$$W(0) = W_b(0) + W_f(0). \quad (256)$$

The bosonic parts are given in appendix A of [80]<sup>14</sup>

$$W_b(0) = \frac{5R(1+R)}{8} - \frac{17}{4} + \frac{5}{8R} - \frac{r_w}{8} + \left[ \frac{9}{4} + \frac{3}{4R} - \frac{3}{1-R} \right] \ln R + \frac{3r_w}{4(1-r_w)} \ln r_w, \quad (257)$$

$$\begin{aligned} W_b(M_w^2) = & -\frac{157}{9} + \frac{23}{12R} + \frac{1}{12R^2} - \frac{r_w}{2} + \frac{r_w^2}{12} + \frac{1}{R} \left[ -\frac{7}{2} + \frac{7}{12R} + \frac{1}{24R^2} \right] \ln R \\ & + r_w \left( -\frac{3}{4} + \frac{r_w}{4} - \frac{r_w^2}{24} \right) \ln r_w + \left( \frac{1}{2} - \frac{r_w}{6} + \frac{r_w^2}{24} \right) \frac{L_{WH}(M_w^2)}{M_w^2} \\ & + \left( -2R - \frac{17}{6} + \frac{2}{3R} + \frac{1}{24R^2} \right) \frac{L_{WZ}(M_w^2)}{M_w^2}, \end{aligned} \quad (258)$$

$$Z_b(M_z^2) = -8R^2 - \frac{34R}{3} + \frac{35}{18} \left( 1 + \frac{1}{R} \right) - \frac{r_w}{2} + \frac{r_z^2}{12R} + r_w \left( -\frac{3}{4} + \frac{r_z}{4} - \frac{r_z^2}{24} \right) \ln r_z$$

---

<sup>14</sup>One should eliminate there the (approximate) fermionic parts proportional to  $\text{Tr}Q_f^2$  and  $N_f$ .

$$\begin{aligned}
& + \frac{5 \ln R}{6R} + \left( \frac{1}{2} - \frac{r_z}{6} + \frac{r_z^2}{24} \right) \frac{L_{ZH}(M_z^2)}{M_w^2} \\
& + \left[ -2R^3 - \frac{17}{6}R^2 + \frac{2}{3}R + \frac{1}{24} \right] \frac{L_{WW}(M_z^2)}{M_w^2}, \tag{259}
\end{aligned}$$

$$\begin{aligned}
Z_b^F(M_z^2) = & -4R^2 + \frac{17R}{3} - \frac{23}{9} + \frac{5}{18R} - \frac{r_w}{2} + \frac{r_w r_z}{6} + r_w \left( -\frac{3}{4} + \frac{3r_z}{8} - \frac{r_z^2}{12} \right) \ln r_z \\
& - \frac{1}{12R} \ln R + \frac{\ln r_z}{2R} + \left( -R^3 + \frac{7R^2}{6} - \frac{17R}{12} - \frac{1}{8} \right) \frac{L_{WW}(M_z^2)}{M_w^2} \\
& + \left[ \frac{1}{2} - \frac{5r_z}{24} + \frac{r_z^2}{12} + \frac{1}{2(r_z - 4)} \right] \frac{L_{ZH}(M_z^2)}{M_w^2}, \tag{260}
\end{aligned}$$

Function  $L_{v_1 v_2}(s) \equiv L(-s; M_{v_1}^2, M_{v_2}^2)$  is defined in (2.14) of Ref. [82] and  $\mathcal{F}_n$  and  $\mathbf{I}_n(Q^2; M_1^2, M_2^2)$  in appendices C and D of Ref. [83]. The fermionic corrections are:

$$Z_f(s) = \frac{1}{2R} \sum_f N_c^f \left[ \frac{-s}{M_z^2} (1 + v_f^2) \mathbf{I}_3(-s; m_f^2, m_f^2) + \frac{m_f^2}{M_z^2} \mathbf{I}_0(-s; m_f^2, m_f^2) \right], \tag{261}$$

$$\begin{aligned}
W_f(s) = & \sum_{f=(f_u, f_d)} N_c^f \left[ 2 \frac{-s}{M_w^2} \mathbf{I}_3(-s; m_{f_u}^2, m_{f_d}^2) + \frac{m_{f_u}^2}{M_w^2} \mathbf{I}_1(-s; m_{f_u}^2, m_{f_d}^2) \right. \\
& \left. + \frac{m_{f_d}^2}{M_w^2} \mathbf{I}_1(-s; m_{f_d}^2, m_{f_u}^2) \right], \tag{262}
\end{aligned}$$

$$\begin{aligned}
Z_f^F(M_z^2) = & - \sum_f N_c^f \left\{ \frac{r_f}{2} [1 - r_f M_w^2 \mathcal{F}(-M_z^2, m_f^2, m_f^2)] + \frac{1}{6R} (1 + v_f^2) \right. \\
& \left. \times \left[ \frac{1}{2} \ln(r_f R) + r_f R + \left( -\frac{1}{4R} + \frac{r_f}{2} - r_f^2 R \right) M_w^2 \mathcal{F}(-M_z^2, m_f^2, m_f^2) \right] \right\}, \tag{263}
\end{aligned}$$

with  $r_f = m_f^2/M_w^2$  and the color factor  $N_c^f$ . The  $\gamma Z$ -mixing function is:

$$M(s) = 2 \sum_f N_c^f |Q_f| v_f \mathbf{I}_3(-s; m_f^2, m_f^2). \tag{264}$$

The vertex functions are in the limit of vanishing fermion masses:

$$V_{1V}(s) = -\frac{7}{2} - 2R_V - (3 + 2R_V) \ln(-\tilde{R}_V) + 2(1 + R_V)^2 [\text{Li}_2(1 + \tilde{R}_V) - \text{Li}_2(1)], \tag{265}$$

$$V_{2W}(s) = -\frac{1}{6} - 2R_W - \left( \frac{7}{6} + R_W \right) \frac{L_{WW}(s)}{s} + 2R_W (R_W + 2) \mathcal{F}_3(s, M_W^2), \tag{266}$$

with

$$\tilde{R}_V = R_V - i\gamma_V, \quad \gamma_V = \frac{M_V \Gamma_V}{s}, \quad R_V = \frac{M_V^2}{s}. \tag{267}$$



The additional  $t$  mass corrections to the  $Zb\bar{b}$  vertex and the counter term are at the  $Z$  resonance<sup>15</sup>:

$$\begin{aligned}
V_{1W}^t(M_Z^2) &= \frac{1}{R} \int_0^1 dy \left\{ \left[ \frac{1}{2} - 3y(1-y) \right] \ln|r_1| + 2rR \ln|r_2| - rR + (2+R) \right. \\
&\quad \times \left[ \bar{F}_1(r) - \bar{F}_1(0) \right] - \left( \frac{3}{2} + R \right) \left[ \bar{F}_2(r) - \bar{F}_2(0) \right] + \frac{1}{2} rR(2+R) \bar{F}_2(r) \\
&\quad \left. - \frac{2rR(1-R)}{(1-4R)} \left[ 1 + \ln|r_2| - 4\bar{F}_1(r) + \frac{1-r}{2} \bar{F}_2(r) \right] \right\}, \quad (268)
\end{aligned}$$

$$\begin{aligned}
V_{2W}^t(M_Z^2) &= \frac{1}{R} \int_0^1 dy \left\{ -(2+R) \left[ \bar{F}_2(r) - \bar{F}_2(0) \right] + r \left[ 2R \ln|r_3| + \frac{1-2R}{4} (\ln|r_4| - 1) \right. \right. \\
&\quad \left. \left. + \frac{1}{2} (r - 2rR - 4R - 4) F_1(r) + \frac{1}{4} (1 - r + 2R + 2rR) F_2(r) \right] \right\}, \quad (269)
\end{aligned}$$

$$\delta\rho_{ct,b}^t = -\frac{r(1+2R)}{6(1-r)} \left[ \frac{1}{2} (5r-11) + \frac{3r(r-2)}{1-r} \ln r \right], \quad (270)$$

with  $r = r_t$  and

$$\begin{aligned}
r_1 &= \frac{rR}{y(1-y)} - 1, & r_2 &= r - (1-y) \frac{y}{R}, \\
r_3 &= y + (1-y)r, & r_4 &= 1 - (1-y) \frac{y}{R}, \\
F_i(r) &= f_i(1, r), & \bar{F}_i(r) &= f_i(r, 1), \quad i = 1, 2,
\end{aligned}$$

$$\begin{aligned}
f_1(a, b) &= \frac{1}{a-b-y/R} \ln \frac{a-y(1-y)/R}{ay+b(1-y)}, \\
f_2(a, b) &= \frac{1-y}{a-b-y/R} - \left( b + \frac{y^2}{R} \right) f_1(a, b). \quad (271)
\end{aligned}$$

A completely analytical expression, valid at arbitrary  $s$  may be found in [84]. In the next section, we will need in addition the photonic self energy function  $A(s)$ , and  $D_Z(s)$ :

$$A(s) = \frac{34}{3} + 8R_w + \left( \frac{17}{6} + 2R_w \right) \frac{L_{ww}(s)}{s}, \quad (272)$$

$$\begin{aligned}
D_{z,b}(s) &= \frac{34R}{3} - \frac{35}{18} - \frac{4}{9R} - \frac{\ln R}{12R} - 2R^2 \frac{L_{ww}(s)}{s} + \left( -2R^2 - \frac{17R}{6} + \frac{2}{3} + \frac{1}{24R} \right) \\
&\quad \times \frac{L_{ww}(s) - \mathcal{R}e L_{ww}(M_Z^2)}{-s + M_Z^2} + \frac{1}{R} \left\{ \frac{R_z}{12} (1-r_z)^2 + [1 + (1-r_z) \right. \\
&\quad \times (10 - 5r_z + r_z^2) R_z + (1-r_z)^3 R_z^2] \frac{\ln r_z}{24} + [11 - 4r_z + r_z^2 \\
&\quad \left. + (1-r_z) R_z] \frac{L_{zh}(s)}{24s} + \left( \frac{1}{2} - \frac{r_z}{6} + \frac{r_z^2}{24} \right) \frac{L_{zh}(s) - \mathcal{R}e L_{zh}(M_Z^2)}{-s + M_Z^2} \right\}, \quad (273)
\end{aligned}$$

$$D_{z,f}(s) = \frac{M_Z^2}{M_Z^2 - s} [Z_f(s) - \mathcal{R}e Z_f(M_Z^2)]. \quad (274)$$

---

<sup>15</sup> The net one loop finite  $t$  mass effect from the two vertices and the counter term is taken into account in ZFITTER by a variable VTB.

#### 4.4.4 Form factors of the process $e^+e^- \rightarrow f\bar{f}$

The virtual, non-photon corrections to fermion pair production, including Bhabha scattering, may be described by four form factors per production channel as is indicated in Eq. (21). The contributions from the  $ZZ, WW$  box diagrams are vanishingly small at the  $Z$  peak. Leaving them out<sup>16</sup>, it is [83]:

$$\begin{aligned} \rho_{ef}(s)^{\text{1loop},\alpha} = & 1 + \frac{\alpha}{4\pi(1-R)} \left\{ Z(M_z^2) - W_f(0) + \frac{19}{12} - \frac{5}{8R} + \frac{r_w}{8} + \frac{3}{4} \left[ -\frac{r_w \ln r_w}{1-r_w} \right. \right. \\ & + \left. \left( \frac{1}{1-R} - \frac{1}{R} \right) \ln R \right] + \frac{5L_{ww}(s)}{6s} + D_z(s) + 2RV_{2w}(s) + \left[ -2R + \frac{1}{2} \right. \\ & \left. \left. + \frac{1}{4}(v_e + v_f) \right] V_{1w}(s) + \frac{1}{8R} \left[ 1 + \frac{3}{2}(v_e^2 + v_f^2) \right] V_{1z}(s) + \frac{1}{2} \delta \rho_{ct,f}^t \right\}, \quad (275) \end{aligned}$$

$$\begin{aligned} \kappa_f(s)^{\text{1loop},\alpha} = & 1 + \frac{\alpha}{4\pi(1-R)} \left\{ \frac{R}{1-R} [Z(M_z^2) - W(M_w^2)] \right. \\ & - \frac{4}{9} - \frac{L_{ww}(s)}{12s} - M(s) - RA(s) + (R_w - 2R) V_{2w}(s) \\ & + \left[ 2R - |Q_f| - \frac{1}{4}(v_e + v_f) + (|Q_f| - 1) R_z \right] V_{1w}(s) \\ & \left. + \left[ -\frac{1}{8R} v_e(1+v_e) - \frac{1}{2} |Q_f| v_f(1-R_z) \right] V_{1z}(s) - \frac{1}{2} \delta \rho_{ct,f}^t \right\}, \quad (276) \end{aligned}$$

$$\begin{aligned} \kappa_{ef}(s)^{\text{1loop},\alpha} = & 1 + \frac{\alpha}{4\pi(1-R)} \left\{ \frac{2R}{1-R} [Z(M_z^2) - W(M_w^2)] - \frac{8}{9} - \frac{L_{ww}(s)}{6s} \right. \\ & - 2M(s) - \frac{4}{3}R - 2RV_{2w}(s) - (R + R_w) \left[ A(s) - \frac{2}{3} \right] \\ & + \left[ 2R - \frac{1}{2} - \frac{1}{4}(v_e + v_f) \right] V_{1w}(s) + \left[ -\frac{1}{8R} - \frac{3}{16R} (v_e^2 + v_f^2) \right. \\ & \left. \left. + \frac{1-R}{R} (Q_e^2 + Q_f^2) (1-R_w) \right] V_{1z}(s) - \frac{1}{2} \delta \rho_{ct,f}^t \right\}. \quad (277) \end{aligned}$$

#### 4.4.5 The $\mathcal{O}(\alpha\alpha_s)$ corrections to electroweak observables

Here we follow presentation of Ref. [85], based on the second Ref. [52].

$$\Delta\alpha^{2\text{loop},\alpha\alpha_s} = \frac{\alpha\alpha_s}{3\pi^2} Q_t^2 \frac{m_t^2}{Q^2} \mathcal{R}e \left\{ \Pi_t^{VF}(Q^2) + \frac{45}{4} \frac{Q^2}{m_t^2} \right\}, \quad (278)$$

$$\Delta r^{2\text{loop},\alpha\alpha_s} = \frac{\alpha\alpha_s}{12\pi^2 s_W^2} \frac{m_t^2}{M_W^2} \mathcal{R}e \left\{ -4s_W^2 \left[ Q_b^2 \Pi_b^F(M_W^2) + Q_t^2 \Pi_t^{VF}(M_W^2) \right] \right.$$

<sup>16</sup> The interested reader may find expressions for  $WW, ZZ$  boxes in Ref. [83] and in the subroutine `ROKANC(..., t-s, -s, -t, ...)` of `ZFITTER` for the s channel ( $t > 0$ ). For the t channel (used in Bhabha scattering) the call is `ROKANC(..., s, t, u, ...)`.

$$\begin{aligned}
& + \frac{R}{4s_W^2} \left[ (v_b^2 + 1) \Pi_b^F(M_Z^2) + v_t^2 \Pi_t^{VF}(M_Z^2) + \Pi_t^{AF}(M_Z^2) \right] \\
& - \frac{1}{s_W^2} (c_W^2 - s_W^2) \Pi_t^{WF}(M_W^2) - \Pi_0^{WF} \Big\} , \tag{279}
\end{aligned}$$

$$\begin{aligned}
\Delta\kappa^{2\text{loop},\alpha\alpha_s} &= \frac{\alpha\alpha_s}{12\pi^2 s_W^2} \frac{m_t^2}{M_W^2} \mathcal{R}e \left\{ -\frac{R}{4s_W^2} \left[ (v_b^2 + 1) \Pi_b^F(M_Z^2) + v_t^2 \Pi_t^{VF}(M_Z^2) + \Pi_t^{AF}(M_Z^2) \right] \right. \\
& \left. + \frac{c_W^2}{s_W^2} \Pi_t^{WF}(M_W^2) - \frac{M_W^2}{Q^2} \left[ v_b |Q_b| \Pi_b^F(Q^2) + v_t |Q_t| \Pi_t^{VF}(Q^2) \right] \right\} , \tag{280}
\end{aligned}$$

$$\begin{aligned}
\Delta\rho^{2\text{loop},\alpha\alpha_s} &= \frac{\alpha\alpha_s}{48\pi^2 s_W^2} \frac{m_t^2}{M_W^2} \mathcal{R}e \left\{ -\frac{Q^2}{m_t^2} (v_b^2 + 1) \frac{\ln(Q^2/M_Z^2)}{1 - Q^2/M_Z^2} + 4\Pi_0^{WF} \right. \\
& + \left[ \frac{1}{1 - Q^2/M_Z^2} \left( v_t^2 \left[ \Pi_t^{VF}(M_Z^2) - \Pi_t^{VF}(Q^2) \right] \right. \right. \\
& \left. \left. + \Pi_t^{AF}(M_Z^2) - \Pi_t^{AF}(Q^2) \right) - v_t^2 \Pi_t^{VF}(M_Z^2) - \Pi_t^{AF}(M_Z^2) \right] \Big\} , \tag{281}
\end{aligned}$$

and, when  $Q^2 = M_Z^2$ ,

$$\begin{aligned}
\Delta\rho^{2\text{loop},\alpha\alpha_s} &= \frac{\alpha\alpha_s}{48\pi^2 s_W^2} \frac{m_t^2}{M_W^2} \mathcal{R}e \left\{ \frac{M_Z^2}{m_t^2} (v_b^2 + 1) + \left[ v_t^2 \left( M_Z^2 \frac{d\Pi_t^{VF}(Q^2)}{dQ^2} \Big|_{Q^2=M_Z^2} \right. \right. \right. \tag{282} \\
& \left. \left. - \Pi_t^{VF}(M_Z^2) \right) + M_Z^2 \frac{d\Pi_t^{AF}(Q^2)}{dQ^2} \Big|_{Q^2=M_Z^2} - \Pi_t^{AF}(M_Z^2) \right] + 4\Pi_0^{WF} \Big\} .
\end{aligned}$$

Here, the two-loop functions are:

$$\begin{aligned}
\Pi_t^{VF}(Q^2) &= \frac{1}{\alpha} \left\{ \frac{55}{4} - 26\alpha + 3(1 + x_\alpha)(1 - 6\alpha)f_\alpha - 2 \left[ \alpha(2x_\alpha^2 - 3x_\alpha + 2) + 2x_\alpha \right] f_\alpha^2 \right. \\
& \left. + 2(4\alpha^2 - 1)I_\alpha + 4\alpha(2\alpha - 1)(4\alpha + 1)J_\alpha \right\} , \tag{283}
\end{aligned}$$

$$\begin{aligned}
\Pi_t^{AF}(Q^2) &= \frac{1}{\alpha} \left\{ \frac{55}{4} - \frac{19}{2}\alpha + 12\alpha^2 + 3(1 + x_\alpha)(1 + 12\alpha + 4\alpha^2)f_\alpha + 2 \left[ 2x_\alpha(3\alpha^2 - 1) \right. \right. \\
& \left. \left. + \alpha(7x_\alpha^2 - 3x_\alpha + 7) \right] f_\alpha^2 - 2(1 + 2\alpha)(1 + 4\alpha)I_\alpha - 4\alpha(1 + 4\alpha)^2 J_\alpha \right\} , \tag{284}
\end{aligned}$$

$$\begin{aligned}
\Pi_t^{WF}(Q^2) &= \frac{1}{4\alpha} \left\{ 55 - \frac{71}{2}\alpha - 10\alpha^2 - 8\alpha G(x_b) + 2(6 + 9\alpha - 5\alpha^2)f_b \right. \\
& + 2 \left[ 4x_b(\alpha^2 - \alpha - 1) + \alpha(5 - 4\alpha) \right] f_b^2 \\
& \left. + 4(\alpha - 2)(\alpha + 1)^2 I_b + 8\alpha(\alpha - 2)(\alpha + 1)J_b \right\} , \tag{285}
\end{aligned}$$

$$\frac{d\Pi_t^{VF}(Q^2)}{dQ^2} = -\frac{1}{m_t^2} \left[ \frac{43}{4} + 18\alpha + (10\alpha + 3)(1 + x_\alpha)f_\alpha + 2(5\alpha - 2)x_\alpha f_\alpha^2 \right]$$

$$- 8 (2\alpha - 1) x_\alpha^2 f_\alpha^2(x_\alpha^2) - 2 (4\alpha^2 + 1) I_\alpha - 8\alpha^2 (1 + 4\alpha) J_\alpha \Big] , \quad (286)$$

$$\begin{aligned} \frac{d\Pi_t^{AF}(Q^2)}{dQ^2} = & -\frac{1}{m_t^2} \left[ \frac{43}{4} - 12\alpha (2\alpha + 3) - (24\alpha^2 + 26\alpha - 3) (1 + x_\alpha) f_\alpha \right. \\ & - 2(12\alpha^2 + 19\alpha + 2) x_\alpha f_\alpha^2 + 8(1 + 4\alpha) x_\alpha^2 f_\alpha^2(x_\alpha^2) + 2(8\alpha^2 - 1) I_\alpha \\ & \left. + 16\alpha^2 (1 + 4\alpha) J_\alpha \right] , \end{aligned} \quad (287)$$

where

$$\begin{aligned} x_\alpha &= \frac{2\alpha}{1 + 2\alpha + \sqrt{1 + 4\alpha}} , & \alpha &= -\frac{m_t^2}{Q^2} , & x_b &= \frac{\alpha}{1 + \alpha} , \\ I_\alpha &= F(1) + F(x_\alpha^2) - 2F(x_\alpha) , & I_b &= F(1) - F(x_b) , & f_\alpha &= \frac{\ln x_\alpha}{1 - x_\alpha} , \\ J_\alpha &= \frac{1 - x_\alpha}{(1 + x_\alpha)\alpha} [G(x_\alpha^2) - G(x_\alpha)] , & J_b &= -\frac{1}{2\alpha} G(x_b) , & f_b &= \frac{\ln x_b}{1 - x_b} , \end{aligned}$$

$$F(x) = \int_0^x dy \left( \frac{\ln y}{1 - y} \right)^2 \ln \frac{x}{y} , \quad G(x) = \int_0^x dy \left( \frac{\ln y}{1 - y} \right)^2 . \quad (288)$$

The  $\Pi_b^F(Q^2)$  is a common asymptotic expression for functions (283–285) for  $m_t \rightarrow 0$ :

$$\alpha \Pi_b^F(Q^2) = [\alpha \Pi^{VF}]_{m_t=0} = [\alpha \Pi^{AF}]_{m_t=0} = [\alpha \Pi^{WF}]_{m_t=0} = \frac{55}{4} - 12\zeta(3) + 3 \ln \alpha , \quad (289)$$

with  $\zeta(3) = 1.0202\dots$  Further,

$$\Pi_0^{WF} = \lim_{Q^2 \rightarrow 0} \Pi_0^{WF}(Q^2) = -\frac{1}{4} \left[ \frac{105}{2} + 2\pi^2 \right] . \quad (290)$$

## 5 Description of options in different approaches

### 5.1 BHM options

In this subsection we describe the main options implemented in the version of **BHM** used for the present study to estimate the theoretical uncertainties. Out of the actual different user-accessible flags and their possible values, only the ones used in the present analysis are discussed. The rest of the flags and/or values either have a negligible effect on the predictions or exist only for testing purposes.

- **IRES=0,1,2**

The resummation of the one-loop one-particle irreducible contributions in  $\Delta r$  and, in general, in the whole set of self-energies is implemented in **BHM** in three different ways. These can be considered representative of at least two rather different philosophies. The basic difference comes from the treatment of the  $(\hat{\Sigma}^{\gamma Z})^2$  mixing term. If **IRES=0**, then the resummation comes from the resolution of the renormalization equations keeping that term (see for instance W.Hollik in Ref. [2]). In this case, not only

leading top and Higgs terms are re-summed but also non-leading ones. This is the default working option. If  $\text{IRES}=1,2$ , then the renormalization equations are solved keeping strictly one-loop contributions and the inclusion of higher-order terms coming from one-loop one-particle irreducible diagrams is explicitly done for  $\Delta r$  and for each self-energy. If  $\text{IRES}=1$ , the prescription used to treat the top, Higgs and remainder terms follows the suggestions of Halzen, Kniehl and Stong [86], whereas if  $\text{IRES}=2$ , then it follows the suggestions from S.Fanchiotti and A.Sirlin [49]. Both differ in the detailed treatment of the Higgs and remainder terms.

- $\text{ITWO}=1,2$

This flag allows the choice of scale in vertex corrections. The dominant effect happens in the b-vertex. If  $\text{ITWO}=1$ , then the  $\alpha(0)$  scale is used whereas, if  $\text{ITWO}=2$ , then the  $G_\mu$  scale is used. The later is the default working option.

- $\text{IFAC}=0,1,2$

This flag allows the choice of different factorization schemes for the final-state corrections. If  $\text{IFAC}=0$  then no factorization at all is applied for weak vertex, QED and QCD final-state corrections. That means that these three kinds of corrections are independently applied to the vacuum-polarization dressed amplitudes. This is the default working option. If  $\text{IFAC}=1$ , then QED corrections are applied on top of weak vertex ones, and if  $\text{IFAC}=2$ , then QCD corrections are also applied on top of weak vertex and QED ones.

- $\text{IQCD}=3,4$  This flag allows the choice of different treatments of the QCD corrections to electroweak loops. Of its possible values, only two have been used in the present study: if  $\text{IQCD}=3$ , then the exact AFMT correction is implemented, whereas if  $\text{IQCD}=4$ , then the Sirlin's scale  $\xi = 0.248$  is used. These two approaches have already been discussed elsewhere in the text.

To summarize, **BHM** runs in  $3 \times 2 \times 3$  electroweak  $\times 2$  QCD options. We have added Table 26, showing the effect of the working options of **BHM** on theoretical errors.

## 5.2 LEPTOP options

Several options to the preferred formulas used in **LEPTOP** have been chosen and variations of these formulae have been made. Usually each option consists of the addition of an extra term corresponding to a rough guess of the value of the uncalculated higher-order terms. We then make all possible combinations of these options —  $2^n$  in total, where  $n$  is the number of options. Among all these  $2^n$  combinations we locate those yielding the minimum and the maximum values of the observables and take as the estimate of the theoretical errors their deviations from the central values.

Theoretical uncertainties come from two different sources: 1) not yet calculated Feynman diagrams, 2) not yet calculated terms in a given diagram. The first source is represented in **LEPTOP** by the gluonic corrections to the electroweak vertices of light quarks,  $F_{iq}$ , where  $q = u, d, s, c$ ;  $i = V, A$ . In this case as a basis for options a crude estimate of these corrections is used:

$$\delta F_{iq} = \frac{\hat{\alpha}_s}{\pi} F_{iq} . \quad (291)$$

The second source is represented by non-leading terms of a) higgs and b)  $\alpha_s^2$  corrections to the  $t\bar{t}$  loop in  $Z$  boson self energy and  $t - b$  loop in  $W$  boson self energy denoted by  $\delta V_i^{t^2}$  and  $\delta V_i^{\alpha_s^2}$  respectively and c) by the  $t\bar{t}$  vertex contribution to  $Z \rightarrow b\bar{b}$  decay denoted by  $\delta\phi^{t^2}$ .

In cases a) and b) the missing non-leading terms are estimated by multiplying the corresponding leading terms by a factor  $2/t$ , where  $t = (m_t/M_Z)^2$ . In the case c) the leading correction itself is so small that it is taken as a measure of uncertainty. Thus the LEPTOP uncertainties are:

$$\Delta V_i^{t^2} = (2/t)\delta V_i^{t^2} = (2/t) \left( -\frac{\bar{\alpha}}{\pi} \frac{A(M_H/m_t)t^2}{16s^2c^2} \right) \quad (292)$$

in accord with Eq. (206);

$$\Delta V_i^{\alpha_s^2} = (2/t)\delta V_i^{\alpha_s^2} = (2/t)(-1.25\hat{\alpha}_s^2(m_t)t) \quad (293)$$

in accord with Eq. (205);

$$\Delta\phi^{\alpha_s^2} = -1.37 \frac{3-2s^2}{2s^2c^2} \frac{\pi}{3} \hat{\alpha}_s^2(m_t)t \quad (294)$$

in accord with the first term in Eq. (220);

$$\Delta\phi^{t^2} = \delta\phi^{t^2} = \frac{3-2s^2}{2s^2c^2} \frac{\bar{\alpha}t^2}{16\pi s^2c^2} \tau_b^{(2)} \quad (295)$$

in accord with the second term in Eq. (220), as  $\Delta\phi^{\alpha_s^2}$  is much larger then  $\delta\phi^{t^2}$ , the latter will be neglected;

$$\Delta F_{iq}^{\alpha_s} = \delta F_{iq}^{\alpha_s} = \frac{\hat{\alpha}_s}{\pi} F_{iq} \quad (296)$$

in accord with Eq. (291).

Explicit calculations [1, 76] give:

$$F_{Vu} = -0.00169 , \quad F_{Au} = -0.00165 , \quad (297)$$

$$F_{Vd} = 0.00138 , \quad F_{Ad} = 0.00137 . \quad (298)$$

Note that the uncertainties  $\Delta F_{iq}^{\alpha_s}$  produce corresponding uncertainties in electroweak corrections  $\delta\Gamma_q$  to the partial widths  $Z \rightarrow q\bar{q}$ :

$$\delta\Gamma_q = 24sc\Gamma_0 2I_q^{(3)} [(1-4|Q_q|s^2)F_{Vq} + F_{Aq}] . \quad (299)$$

With above numbers

$$\Delta\Gamma_u = \Delta\Gamma_c = -1.9 \left( \frac{\alpha_s}{\pi} \right) \text{MeV} \simeq -0.08 \text{ MeV} , \quad (300)$$

$$\Delta\Gamma_d = \Delta\Gamma_s = -2.0 \left( \frac{\alpha_s}{\pi} \right) \text{ MeV} \simeq -0.08 \text{ MeV} . \quad (301)$$

So that the sum over four light quarks is

$$\Sigma_1^4 \Delta\Gamma_q = -0.3 \text{ MeV} . \quad (302)$$

Now the options of LEPTOP can be formulated:

- Options 1,2

Uncertainty  $\Delta V_i^{t^2}$  given by Eq. (292) is added to (option 1), or subtracted from (option 2) the functions  $V_i$ ,  $i = m, A, R$ .

- Options 3,4

Uncertainty  $\Delta V_i^{\alpha_s^2}$  given by Eq.(293) is added to (option 3), or subtracted from (option 4) the function  $V_i$ ,  $i = m, A, R$ .

- Options 5,6

Uncertainties  $\Delta\Gamma_q (q = u, d, s, c)$  given by Eqs. (300), (301) are added to (option 5) or subtracted from (option 6) the partial widths  $\Gamma_q$ .

- Option 7

Uncertainty  $\Delta\phi^{\alpha_s^2}$  is added to the function  $\phi(t)$  given by Eq. (219).

Theoretical uncertainties for observables, assuming  $M_H = 300 \text{ GeV}$ ,  $m_t = 175 \text{ GeV}$ ,  $\hat{\alpha}_s(M_Z) = 0.125$  are shown in Table 27.

### 5.3 TOPAZ0 options

In this subsection we describe the options implemented in TOPAZ0 version 2.0 for studying the theoretical uncertainties. A general comment is in order here. Some of the TOPAZ0 electroweak options have been originally designed to produce a conservative estimate of the uncertainty. If nothing stands against a certain option then we accept it, even if it goes against our own philosophy.

- OU0.EQ. 'N' ('Y')

This is the primordial option since it controls the partial resummation of bosonic self-energies. If OU0.EQ. 'N', then in  $\hat{s}^2$  and  $\Delta s^2$ , we use:

$$\begin{aligned} \Sigma &\rightarrow \Sigma^{\text{ferm}} , \\ \Delta s^2 &= \frac{\Sigma^{\text{bos}}}{c^2 - s^2} , \end{aligned} \quad (303)$$

i.e., all bosonic self-energies are expanded. Otherwise for `OU0.EQ.'``Y'` we use:

$$\begin{aligned}\Sigma &\rightarrow \Sigma_R = \Sigma^{\text{tot}} - (c^2 - s^2) \frac{\mathcal{R}e\Sigma_{Z\gamma}(M_Z^2)}{M_Z^2}, \\ M_Z^2 \Delta s^2 &= \mathcal{R}e\Sigma_{Z\gamma}(M_Z^2).\end{aligned}\tag{304}$$

For `OU0.EQ.'``Y'` `TOPAZ0` will automatically select `OU2 = 'N'` and `OU3 = 'Y'`.

- `OU1.EQ.'``N'` (`'Y'`)

The default choice requires that in

$$\begin{aligned}\delta g_V^f &= \frac{\alpha}{4\pi} \left[ \frac{2F_V^f - \frac{1}{2}v_f \Delta\Pi_Z}{c^2 s^2} - 2Q_f \Delta s^2 \right], \\ \delta g_A^f &= \frac{\alpha}{4\pi} \left[ \frac{2F_A^f - \frac{1}{2}I_f^{(3)} \Delta\Pi_Z}{c^2 s^2} \right],\end{aligned}\tag{305}$$

everything must be expanded in terms of  $\alpha \equiv \alpha(0) = 1/137.036\dots$  while for `OU1.EQ.'``Y'` the parameter expansion is selected as  $\alpha \equiv \alpha(M_Z)$ .

- `OU2.EQ.'``N'` (`'Y'`)

This option deals with the so-called problem of expansion. The default for `TOPAZ0` is the expanded solution where, for instance, a  $Z$  partial width is computed according to

$$\begin{aligned}\Gamma_f &= \frac{G_\mu M_Z^3}{6\sqrt{2}\pi} N_c^f \rho_Z \left[ \hat{v}_f^2 + \frac{1}{4} + 2\hat{v}_f \delta g_V^f + 2I_f^{(3)} \delta g_A^f \right], \\ \hat{v}_f &= I_f^{(3)} - 2Q_f \hat{s}^2,\end{aligned}\tag{306}$$

where for the moment we assume that there is no final-state QED + QCD radiation, factor, whose treatment will be explained by one of the following options. If, instead, `OU2.EQ.'``Y'`, then the electroweak corrected vector and axial-vector couplings are squared numerically.

- `OU3.EQ.'``Y'` (`'N'`)

Two different procedures are introduced for dealing with the physical Higgs contribution to the self-energies. If `OU3.EQ.'``Y'`, then by working in a  $\overline{MS}$  environment with a scale  $\mu$  set to  $M_Z$  we extract from  $\Sigma^{\text{bos}}$  the physical Higgs contribution,  $\Sigma^H$ , and redefine

$$\Sigma^{\text{ferm}} \rightarrow \Sigma^{\text{ferm}} + [\Sigma^H]_{\overline{MS}},\tag{307}$$



where  $\Sigma^H$  is subject to no additional expansion, such as leading or sub-leading behavior with  $M_H$ . Of course, **OU3.EQ. 'N'** leaves the Higgs contribution expanded as for any other bosonic contribution. This option reflects and partially illustrates one of the defining rules of **TOPAZO** — a certain reluctance to accept the isolation and a different treatment for something which can be considered as the leading part of some quantity only for *extraordinary* values of some of the parameters.

- **OU4.EQ. 'N' ('Y')**

When we consider the mass corrections to the  $\bar{b}b$  partial decay rate there will be something like

$$-6 \frac{m_b^2}{M_Z^2} \left[ 2I_f^{(3)} \delta g_A^f + (\delta g_A^f)^2 \right] . \quad (308)$$

In these mixed corrections there is an additional uncertainty connected with the choice of  $m_b$  — i.e., pole mass or running mass.

- **OU5.EQ. 'N' ('Y')**

According to the strategy that all non-leading and gauge-variant quantities should be expanded, in Eq.( 305) we use as the zero order approximation,

$$s^2 = \frac{1}{2} \left[ 1 - \sqrt{1 - \frac{4\pi\alpha(M_Z)}{\sqrt{2}G_\mu M_Z^2}} \right] . \quad (309)$$

However, since perturbation theory rearranges itself in such a way that the expansion of  $\sin^2 \theta_{\text{eff}}^l$  starts with  $\hat{s}^2$ , i.e.,

$$\sin^2 \theta_{\text{eff}}^l = \hat{s}^2 + \frac{1}{2} \delta g_V^l + \frac{1}{2} (4\hat{s}^2 - 1) \delta g_A^l , \quad (310)$$

we have envisaged the possibility of reorganizing the structure of the pseudo-observables such that to all orders the bare weak mixing angle has an expansion starting with  $\hat{s}^2$ . Combined with **OU1.EQ. 'N' ('Y')** this option tells us that the expansion parameter, formally  $\alpha/(4\pi s^2 c^2)$ , can be set to

$$\frac{G_\mu M_Z^2}{2\sqrt{2}\pi^2} \times \left\{ 1; \rho_Z^R; 1 - \Delta\alpha; \rho_Z^R(1 - \Delta\alpha) \right\} . \quad (311)$$

- **OU6.EQ. 'N' ('Y')**

This option deals with factorization of electroweak corrected kernels and QCD radiation. For instance, if **OU2.EQ. 'N'** — the expanded solution — we still distinguish between a non-factorized solution,

$$\Gamma_f = \frac{G_\mu M_Z^3}{6\sqrt{2}\pi} N_c^f \rho_Z \left[ \hat{v}_f^2 R_V^f + \frac{1}{4} R_A^f + 2\hat{v}_f \delta g_V^f + 2I_f^{(3)} \delta g_A^f \left( 1 - 6 \frac{m_f^2}{M_Z^2} \right) \right] , \quad (312)$$

and a fully factorized solution. A special treatment is of course devoted to  $b\bar{b}$  final state in order to reproduce the FTJR correction term.

- **OU7.EQ.'N'('Y')**

Higher order QCD corrections to  $\rho_z$  are implemented with the exact AFMT term or by subtracting from  $\Sigma^{\text{ferm}}$  the leading  $m_t$  term and by replacing it with the corresponding one evaluated at a scale of  $\xi = 0.248m_t$ .

To summarize TOPAZ0 runs in  $2^4$  or  $2^6$  electroweak  $\times 2$  QCD options. While we have devoted a special section to the effect of **OU0.EQ.'N'** and **OU2.EQ.'Y'**, here we present a short Table 28 to indicate the increasing spread in the theoretical errors while the various flags are switched on.

## 5.4 ZFITTER options

In this subsection we describe some electroweak and QCD options implemented in **ZFITTER** (version 4.9). Simultaneously, we give a description of the flags, implemented in version 4.9 for studying the theoretical uncertainties.

- **OZ1: IAMT4=3,2,1**

The realization of leading and remainder terms, given by formulae (71–84), is the default, **IAMT4=3**. If **IAMT4=2**, then  $X$  is not included in the leading terms, it remains a part of remainders [87]. If **IAMT4=1**, then both  $X$  and  $2\text{loop-}\alpha\alpha_s$  terms are in the remainders. In the last case the  $3\text{loop-}\alpha\alpha_s^2$  term is also placed in remainders. In the result of numerical investigations it was revealed that for **IAMT4=2** the remainder terms in  $\rho_f$  and  $\kappa_f$  are not small. Since this contradicts our philosophy to keep remainder terms small, one could exclude it from the set of working options. However, it was found that the difference between **IAMT4=3** and **1** is rather small, therefore this option doesn't sizably influence the theoretical errors.

- **OZ2: IHIGS=0,1**

This option governs the resummation of the leading Higgs contribution in  $\Delta r$

$$\Delta r^{\text{Higgs}} \simeq \frac{\sqrt{2}G_\mu M_W^2}{4\pi^2} \frac{11}{12} \left( \ln \frac{M_H^2}{M_W^2} - \frac{5}{6} \right), \quad M_H \gg M_W. \quad (313)$$

If **IHIGS=0** (the default), then the Higgs contribution is not re-summed. If **IHIGS=1** and if

$$\ln \frac{M_H^2}{M_W^2} - \frac{5}{6} \geq 0, \quad (314)$$

then it is re-summed — i.e., it is extracted from remainders with the scale  $\alpha/s_W^2$  and put to the leading terms with the scale  $G_\mu$ , as in (313). We observed, that  $10/12$  of  $\Delta r^{\text{Higgs}}$  is contained in  $X$ . Therefore, if **IAMT4=3**, then only  $1/12$  of it is additionally re-summed. The influence of this option on theoretical errors was found to be tiny. For this reason, the Higgs resummation has not been implemented in  $\rho_f$  and  $\kappa_f$ .

- OZ3: ISCRE=0,1,2

This option defines the scale of the remainder terms. If ISCRE=0 (the default), then the scale is  $\alpha/s_W^2$ , if ISCRE=2 it is  $G_\mu$ . (More precisely,  $G_\mu$  in  $\rho_f$  and  $\kappa_f$  and  $G_\mu(1 - \Delta\alpha)$  in  $\Delta r$ .) For ISCRE=1, the scale of the remainder in  $\Delta r$  is set equal to  $G_\mu(1 - \Delta r_L)$ , which was not included in the set of working options, since its influence is much smaller than the previous one's. The effect of the variation of the scale of the remainder term on the theoretical bands was found to be dominating. Especially influential is the scale variation in  $\Delta r$ , which introduces terms of the order  $c_W^2/s_W^2 \Delta\rho \cdot \Delta r_{\text{rem}}$ . This illustrates the importance in the calculation of the next-to-leading term of the order  $\mathcal{O}(G_\mu^2 m_t^2 M_Z^2)$ .

- OZ4: IFACR=0,1,2,3

It realizes four subsequent expansions of  $\Delta r$  as they are given in (99). The first, fully non-expanded option, is the default. Only the first expansion (the second row) was retained in the set of working options. The last two were excluded, since they contradict Sirlin's theorem on mass singularities. This leads to a visible spread of theoretical bands, although one much smaller than that of the previous option.

- OZ5: IFACT=0,1,2,3,4,5

It realizes six subsequent expansions for  $\rho_f$  and  $\kappa_f$ . The default, IFACT=0, corresponds to the non-expanded realizations (72)–(73). The four first options for  $\rho_f$ , IFACT=0,1,2,3, are exactly the same as are given in (99), while  $\kappa_f$  is expanded for IFACT=1,2,3:

$$\kappa_f = \kappa_L + \Delta\kappa_{f,\text{rem}} = 1 + \frac{c_W^2}{s_W^2} \Delta\rho_X + \Delta\kappa_{f,\text{rem}} . \quad (315)$$

For IFACT=4,5, we linearize the full expression (63). Introducing

$$\rho_L = \frac{1}{1 - \Delta\rho} , \quad (316)$$

$$\bar{g}_{VL}^f = 1 - 4|Q_f|s_W^2 \kappa_L , \quad (317)$$

see (72) and (80), we have for IFACT=4,

$$\begin{aligned} \Gamma_f = & \frac{G_\mu M_Z^3}{24\sqrt{2}\pi} N_c^f \left\{ (\rho_L + \Delta\rho_{f,\text{rem}}) \left[ (\bar{g}_{VL}^f)^2 R_V^f + R_A^f \right] \right. \\ & \left. + \rho_L \left[ -8s_W^2 \bar{g}_{VL}^f \Delta\kappa_{f,\text{rem}} R_V^f \right] \right\} . \end{aligned} \quad (318)$$

Realizing, that

$$R_{V,A}^f = 1 + \Delta R_{V,A}^f , \quad (319)$$

for IFACT=5 we finally end up with a fully expanded equation for the partial widths:

$$\begin{aligned} \Gamma_f = & \frac{G_\mu M_Z^3}{24\sqrt{2}\pi} N_c^f \left\{ \rho_L \left[ (\bar{g}_{VL}^f)^2 R_V^f + R_A^f \right] + \Delta\rho_{f,\text{rem}} \left[ (\bar{g}_{VL}^f)^2 + 1 \right] \right. \\ & \left. + \rho_L \left( -8s_W^2 \bar{g}_{VL}^f \Delta\kappa_{f,\text{rem}} \right) \right\} . \end{aligned} \quad (320)$$

It was found that the spread of error bands gradually grows while coming from `IFACT=0` to `IFACT=5`. For this reason, only these two limiting cases were left among the working options. This option was found to be rather influential.

- `OZ6`: `ISCAL=0,1,2,3,4`  
is the only QCD option. At the default, `ISCAL=0`, we implemented the exact AFMT correction. For `ISCAL=2,1,3` we implemented the  $\xi$ -factor as given in Ref. [65]. Finally, for `ISCAL=4`, Sirlin's scale  $\xi = 0.248$  (see Ref.[62]) was implemented. Only `ISCAL=0,4` were left among working options.

To summarize, `ZFITTER` runs in  $2^5$  electroweak  $\times$  2 QCD options <sup>17</sup>. Table 29 has been added to show the effect of the working options of `ZFITTER` on theoretical errors.

## Acknowledgements

The authors acknowledge G. Altarelli, K. Chetyrkin, G. Degrassi, J. Ellis, S. Fanchiotti, D. Haidt, A. Kataev, B. Kniehl, H. Kühn, A. Kwiatkowski, S. Larin, A. Sirlin, O. Tarasov for useful discussions. We are very much indebted to A.D. Schaile for a critical reading of the manuscript and useful suggestions. The authors of the codes which have presented flowcharts are grateful to V.L. Telegdi for insistence on and help in preparing them.

## References

- [1] *Z Physics at LEP 1*, G. Altarelli, R. Kleiss and C. Verzegnassi eds., CERN 89-08, Vol. 1 (1989) 235.
- [2] G. Burgers, W. Hollik and M. Martinez, program `BHM`;  
W. Hollik, Fortschr. Phys. **38** (1990) 3, 165;  
M. Consoli, W. Hollik and F. Jegerlehner: Proceedings of the Workshop on Z physics at LEP I, CERN Report 89-08 Vol. I, 7;  
G. Burgers, F. Jegerlehner, B. Kniehl and J.H.K ühn: CERN Report 89-08 Vol. I, 55.
- [3] V.A. Novikov, L.B. Okun, M.I. Vysotsky, Nucl. Phys. **B397** (1993) 35;  
V.A. Novikov, L.B. Okun, A.N. Rozanov M.I. Vysotsky and V. Yurov Phys. Lett. **B331** (1994) 433;  
V.A. Novikov, L.B. Okun, A.N. Rozanov and M.I. Vysotsky, CERN preprint CERN-TH.7217/94, Modern Physics Letters **A9** (1994) 2641.
- [4] G. Montagna, O. Nicrosini, G. Passarino, F. Piccinini and R. Pittau, Nucl. Phys. **B401** (1993) 3;  
G. Montagna, O. Nicrosini, G. Passarino, F. Piccinini and R. Pittau, program `TOPAZ0`, Comput. Phys. Commun. **76** (1993) 328.

---

<sup>17</sup>The option `OZ5`, `IFACT=5` also may be ranked among QCD options, since it simulates missing terms of the order  $\mathcal{O}(\alpha_s)$ .

- [5] W. Hollik, program WOH.
- [6] D. Bardin et al., program ZFITTER 4.9, Nucl. Phys. **B351** (1991) 1; Z. Phys. **C44** (1989) 493; Phys. Lett. **B255** (1991) 290; CERN-TH.6443/1992, May 1992; hep-ph/9412201.
- [7] *Review of Particle Properties* Phys. Rev. **D50** (1994) 1173.
- [8] F. Jegerlehner, Z.Phys. C32 (1986) 195;  
F. Jegerlehner, in Proceedings of the 1990 TASI in Elementary Particle Physics, ed. by P. Langacker and M. Cvetič (World Scientific, Singapore, 1991) p. 476.
- [9] Morris L. Swartz, Preprint SCAL-PUB-6710, November 1994; hep-ph/9411353.
- [10] A.D. Martin and D. Zeppenfeld, MAD-PH-855, November 1994; hep-ph/9411377.
- [11] S. Eidelman and F. Jegerlehner, PSI-PR-95-1, Budker INP 95-5, January 1995.
- [12] G. Burgers and F. Jegerlehner: Proceedings of the Workshop on Z physics at LEP I, CERN Report 89-08 Vol. I, 55;  
F. Jegerlehner, PSI-PR-91-08, April 1991.
- [13] W. Hollik, second Ref. [2].
- [14] D. Bardin, B. Kniehl, R. Stuart, private communication, 1992.
- [15] The LEP Electroweak Working Group, CERN-PPE/94-187 November 1994.
- [16] D. Schaile, plenary talk held at the XXXVII Int. Conf. on High Energy Physics, 20–27 July 1994, Glasgow, Scotland (ICHEP94, Glasgow).
- [17] S. Bethke, proceedings of the Linear Collider Workshop in Waikoloa/Hawaii, April 1993.
- [18] CDF Collaboration, F. Abe et al., FERMILAB-PUB-94/097-E (1994).
- [19] D. Bardin, S. Riemann, and T. Riemann, Z. Phys. **C32** (1986) 121;  
F. Jegerlehner, Z.Phys. **C32** (1986) 425;  
A. Denner and T. Sack, Z.Phys. **C46** (1990) 653;  
J. Rosner and M. Worah, Phys. Rev. **D49** (1994) 1363.
- [20] M. Martinez et al., Z.Phys. **C49** (1991) 645.
- [21] A. Leike, J. Rose, T. Riemann, Phys. Lett. **B273** (1991) 513;  
S. Kirsch and T. Riemann, SMATASY, DESY 94-125 (1994), hep-ph/9408365, to appear in Comp. Phys. Comm.
- [22] G. Passarino and M. Veltman, Nucl. Phys. **B160** (1979) 151.
- [23] A. Sirlin, Phys. Rev. **D22** (1980) 971;  
W.J. Marciano and A. Sirlin, Phys. Rev. **D22** (1980) 2695.

- [24] D.Yu. Bardin, P.Ch. Christova and O.M. Fedorenko, Nucl. Phys. **B175** (1980) 235;  
D.Yu. Bardin, P.Ch. Christova and O.M. Fedorenko, Nucl. Phys. **B197** (1982) 1;  
D.Yu. Bardin, M.S. Bilenky, G.V. Mitselmakher, T. Riemann and M. Sachwitz, Z.  
Phys. **C44** (1989) 493.
- [25] J. Fleischer and F. Jegerlehner, Phys. Rev. **D23** (1981) 2001.
- [26] K.I. Aoki, Z. Hioki, R. Kawabe, M. Konuma and T. Muta, Suppl. Prog. Theor. Phys.  
**73** (1982) 1.
- [27] M. Consoli, S. LoPresti and L. Maiani, Nucl. Phys. **B223** (1983) 474.
- [28] M. Böhm, W. Hollik and H. Spiesberger, Fortschr. Phys. **34** (1986) 687;  
W. Hollik, Fortschr. Phys. **38** (1990) 165.
- [29] F. Jegerlehner, Z.Phys. **C32** (1986) 425.
- [30] W. Hollik, H.J. Timme, Z. Phys. **C33** (1986) 125.
- [31] G. Passarino and R. Pittau, Phys. Lett. **B228** (1989) 89;  
G. Passarino, Nucl Phys. **B361** (1991) 351.
- [32] D.C. Kennedy and B.W. Lynn, Nucl. Phys. **B322** (1989) 1.
- [33] W.J. Marciano and A. Sirlin, Phys. rev. Lett. **46** (1981) 163;  
A. Sirlin, Phys. Lett. **B232** (1989) 123;  
G. Degrossi, S. Fanchiotti and A. Sirlin, Nucl. Phys **B351** (1991) 49;  
G. Degrossi and A. Sirlin, Nucl. Phys. **B352** (1991) 342.
- [34] G. Passarino and M. Veltman, Phys. Lett. **B237** (1990) 537.
- [35] A. Sirlin, Phys. Rev. **D22** (1980) 971.
- [36] W.J. Marciano and A. Sirlin, Phys. Rev. **D22** (1980) 2695.
- [37] CDF Collaboration, F. Abe et al., Phys. Rev. Lett. **65** (1990) 2443;  
UA2 Collaboration, Phys. Lett. **B276** (1992) 354 and [7].
- [38] G. 't Hooft and M. Veltman, in Louvain 1973, Particle Interactions at Very High  
Energies, New York, 1973, 177 and CERN 73-9.
- [39] B. Kniehl and J. Kühn, Nucl. Phys. **B329** (1990) 547.
- [40] S. Gorishny, A. Kataev and S. Larin, Phys. Letters **B259** (1991) 144.
- [41] A. L. Kataev, Phys. Lett. **B287** (1992) 209.

- [42] K.G. Chetyrkin, J.H. Kühn, Phys. Lett. **B248** (1990) 359;  
 K.G. Chetyrkin, J.H. Kühn and A.Kwiatkowski, Phys. Lett. **B282** (1992) 221;  
 K.G. Chetyrkin and A. Kwiatkowski, Phys. Lett. **B305** (1993) 285;  
 K.G. Chetyrkin, Phys. Lett. **B307** (1993) 169;  
 K.G. Chetyrkin and J.H. Kühn, Phys. Lett. **B308** (1993) 127;  
 K.G. Chetyrkin and A. Kwiatkowski, Phys. Lett. **B319** (1993) 307.
- [43] K.G. Chetyrkin and A. Kwiatkowski, Z. Phys. **C59** , 525 (1993).
- [44] S.A. Larin, T. van Ritbergen and J.A.M. Vermaseren, Phys. Lett. **B320** (1994) 159  
 and contribution to this Report.
- [45] K.G. Chetyrkin, A. Kwiatkowski and J.H. Kühn, contribution to this Report.
- [46] M. Consoli, W. Hollik and F. Jegerlehner, Phys. Lett. **B227** (1989) 167;  
 M. Consoli, W. Hollik and F. Jegerlehner, in: [1], vol. 1, p. 7;  
 W. Hollik, Lectures at the CERN-JINR School of Physics 1989, Egmond-aan-Zee,  
 Netherlands, in: CERN 91-07 (1991).
- [47] D. Bardin, W. Hollik and T. Riemann, Z.Physik **C49** (1991) 485.
- [48] A. Sirlin, Phys. Rev. **D29** (1984) 89.
- [49] S. Fanchiotti and A. Sirlin, prepr. NYU-TH-91-02-04 (1991), in: *M.A.B. Beg Memorial Volume*, eds. A. Ali et al. (World Scientific, Singapore, 1991), p. 58.
- [50] W. Hollik, in Precision Tests of the Standard Model, ed. by P. Langacker (World Scientific, Singapore, 1993).
- [51] M. Veltman, Nucl. Phys. **B123** (1977) 89.
- [52] A. Djouadi and C. Verzegnassi, Phys. Lett. **B195** (1987) 265;  
 A. Djouadi, Nuovo Cim. **100A** (1988) 357;  
 B.A. Kniehl, Nucl.Phys. **B347** (1990) 86;  
 F. Halzen and B.A. Kniehl, Nucl.Phys. **B353** (1991) 517.
- [53] L. Avdeev, J. Fleischer, S. Mikhailov and O. Tarasov, Phys. Lett. **B336** (1994) 560;  
 hep-ph/9406363, last revision: 16.02.1995.
- [54] J. van der Bij and F. Hoogeveen, Nucl. Phys. **B283** (1987) 477.
- [55] R. Barbieri et al., Phys. Lett. **B288** (1992) 95;  
 R. Barbieri et al., Nucl. Phys. **B409** (1993) 105.
- [56] A. Akhundov, D. Bardin, T. Riemann, Nucl. Phys. **B276** (1986) 1;  
 W. Beenakker and W. Hollik, Z. Physik **C40** (1988) 141;  
 J. Bernabéu, A. Pich and A. Santamaria, Phys. Lett. **B200** (1988) 569; Nucl. Phys.  
**B363** (1991) 326.

- [57] J. Fleischer, O.V. Tarasov, F. Jegerlehner and P. Raczka, Phys. Lett. **B293** (1992) 437;  
 G. Buchalla and A. Buras, Nucl.Phys. **B398** (1990) 285;  
 G. Degrassi, Nucl.Phys. **B407** (1993) 271;  
 K.G. Chetyrkin, A. Kwiatkowski, M. Steinhauser, Mod.Phys.Lett. **A8** (1993) 2785.
- [58] J. Fleischer, O. V. Tarasov and F. Jegerlehner, Preprint BI-TP-93/24 and PSI-PR-93-14 (June, 1993); Phys. Lett. **B319** (1993) 249.
- [59] M. Veltman, Acta Phys. Polon. **B8** (1977) 475.
- [60] G. Degrassi and A. Sirlin, NYU-Tr 92/05/02.
- [61] G. Degrassi, S. Fanchiotti and P. Gambino, CERN-TH.7180/94;  
 G. Degrassi et al., contribution to this Report.
- [62] A. Sirlin, NYU-TH-94/08/01 and contribution to this Report.
- [63] M. Steinhauser, talk given at the Ringberg Workshop on ‘Perspective for Electroweak Interactions in  $e^+e^-$  Collisions’, February 5-8, 1995;  
 K.G. Chetyrkin, J.H. Kühn, M. Steinhauser, Karlsruhe University Report, No. TTP 95-03; hep-ph/9502291, last revision: 15.02.95.
- [64] V.S. Fadin and V.A. Khoze, JETP Lett. **46** (1987) 525;  
 B.A. Kniehl and A. Sirlin, Phys. Rev. **D47** (1993) 883;  
 F.J. Yndurain, Phys. Lett. **B321** (1994) 400;  
 B.A. Kniehl and A. Sirlin, DESY-preprint DESY 93-194;  
 S. Fanchiotti, B.A. Kniehl and A. Sirlin, Phys. Rev. **D48** (1993) 307;  
 M.C. Gonzalez-Garcia, F. Halzen and R.A. Vázquez, Phys. Lett. **B322** (1994) 233;  
 B.H. Smith and M.B. Voloshin, UMN-TH-1241/94, TPI-MINN-94/5-T.
- [65] B.A. Kniehl, contribution to this Report.
- [66] G. Passarino, Nucl. Phys. B(Proc. Suppl.) **37B** (1994) 32;  
 G. Passarino, Precision Calculations for the  $Z$ , talk given at the 27th International Conference on High Energy Physics, Glasgow, 20-27th July 1994.
- [67] T. Hebbeker, M. Martinez, G. Passarino and G. Quast, Phys. Lett. **B331** (1994) 165.
- [68] W. Beenakker, F.A. Berends and S.C. van der Mark, Nucl. Phys. **B349** (1991) 323.
- [69] W. Hollik, in Precision Tests of the Standard Model, ed. by P. Langacker (World Scientific, Singapore, 1993);  
 G. Montagna, O. Nicrosini, G. Passarino, F. Piccinini and R. Pittau, first Ref.[4];  
 D.Yu. Bardin et al., CERN-TH.6443/92 (May 1992);  
 M. Bilenky and A. Sazonov, JINR Preprint E2-89-792 (1989).
- [70] B.A. Kniehl, M. Krawczyk, J.H. Kühn and R.G. Stuart, Phys. Lett. **B209** (1988) 337.



- [71] S. Jadach, M. Skrzypek and M. Martinez, Phys. Lett. **B280** (1992) 129.
- [72] V.A. Novikov, L.B. Okun and M.I. Vysotsky, Nucl.Phys. **B397** (1993) 35.
- [73] N.A. Nekrasov, V.A. Novikov, L.B. Okun and M.I. Vysotsky, Yad.Fiz. **57** (1994) 883.
- [74] V.A. Novikov, L.B. Okun and M.I. Vysotsky, Phys.Lett. **B324** (1994) 89.
- [75] J. van der Bij and M. Veltman, Nucl. Phys. **231** (1984) 205 ;  
J.J. van der Bij, Nucl. Phys. **B248** (1984) 141.
- [76] V.A. Novikov, L.B. Okun and M.I. Vysotsky, Phys.Lett. **B320** (1994) 388.
- [77] G. Passarino, second Ref.[31];  
G. Passarino, in '91 Electroweak Interactions and Unified Theories, J.Tran Thanh Van ed., p. 119 (Edition Frontieres).
- [78] M. Green and M. Veltman, Nucl/ Phys. **B169** (1980) 137.
- [79] G. 't Hooft and M. Veltman, Nucl. Phys. **B153** (1979) 365.
- [80] D. Bardin et al., second Ref. [24].
- [81] A. Akhundov et al., first Ref. [56].
- [82] D. Bardin et al., first Ref. [24].
- [83] D. Bardin et al., third Ref. [24].
- [84] G. Mann and T. Riemann, Annalen der Physik **40** (1983) 334.
- [85] D. Bardin and A. Chizhov, in: *Proc. Int. Topical Meeting on Physics of  $e^+e^-$  Interactions at LEP Energies*, ed. D. Bardin (Dubna, 1988), JINR Dubna E2-89-525 (1989), p. 42.
- [86] F. Halzen, B. Kniehl and M.L. Stong, Z. Phys. **C58** (1993).
- [87] F. Halzen and B. Kniehl Nucl. Phys. **B353** (1991) 567.

# Figures

## Pseudo-observables

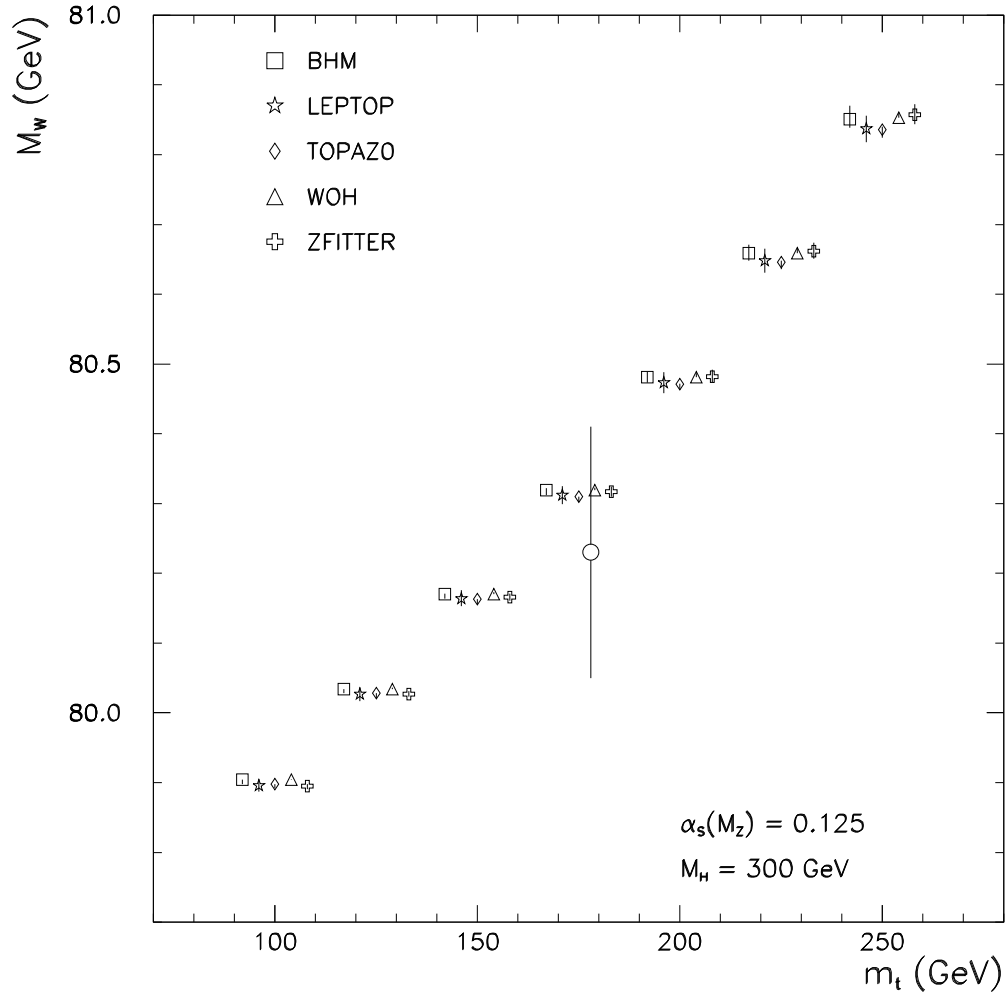


Figure 11: The BHM, LEPTOP, TOPAZO, ZFITTER, WOH predictions for  $M_W$ , including an estimate of the theoretical error as a function of  $m_t$ , for  $M_H = 300 \text{ GeV}$  and  $\hat{\alpha}_s = 0.125$ .

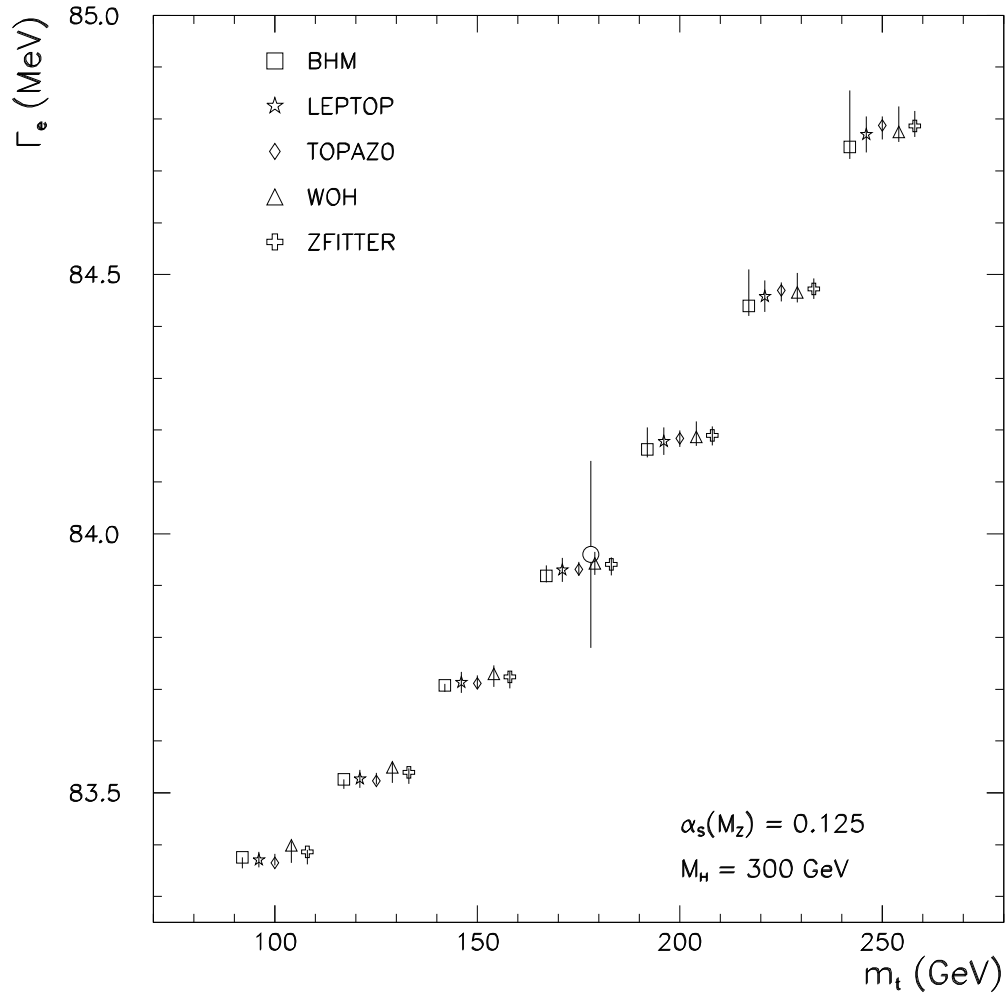


Figure 12: The BHM, LEPTOP, TOPAZO, ZFITTER, WOH predictions for  $\Gamma_e$ , including an estimate of the theoretical error as a function of  $m_t$ , for  $M_H = 300$  GeV and  $\hat{\alpha}_s = 0.125$ .

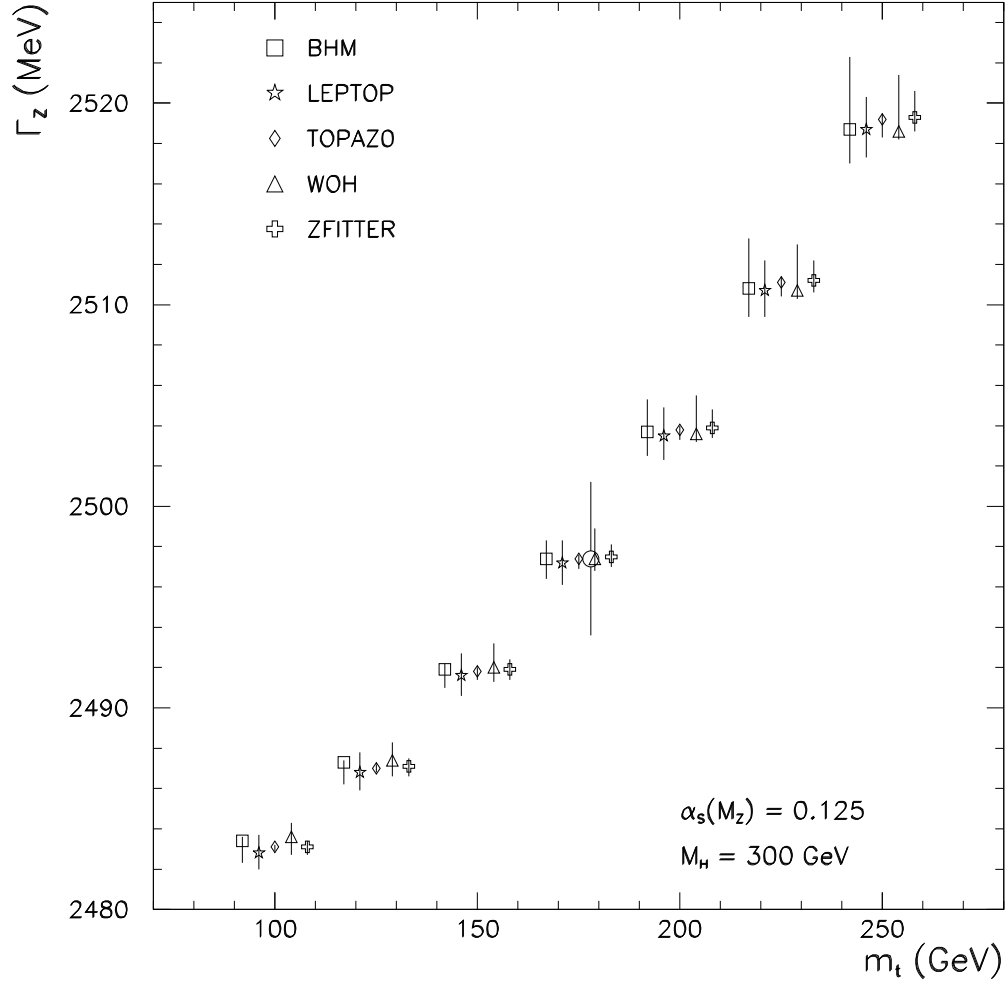


Figure 13: The BHM, LEPTOP, TOPAZ0, ZFITTER, WOH predictions for  $\Gamma_z$ , including an estimate of the theoretical error as a function of  $m_t$ , for  $M_H = 300$  GeV and  $\hat{\alpha}_s = 0.125$ .

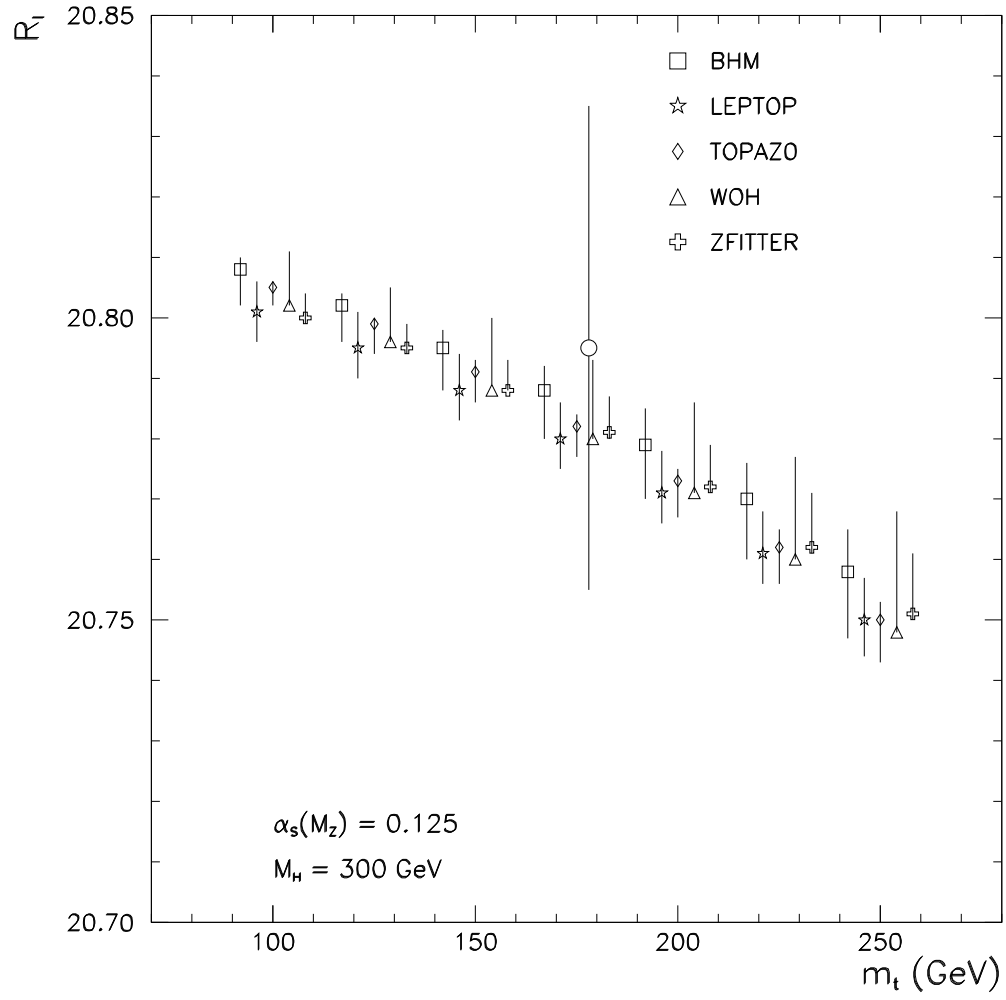


Figure 14: The BHM, LEPTOP, TOPAZ0, ZFITTER, WOH predictions for  $R_l$ , including an estimate of the theoretical error as a function of  $m_t$ , for  $M_H = 300 \text{ GeV}$  and  $\hat{\alpha}_s = 0.125$ .

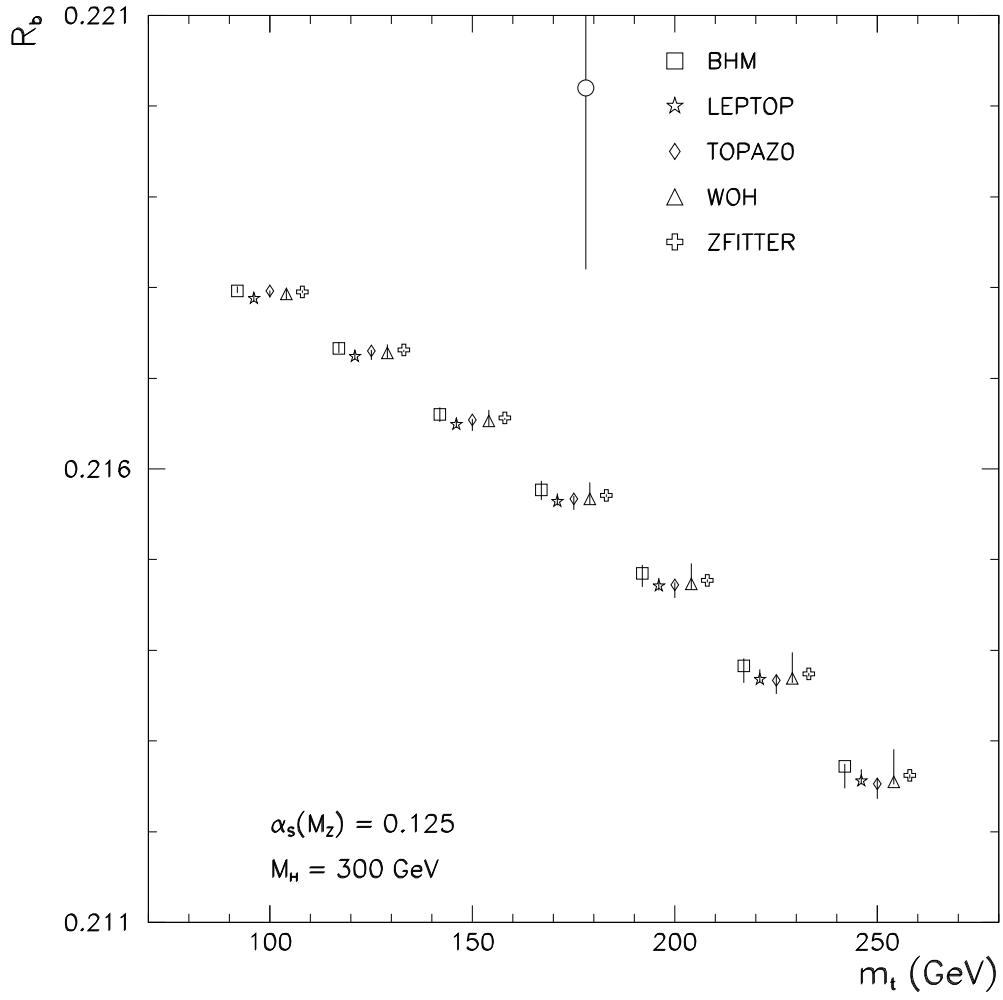


Figure 15: The BHM, LEPTOP, TOPAZO, ZFITTER, WOH predictions for  $R_b$ , including an estimate of the theoretical error as a function of  $m_t$ , for  $M_H = 300 \text{ GeV}$  and  $\hat{\alpha}_s = 0.125$ .

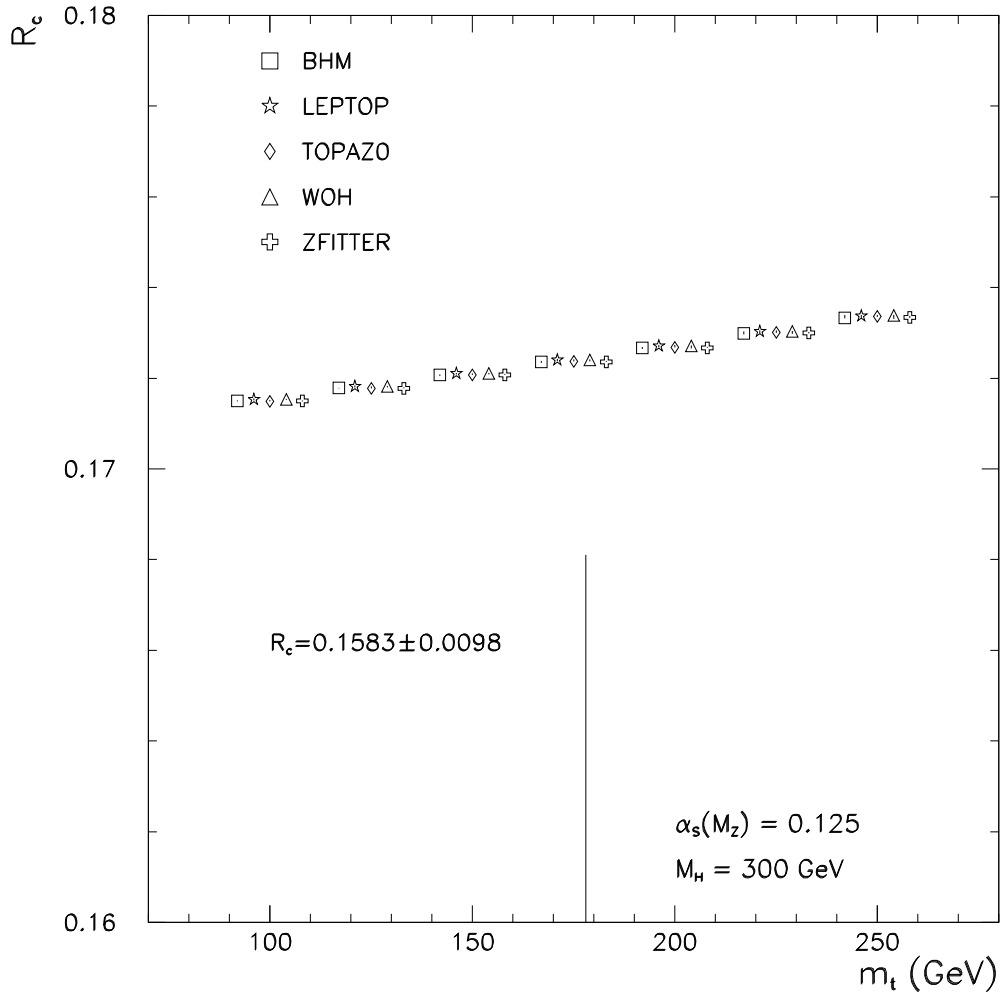


Figure 16: The BHM, LEPTOP, TOPAZO, ZFITTER, WOH predictions for  $R_c$ , including an estimate of the theoretical error as a function of  $m_t$ , for  $M_H = 300 \text{ GeV}$  and  $\hat{\alpha}_s = 0.125$ .

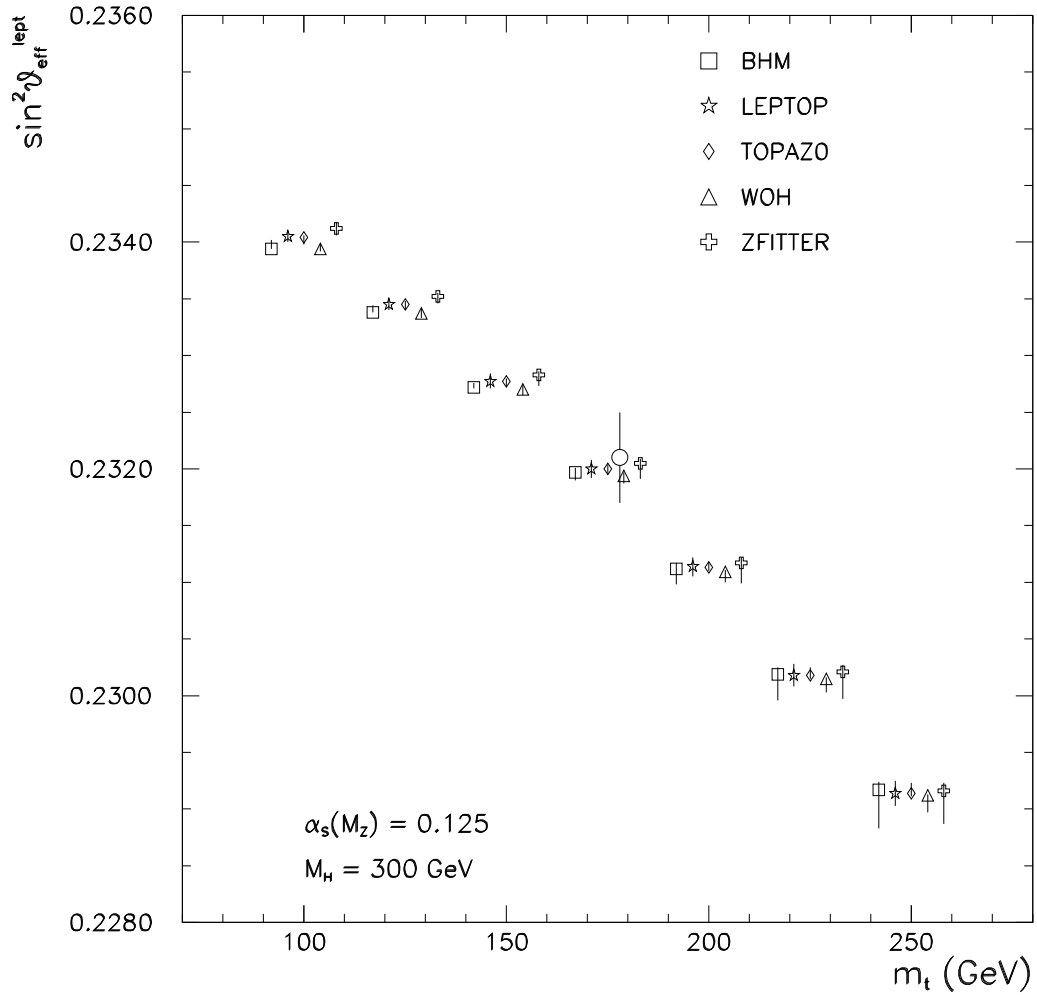


Figure 17: The BHM, LEPTOP, TOPAZO, ZFITTER, WOH predictions for  $\sin^2 \theta_{\text{eff}}^l$ , including an estimate of the theoretical error as a function of  $m_t$ , for  $M_H = 300$  GeV and  $\hat{\alpha}_s = 0.125$ .



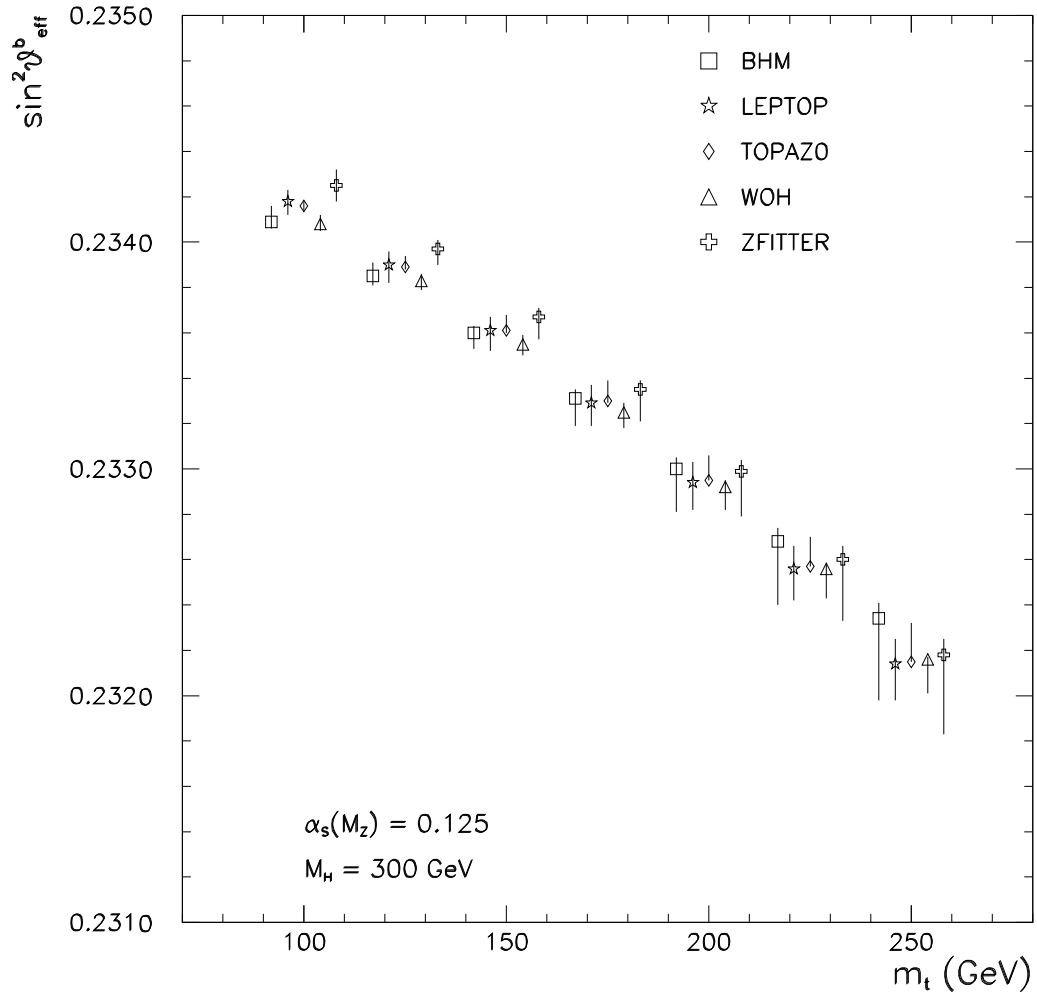


Figure 18: The BHM, LEPTOP, TOPAZ0, ZFITTER, WOH predictions for  $\sin^2 \theta_{\text{eff}}^b$ , including an estimate of the theoretical error as a function of  $m_t$ , for  $M_H = 300 \text{ GeV}$  and  $\hat{\alpha}_s = 0.125$ .

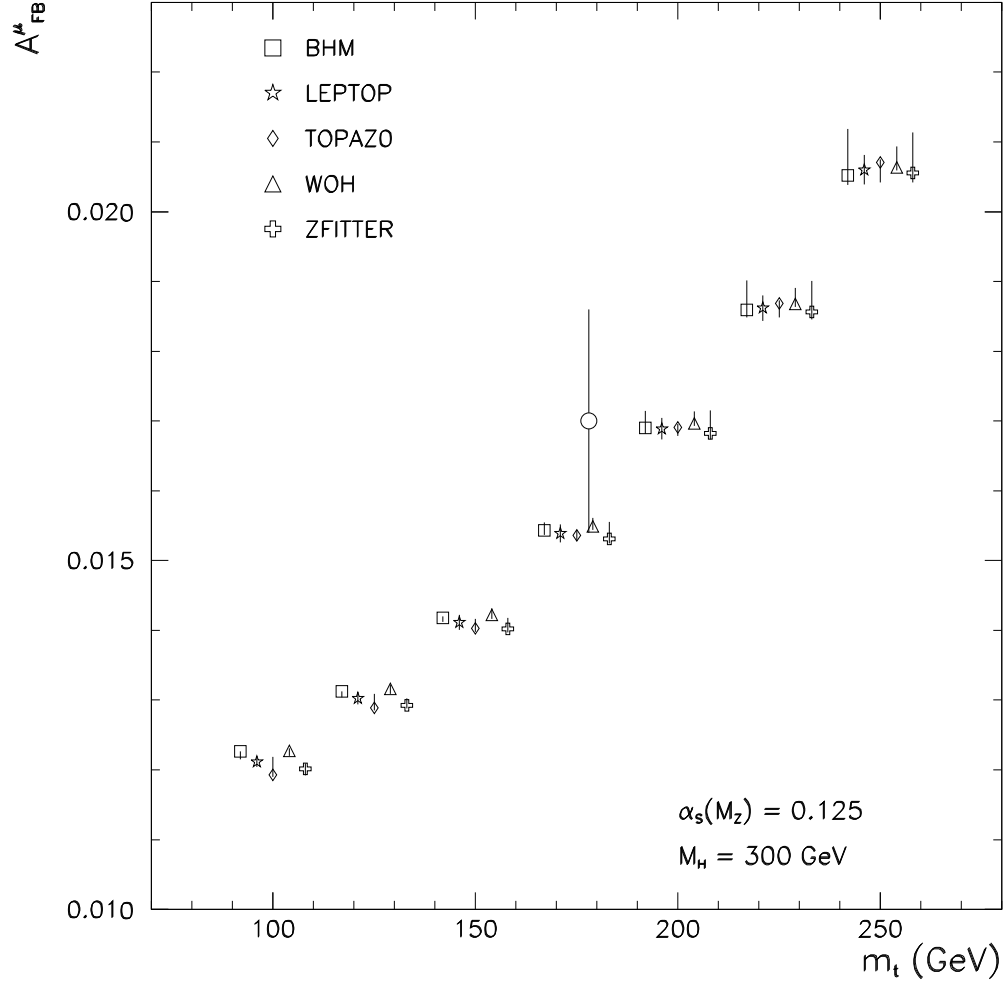


Figure 19: The BHM, LEPTOP, TOPAZO, ZFITTER, WOH predictions for  $A_{\text{FB}}^\mu$ , including an estimate of the theoretical error as a function of  $m_t$ , for  $M_H = 300$  GeV and  $\hat{\alpha}_s = 0.125$ .

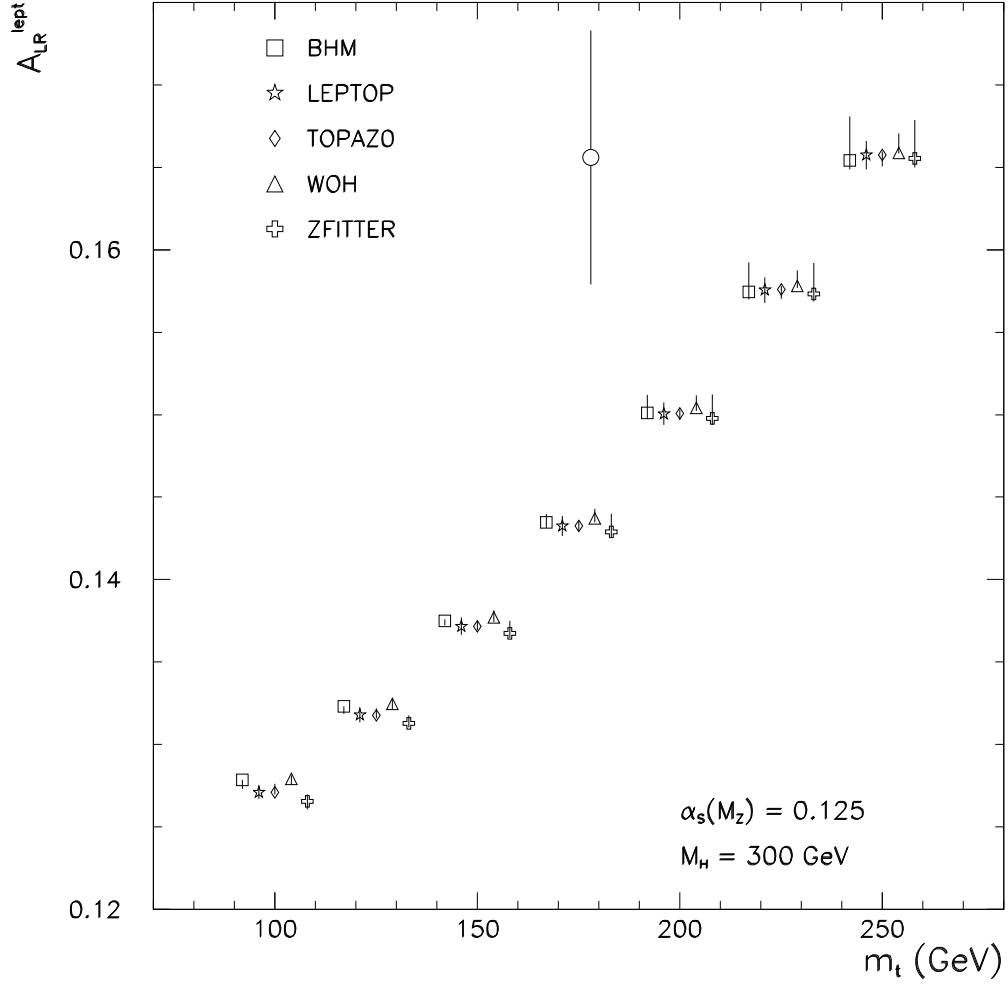


Figure 20: The BHM, LEPTOP, TOPAZO, ZFITTER, WOH predictions for  $A_{LR}^{\text{lept}}$ , including an estimate of the theoretical error as a function of  $m_t$ , for  $M_H = 300$  GeV and  $\hat{\alpha}_s = 0.125$ .

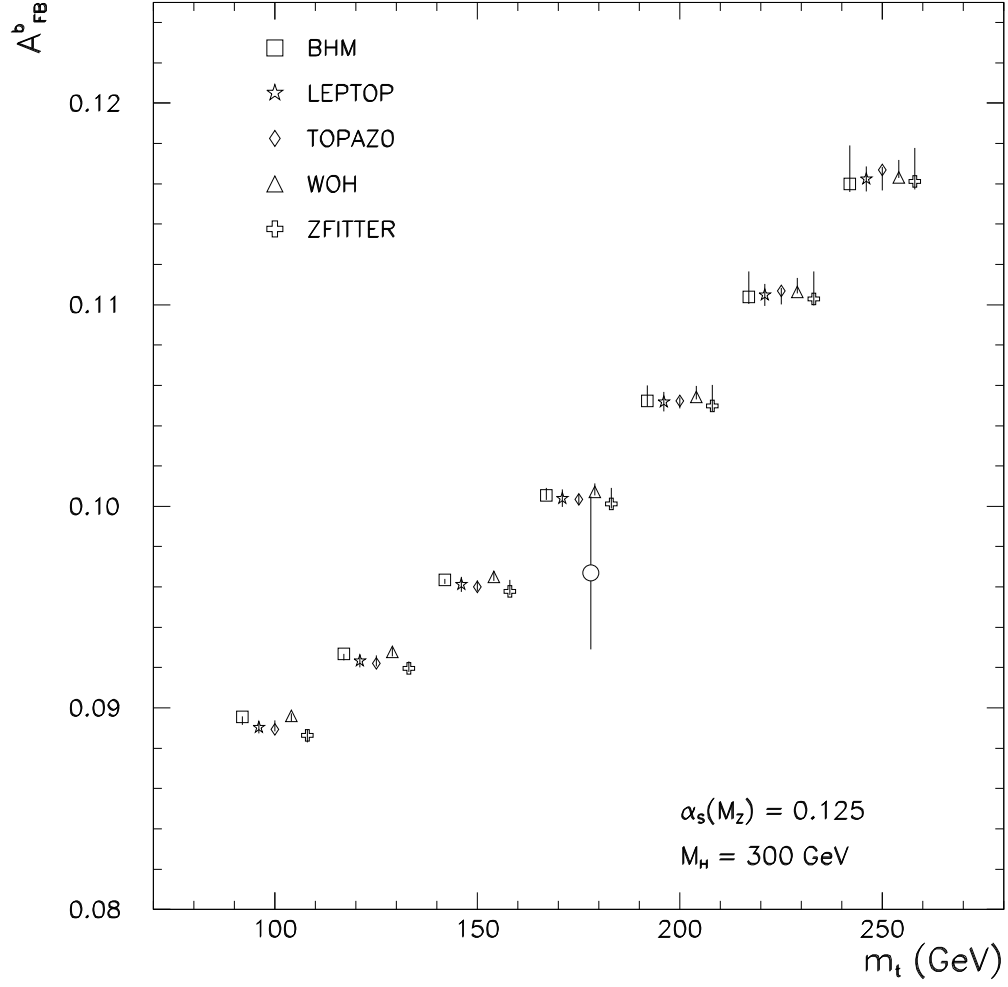


Figure 21: The BHM, LEPTOP, TOPAZO, ZFITTER, WOH predictions for  $A_{\text{FB}}^b$ , including an estimate of the theoretical error as a function of  $m_t$ , for  $M_H = 300 \text{ GeV}$  and  $\hat{\alpha}_s = 0.125$ .

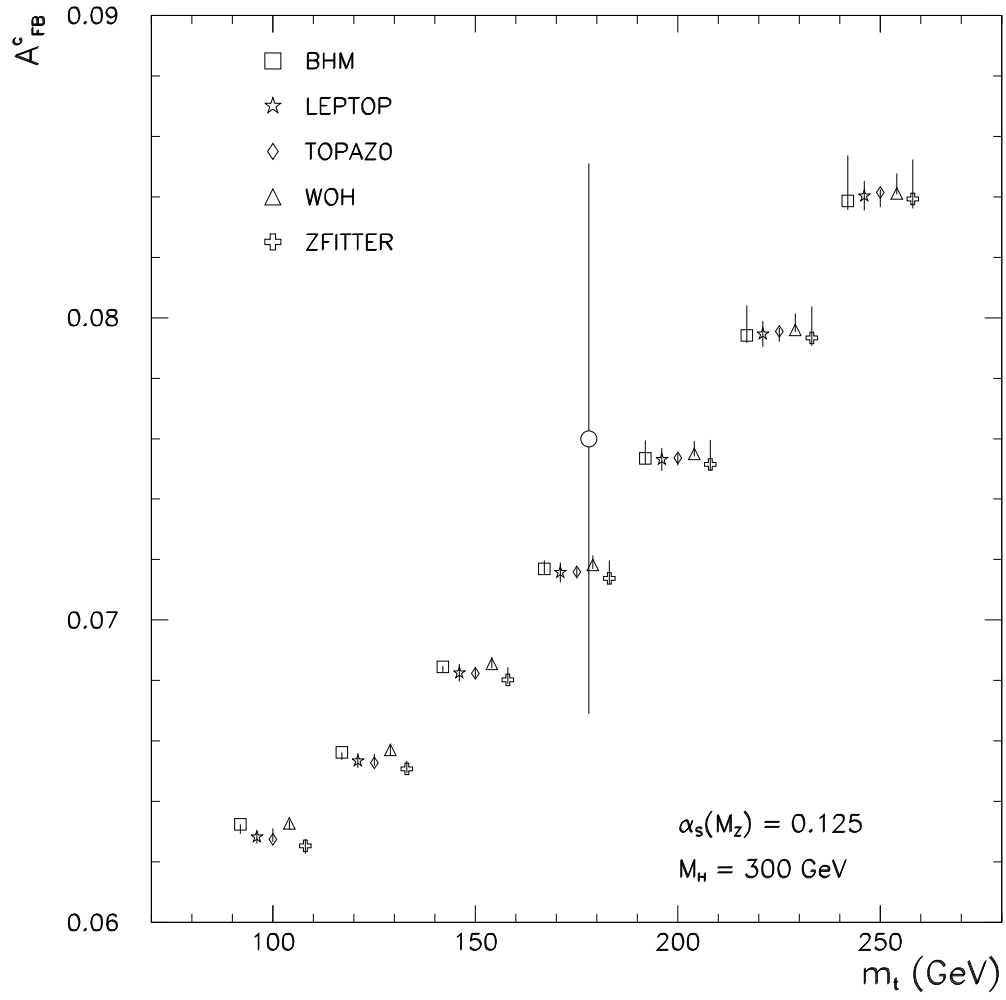


Figure 22: The BHM, LEPTOP, TOPAZO, ZFITTER, WOH predictions for  $A_{\text{FB}}^c$ , including an estimate of the theoretical error as a function of  $m_t$ , for  $M_H = 300 \text{ GeV}$  and  $\hat{\alpha}_s = 0.125$ .

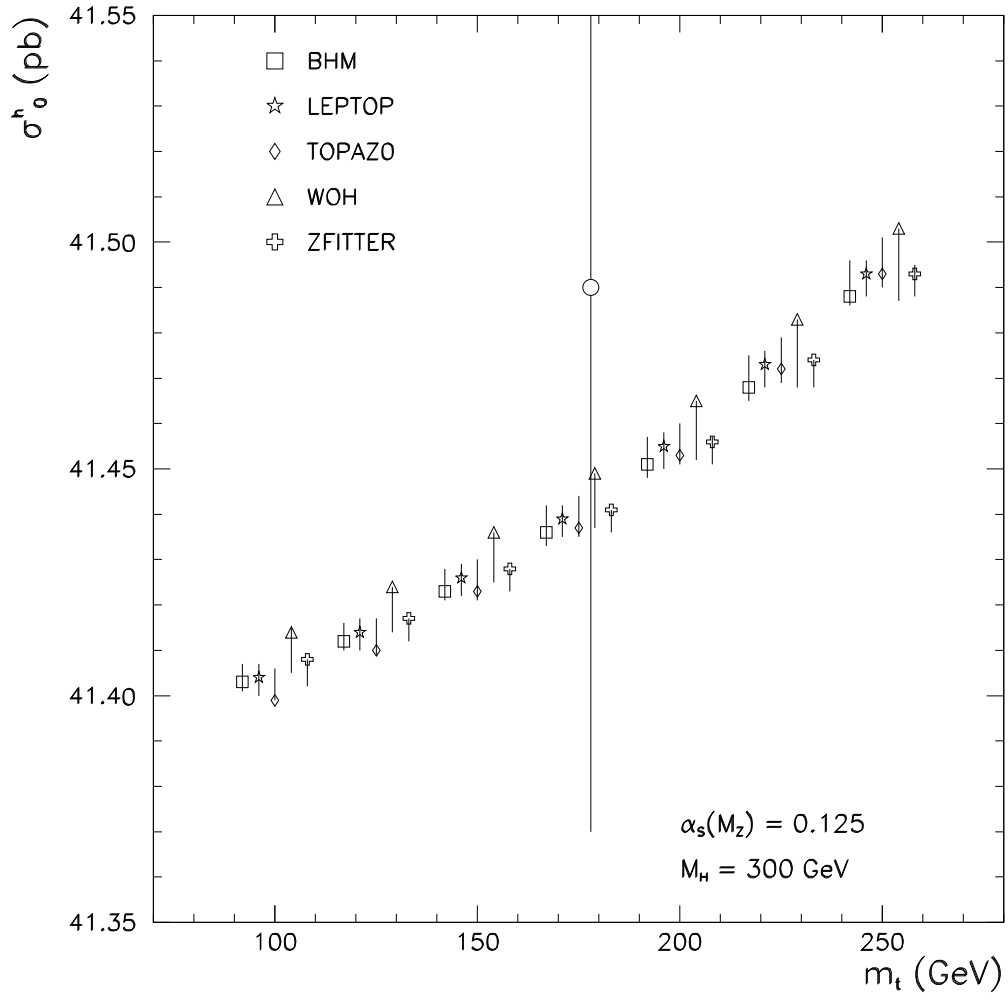


Figure 23: The BHM, LEPTOP, TOPAZO, ZFITTER, WOH predictions for  $\sigma_0^h$ , including an estimate of the theoretical error as a function of  $m_t$ , for  $M_H = 300$  GeV and  $\hat{\alpha}_s = 0.125$ .

## Realistic-observables

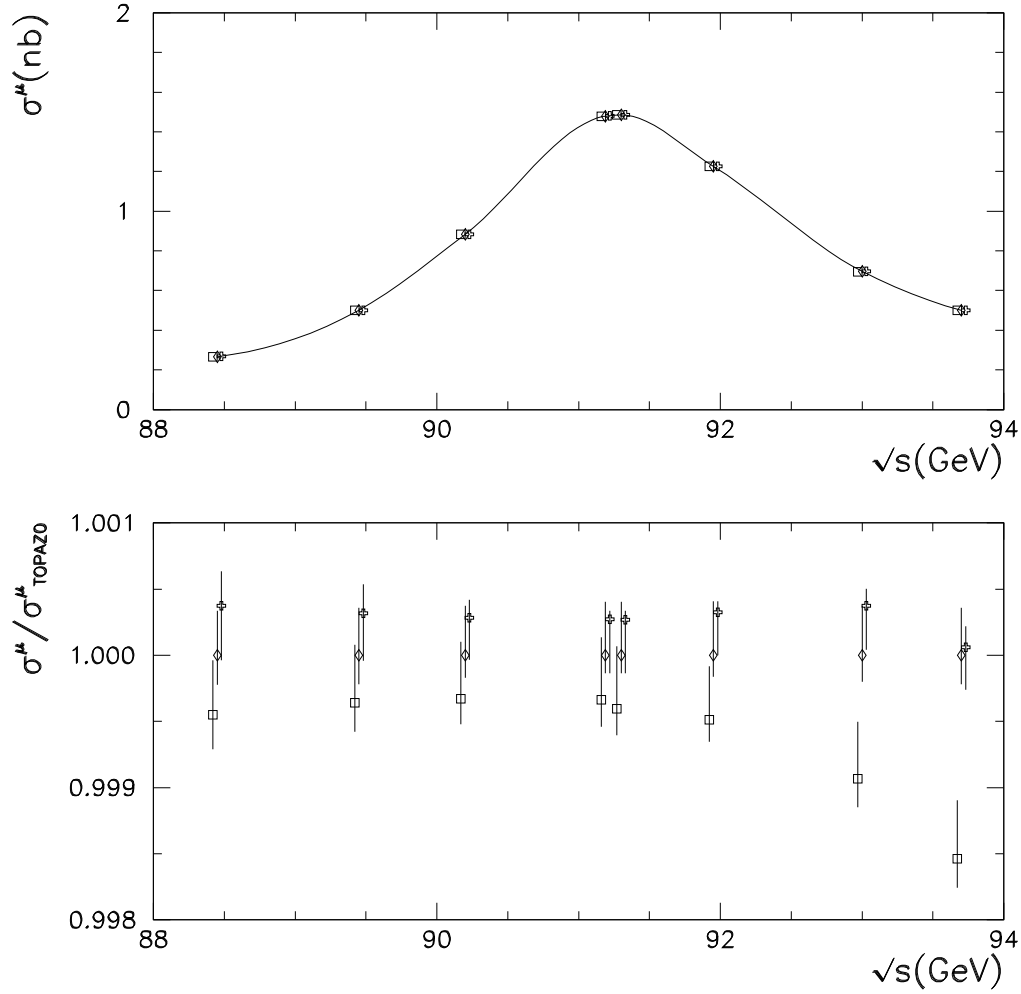


Figure 24: The BHM (square), TOPAZO (diamond) and ZFITTER (cross) predictions, including an estimate of the theoretical error, for  $\sigma^\mu$  in a fully extrapolated set-up. Here  $m_t = 175$  GeV,  $M_H = 300$  GeV and  $\hat{\alpha}_s = 0.125$ . In the lower part a comparison is also shown with the relative deviation of BHM, ZFITTER versus TOPAZO.

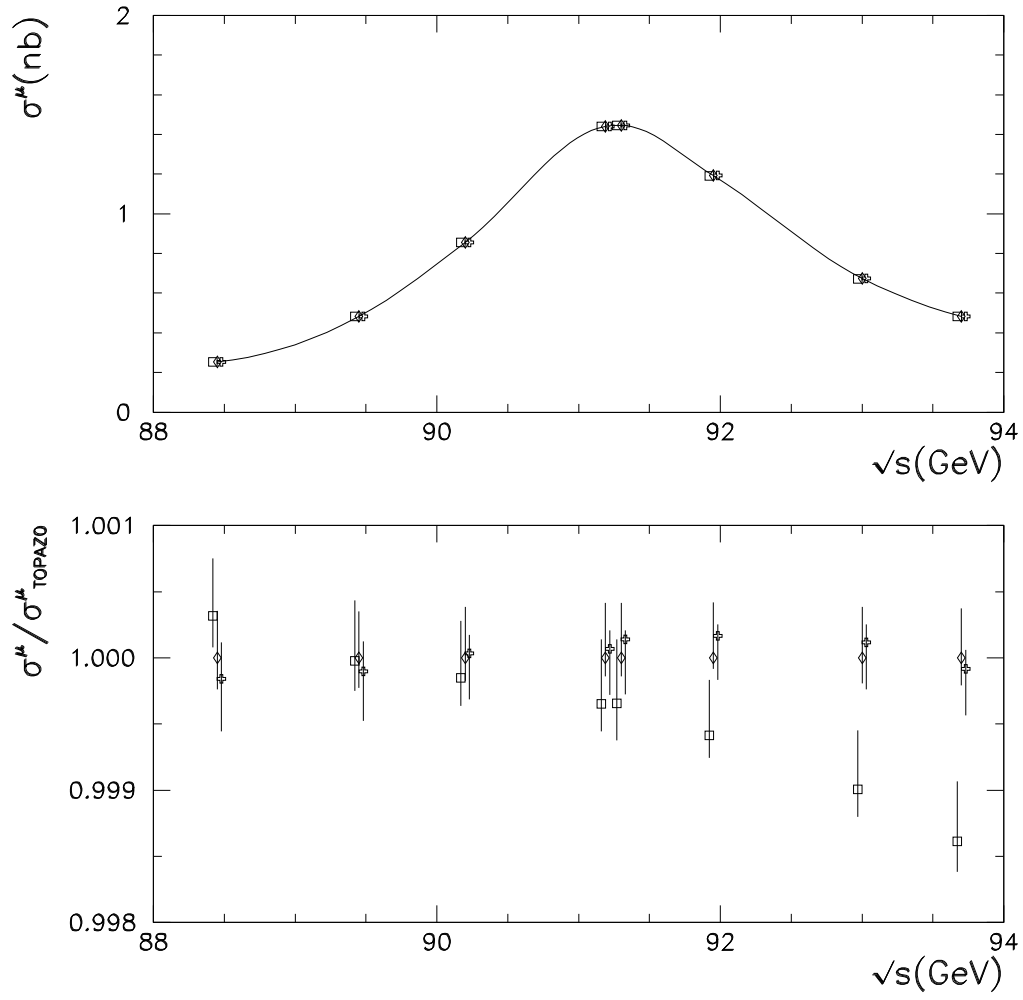


Figure 25: The same as in Fig. 24 with an  $s'$  cut,  $s' = 0.5s$ .



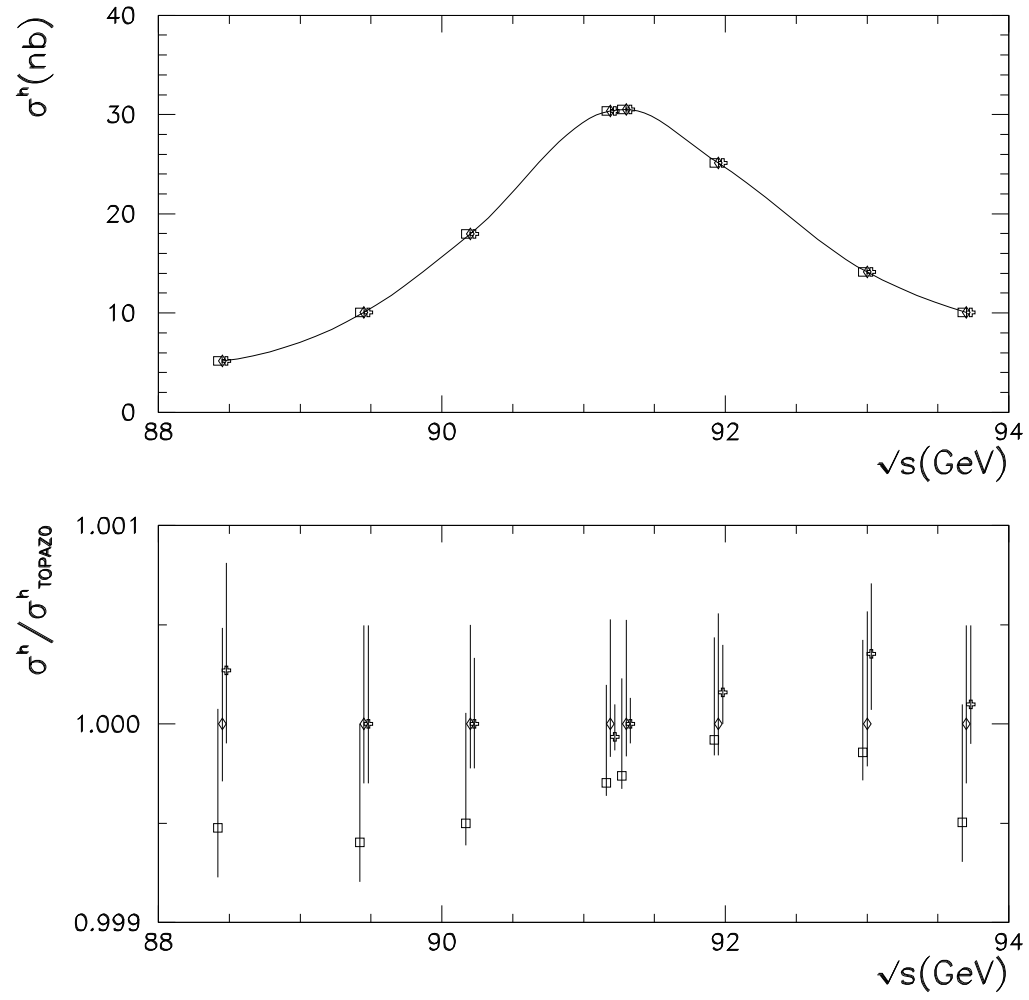


Figure 26: The same as in Fig. 24 for the hadronic cross-section,  $\sigma^h$ .

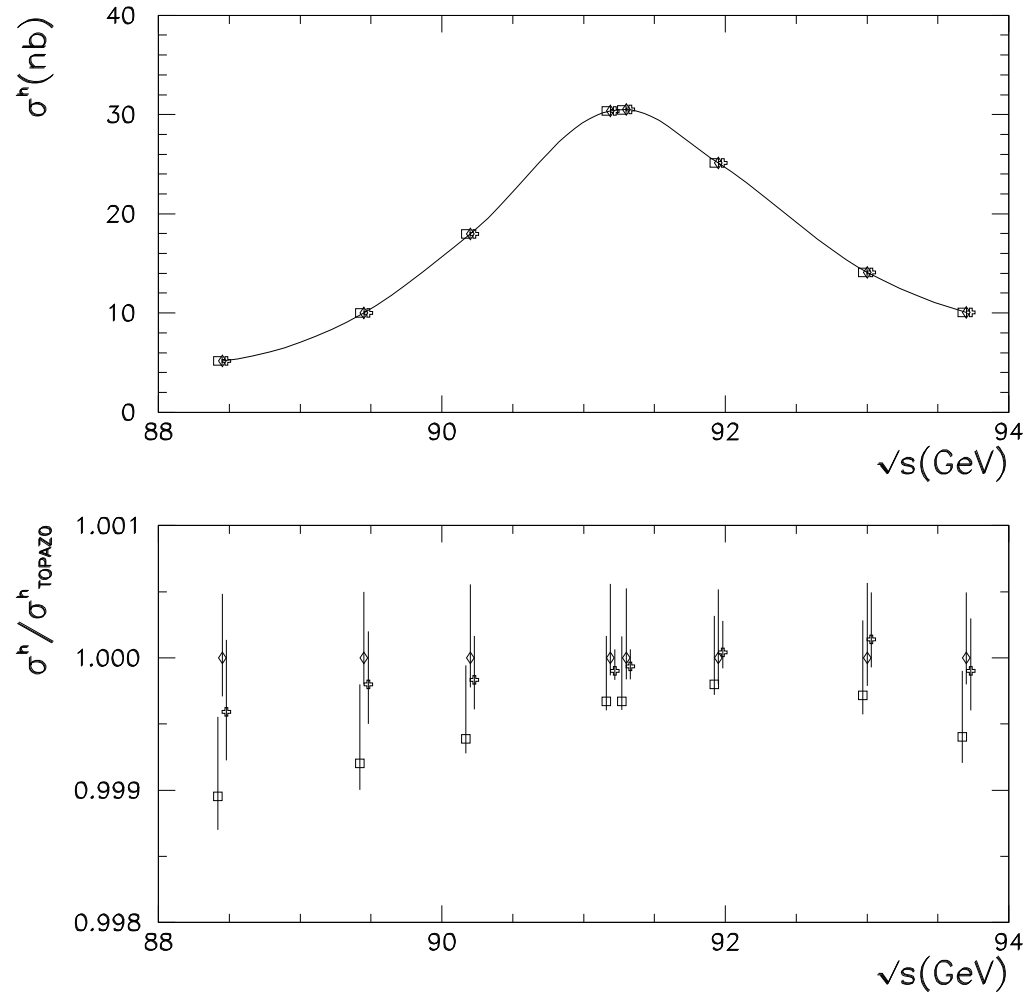


Figure 27: The same as in Fig. 26 with an  $s'$  cut,  $s' = 0.01s$ .

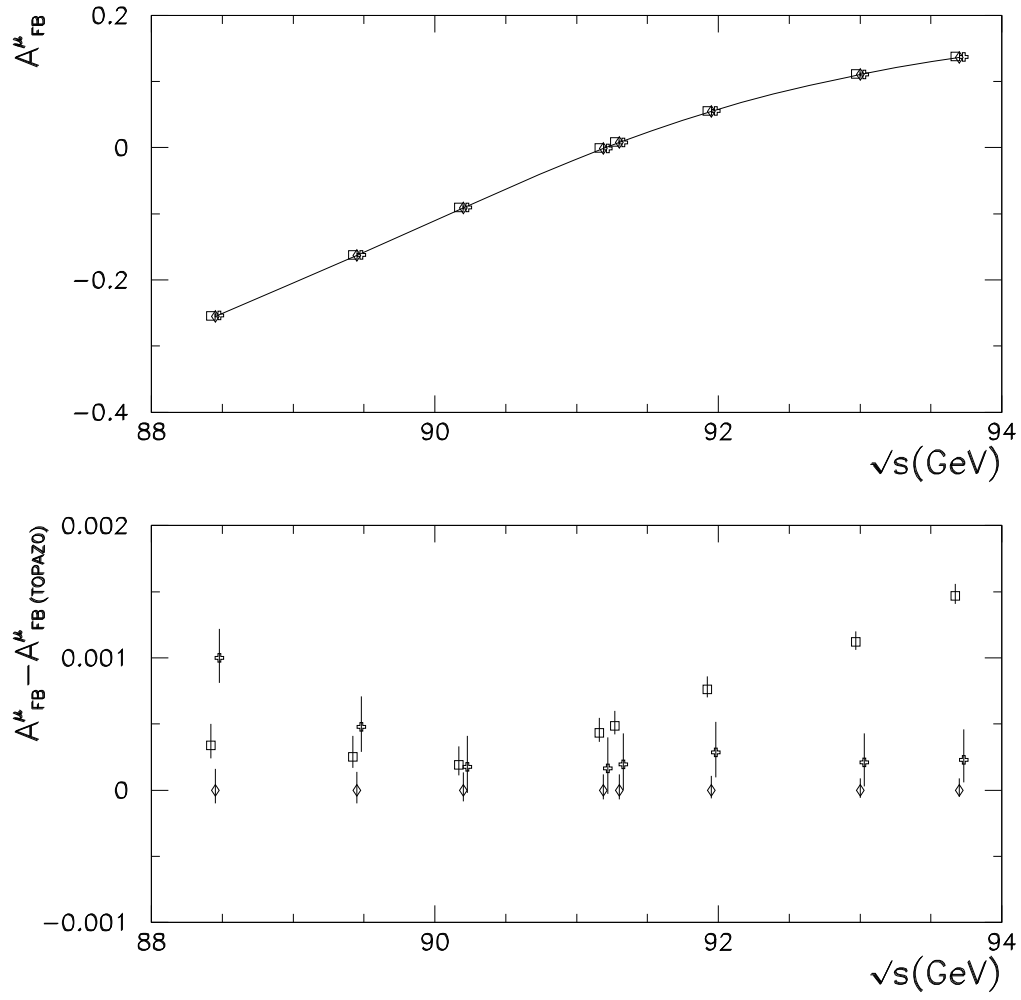


Figure 28: The same as in Fig. 24 for the leptonic forward-backward asymmetry. In the lower part a comparison is also shown with the absolute deviation of BHM, ZFITTER versus TOPAZO.

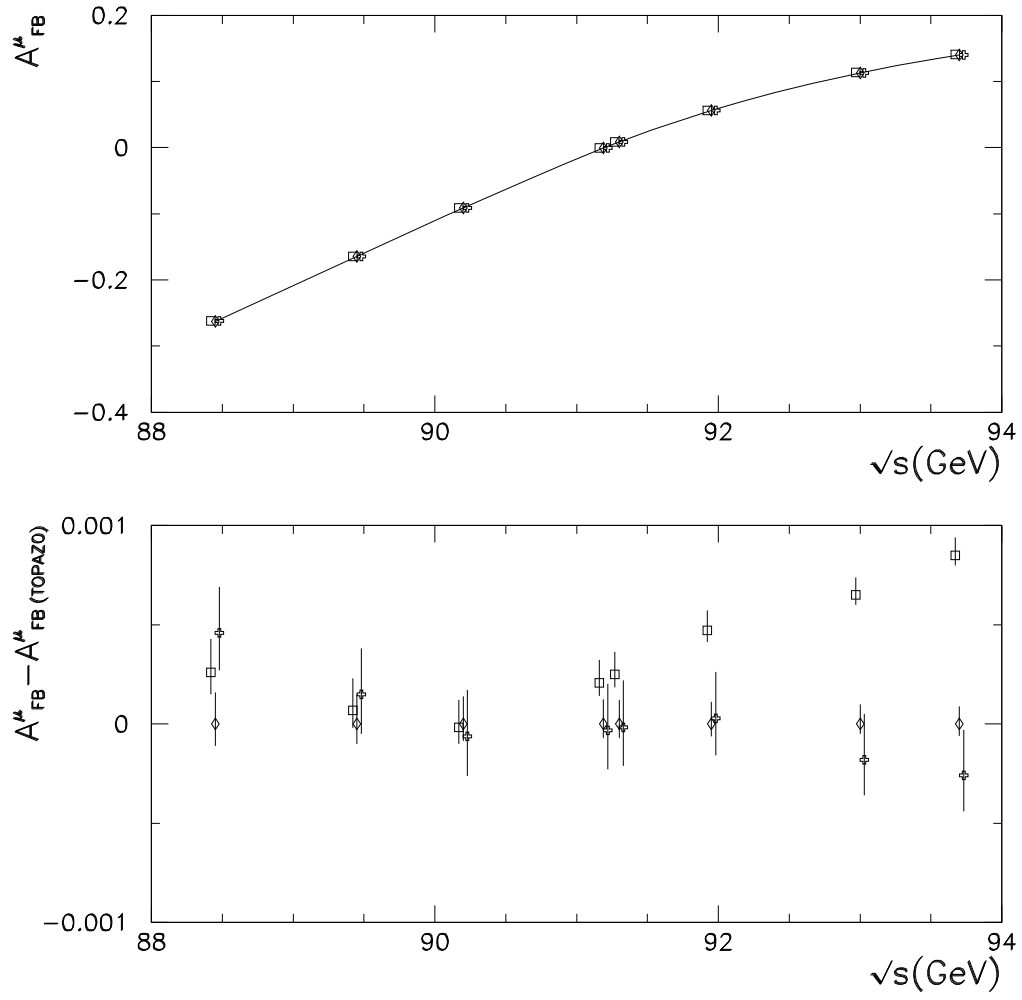


Figure 29: The same as in Fig. 28 with an  $s'$  cut,  $s' = 0.5s$ .

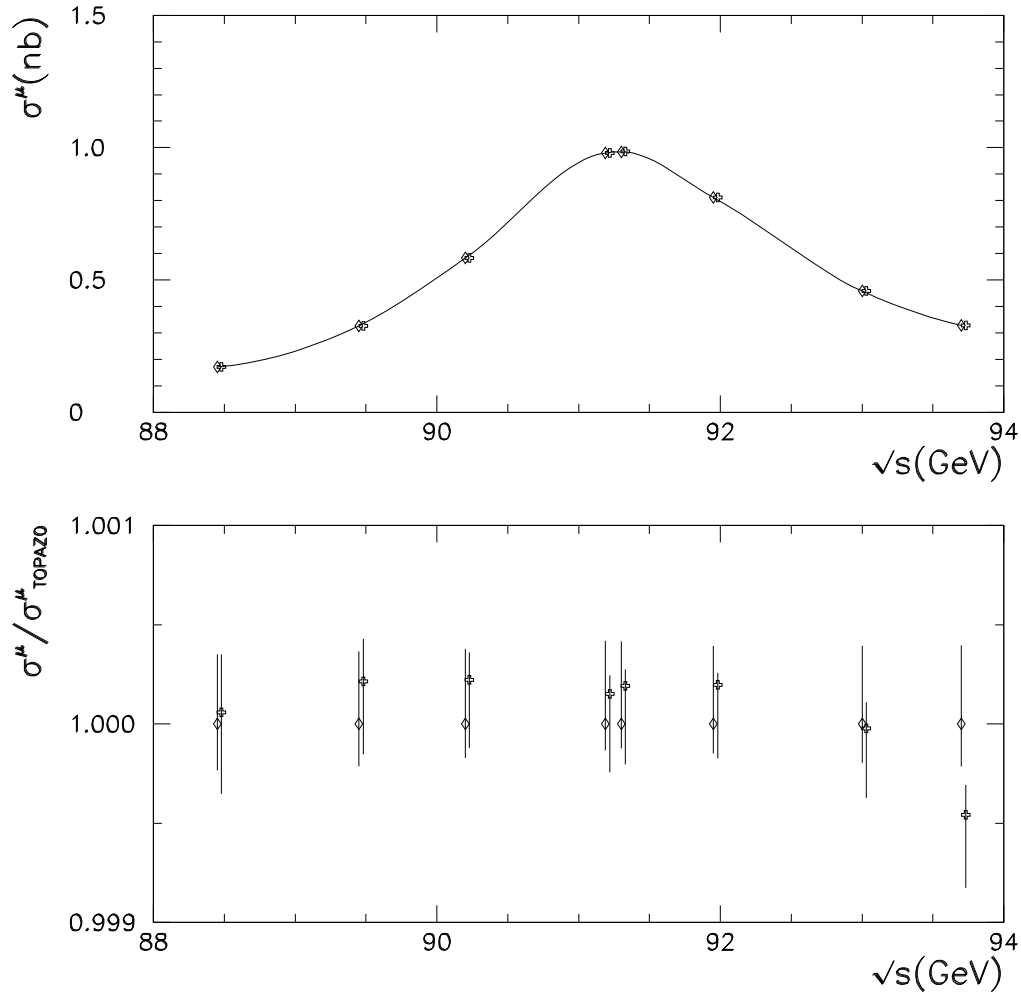


Figure 30: The TOPAZ0 (diamond) and ZFITTER (cross) predictions , including an estimate of the theoretical error, for  $\sigma^\mu$  in the following set-up:  $40^\circ < \theta_- < 140^\circ$ ,  $\theta_{\text{acoll}} < 10^\circ$  and  $E_{\text{th}} = 20$  GeV. Here  $m_t = 175$  GeV,  $M_H = 300$  GeV and  $\hat{\alpha}_s = 0.125$ . In the lower part a comparison is also shown with the relative deviation of ZFITTER versus TOPAZ0.

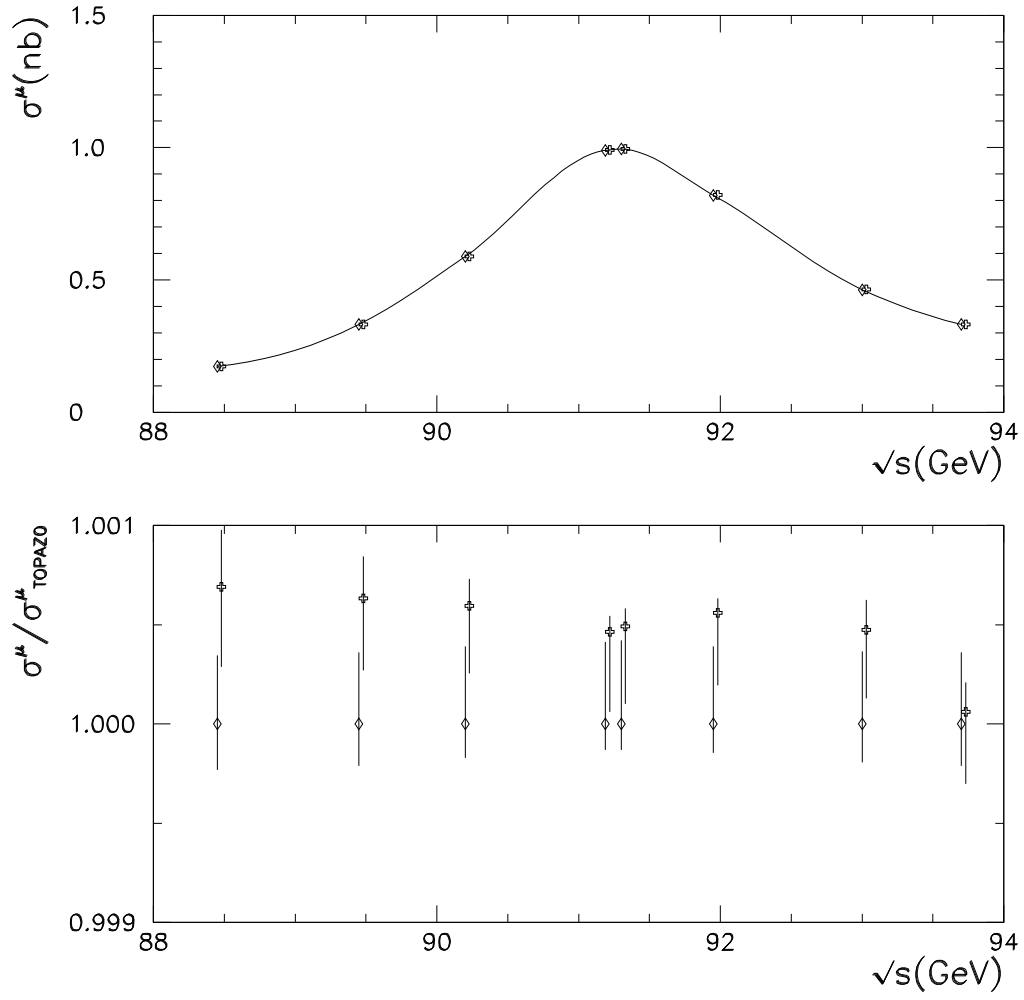


Figure 31: The same as in Fig. 30 for  $\theta_{\text{acoll}} < 25^\circ$ .

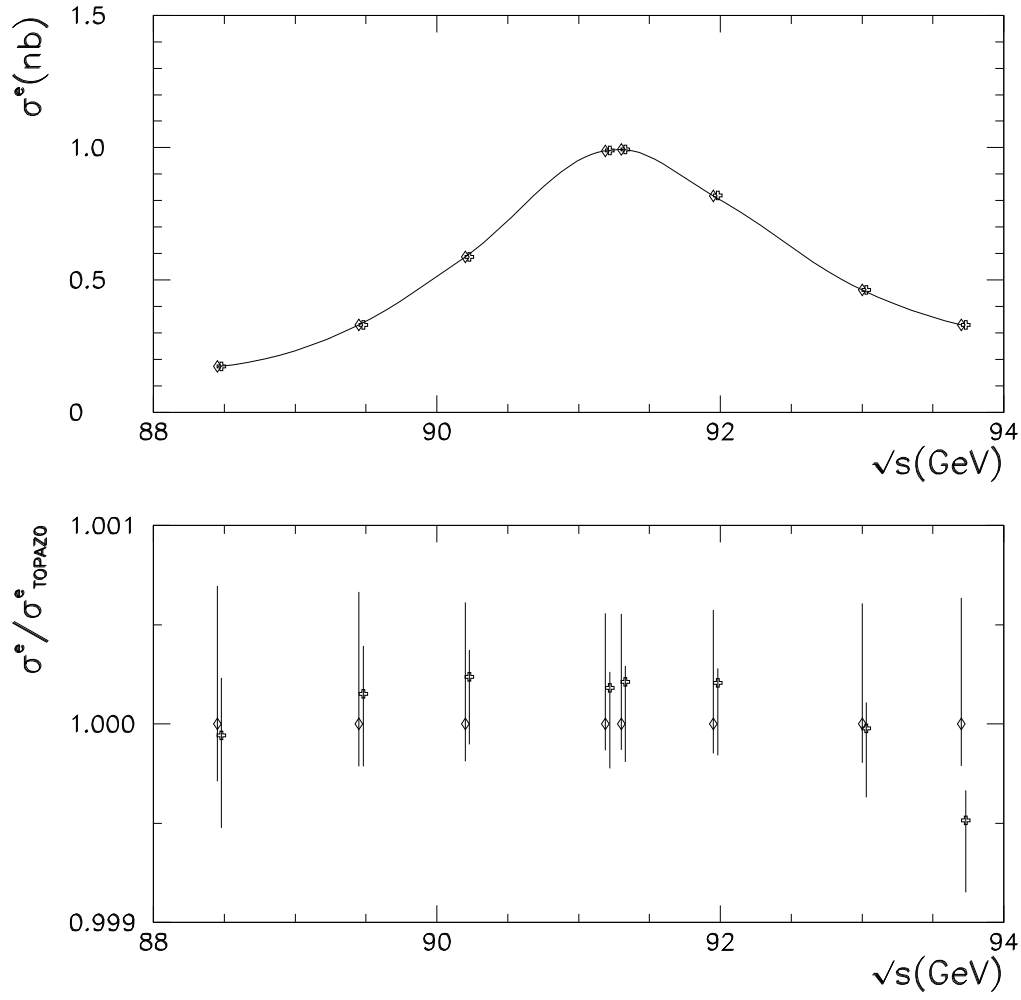


Figure 32: The TOPAZO (diamond) and ZFITTER (cross) predictions, including an estimate of the theoretical error, for  $\sigma^e$  with  $s$ -channel electrons, in the following set-up:  $40^\circ < \theta_- < 140^\circ$ ,  $\theta_{\text{acoll}} < 10^\circ$  and  $E_{\text{th}} = 1$  GeV. Here  $m_t = 175$  GeV,  $M_H = 300$  GeV and  $\hat{\alpha}_s = 0.125$ . In the lower part a comparison is also shown with the relative deviation of ZFITTER versus TOPAZO.

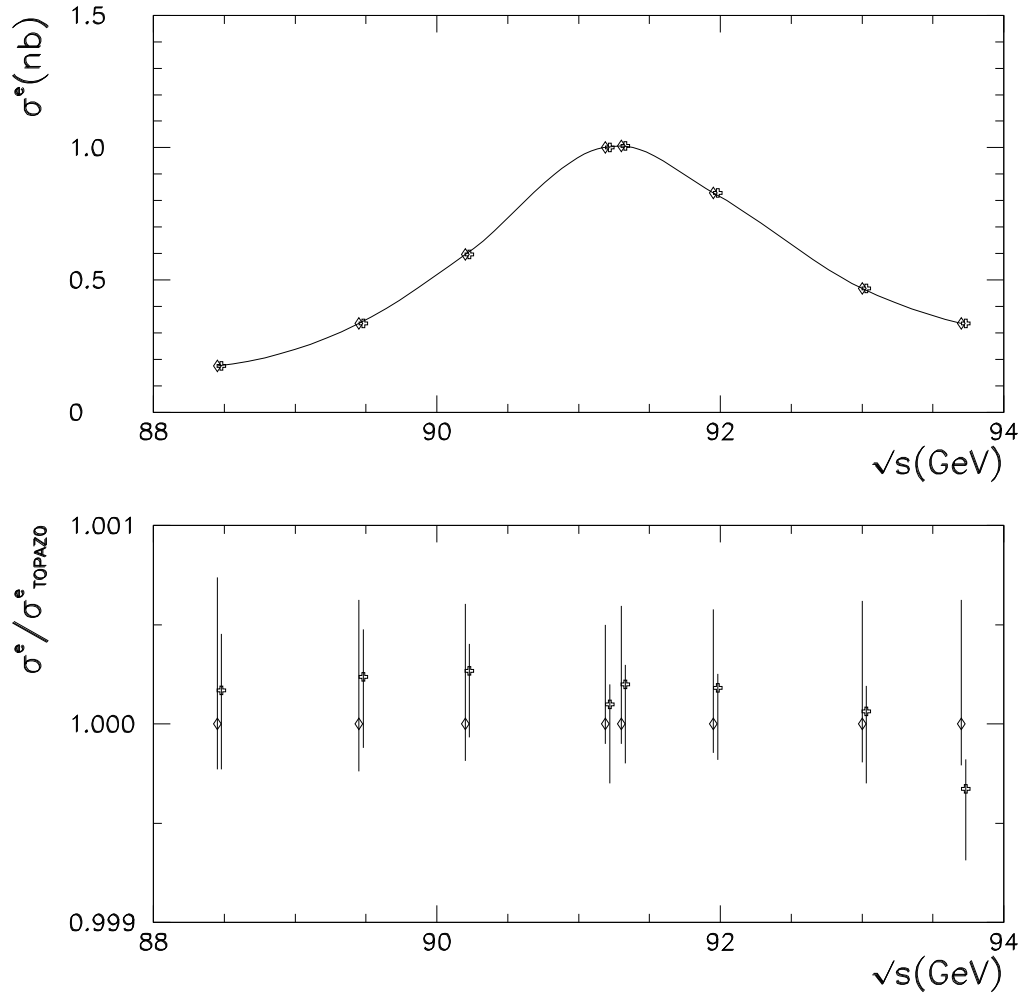


Figure 33: The same as in Fig. 32 for  $\theta_{\text{acoll}} < 25^\circ$ .



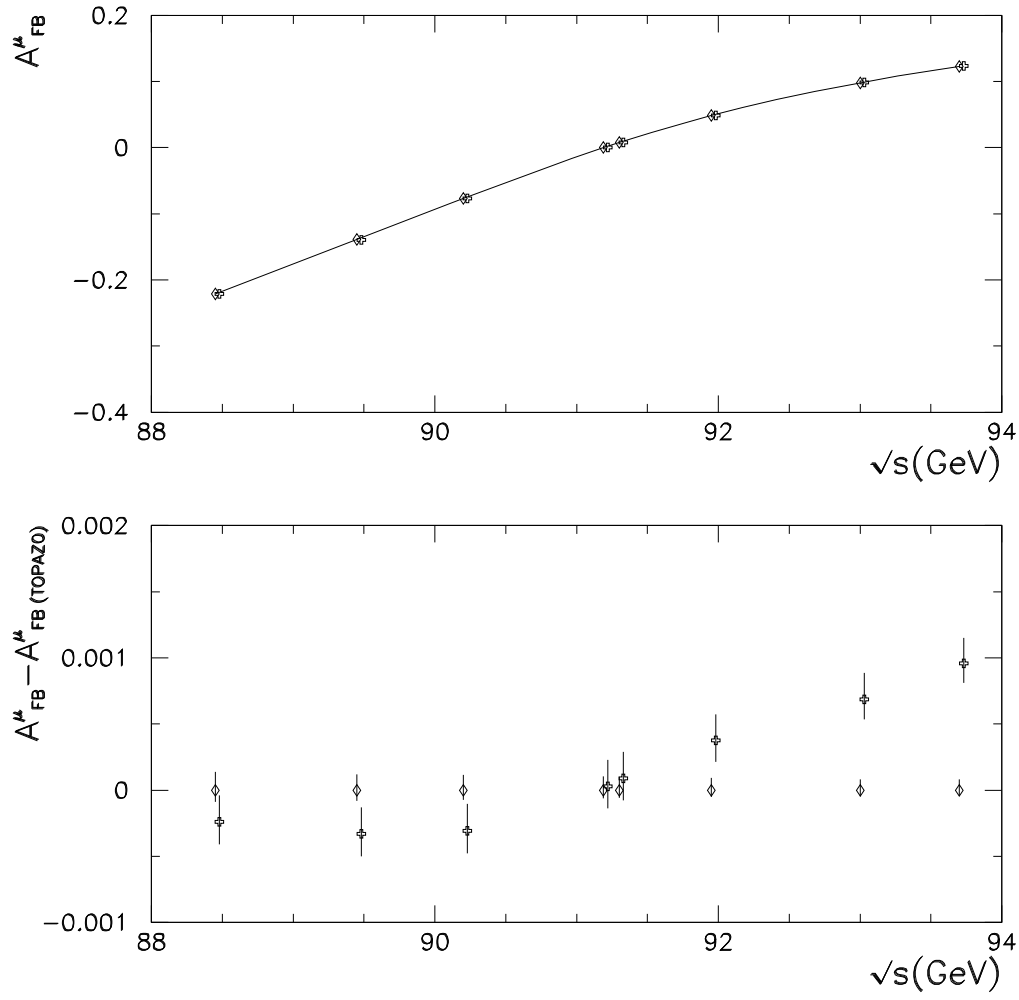


Figure 34: The TOPAZO (diamond) and ZFITTER (cross) predictions, including an estimate of the theoretical error, for  $A_{\text{FB}}^{\mu}$  in the following set-up:  $40^{\circ} < \theta_{-} < 140^{\circ}$ ,  $\theta_{\text{acoll}} < 10^{\circ}$  and  $E_{\text{th}} = 20$  GeV. Here  $m_t = 175$  GeV,  $M_H = 300$  GeV and  $\hat{\alpha}_s = 0.125$ . In the lower part a comparison is also shown with the absolute deviation of ZFITTER versus TOPAZO.

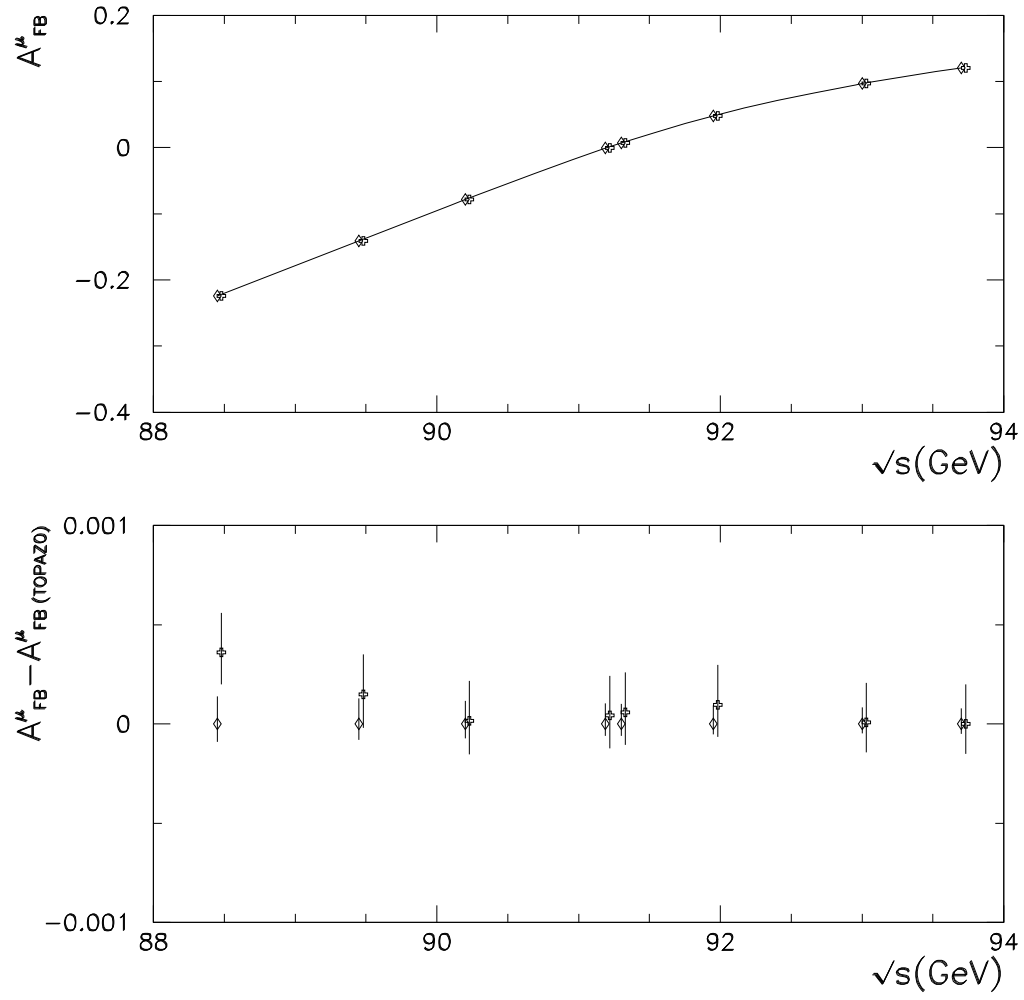


Figure 35: The same as in Fig. 34 for  $\theta_{\text{acoll}} < 25^\circ$ .

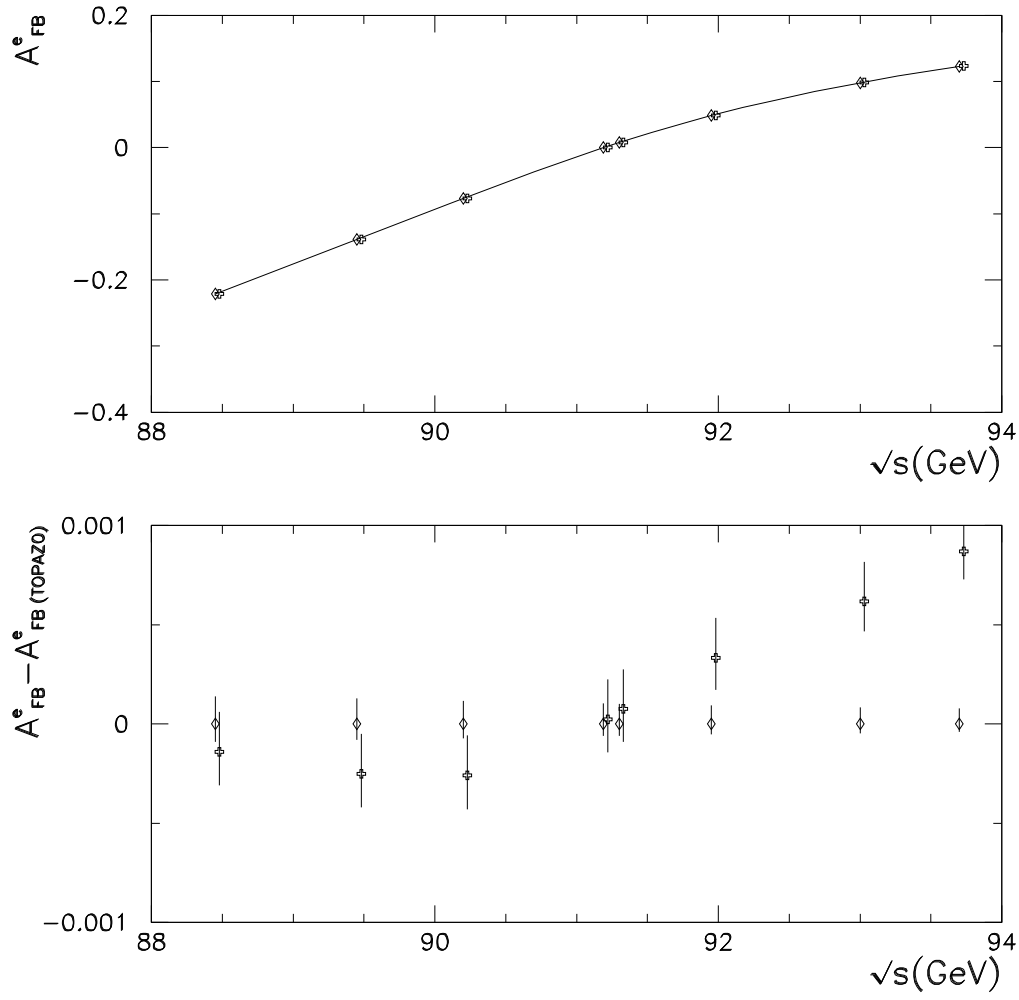


Figure 36: The TOPAZO (diamond) and ZFITTER (cross) predictions, including an estimate of the theoretical error, for  $A_{\text{FB}}^e$  with  $s$ -channel electrons in the following set-up:  $40^\circ < \theta_- < 140^\circ$ ,  $\theta_{\text{acoll}} < 10^\circ$  and  $E_{\text{th}} = 1$  GeV. Here  $m_t = 175$  GeV,  $M_H = 300$  GeV and  $\hat{\alpha}_s = 0.125$ . In the lower part a comparison is also shown with the absolute deviation of ZFITTER versus TOPAZO.

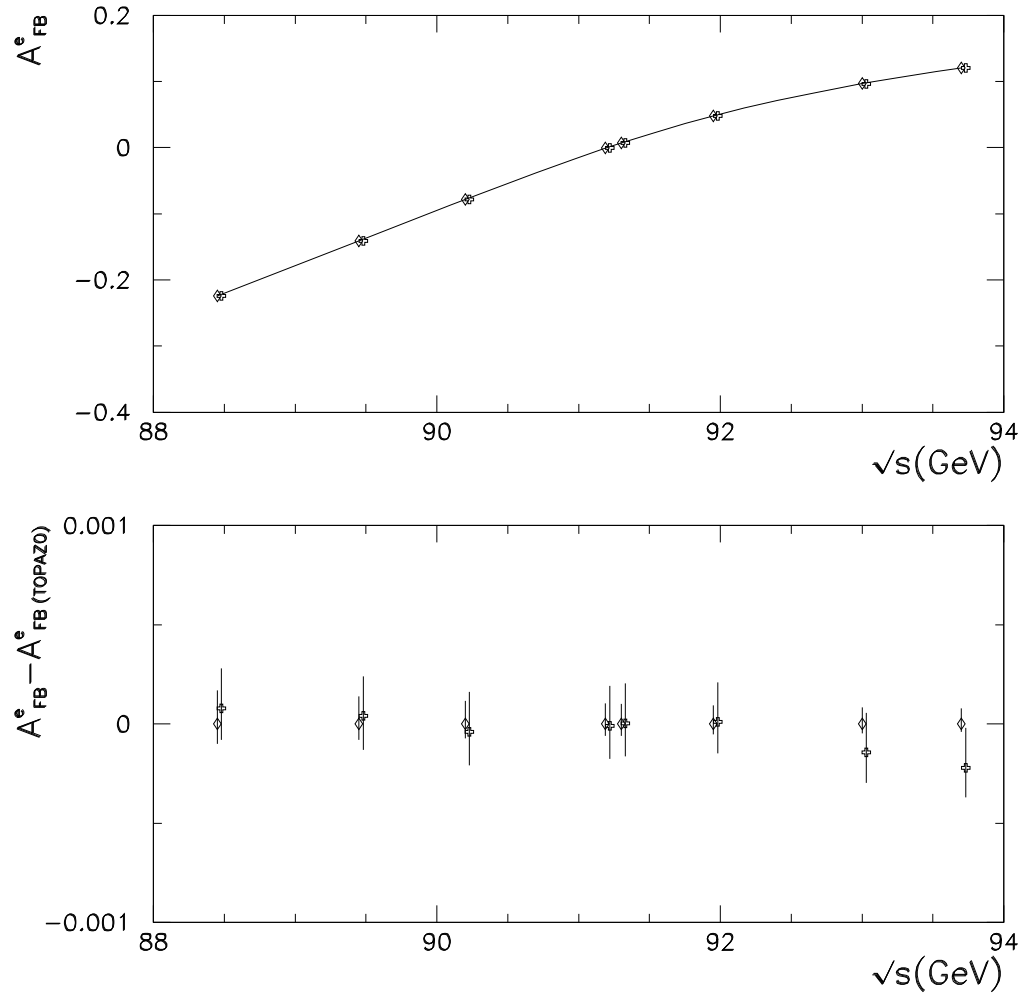


Figure 37: The same as in Fig. 36 for  $\theta_{\text{acoll}} < 25^\circ$ .

# Tables

## Pseudo-observables

Table 1: Maximum Derivatives with respect to  $\bar{\alpha}^{-1}$ .

Observables	BHM	LEPTOP	TOPAZO	ZFITTER
$M_w$ (GeV)	0.13586	0.13537	0.13541	0.13546
$\Gamma_\nu$ (MeV)	$-0.66258 \times 10^{-2}$	$-0.12495 \times 10^{-2}$	$-0.12805 \times 10^{-2}$	$-0.18897 \times 10^{-2}$
$\Gamma_e$ (MeV)	0.11994	0.12411	0.12413	0.12174
$\Gamma_\mu$ (MeV)	0.11994	0.12411	0.12413	0.12174
$\Gamma_\tau$ (MeV)	0.11995	0.12411	0.12413	0.12175
$\Gamma_u$ (MeV)	1.3561	1.3656	1.3664	1.3613
$\Gamma_d$ (MeV)	1.2252	1.2371	1.2374	1.2341
$\Gamma_c$ (MeV)	1.3562	1.3656	1.3665	1.3613
$\Gamma_b$ (MeV)	1.2143	1.2282	1.2330	1.2235
$\sin^2 \theta_{\text{eff}}^l$	$-0.25824 \times 10^{-2}$	$-0.25781 \times 10^{-2}$	$-0.25781 \times 10^{-2}$	$-0.25798 \times 10^{-2}$
$\sin^2 \theta_{\text{eff}}^b$	$-0.25968 \times 10^{-2}$	$-0.25925 \times 10^{-2}$	$-0.25930 \times 10^{-2}$	$-0.25947 \times 10^{-2}$
$A_{\text{FB}}^l$	$0.43992 \times 10^{-2}$	$0.43863 \times 10^{-2}$	$0.43863 \times 10^{-2}$	$0.43781 \times 10^{-2}$
$A_{\text{LR}}$	$0.20344 \times 10^{-1}$	$0.20312 \times 10^{-1}$	$0.20312 \times 10^{-1}$	$0.20327 \times 10^{-1}$
$\Gamma_z$ (MeV)	6.7115	6.7968	6.8041	6.7685
$R_l$	$0.46721 \times 10^{-1}$	$0.46367 \times 10^{-1}$	$0.46446 \times 10^{-1}$	$0.46719 \times 10^{-1}$
$\sigma_0^h$ (nb)	$-0.12890 \times 10^{-1}$	$-0.12305 \times 10^{-1}$	$-0.12363 \times 10^{-1}$	$-0.13001 \times 10^{-1}$
$R_b$	$-0.92933 \times 10^{-4}$	$-0.91531 \times 10^{-4}$	$-0.89791 \times 10^{-4}$	$-0.92040 \times 10^{-4}$
$A_{\text{FB}}^b$	$0.14434 \times 10^{-1}$	$0.14411 \times 10^{-1}$	$0.14411 \times 10^{-1}$	$0.14421 \times 10^{-1}$
$\Gamma_h$ (MeV)	6.3768	6.4335	6.4408	6.4143
$P^b$	$0.16748 \times 10^{-2}$	$0.16718 \times 10^{-2}$	$0.16722 \times 10^{-2}$	$0.16738 \times 10^{-2}$
$\Gamma_{\text{inv}}$ (MeV)	$-0.19877 \times 10^{-1}$	$-0.37484 \times 10^{-2}$	$-0.38416 \times 10^{-2}$	$-0.56691 \times 10^{-2}$
$A_{\text{FB}}^c$	$0.11116 \times 10^{-1}$	$0.11095 \times 10^{-1}$	$0.11098 \times 10^{-1}$	$0.11098 \times 10^{-1}$
$R_c$	$0.14772 \times 10^{-3}$	$0.14744 \times 10^{-3}$	$0.14730 \times 10^{-3}$	$0.14698 \times 10^{-3}$

Table 2: Maximum Derivatives with respect to  $m_b$ .

Observables	BHM	LEPTOP	TOPAZO	ZFITTER
$\Gamma_b$ (MeV)	-0.77934	-0.81333	-0.80247	-0.79613
$\Gamma_z$ (MeV)	-0.81949	-0.81344	-0.84278	-0.79462
$R_l$	$-0.92763 \times 10^{-2}$	$-0.96913 \times 10^{-2}$	$-0.95275 \times 10^{-2}$	$-0.94665 \times 10^{-2}$
$\sigma_0^h$ (nb)	$0.73002 \times 10^{-2}$	$0.76691 \times 10^{-2}$	$0.74958 \times 10^{-2}$	$0.74927 \times 10^{-2}$
$R_b$	$-0.34685 \times 10^{-3}$	$-0.36581 \times 10^{-3}$	$-0.35739 \times 10^{-3}$	$-0.35819 \times 10^{-3}$
$\Gamma_h$ (MeV)	-0.80799	-0.81344	-0.83069	-0.79462
$R_c$	$0.76013 \times 10^{-4}$	$0.80403 \times 10^{-4}$	$0.78998 \times 10^{-4}$	$0.79395 \times 10^{-4}$

Table 3: The experimental data.

Observables	Data
$M_w(\text{GeV})$	$80.22 \pm 0.18$
$\Gamma_l(\text{MeV})$	$83.96 \pm 0.18$
$\Gamma_z(\text{MeV})$	$2497.4 \pm 3.8$
$\sigma^h(\text{nb})$	$41.49 \pm 0.12$
$R_l$	$20.795 \pm 0.040$
$R_b$	$0.2202 \pm 0.0020$
$R_c$	$0.1583 \pm 0.0098$
$\sin^2 \theta_{\text{eff}}^l$	$0.2321 \pm 0.0004$
$A_{\text{FB}}^l$	$0.0170 \pm 0.0016$
$A_{\text{FB}}^b$	$0.0967 \pm 0.0038$
$A_{\text{FB}}^c$	$0.0760 \pm 0.0091$
$A_{\text{LR}}(\text{SLD})$	$0.1668 \pm 0.0077$

Table 4: The experimental data for  $M_w, \Gamma_l = \Gamma_e, \Gamma_z$  and the theoretical predictions corresponding to  $m_t = 175 \text{ GeV}$ ,  $M_H = 300 \text{ GeV}$  and  $\hat{\alpha}_s(M_z) = 0.125$ . The first entry is BHM then LEPTOP, TOPAZ0, WOH and ZFITTER. The uncertainties quoted are obtained from a variation of program options as described in Section 5.

Observable	Exp.	Theor. Predictions	Average
$M_w \text{ (GeV)}$	$80.22 \pm 0.18$	$80.319^{+0.003}_{-0.007}$ $80.312^{+0.013}_{-0.013}$ $80.310^{+0.000}_{-0.007}$ $80.319^{+0.004}_{-0.000}$ $80.317^{+0.007}_{-0.007}$	80.315
$\Gamma_l \text{ (MeV)}$	$83.96 \pm 0.18$	$83.919^{+0.020}_{-0.013}$ $83.930^{+0.023}_{-0.023}$ $83.931^{+0.015}_{-0.012}$ $83.943^{+0.022}_{-0.022}$ $83.941^{+0.013}_{-0.021}$	83.933
$\Gamma_z \text{ (MeV)}$	$2497.4 \pm 3.8$	$2497.4^{+0.9}_{-1.0}$ $2497.2^{+1.1}_{-1.1}$ $2497.4^{+0.2}_{-0.5}$ $2497.4^{+1.5}_{-0.6}$ $2497.5^{+0.6}_{-0.5}$	2497.4



Table 5: The same as in Table 4 for  $R_l, R_b, R_c$ .

Observable	Exp.	Theor. Predictions	Average
$R_l$	$20.795 \pm 0.040$	$20.788^{+0.004}_{-0.008}$ $20.780^{+0.006}_{-0.005}$ $20.782^{+0.002}_{-0.005}$ $20.780^{+0.013}_{-0.000}$ $20.781^{+0.006}_{-0.001}$	20.782
$R_b$	$0.2202 \pm 0.0020$	$0.21577^{+0.00010}_{-0.00011}$ $0.21564^{+0.00009}_{-0.00004}$ $0.21567^{+0.00003}_{-0.00012}$ $0.21567^{+0.00018}_{-0.00006}$ $0.21571^{+0.00001}_{-0.00002}$	0.21569
$R_c$	$0.1583 \pm 0.0098$	$0.17236^{+0.00002}_{-0.00002}$ $0.17240^{+0.00002}_{-0.00003}$ $0.17237^{+0.00004}_{-0.00000}$ $0.17240^{+0.00001}_{-0.00003}$ $0.17236^{+0.00002}_{-0.00000}$	0.17238

Table 6: The same as in Table 4 for  $\sin^2 \theta_{\text{eff}}^l, \sin^2 \theta_{\text{eff}}^b, A_{\text{FB}}^l$ .

Observable	Exp.	Theor. Predictions	Average
$\sin^2 \theta_{\text{eff}}^l$	$0.2321 \pm 0.0004$	$0.23197^{+0.00004}_{-0.00007}$ $0.23200^{+0.00008}_{-0.00008}$ $0.23200^{+0.00004}_{-0.00004}$ $0.23194^{+0.00003}_{-0.00007}$ $0.23205^{+0.00004}_{-0.00014}$	0.23199
$\sin^2 \theta_{\text{eff}}^b$		$0.23331^{+0.00004}_{-0.00012}$ $0.23329^{+0.00008}_{-0.00010}$ $0.23330^{+0.00009}_{-0.00001}$ $0.23325^{+0.00004}_{-0.00007}$ $0.23335^{+0.00004}_{-0.00014}$	0.23330
$A_{\text{FB}}^l$	$0.0170 \pm 0.0016$	$0.01544^{+0.00011}_{-0.00007}$ $0.01539^{+0.00013}_{-0.00013}$ $0.01536^{+0.00008}_{-0.00007}$ $0.01549^{+0.00012}_{-0.00005}$ $0.01531^{+0.00024}_{-0.00007}$	0.01540

Table 7: The same as in Table 4 for  $A_{\text{LR}}, A_{\text{FB}}^b, A_{\text{FB}}^c$ .

Observable	Exp.	Theor. Predictions	Average
$A_{\text{LR}}$	$0.1668 \pm 0.0077$	$0.14346^{+0.00052}_{-0.00031}$ $0.14326^{+0.00060}_{-0.00060}$ $0.14327^{+0.00028}_{-0.00031}$ $0.14372^{+0.00057}_{-0.00024}$ $0.14289^{+0.00110}_{-0.00032}$	0.14332
$A_{\text{FB}}^b$	$0.0967 \pm 0.0038$	$0.10053^{+0.00038}_{-0.00022}$ $0.10040^{+0.00043}_{-0.00042}$ $0.10033^{+0.00023}_{-0.00023}$ $0.10072^{+0.00041}_{-0.00006}$ $0.10013^{+0.00079}_{-0.00022}$	0.10042
$A_{\text{FB}}^c$	$0.0760 \pm 0.0038$	$0.07169^{+0.00029}_{-0.00017}$ $0.07158^{+0.00033}_{-0.00033}$ $0.07159^{+0.00016}_{-0.00017}$ $0.07183^{+0.00032}_{-0.00013}$ $0.07138^{+0.00061}_{-0.00017}$	0.07161

Table 8: Largest half-differences among central values ( $d_c$ ) and among maximal and minimal predictions ( $d_g$ ) for  $150 \text{ GeV} < m_t < 200 \text{ GeV}$ ,  $60 \text{ GeV} < M_H < 1 \text{ TeV}$  and  $0.118 < \alpha_s(M_Z) < 0.125$ .

Observable $O$	$d_c O$	$d_g O$
$M_W$ (GeV)	$6.5 \times 10^{-3}$	$1.9 \times 10^{-2}$
$\Gamma_e$ (MeV)	$1.7 \times 10^{-2}$	$3.7 \times 10^{-2}$
$\Gamma_z$ (MeV)	0.3	1.6
$\sin^2 \theta_{\text{eff}}^l$	$6.5 \times 10^{-5}$	$1.5 \times 10^{-4}$
$\sin^2 \theta_{\text{eff}}^b$	$6.0 \times 10^{-5}$	$1.6 \times 10^{-4}$
$R_l$	$4.0 \times 10^{-3}$	$1.0 \times 10^{-2}$
$R_b$	$7.0 \times 10^{-5}$	$2.0 \times 10^{-4}$
$R_c$	$3.0 \times 10^{-5}$	$5.0 \times 10^{-5}$
$\sigma_0^h$ (nb)	$7.5 \times 10^{-3}$	$8.5 \times 10^{-3}$
$A_{\text{FB}}^l$	$1.2 \times 10^{-4}$	$2.5 \times 10^{-4}$
$A_{\text{FB}}^b$	$3.5 \times 10^{-4}$	$8.2 \times 10^{-4}$
$A_{\text{FB}}^c$	$2.7 \times 10^{-4}$	$6.3 \times 10^{-4}$
$A_{\text{LR}}$	$5.0 \times 10^{-4}$	$1.1 \times 10^{-3}$

Table 9: Largest half-differences among central values ( $d_c$ ) and among maximal and minimal predictions ( $d_g$ ) for  $m_t = 175$  GeV,  $60 \text{ GeV} < M_H < 1 \text{ TeV}$  and  $\hat{\alpha}_s(M_Z) = 0.125$ .

Observable $O$	$d_c O$	$d_g O$
$M_W$ (GeV)	$4.5 \times 10^{-3}$	$1.6 \times 10^{-2}$
$\Gamma_e$ (MeV)	$1.3 \times 10^{-2}$	$3.1 \times 10^{-2}$
$\Gamma_Z$ (MeV)	0.2	1.4
$\sin^2 \theta_{\text{eff}}^l$	$5.5 \times 10^{-5}$	$1.4 \times 10^{-4}$
$\sin^2 \theta_{\text{eff}}^b$	$5.0 \times 10^{-5}$	$1.5 \times 10^{-4}$
$R_l$	$4.0 \times 10^{-3}$	$9.0 \times 10^{-3}$
$R_b$	$6.5 \times 10^{-5}$	$1.7 \times 10^{-4}$
$R_c$	$2.0 \times 10^{-5}$	$4.5 \times 10^{-5}$
$\sigma_0^h$ (nb)	$7.0 \times 10^{-3}$	$8.5 \times 10^{-3}$
$A_{\text{FB}}^l$	$9.3 \times 10^{-5}$	$2.2 \times 10^{-4}$
$A_{\text{FB}}^b$	$3.0 \times 10^{-4}$	$7.4 \times 10^{-4}$
$A_{\text{FB}}^c$	$2.3 \times 10^{-4}$	$5.7 \times 10^{-4}$
$A_{\text{LR}}$	$4.2 \times 10^{-4}$	$8.7 \times 10^{-4}$

Table 10: Largest half-differences among central values ( $d_c$ ) and among maximal and minimal predictions ( $d_g$ ) for  $m_t = 175$  GeV,  $M_H = 300$  GeV and  $0.118 < \hat{\alpha}_s(M_Z) < 0.125$ .

Observable $O$	$d_c O$	$d_g O$
$M_W$ (GeV)	$4.5 \times 10^{-3}$	$1.3 \times 10^{-2}$
$\Gamma_e$ (MeV)	$1.2 \times 10^{-2}$	$3.0 \times 10^{-2}$
$\Gamma_Z$ (MeV)	0.15	1.4
$\sin^2 \theta_{\text{eff}}^l$	$5.5 \times 10^{-5}$	$1.1 \times 10^{-4}$
$\sin^2 \theta_{\text{eff}}^b$	$5.0 \times 10^{-5}$	$1.1 \times 10^{-4}$
$R_l$	$4.0 \times 10^{-3}$	$9.0 \times 10^{-3}$
$R_b$	$6.5 \times 10^{-5}$	$1.6 \times 10^{-4}$
$R_c$	$2.5 \times 10^{-5}$	$4.5 \times 10^{-5}$
$\sigma_0^h$ (nb)	$6.5 \times 10^{-3}$	$8.0 \times 10^{-3}$
$A_{\text{FB}}^l$	$8.9 \times 10^{-5}$	$1.9 \times 10^{-4}$
$A_{\text{FB}}^b$	$3.0 \times 10^{-4}$	$6.1 \times 10^{-4}$
$A_{\text{FB}}^c$	$2.3 \times 10^{-4}$	$4.7 \times 10^{-4}$
$A_{\text{LR}}$	$4.2 \times 10^{-4}$	$8.6 \times 10^{-4}$

Table 11: Effects of additional options in TOPAZ0 for  $m_t = 175$  GeV,  $M_H = 300$  GeV and  $\hat{\alpha}_s(M_Z) = 0.125$ .

Observables	Predictions
$M_W$ (GeV)	$80.310^{+0.000}_{-0.007} \rightarrow 80.310^{+0.005}_{-0.007}$
$\Gamma_l$ (MeV)	$83.931^{+0.015}_{-0.012} \rightarrow 83.931^{+0.043}_{-0.031}$
$\Gamma_Z$ (MeV)	$2497.4^{+0.2}_{-0.5} \rightarrow 2497.4^{+1.3}_{-0.6}$
$R_l$	$20.782^{+0.002}_{-0.005} \rightarrow 20.782^{+0.010}_{-0.004}$
$R_b$	$0.21567^{+0.00003}_{-0.00012} \rightarrow 0.21569^{+0.00000}_{-0.00016}$
$R_c$	$0.17237^{+0.00004}_{-0.00000} \rightarrow 0.17237^{+0.00007}_{-0.00001}$
$\sin^2 \theta_{\text{eff}}^l$	$0.23200^{+0.00004}_{-0.00004} \rightarrow 0.23201^{+0.00004}_{-0.00026}$
$A_{\text{FB}}^l$	$0.01536^{+0.00008}_{-0.00007} \rightarrow 0.01538^{+0.00075}_{-0.00074}$
$A_{\text{FB}}^b$	$0.10033^{+0.00023}_{-0.00023} \rightarrow 0.10037^{+0.00137}_{-0.00067}$
$A_{\text{FB}}^c$	$0.07159^{+0.00016}_{-0.00017} \rightarrow 0.07157^{+0.00115}_{-0.00053}$
$A_{\text{LR}}$	$0.14327^{+0.00028}_{-0.00031} \rightarrow 0.14320^{+0.00193}_{-0.00039}$

## Realistic-observables

Table 12: The hadronic cross-section (nb) in two different configurations, NN=NY/  
YN=YY for inclusion of initial state pair production.

$\sqrt{s}$ (GeV)	BHM	TOPAZO	ZFITTER
88.45	5.181	5.184	5.185
	5.168	5.171	5.172
89.45	10.062	10.068	10.067
	10.036	10.042	10.042
90.20	18.033	18.040	18.039
	17.983	17.992	17.992
91.1887	30.446	30.452	30.451
	30.366	30.375	30.373
91.30	30.585	30.590	30.590
	30.506	30.514	30.514
91.95	25.176	25.176	25.181
	25.124	25.126	25.130
93.00	14.131	14.127	14.134
	14.117	14.119	14.124
93.70	10.070	10.065	10.072
	10.068	10.073	10.074



Table 13: The  $\mu$  forward-backward asymmetry in four different configurations, NN/YN/NY/YY for inclusion of initial state pair production and initial-final QED interference.

$\sqrt{s}$ (GeV)	BHM	TOPAZ0	ZFITTER
88.45	-0.2552	-0.2551	-0.2546
	-0.2552	-0.2557	-0.2544
	-0.2546	-0.2543	-0.2541
	-0.2546	-0.2549	-0.2539
89.45	-0.1631	-0.1632	-0.1630
	-0.1631	-0.1636	-0.1628
	-0.1626	-0.1624	-0.1625
	-0.1626	-0.1628	-0.1623
90.20	-0.0912	-0.0914	-0.0913
	-0.0912	-0.0917	-0.0912
	-0.0907	-0.0907	-0.0908
	-0.0907	-0.0909	-0.0907
91.1887	-0.0012	-0.0015	-0.0014
	-0.0012	-0.0014	-0.0014
	-0.0008	-0.0011	-0.0011
	-0.0008	-0.0011	-0.0011
91.30	0.0080	0.0076	0.0077
	0.0080	0.0076	0.0077
	0.0083	0.0078	0.0080
	0.0083	0.0078	0.0083
91.95	0.0556	0.0550	0.0552
	0.0556	0.0551	0.0551
	0.0558	0.0549	0.0554
	0.0558	0.0550	0.0553
93.00	0.1114	0.1105	0.1108
	0.1114	0.1106	0.1106
	0.1116	0.1104	0.1109
	0.1116	0.1104	0.1106
93.70	0.1379	0.1368	0.1372
	0.1379	0.1367	0.1367
	0.1380	0.1367	0.1372
	0.1380	0.1366	0.1368

Table 14: De-convoluted  $A_{\text{FB}}^\mu$  at  $s = M_Z^2$ , first entry is the  $ZZ$  part, then  $ZZ + \gamma\gamma$ ,  $ZZ + Z\gamma$  and total.

Contribution	BHM	TOPAZO	ZFITTER
$ZZ$	0.015443	0.015358	0.015279
$ZZ + \gamma\gamma$	0.015351	0.015267	0.015189
$ZZ + Z\gamma$	0.017026	0.016735	0.016725
Total	0.016925	0.016636	0.016627

Table 15: The de-convoluted  $\sigma^\mu, \sigma^h$  and  $A_{\text{FB}}^\mu$ .

$\sqrt{s}$ (GeV)	BHM	TOPAZ0	ZFITTER
88.45	0.3491	0.3492	0.3492
	7.020	7.026	7.022
	-0.2386	-0.2388	-0.2384
89.45	0.6884	0.6887	0.6887
	14.073	14.083	14.077
	-0.1454	-0.1456	-0.1453
90.20	1.2453	1.2457	1.2458
	25.650	25.663	25.655
	-0.0749	-0.0751	-0.0750
91.1887	2.0015	2.0019	2.0022
	41.400	41.409	41.402
	0.0169	0.0166	0.0166
91.30	1.9812	1.9816	1.9820
	40.983	40.991	40.987
	0.0271	0.0268	0.0268
91.95	1.4486	1.4488	1.4492
	29.935	29.936	29.937
	0.0855	0.0853	0.0851
93.00	0.6534	0.6533	0.6536
	13.411	13.408	13.411
	0.1757	0.1755	0.1751
93.70	0.4105	0.4104	0.4106
	8.362	8.358	8.361
	0.2323	0.2320	0.2316

Table 16:  $\delta_{\text{conv}}$ , as defined by Eq.( 136) for the hadronic cross-section.

$\sqrt{s}$ (GeV)	BHM	TOPAZ0	ZFITTER
88.450	-0.2638	-0.2640	-0.2634
89.450	-0.2869	-0.2869	-0.2866
90.200	-0.2989	-0.2989	-0.2987
91.189	-0.2665	-0.2665	-0.2664
91.300	-0.2556	-0.2556	-0.2555
91.950	-0.1607	-0.1607	-0.1606
93.000	+0.0526	+0.0530	+0.0532
93.700	+0.2040	+0.2052	+0.2049

## Bhabha scattering

Table 17: The ALIBABA(A) - TOPAZO(T) comparison for the full Bhabha cross-section (in pb) for the following set-up:  $40^\circ < \theta_- < 140^\circ$ ,  $\theta_{\text{acoll}} < 10^\circ$  and  $E_{\text{th}} = 1$  GeV. I is the TOPAZO default for QED final state radiation, II is the ZFITTER-like default for QED final state radiation and III includes initial state pair production.

$\sqrt{s}$ GeV	A	T(I)	T(II)	T (III)
88.45	$457.52 \pm 0.27$	$457.30^{+0.17}_{-0.06} \pm 0.25$	457.20	456.14
89.45	$643.95 \pm 0.31$	$644.37^{+0.26}_{-0.09} \pm 0.24$	644.23	642.60
90.20	$908.99 \pm 0.39$	$910.46^{+0.38}_{-0.11} \pm 0.24$	910.26	907.86
91.19	$1183.99 \pm 0.39$	$1184.03^{+0.48}_{-0.13} \pm 0.24$	1183.78	1180.79
91.30	$1163.56 \pm 0.45$	$1163.51^{+0.47}_{-0.13} \pm 0.24$	1163.26	1160.38
91.95	$876.90 \pm 0.28$	$874.02^{+0.35}_{-0.12} \pm 0.24$	873.83	872.13
93.00	$481.35 \pm 0.14$	$477.51^{+0.17}_{-0.08} \pm 0.24$	477.41	477.18
93.70	$355.57 \pm 0.13$	$352.52^{+0.14}_{-0.06} \pm 0.25$	352.45	352.72

Table 18: The same as in Table 17 for the forward backward asymmetry.

$\sqrt{s}$ GeV	A	T(I)	T(III)
88.45	$0.44611 \pm 1.06 \times 10^{-3}$	$0.44534^{+0.02}_{-0.08} \pm 0.79 \times 10^{-3}$	0.44637
89.45	$0.34250 \pm 0.90 \times 10^{-3}$	$0.34166^{+0.01}_{-0.07} \pm 0.51 \times 10^{-3}$	0.34252
90.20	$0.24956 \pm 0.81 \times 10^{-3}$	$0.24977^{+0.02}_{-0.05} \pm 0.33 \times 10^{-3}$	0.25043
91.19	$0.13925 \pm 0.66 \times 10^{-3}$	$0.13916^{+0.03}_{-0.08} \pm 0.23 \times 10^{-3}$	0.13951
91.30	$0.13050 \pm 0.70 \times 10^{-3}$	$0.13035^{+0.03}_{-0.08} \pm 0.23 \times 10^{-3}$	0.13067
91.95	$0.10169 \pm 0.63 \times 10^{-3}$	$0.10139^{+0.03}_{-0.09} \pm 0.30 \times 10^{-3}$	0.10158
93.00	$0.13110 \pm 0.61 \times 10^{-3}$	$0.13055^{+0.03}_{-0.12} \pm 0.57 \times 10^{-3}$	0.13061
93.70	$0.18157 \pm 0.68 \times 10^{-3}$	$0.17957^{+0.02}_{-0.10} \pm 0.83 \times 10^{-3}$	0.17944

Table 19: The same as in Table 17 for  $\theta_{\text{acoll}} < 25^\circ$ .

$\sqrt{s}$ GeV	A	T(I)	T(II)	T (III)
88.45	$483.27 \pm 0.25$	$484.97^{+0.07}_{-0.06} \pm 0.22$	484.86	483.74
89.45	$672.67 \pm 0.29$	$673.99^{+0.13}_{-0.09} \pm 0.22$	673.84	672.13
90.20	$942.52 \pm 0.34$	$942.96^{+0.25}_{-0.12} \pm 0.22$	942.76	940.27
91.19	$1218.66 \pm 0.40$	$1219.24^{+0.36}_{-0.13} \pm 0.21$	1218.98	1215.90
91.30	$1198.23 \pm 0.36$	$1198.42^{+0.35}_{-0.13} \pm 0.21$	1198.17	1195.20
91.95	$908.87 \pm 0.30$	$905.35^{+0.24}_{-0.12} \pm 0.20$	905.16	903.39
93.00	$505.38 \pm 0.15$	$504.24^{+0.10}_{-0.08} \pm 0.20$	504.13	503.88
93.70	$378.20 \pm 0.13$	$377.94^{+0.06}_{-0.06} \pm 0.20$	377.86	378.14

Table 20: The same as in Table 18 for  $\theta_{\text{acoll}} < 25^\circ$ .

$\sqrt{s}$ GeV	A	T(I)	T(III)
88.45	$0.45843 \pm 0.94 \times 10^{-3}$	$0.46061^{+0.02}_{-0.19} \pm 0.65 \times 10^{-3}$	0.46168
89.45	$0.35479 \pm 0.77 \times 10^{-3}$	$0.35560^{+0.01}_{-0.17} \pm 0.43 \times 10^{-3}$	0.67213
90.20	$0.26121 \pm 0.67 \times 10^{-3}$	$0.26165^{+0.02}_{-0.14} \pm 0.29 \times 10^{-3}$	0.26235
91.19	$0.15114 \pm 0.70 \times 10^{-3}$	$0.15045^{+0.03}_{-0.12} \pm 0.20 \times 10^{-3}$	0.15083
91.30	$0.14067 \pm 0.62 \times 10^{-3}$	$0.14203^{+0.03}_{-0.12} \pm 0.20 \times 10^{-3}$	0.14238
91.95	$0.11466 \pm 0.62 \times 10^{-3}$	$0.11773^{+0.03}_{-0.17} \pm 0.25 \times 10^{-3}$	0.11795
93.00	$0.15628 \pm 0.59 \times 10^{-3}$	$0.15838^{+0.03}_{-0.29} \pm 0.45 \times 10^{-3}$	0.15845
93.70	$0.21239 \pm 0.66 \times 10^{-3}$	$0.21360^{+0.02}_{-0.36} \pm 0.65 \times 10^{-3}$	0.21344

Table 21: The same as in Table 17 with the percentage relative deviation.

$\sqrt{s}$ GeV	A	T(II)	%
88.45	457.52	457.20	+0.07
89.45	643.95	644.23	-0.04
90.20	908.99	910.26	-0.14
91.19	1183.99	1183.78	+0.02
91.30	1163.56	1163.26	+0.03
91.95	876.90	873.83	+0.35
93.00	481.35	477.41	+0.82
93.70	355.57	352.45	+0.88



Table 22: The same as in Table 21 for  $s$ -channel alone.

$\sqrt{s}$ GeV	A	T(II)	%
88.45	173.01	172.71	+0.17
89.45	330.62	330.70	-0.02
90.20	588.47	588.81	-0.06
91.19	989.81	990.90	-0.11
91.30	994.07	995.38	-0.13
91.95	819.56	819.97	-0.05
93.00	463.72	461.68	+0.44
93.70	331.78	329.83	+0.59

Table 23: ALIBABA-TOPAZ0 comparison for  $s-t$  and  $t-t$  contributions with the following set-up:  $40^\circ < \theta_- < 140^\circ$ ,  $\theta_{\text{acoll}} < 10^\circ$  and  $E_{\text{th}} = 1$  GeV.

$\sqrt{s}$ GeV	$\sigma - \sigma(s)$ A	$\sigma - \sigma(s)$ T	$\delta(\text{A})$	$\delta(\text{T})$	%
88.45	284.51	284.49	1.644	1.647	-0.18
89.45	313.33	313.53	0.948	0.948	+0.00
90.20	320.52	321.45	0.545	0.546	-0.18
91.19	194.18	192.88	0.196	0.195	+0.51
91.30	169.49	167.88	0.171	0.169	+1.18
91.95	57.34	53.86	0.070	0.066	+5.88
93.00	17.63	15.75	0.038	0.034	+11.11
93.70	23.79	22.62	0.072	0.069	+4.26

Table 24: The same as in Table 23 for the forward-backward asymmetry.

$\sqrt{s}$ GeV	A s+t	T s+t	A s	T s	A t	T t
88.45	0.44611	0.44534	-0.22019	-0.22060	0.66630	0.66594
89.45	0.34250	0.34166	-0.13754	-0.13847	0.48004	0.48013
90.20	0.24956	0.24977	-0.07774	-0.07649	0.32730	0.32626
91.19	0.13925	0.13916	-0.00102	0.00001	0.14027	0.13915
91.30	0.13050	0.13035	0.00745	0.00779	0.12305	0.12256
91.95	0.10169	0.10139	0.05059	0.04851	0.05110	0.05288
93.00	0.13110	0.13055	0.09863	0.09789	0.03247	0.03266
93.70	0.18157	0.17957	0.12237	0.12248	0.05920	0.05709

Table 25: Comparison for the full Bhabha cross-section (in pb) for the following set-up:  $40^\circ < \theta_- < 140^\circ$ ,  $\theta_{\text{acoll}} < 10^\circ$  and  $E_{\text{th}} = 1$  GeV. First entry is **ALIBABA**, second entry is the TOPAZ0 default for QED final state radiation and no pair production,  $\delta_{\text{FSR}}$  is the uncertainty on final-state QED radiation estimated by **TOPAZ0**, while  $\Delta_g$  is the relative difference between the maximal and minimal predictions of **ALIBABA-TOPAZ0**.

$\sqrt{s}$ GeV	A	T(I)	$\delta_{\text{FSR}}(T)\%$	$\Delta_g\%$
88.45	$457.52 \pm 0.27$	$457.30^{+0.17}_{-0.06} \pm 0.25$	0.02	0.15
89.45	$643.95 \pm 0.31$	$644.37^{+0.26}_{-0.09} \pm 0.24$	0.02	0.19
90.20	$908.99 \pm 0.39$	$910.46^{+0.38}_{-0.11} \pm 0.24$	0.02	0.27
91.19	$1183.99 \pm 0.39$	$1184.03^{+0.48}_{-0.13} \pm 0.24$	0.02	0.10
91.30	$1163.56 \pm 0.45$	$1163.51^{+0.47}_{-0.13} \pm 0.24$	0.02	0.10
91.95	$876.90 \pm 0.28$	$874.02^{+0.35}_{-0.12} \pm 0.24$	0.02	0.37
93.00	$481.35 \pm 0.14$	$477.51^{+0.17}_{-0.08} \pm 0.24$	0.02	0.86
93.70	$355.57 \pm 0.13$	$352.52^{+0.14}_{-0.06} \pm 0.25$	0.02	0.95

## Effect of working options for different codes

Table 26: The effect of the working options of BHM on theoretical errors.

Observable	Default	IRES err	+IQCD err	+IFAC err	+ITWO err
$M_W$ (GeV)	80.319	0.004	0.010	0.010	0.010
$\Gamma_e$ (MeV)	83.919	0.020	0.032	0.033	0.033
$\Gamma_z$ (MeV)	2497.4	0.68	1.07	1.71	1.92
$R_l$	20.788	0.001	0.002	0.010	0.012
$R_b$	0.21577	0.00000	0.00000	0.00011	0.00020
$A^l$	0.015435	0.00011	0.00018	0.00018	0.00018
$A_{\text{FB}}^b$	0.10053	0.00037	0.00059	0.00059	0.00059
$\sin^2 \theta_{\text{eff}}^l$	0.23197	0.00007	0.00011	0.00011	0.00011
$\sin^2 \theta_{\text{eff}}^b$	0.23331	0.00007	0.00011	0.00011	0.00016

Table 27: The effect of the working options of LEPTOP on theoretical errors. The first two lines indicate parametric uncertainties caused by  $\delta s^2 = 0.0003$  (which is equivalent to  $\delta \bar{\alpha}^{-1} = 0.12$ ) and by  $\delta m_b = 0.3 \text{ GeV}$ . The next six lines refer to the intrinsic theoretical uncertainties. This table was calculated with  $m_t=175 \text{ GeV}$ ,  $M_H=300 \text{ GeV}$  and  $\hat{\alpha}_s=0.125$ .

	$M_W$ (MeV)	$\Gamma_l$ (MeV)	$\sin^2 \theta_{\text{eff}}^l$	$\sigma_0^h(nb)$	$\Gamma_z$ (MeV)	$\Gamma_h$ (MeV)	$R_l$	$\Gamma_b$ (MeV)	$R_b \times 10^5$	$R_c \times 10^5$
$\delta s^2$	16	.015	.00031	.0014	.8	.8	.0055	.15	1.1	1.8
$\delta m_b$	-	-	-	.0023	.2	.2	.0029	.24	11.0	2.4
$\Delta V_i^{t^2}$	9	.015	.00005	.0002	.5	.4	.0009	.08	.2	.3
$\Delta V_i^{\alpha_s^2}$	5	.008	.00003	.0001	.3	.2	.0005	.04	.1	.2
$\Delta \Gamma_q$	-	-	-	.0029	.3	.3	.0037	-	3.8	1.5
$\Delta \phi^{\alpha_s^2}$	-	-	-	.0010	.1	.1	.0012	.10	4.6	1.0
total	+13 -13	+.023 -.023	+.00008 -.00008	+.0032 -.0042	+1.2 -1.1	+1.0 -0.9	+.0063 -.0051	+.23 -.13	+8.7 -4.1	+1.9 -2.9

Table 28: The effect of the working options of **TOPAZ0** on theoretical errors.

Observable	Default	OU1 err	+ OU4 err	+ OU5 err	+ OU6 err	+OU7 err
$M_W$ (GeV)	80.310	-	-	0.001	0.001	0.007
$\Gamma_e$ (MeV)	83.931	0.014	0.014	0.015	0.015	0.027
$\Gamma_z$ (MeV)	2497.4	0.10	0.10	0.10	0.30	0.70
$R_l$	20.782	0.004	0.004	0.004	0.006	0.007
$R_b$	0.21567	0.00012	0.00012	0.00013	0.00014	0.00015
$A_{\text{FB}}^l$	0.015362	0.00006	0.00006	0.00008	0.00008	0.00015
$A_{\text{FB}}^b$	0.10033	0.00018	0.00019	0.00024	0.00024	0.00046
$\sin^2 \theta_{\text{eff}}^l$	0.23200	0.00004	0.00004	0.00004	0.00004	0.00008
$\sin^2 \theta_{\text{eff}}^b$	0.23330	0.00005	0.00005	0.00006	0.00006	0.00010

Table 29: The effect of the working options of **ZFITTER** on theoretical errors.

Observable	Default	OZ1 err	+OZ2 err	+OZ3 err	+OZ4 err	+OZ5 err	+OZ6 err
$M_W$ (GeV)	80.317	0.001	0.002	0.005	0.007	0.007	0.014
$\Gamma_e$ (MeV)	83.941	0.004	0.006	0.014	0.014	0.021	0.034
$\Gamma_z$ (MeV)	2497.5	0.1	0.2	0.2	0.2	0.6	1.1
$R_l$	20.781	-	0.001	0.002	0.003	0.005	0.007
$R_b$	0.21571	-	-	0.00001	0.00001	0.00002	0.00003
$A_{\text{FB}}^l$	0.01531	0.00003	0.00009	0.00015	0.00024	0.00024	0.00030
$A_{\text{FB}}^b$	0.10013	0.00011	0.00029	0.00050	0.00078	0.00079	0.00101
$\sin^2 \theta_{\text{eff}}^l$	0.23205	0.00002	0.00005	0.00009	0.00014	0.00014	0.00018
$\sin^2 \theta_{\text{eff}}^b$	0.23335	0.00002	0.00005	0.00009	0.00014	0.00014	0.00018

## Note added in proof

While making proof-reading of this contribution we have been informed on some recent development concerning the AFMT term in  $\Delta\rho$ . A recent calculation by K.G. Chetyrkin, J.H. Kühn and M. Steinhauser [63] as well as a revised version of the AFMT calculation [53] have shown that the correct coefficient of  $\zeta(4)$  in a term proportional to  $C_F^2$  of  $\delta_{(3)}^{\text{QCD}}$  is 4 and not 188/5. This will correspond to some shift in our predictions for the central values of the pseudo-observables, as a matter of fact a shift common to all codes since the AFMT term is a common external block. We have shown this shift in the following Table, where we compare our error bands with the shifted central values at the standard reference point. The result can be simply summarized by saying that the updated central values remain within our theoretical error bands. As for the theoretical bands is concerned, we note first, that they are not dominated by the QCD-uncertainty in the calculation of the  $\rho$ -parameter. Second, as it seen from the Table added, the widths of the uncertainty bands is only marginally affected by the shift of the AFMT correction.

Table 30: Change of some of the observables due to the introduction of the revised AFMT formulas. Here  $m_t = 175 \text{ GeV}$ ,  $M_H = 300 \text{ GeV}$  and  $\alpha_s = 0.125$ . In order to estimate the size of the non-leading QCD effects, the  $\delta^{\text{QCD}}$  correction factor has been implemented according to the formulation of Ref. [62], with a scale which gives the maximum variation with respect to the AFMT(revised) term —  $\xi = 0.248(0.204)$  — and the difference between this and the AFMT (revised) calculation is used as an estimate of the corresponding uncertainty. The numbers are calculated by TOPAZ0, first row, and ZFITTER, second row.

Observable	New AFMT	AFMT	Central difference
$M_W \text{ (GeV)}$	$80.307^{+0.000}_{-0.007}$	$80.310^{+0.000}_{-0.007}$	$-3 \text{ MeV}$
	$80.314^{+0.007}_{-0.007}$	$80.317^{+0.007}_{-0.007}$	$-3 \text{ MeV}$
$\Gamma_l \text{ (MeV)}$	$83.926^{+0.015}_{-0.012}$	$83.931^{+0.015}_{-0.012}$	$-0.005 \text{ MeV}$
	$83.936^{+0.013}_{-0.021}$	$83.941^{+0.013}_{-0.021}$	$-0.005 \text{ MeV}$
$\Gamma_Z \text{ (MeV)}$	$2497.2^{+0.2}_{-0.4}$	$2497.4^{+0.2}_{-0.5}$	$-0.2 \text{ MeV}$
	$2497.3^{+0.7}_{-0.5}$	$2497.5^{+0.6}_{-0.5}$	$-0.2 \text{ MeV}$
$R_l$	$20.782^{+0.002}_{-0.005}$	$20.782^{+0.002}_{-0.005}$	$0.000$
	$20.780^{+0.006}_{-0.000}$	$20.781^{+0.006}_{-0.001}$	$-0.001$
$R_b$	$0.21568^{+0.00002}_{-0.00013}$	$0.21567^{+0.00003}_{-0.00012}$	$+1 \times 10^{-5}$
	$0.21571^{+0.00001}_{-0.00002}$	$0.21571^{+0.00001}_{-0.00002}$	$0 \times 10^{-5}$
$\sin^2 \theta_{\text{eff}}^l$	$0.23201^{+0.00004}_{-0.00003}$	$0.23200^{+0.00004}_{-0.00004}$	$+1 \times 10^{-5}$
	$0.23206^{+0.00004}_{-0.00014}$	$0.23205^{+0.00004}_{-0.00014}$	$+1 \times 10^{-5}$
$\sin^2 \theta_{\text{eff}}^b$	$0.23331^{+0.00009}_{-0.00000}$	$0.23330^{+0.00009}_{-0.00001}$	$+1 \times 10^{-5}$
	$0.23337^{+0.00004}_{-0.00015}$	$0.23335^{+0.00004}_{-0.00014}$	$+2 \times 10^{-5}$
$A_{\text{FB}}^l$	$0.01533^{+0.00008}_{-0.00007}$	$0.01536^{+0.00008}_{-0.00007}$	$-3 \times 10^{-5}$
	$0.01528^{+0.00024}_{-0.00007}$	$0.01531^{+0.00024}_{-0.00007}$	$-3 \times 10^{-5}$
$A_{\text{LR}}$	$0.14314^{+0.00028}_{-0.00030}$	$0.14327^{+0.00028}_{-0.00031}$	$-1.3 \times 10^{-4}$
	$0.14275^{+0.00111}_{-0.00030}$	$0.14289^{+0.00110}_{-0.00032}$	$-1.4 \times 10^{-4}$
$A_{\text{FB}}^b$	$0.10024^{+0.00022}_{-0.00023}$	$0.10033^{+0.00023}_{-0.00023}$	$-9 \times 10^{-5}$
	$0.10004^{+0.00078}_{-0.00022}$	$0.10013^{+0.00079}_{-0.00022}$	$-9 \times 10^{-5}$